AD-A216 740 MENTATION PAGE

Form Approved
OMB No. 0704-0188

PORT SECURITY CLASSIFICATION	1b. RESTRICTIVE MARKINGS
Unclassified	
CURITY CLASSIFICATION AUTHORITY	3. DISTRIBUTION / AVAILABILITY OF REPORT
	Approved for public release;
CLASSIFICATION / DOWNGRADING SCHEDULE	distribution unlimited.

FORMING ORGANIZATION REPORT NUMBER(S)	5. MONITORING ORGANIZATION REPORT NUMBER(S)
	AFOSR·TR. 8 5 - 0 4 6 0

6a. NAME OF PERFORMING ORGANIZATION	6b. OFFICE SYMBOL (If applicable)	7a. NAME OF MONITORING ORGANIZATION
Georgie Institute of Technology		Air Force Office of Scientific Research
6c. ADDRESS (City, State, and ZIP Code)		7b. ADDRESS (City, State, and ZIP Code)
Atlanta, Georgia 30332		AFOSR/NA Bldg 410
		Bolling AFB, Washington D.C. 20332-6448

8a. NAME OF FUNDING / SPONSORING ORGANIZATION	8b. OFFICE SYMBOL (If applicable)	9 PROCUREMENT INSTRUMENT IDENTIFICATION NUMBER
Air Force Office of Scientific Research	NA	AF-AFOSR/DCASR F49620-86-C-0005

8c. ADDRESS (City, State, and ZIP Code)	10 SOURCE OF FUNDING NUMBERS			
AFOSR/NA Bldg 410 Bolling AFB, Washington D.C. 20332-6448	PROGRAM ELEMENT NO.	PROJECT NO.	TASK NO	WORK UNIT ACCESSION NO
	61102F	2308	A1	

11. TITLE (Include Security Classification) Propellant Rockets
Combustion Instability in Solid ~~Rocket Motors~~ (Unclassified)

12. PERSONAL AUTHOR(S)
E. W. Price and G. A. Flandro

13a. TYPE OF REPORT	13b TIME COVERED	14 DATE OF REPORT (Year, Month, Day)	15. PAGE COUNT
Final	FROM 10/85 TO 3/89	March 21, 1989	288

16. SUPPLEMENTARY NOTATION

17.	COSATI CODES		18 SUBJECT TERMS (Continue on reverse if necessary and identify by block number)
FIELD	GROUP	SUB-GROUP	Combustion Instability, Solid Propellants, Rocket Motors, Solid ... ...

19. ABSTRACT (Continue on reverse if necessary and identify by block number)

This report consists of a partial manuscript of a book on combustion instability, and plans for future work to complete the book. The manuscript is submitted in its present form as a report of work completed on Contract # F49620-86-C-0005.

DTIC
ELECTE
JAN 12 1990
S D
D

9U 01 11 120

20 DISTRIBUTION / AVAILABILITY OF ABSTRACT	21 ABSTRACT SECURITY CLASSIFICATION
☒ UNCLASSIFIED/UNLIMITED ☐ SAME AS RPT ☐ DTIC USERS	Unclassified
22a NAME OF RESPONSIBLE INDIVIDUAL	22b TELEPHONE (Include Area Code)	22c. OFFICE SYMBOL
Mike H. Buzkan	(202) 767-4938	NA

DD Form 1473, JUN 86   Previous editions are obsolete   SECURITY CLASSIFICATION OF THIS PAGE

UNCLASSIFIED

INTRODUCTION

This report constitutes the principal part of a book on combustion stability in solid propellant rockets. While the manuscript is not complete, an Air Force contract to support the writing has run out, and it has been requested that the manuscript be submitted as is so that the contract can be closed out. The authors thank the Air Force Office of Scientific Research for its support, and for its patience in allowing further time to work on the manuscript beyond the originally scheduled completion date of September 30, 1987.

The present report contains nine chapters that are each substantially complete except for some editorial, bibliographical and art work in some chapters. Work is continuing, with highest priority on these chapters. It is proposed that completed versions of these nine chapters will be sent to the contract monitor informally as they become available. It is also planned to publish these chapters along with several new ones at a later date (estimated June 1990).

In addition to the text, extensive bibliographical work has been involved in this project. A computerized data storage, retrieval and search system was developed and relevant information on publications actually on hand is being entered in the data base. The program and data base can be provided on two 5-inch floppy disks suitable for use in IBM PCs with two-disk capacity. When all of the (subject-coded) entries from on-hand publications have been entered, the disks will be sent to the Air Force monitor along with an instruction manual for operation of the program (estimated May 1989). The authors intend to continue to add to the data base, and hope that arrangements can be made to make the bibliography widely available.

The authors have designed this book to consolidate a vast body of research during the last 30 years, research on a complex, sometimes mystical or frustrating, but intensely challenging topic. Our goal is to present a coherent, reasonably complete summary of current knowledge, arranged in a way that satisfies the needs of a variety of users with a variety of technical backgrounds. While this need is not fully served by the present nine chapters,

the reader is carried (in progressive chapters) from general introductory material on into the basic theory of combustion, flow, and instability. The "broad audience" approach is also embodied in the format of each chapter. No matter how complex the content, most chapters start with a section describing in qualitative terms what material will be covered and why. A section at the end of the chapter then reviews what was done, and how well the topics have been treated to date--i.e., where we stand. An ambitious goal is to reduce the chaos of the literature to an orderly and lucid form that will lead to more effective use and extension. To the extent that this goal is achieved, it will be rewarded 100-fold for time spent and financial support provided. To the extent that this goal eludes us, we solicit suggestions from fellow members of the "combustion instability community" on how to better serve that community.

CONTENTS

Combustion Instability in Solid Propellant Rockets

Edward W. Price

Regents Professor of Aerospace Engineering
Georgia Institute of Technology

Gary A. Flandro

Professor of Aerospace Engineering
Georgia Institute of Technology

Approved for public release;

Accesion For

NTIS	CRA&I	
DTIC	TAB	
U		
J		

By

D

Dist

A-1

Air Force Office of Scientific Research

INTRODUCTION TO COMBUSTION INSTABILITY

Secondary pressure peaks and grain erosion characteristic of unstable burning are due to some abnormal flow or oscillation ... as if the gas were swirling with a high velocity

S. F. Boys & A. Schofield 1942

1.1 INTRODUCTION

High capacity combustors such as those used in jet propulsion systems are supposed to give smooth combustion at some design level determined by fuel-flow settings or design. However, such high-energy systems sometimes operate instead spontaneously in an oscillatory fashion, with gas flow and combustion processes interacting periodically to produce severe pressure oscillations. Unless the combustor is specially designed for such conditions, it can be destroyed by pressure excesses, severe heating, or vibration-induced mechanical failures. Even if outright destruction does not occur, the oscillations can induce a variety of malfunctions in the flight vehicle.

Oscillatory modes of operation, while not ordinarily desired, are completely natural. If unwanted, their avoidance may require overt design consideration or experimental evaluation, and failure to do so often causes serious delays and costs in development programs for new propulsion systems. However, the physio-chemical processes involved in nonsteady combustion-flow systems are very complex and "overt design considerations" mentioned above are by no means straightforward. Indeed, the relevant technical literature is very abstruse, as are the experimental strategies. While the practical problem has stimulated consider-able research, the results are not usually effectively applied to system design until unacceptable oscillatory behavior is encountered in prototype or production systems. This tardy application of the available knowledge severely limits its utility because of the many commitments already made to design, and the high cost of making changes to control oscillatory behavior.

In the case of solid propellant rocket motors, the body of research is quite respectable, but poorly used because documentation of results is in the fragmentary form of several hundred research publications. In addition, the encounters with oscillatory combustion in development programs are so poorly documented that the seriousness of the problem is often underrated. The purpose of this text is to consolidate the research results and development program experiences in a manner that makes the results more accessible and more easily understood. The manner of presentation is designed to serve the needs of a wide spectrum of readers.

1.2 ELEMENTARY ASPECTS OF OSCILLATORY COMBUSTION

The normal function of a solid rocket motor is to produce a controlled flow of high pressure, high temperature gas and accelerate it through a nozzle, thus producing thrust. The source of the hot gas is a solid propellant charge, and generation of the gas is accomplished by combustion of the solid at its exposed surfaces. The pressure is maintained by a balance between the rate of formation of gas by combustion and the rate of discharge through the nozzle. The formation

r determined by high pressure, low mainstream flow velocity

r determined by lower pressure, high mainstream flow velocity

– – – Burning Surface of Propellant

Path of Gases Leaving the Burning Surface

Pressure

Velocity
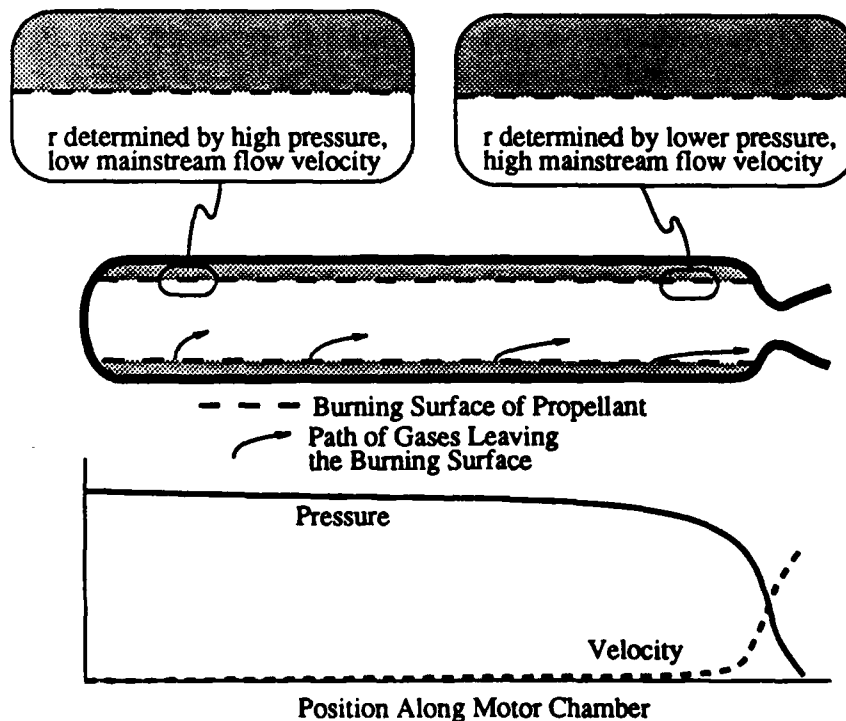
Position Along Motor Chamber

Fig. 1.1 Sketch of combustor, showing location of burning surface and orientation of gas flow (top), and variation of pressure and mean axial flow velocity with axial location (bottom).

rate depends on the area of exposed propellant, and the surface burning characteristics of the solid propellant. Prediction of mass rate is complicated by the fact that the propellant burning rate is dependent on pressure and other features of the gas flow environment. This complicates design somewhat, but is accommodated in conventional "internal ballistics" theory (Ref. 1.1-1.4). Such theory is based on steady state descriptions of combustor and nozzle flow, which are used as the basis for design of the propellant charge and nozzle. The dependence of the burning rate of each propellant (i.e., regression rate of the burning surface into the solid) on pressure and other variables is determined by separate "ballistic" tests, of which the simplest is the "strand burner" method (Ref. 1.5-1.7) for determining pressure dependence (it should be understood that any propellant is useful only if it has predictable burning rate, and that preparation procedures must be capable of making reproducible "batches"). Figure 1.1 shows a motor of very elementary configuration, in which the burning surface and gas flow are indicated, along with typical spatial distribution of pressure, velocity, and mass flow rates. Figure 1.2 shows some examples of experimentally determined burning rate over a range of pressure and propellant temperature.

The design procedures of internal ballistics do not take into account what would happen if there were a disturbance of the equilibrium between mass burning rate and nozzle discharge rate. The internal ballistics equations and laboratory burning rate measurements are based on steady state behavior. Those relations suggest (Fig. 1.3) that, if the pressure were for some reason off of equilibrium, the difference between mass burning rate and mass discharge rate would tend to cause the pressure to change toward the equilibrium value (indeed, a propellant with steady state burning rate characteristics that did not show this property would be useless for most rocket applications). The details of how a combustor would recover from an off-equilibrium state depend on many non-steady features of the system, the most obvious of which is the accumulation of gas in the combustor necessary for pressure change. However, a complete representation of response to disturbances must consider how the combustion, flow, and mechanical system respond to transient disturbances. For example, a transient disturbance of the steady flow can induce disturbances in combustion, which can produce reinforcing pressure disturbances. The usual internal ballistic equations do not contain transient terms, and the response of combustion to transient flow is not generally known, so prediction of response to disturbances is not forthcoming. But in practice we find that disturbances do occur, and sometimes grow to intolerable levels. As a result, there is a special branch of the applied science of internal ballistics concerned with transient behavior of combustion-flow systems. As one might guess, this special "transient" branch of internal ballistics involves much tougher science, and is in a much less complete state of development than steady state ballistics. Further, it is much more difficult for a novice to understand. However, its general features can be understood by anyone with modest training in physical science and the determination to read on here.
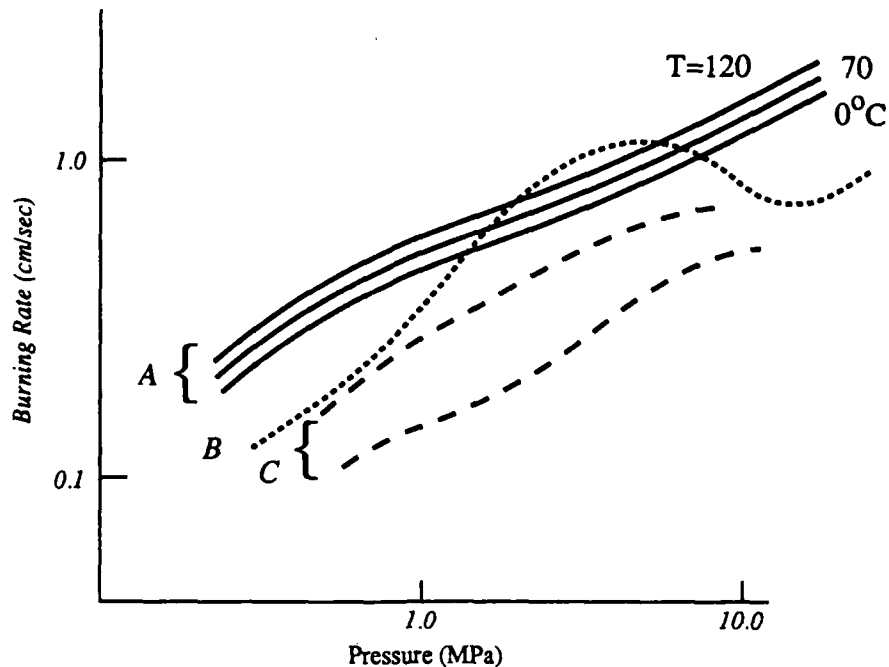
Fig. 1.2 - Burning Rate of propellant strands as measured in a constant-pressure "strand burner." Curves A indicate typical dependence on pressure at three different propellant temperatures. Curves B show the rate for a double base propellant with catalyst that produces enhanced rate at low pressures and a desirably low or negative dependence of rate on pressure at motor design presssure. Curves C show effect of oxidizer particle size on burning rate of an ammonium perchlorate-HTPB binder propellant.
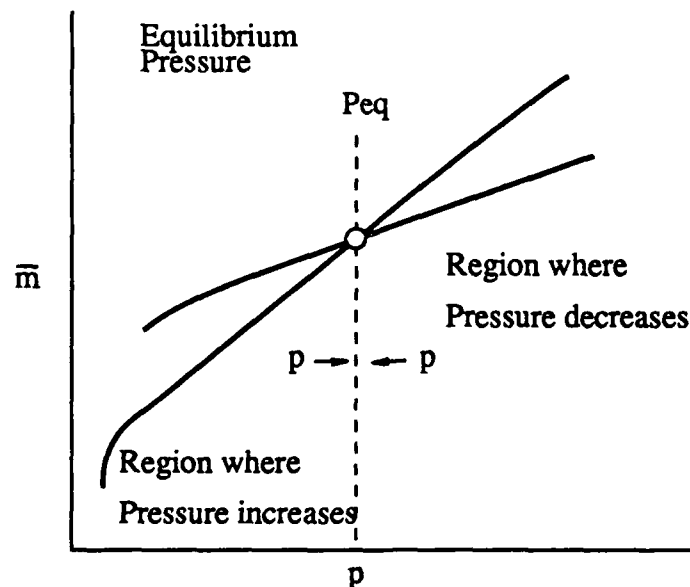
Fig. 1.3 Balance between mass burning rate and mass discharge rate to determine equilibrium pressure (pertains to a specific ratio of area of propellant burning surface to nozzle throat area. Peq is equilibrium pressure and other pressures represent off-equilibrium situations

When a local pressure disturbance occurs in the combustion chamber of the rocket motor, it propagates and is reflected repeatedly from walls and burning surfaces. In the process, the wave may strengthen due to interaction with combustion and mean flow in the cavity. Such repeatedly reflected waves tend to develop into discrete frequencies of oscillation characteristic of the cavity shape and size (Fig. 1.4). Under some conditions, such oscillations grow from minor disturbances present in any flow system. It often happens that some specific frequency of oscillation grows, a frequency corresponding to a specific mode of gas oscillation that is particularly suited to combustion "amplification".
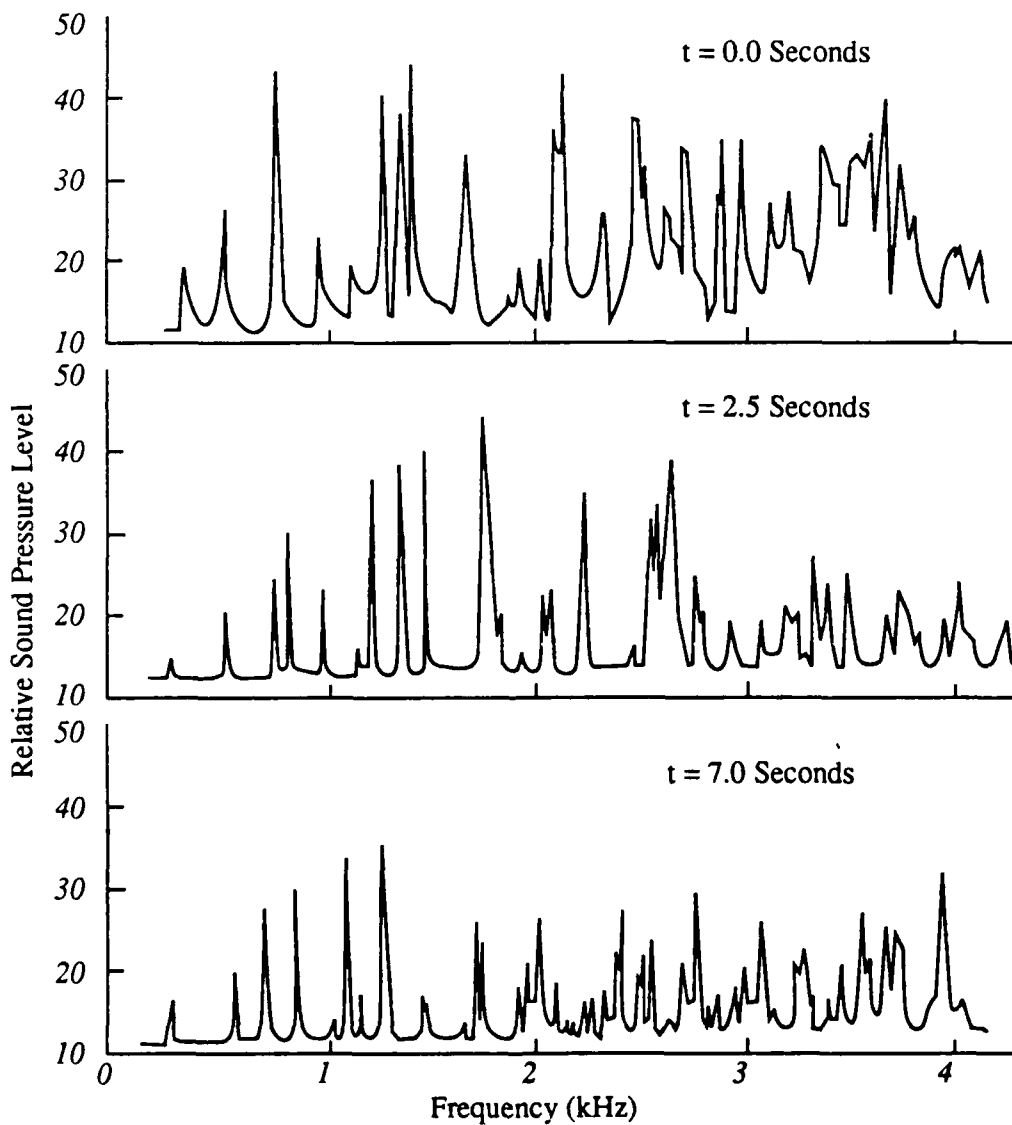
Fig. 1.4 Combustor sound level response to a variable frequency sound input

The above behavior is illustrated schematically in Fig. 1.5a by pressure at a particular point in the motor, which is typical of thousands of motor test records. Oscillations develop at a characteristic time during burning, grow to peak-to-peak amplitudes that are often much more than 10% of the mean pressure, and then die off at some later point in burning of the propellant charge. Such behavior is often accompanied by large increases in mean pressure, and by severe vibrations in the motor case and other parts of the flight vehicle. In such systems we have come to realize that a sort of dynamic instability exists for the motor during part of its burning period. Under those particular conditions, steady state operation is simply not a normal mode of behavior. Depending on the severity of oscillations, and the sensitivity of the flight vehicle to the oscillatory behavior, the motor may be unsuitable for use without modification of design or propellant. One of the most troublesome features of this instability behavior is its sensitivity to rather
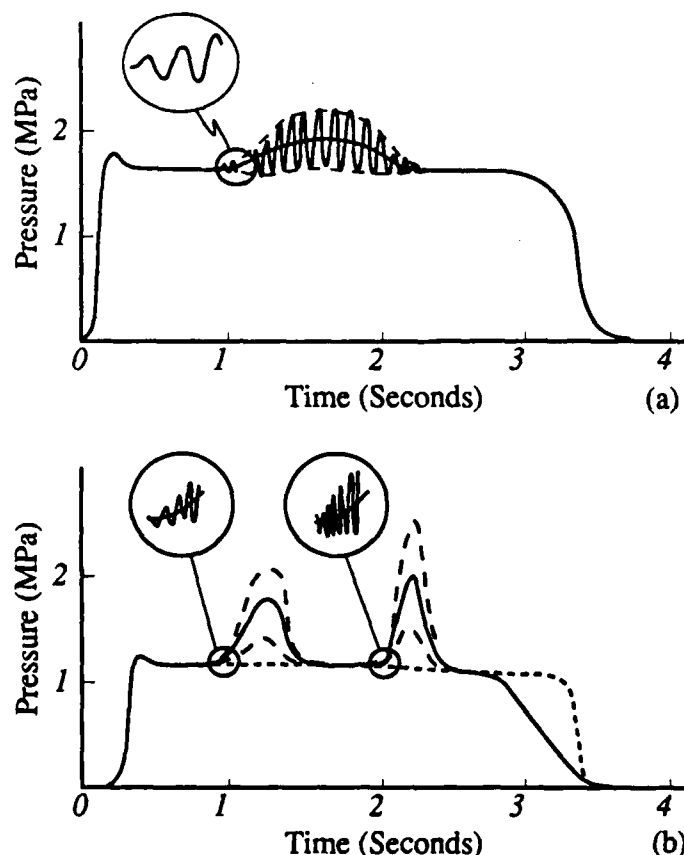
Fig. 1.5 Sketch illustrating spontaneous occurrence of oscillatory instability with associated increase in mean burning rate and pressure.

(a) The solid curve is the actual pressure; the broken line is the pressure to be expected in the absence of oscillatory combustion. The dotted curve is the pressure indicated by low frequency response instrumentation.

(b) Example of different modes of instability occurring at different (characteristic) times during a single test.

small changes in propellant, design, or operating conditions (pressure, temperature, etc.). This is illustrated by its appearance and disappearance in the way shown in Fig. 1.5b, where changes related to burning away of the propellant charge carry the system in and out of unstable domains. This property means that some motors that seem to be free of the problem are later found to be unstable at extreme operating temperatures, or exhibit instability in production motors because of some small change in charge geometry or propellant characteristics part way through production. Such encounters with combustion instability can be extraordinarily costly to a weapons system program, causing rejected production, disrupted supplies of weapons, and loss of confidence in the weapon system (Ref. 1.8).

Fortunately, the risk of such costly encounters with combustion instability in service-qualified systems can be reduced by careful consideration of the problem during development. There is a tendency to shortchange these precautions because of unawareness of the risk or appropriate precautionary measures, and because of complacency after two or three motor programs in which no instability problems showed up. But the track record does not justify complacency, as instability has exacted severe penalties in many development programs. Even a careful use of current knowledge cannot absolutely assure avoidance of instability, but timely use of that knowledge can provide information about risk and reduction of risk early in a program when costs are low. The failure to use that knowledge can be very costly.

1.3 A BRIEF HISTORY OF COMBUSTION INSTABILITY IN SOLID ROCKET MOTORS

To the non-specialist, a deeper insight into the full scope of the combustion instability problem can probably be gained from a historical review than from any other description of the problem. That context provides a framework in which the reader can identify with his own situation and see the interplay of many factors such as evolution of the scientific base; interplay of time and cost considerations with technical ones; interplay of propellant development, motor design and vehicle considerations; and the ever present problem of bringing the scientific base to bear on the problem at all relevant levels of system R and D.

The first encounters with combustion instability in solid rockets may have been in the pioneering work of Poole (Ref. 1.9) on internal burning cordite propellant charges in 1937. Performance of Poole's motors was reported to have been erratic, and there may have been a variety of causes. However, later experiences suggest that his combination of design and propellant would probably yield oscillatory combustion. There were no pressure measuring systems available then (or for the following ten years) that would show the presence of high frequency oscillations. Without such instrumentation, the excursions in mean burning rate (and corresponding excursions in mean pressure as in Fig. 1.5) that

are caused by the oscillations are not distinguishable from those caused by a variety of other problems encountered in early developments, problems such as break up of propellant charges, plugged nozzles, and non-reproducible propellant properties.

Around 1940, some clues began to emerge in work in the United Kingdom and soon after at California Institute of Technology in the U.S.A. (Ref. 1.10-1.12) that pointed the way to recognition of oscillatory combustion even though the oscillations could not be measured. Dry-extruded double base propellant charges that were ejected during nozzle release (due to over-pressure) were found to be heated in a way not attributable to any conductive means, suggesting dissipation of vibration energy in the solid (Ref. 1.10). Twenty years later, this absorption of oscillatory energy was measured concurrently with measured oscillations (Ref. 1.13), and proposed as a significant factor in damping oscillations (Ref. 1.14).

Another feature of propellant charges recovered after erratic burning was evidence of localized enhanced burning rate, particularly in the perforations of internal-external burning charges (Fig. 1.6). The internal conduit often showed rippled surfaces. Sometimes these charges were burst due to excessive pressure in the perforation (Ref. 1.4). These effects were believed to be due to some unidentified gas flow effect, and there was some evidence that burning returned to normal after fracture of the propellant tube. Charges were then tested in which holes were provided ahead of time to connect internal and external flow conduits (Fig. 1.7). It was found that the effectiveness of such web perforations depended on the *pattern* of the holes rather than their area, a result that led to speculation about the possible role of oscillatory flow. During the early '40s, many service rockets used internal-external burning solid double-base propellant charges stabilized by radial perforations, arranged in patterns determined by trial-and-error methods (Ref. 1.4). While the combined results suggested that oscillatory gas motion was involved in the erratic burning, no theory or measurements for oscillations were available until 1948.

While the studies with dry-extruded double base propellants were in progress at Cal Tech, oscillatory combustion was also suspected in testing by Hickman of solvent-extruded propellant charges using multiple tubular "grains" (Ref. 1.15). These "bundles" consisted of tubular grains that were small, and thin walled to provide large burning area and short burning time (suitable for certain Army applications). The grains were supported on an aft end grid plate, and erratic behavior was initially blamed on break up of the charges due to differential pressure, and high acceleration forces in flight tests. It was suggested that these problems would be minimized if a metal cage structure were used in which each "grain" of the propellant charge was strung on a support rod. This resulted in elimination of irregular behavior. Word of this result led the dry-extruded propellant team at Cal Tech to use a longitudinal rod in the perforation of their larger single charges. Test results showed similar stabilizing effects. Since the rod *reduced* the area of the interior duct of the charge, it was concluded that

Abnormally High Surface Regression
Near Midposition of Port

Burned Surface

Direction of Oscillations
During Burning
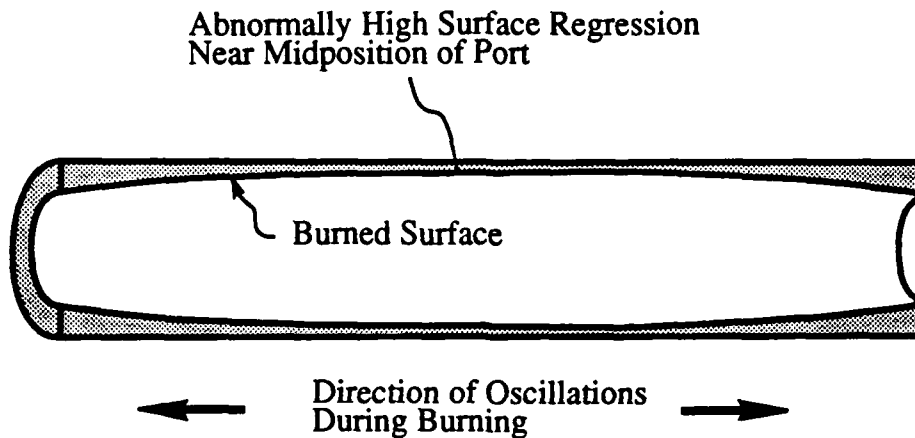
Fig. 1.6 Sketch of a cross section of a quenched internal-external burning propellant charge, showing evidence of local enhancement of burning rate (Ref. 1.4).
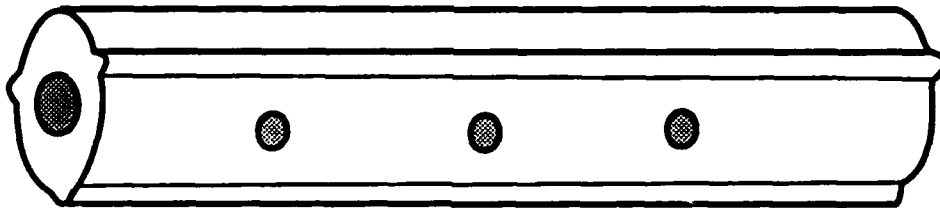
Fig. 1.7 Internal-External burning charge with radial holes to suppress instability in the inner conduit.

pressure excess in the perforation was not the primary cause of irregular burning, but rather that oscillatory burning caused the excess pressure. On the other hand, stabilization by rods seemed to be contrary to the then prevalent speculation that the oscillations were analogous to "organ pipe" modes, as a continuous circular rod offered only limited means to interfere with longitudinal oscillations. This result led to the speculation that the oscillations were in transverse "modes", i.e., the pressure waves were reflected back and forth crossways in the perforation (for the designs then in use, the frequency of such oscillations would be 20,000 Hz, which explains why they could not be measured).

The above reasoning was largely intuitive, as the investigators were not trained in acoustic theory. However, it was reasoned that a modification of the shape of the internal conduit of the propellant charge might have a stabilizing effect analogous to the effect of the axial rod. This reasoning was tested first by

cementing small longitudinal plastic ribs in the perforation, and then by extrusion of charges with propellant "ribs" (Ref. 1.4). Those methods were found to be completely successful in the charges tested, and provided the confidence needed for the important later transition to propellant charges with only internal burning surfaces (i.e., with external surfaces bonded to, or inhibited and close-fitted to the motor walls, Fig. 1.8). This transition in charge design (tried by Poole in 1937) was under active consideration in several laboratories in 1945-1946 (Allegany Ballistics Laboratory, Naval Weapons Center, and Jet Propulsion Laboratory (CIT)). It should be noted that however suspicious investigators were of the involvement of oscillatory behavior in the experiences with irregular combustion, no measurements of such oscillations were available; the evidence was all indirect and the result of speculative interpretation. Only in the case of a very low frequency form of instability then referred to as "chuffing" were there direct measurements of pseudo-periodic behavior (Ref. 1.16).
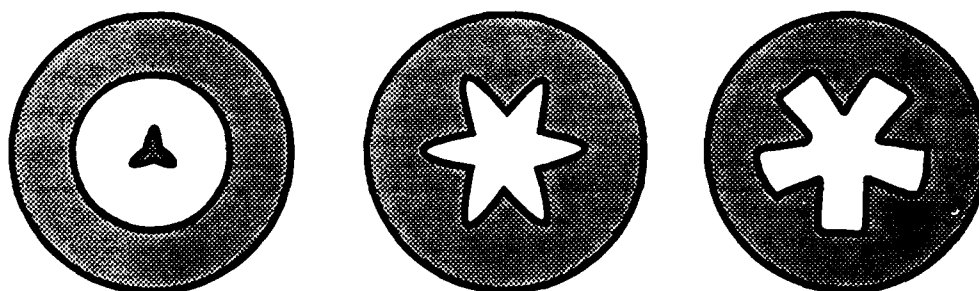
Fig. 1.8 Configurations of internal-burning charges that protect the motor case and have non-circular internal conduits that are relatively unsusceptible to transverse mode instabilities.

As of 1946 it seemed significant that the irregular burning we now associate with oscillatory instability was observed only with double base propellants and charges with internal burning conduits. Tests on composite propellants (mainly hydrocarbon fuel with potassium perchlorate oxidizers) did not exhibit such behavior, and later work using ammonium-nitrate oxidizer also was free of oscillatory instability. This early result was sustained in later years, indicating that combustion of some propellants is "inherently stable". At the time, it was widely thought that the problem was uniquely characteristic of propellants based on nitrocellulose and nitroglycerin. The error of this judgement became evident when more energetic composite propellants based on ammonium perchlorate were introduced in the period 1947-1950 (e.g., Ref. 1.17). By this time most new designs involved internal burning propellant charges, which are much more susceptible to combustion instability than the external burning charges used in several World War II weapons (Fig. 1.9).

Inhibitor - Support Strips
(Plastic)

Extruded "Cruciform" Charge
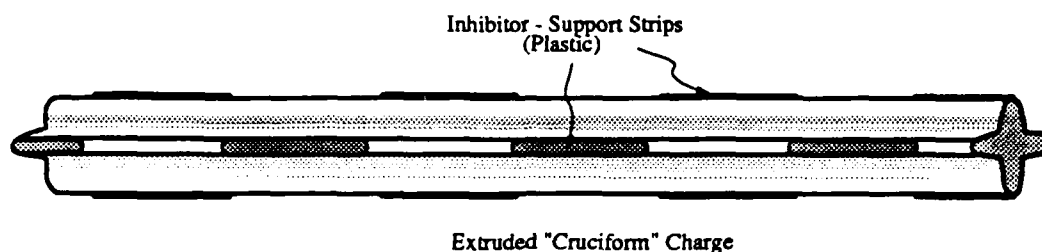
Fig. 1.9 External-burning charge typical of the 1943-1948 designs that were less prone to combustion instability.

By 1948, it was established conclusively that the irregular burning problem was linked to oscillatory gas motions in the combustion cavity. Although still difficult, it became possible to measure the pressure oscillations and to relate them to natural modes of oscillation of the combustor cavity. The first direct measurements were reported by Hunt, Anderson and Swanson at the U. S. Naval Weapons Center (NWC) (Ref. 1.18). A classic paper by Smith and Sprenger of Aerojet Corporation (Ref. 1.17) showed the trend in oscillatory behavior in a study of an AP composite propellant in a family of charge configurations. The first paper presenting an analytical model of solid rocket combustion instability theory was written by Grad at New York University, apparently in collaboration with McDonald, who worked at both NWC and NYU (Ref. 1.19). These works were the first to establish the concept of spontaneous growth of oscillations in natural acoustic modes of the combustion chamber, and to point out the distinction between the well established dependence of steady state burning rate on pressure and the dynamic combustion response under non-steady (oscillatory) conditions. This latter (dynamic response) concept was examined by several investigators in the 1950s (Ref. 1.20-1.22), but was not formalized in a realistic way until ten years later in 1959 with the classic work of Hart and McClure (Ref. 1.23).

During the period 1948-1958, combustion instability was a common problem in motor development programs. The encounters were substantially summarized by Price in 1961 (Ref. 1.24). No strategy of avoidance of the problem was evolved, partly because motor developers did not understand the problem, and partly because correction was not prohibitively expensive with the moderate size motors of the time. When instability was encountered, it was controlled by trial-and-error modifications of charge geometry, or introduction of "resonance" rods (Fig. 1.8) (Ref. 1.25) analogous to those discovered in the mid-'40s. Remedy was aided by measurement of the oscillation frequency, identification of the unstable mode of oscillation, and adoption of geometries that blocked the oscillatory motions of that mode (Fig. 1.10). This was not always simple because the remedial measures, often referred to as "black magic", were inexact, because the oscillation measurements were often lacking or poor, and because modified designs had to be qualified over a wide range of operational temperatures. Some

FIGURE IN PREPARATION

Fig. 1.10 Mode Shapes and Blocking Geometries

motors went into service with designs that consistently gave moderate oscillations that were either not recognized, or deemed to be tolerable. In some cases, this "residual" oscillatory behavior proved later to be quite intolerable due to unexpected interaction with guidance, control and fuse function in the all-up service systems. Such revelations later in the system development or after start of production can be very costly because of the necessity to go back and requalify a modified propulsion system, and because of the high cost of development and production delays. In some cases, restricted service limits were accepted (e.g., narrower operational temperature limits) in preference to accepting the costs of modification and requalification of the motor.

Obviously, the "easy out" from all these problems with oscillatory combustion would be to use a "stable" propellant, such as the potassium perchlorate or ammonium nitrate formulations. Unfortunately, these propellants had several undesirable characteristics, the most important of which was low specific impulse. No higher energy propellants have exhibited the consistent stability of these propellants. As understanding of the phenomenon has increased, it has become evident that susceptibility to instability is closely related to several of the more desirable propellant characteristics such as high energy, high burning rate, and low concentration of condensed reaction products ("lo-smoke" characteristics). Thus, nature offers no easy out for the instability problem, but instead demands continuing vigilance and compromise. This is nothing new in the high energy propellant and rocket motor business, which is constantly concerned with courting disaster in the quest for higher performance. However, propellant formulators are more directly motivated to recognize more direct hazards (e.g., susceptibility to unwanted ignition, detonation, or mechanical failure) than the vaguely understood possibility that their newest propellant might exhibit oscillatory combustion in a motor. In the 1950s there were no handy tests to rate the susceptibility of a propellant to oscillatory combustion (and even today it is a costly and inexact business).

In the late 1950s, powdered aluminum was introduced as a fuel ingredient in composite propellants. This modification offered more dense propellants and higher specific impulse. It also resulted in complete elimination of oscillatory combustion in the motors of that period. Aluminum looked like the "easy out", particularly at that time when the penalty of a smoky exhaust plume was deemed acceptable in exchange for higher performance. However, this was also the time when serious commitments were being made to development of much larger motors with the high energy propellants, and there was an uneasy feeling that the reprieve from instability problems brought about by introduction of aluminum powder might not apply to large motors.

In the U.S.A., a Defense Department Committee was set up to examine the risk of combustion instability in future programs. The risk was deemed to be particularly important for large motors because the cost of testing was so great that trial-and-error methods of correction would be very costly. After thorough review, the

committee (Sage, Ball and Avery, Ref. 1.26) warned that there was no basis for confidence that aluminized propellants would be stable in large motors, and that a better fundamental understanding should be sought to avoid costly problems in large-motor development programs. Even before that report was made, considerably expanded research was begun at the Naval Weapons Center under sponsorship of the Polaris program, and at other laboratories under U. S. AFOSR, ONR and Army support. As a result of the DoD study, the Advanced Research Projects Agency of the U. S. DoD established a further series of studies, including an assignment to F. T. McClure at Johns Hopkins University Applied Physics Lab to organize a technical panel for coordination of research and exchange of information. This was the beginning of an intensive effort to enhance information exchange and evaluation, which continues to the present as the Combustion Subcommittee of the Joint Army-Navy-NASA-Air Force Interagency Propulsion Committee.

During the 1956-1966 period, the magic of aluminum as a suppressant became better understood, as did its limitations. It was shown that the fine oxide smoke resulting from aluminum combustion acted very effectively to damp high frequency gas oscillations. Even a few percent of aluminum was often sufficient to yield stable combustion. However, the damping effect was small at the low oscillation frequencies of large rocket motors, and oscillatory behavior was encountered in several motor programs at frequencies in the 200-2000 Hz range (thus validating the concern expressed in the 1959 DoD committee report (Ref. 1.26). In addition, concern developed over three new trends in motor development. One was the thrust toward evaluation and use of technology for very large motors that would have natural combustor mode frequencies down to 10 Hz. Another was a return to low smoke propellants in many tactical applications as a means to frustrate countermeasures. The third trend was toward complicated charge and motor geometries, especially in upper stage and space motors. The risk of combustor instability in the large motors (such as the Titan IIIC and Space Transportation System ("Shuttle") boosters) was unknown, and the return to low smoke propellants in tactical missiles was guaranteed to bring instability troubles. The motors with complex interior geometries gave rise to complicated internal gas flow fields and interactions with combustion. These new developments, along with the problems with existing motors, led to increased pressure for procedures for *prediction* of motor stability as part of the design-proposal activity. We will return to this point shortly, but divert now to a related development case history that serves well to illustrate more clearly some of the vague generalizations in the foregoing regarding the compromise of missile systems by combustion instability.

In 1959, the U. S. Navy started development of a motor for a torpedo tube launched surface-to-surface weapon called Sub Roc. The motor used an ammonium perchlorate-polyurethane-aluminum propellant. No serious consideration was given to the possibility of combustion instability, primarily because aluminum had become accepted as an "easy out" cure for instability. The motor

involved considerable new hardware technology, which was evaluated first in static firing tests in 1/4 length motors for economy reasons. No problems were encountered with instability in these tests or later 1/2 length motor tests, or in several full length motor tests. Then an abrupt transition from steady burning to severe oscillations at 180 Hz occurred during one firing (Ref. 1.27). The oscillatory behavior (first axial mode) was accompanied by a 30% increase in mean pressure. After several stable firings, the instability was repeated. No special conditions could be linked to the unstable motors, except that oscillations started with a strong initial pulse. Such behavior had been observed in earlier research studies where nominally stable motors were found to develop growing oscillations when pulsed by firing of a powder charge into the motor (Ref. 1.28, 1.29). The sporadic nature of occurrences of instability in the Sub Roc program posed a serious problem, because it indicated that identification of a statistically reliable "fix" for the motor would require a large number of costly full scale motor tests. A panel of experts proposed a set of 19 possible fixes. It was recognized that some cause for spurious initiation of oscillations was present, and that the problem could possibly be solved by elimination of that cause. However, it was also considered to be desirable for the motor to be stable even when a pulse occurred. Ejection of parts of the spent igniter case was considered as a possible source of pulsing, and the igniter was modified to assure retention in the motor. Based on research studies of similar behavior at NWC (Ref. 1.28, 1.30), it was also proposed that a finer aluminum powder be used in the propellant. After these two changes were made, no further encounter with oscillatory behavior occurred. Comparison of the original and the modified propellants in the NWC laboratory burner showed the modified propellant to be more stable in the NWC burner (Fig. 1.11), even when the burner was pulsed (Ref. 1.30). It was not determined whether the change in aluminum particle size improved stability by increased damping (more favorable aluminum oxide droplet size) or by a less destabilizing response of combustion to flow disturbances. Whatever the mechanisms, this motor program dispelled the myth that aluminized propellants were inherently stable. It also introduced the development community to: a nonlinear (pulse initiated) form of instability that was under investigation by the research community; the nightmare statistics of a phenomenon that gave no symptoms in repeated tests and then appeared in catastrophic form; the need to avoid designs that allowed ejection of solid debris from the motor; and the complexity of scaling laws for combustion instability. These aspects of the instability problem were to be encountered in later programs, and became major aspects of research programs. It is worthy of note that the complex nonlinear interactions of the side-burning propellant charge with large amplitude axially oscillating flow in the combustor (as in the Sub Roc system) is a very complicated phenomenon that has only recently (in the 1980s) begun to receive rigorous modeling efforts. This case history illustrates another important lesson about dealing with the problems of combustion instability, one that is all-too-little recognized. The changes in the

FIGURE IN PREPARATION

Fig. 1.11 Comparison of pulsed instability of original and"stabilized" Subroc propellants in research burner.

Sub Roc propellant and igniter design that so quickly resolved the problem were proposed as a result of research sponsored at an entirely different laboratory by an entirely different development program (Polaris). This research was part of the expanded research motivated by the risk so well stated by the DoD Committee in 1959. The communication that led to timely transfer of the critical information to the Sub Roc program was due to the enhanced efforts at communication of current results. If this atmosphere of timely and vigorous collaboration had not existed, the Sub Roc program would have experienced major delays. In the last 20 years, this kind of collaboration among research and development teams regarding combustion instability has become commonplace, although poorly documented and sometimes absent. Since the administrative context provides few clear-cut incentives for such collaborative efforts (such as funding for special tests or travel expenses), its success is a testimonial to the dedication of the working level participants and the desire to bring current research to bear on practical problems. A development program in trouble rarely has, or will allocate, funds to meet the extra costs of outside participants. Further, the contributions of the outside participants are rarely acknowledged in any formal way.

Returning to the progress and problems in the early 1960s, some of the notable advances were:

a.   Some significant progress in basic understanding of propellant com-
     bustion was made, which was essential to realistic analytical modeling
     of dynamic combustion response. These advances included clarification
     of the self-deflagration process of ammonium perchlorate, combustion of
     aluminum, and surface features of burning composite propellants.
     Methods of combustion photography, interrupted burning, and microscopic
     analysis of quenched samples played important roles in these advances.
b.   Laboratory scale tests were developed for determination of the relative
     susceptibility of propellants to oscillatory combustion. The "T" burner,
     developed originally at NWC in the late 1950s (Ref. 1.31-1.33),
     evolved into several forms, and was used in around 20,000 tests in the
     1960s to show the trends of combustion response with frequency, mean
     pressure, and propellant variables.
c.   Several analytical models of the dynamic response of combustion to
     incident pressure disturbances were developed, which provided a much
     better understanding of how propellant combustion responds to flow
     disturbances (Ref. 1.34).
d.   More realistic analyses were made of the acoustic modes that occur in
     combustors, including the description of the effect of the mean flow
     field, nozzle, and coupled vibration of the propellant charge and motor
     case (Ref. 1.35-1.38).
e.   Advances were made in overall stability analyses (e.g., Ref. 1.39,
     1.40) and physical insight.

Progress in the 1960s and 1970s was intensively reported in the literature, particularly in the annual proceedings of the meetings of the U. S. Joint Army-Navy-NASA-Air Force Combustion Working Group, published by the Chemical Propulsion Information Agency. In addition to continuing improvement of basic experimental and analytical methods, attention was focused particularly on the emerging problems noted above (e.g., stability characteristics of new low-smoke propellants, stability of aluminized propellants in large motors, and stability of motors with complex geometrical features). A problem in a major operational system in 1969 led to intensified efforts to conduct analytical-computational evaluations of motor stability prior to final design and testing. Intensified research efforts also were stimulated by this operational system problem, illustrating the positive side of an unfortunate tendency for national efforts to peak and decline according to the severity of current operational problems with combustion instability. The system problem referred to above provides so much insight into the realities of "managing" the combustion instability problem that it is described in more detail in the following.

The case history of the Sub Roc system described previously illustrated the problem of nonlinear axial mode instability, in which a margin of stability exists that leads to stable tests until finite disturbances trigger severe instability. In that case history the problem was resolved by propellant changes *during the development program*. A rather different scenario was presented *during production* of the Minute Man Wing II Stage III motor (Ref. 1.41), with consequences so serious that the U. S. Air Force and its Rocket Propulsion Laboratory initiated a substantially enlarged program of combustion instability research to forestall recurrence of such program problems (Ref. 1.42).

The Stage III motor went into production with a recognized oscillatory instability that gave pressure oscillations with peak-to-peak amplitude of approximately 10% of mean pressure, with primary frequency of around 450 Hz. Production specifications set a limit on amplitude, and no problem was encountered with staying within this specification in quality control testing (the instability was surprisingly reproducible, and functioning of the missile system was not initially impaired). However, about halfway through the production program an undetected change in oscillatory behavior occurred, that later led to several flight failures. A review of test records showed that the predominant oscillatory frequency had changed from 450 Hz to 1250 Hz. The review traced the failure to a resonant vibration-induced failure of the thrust direction control system. Review of the production records linked the change in oscillatory behavior to a change in the supply source of the aluminum powder in the propellant. The powder met the usual specifications, but combustion studies on the propellant showed a substantial difference in combustion behavior of the "new" aluminum. While the exact mechanism responsible for the change in frequency of the oscillatory behavior was not determined, the most likely cause was a change in damping behavior of the aluminum oxide products of combustion. The modified

combustion led to a change in the size distribution of the product oxide droplets that was conducive to better damping at 450 Hz and less damping at the third axial mode frequency of 1250 Hz. At the time, methods for measuring the change in dynamic response of the combustion were only marginally adequate, so that the importance of this as a contributing effect in the change in instability was not evaluated.

After the link with aluminum sources was established, motors using the modified aluminum were recalled from service and a modification of the control system was made to prevent the vibration-induced failure.

This case history serves to illustrate several aspects of the combustion instability problem that deserve emphasis:

1. The total cost was very large because it emerged after the missile system was deployed.
2. The problem arose because of a change in a propellant ingredient supply that was not (and still is not) covered by quality specifications. *
3. The motor was qualified for production with recognized combustor instability, and the failures resulted from changes in stability that were not covered by quality acceptance criteria or recognized in routine acceptance firings.
4. The motor failures were due to a mechanical resonance with combustor frequency, indicating the importance of "hardening the bird" to combustor frequencies if combustor stability is not assured.
5. The technical capability to diagnose the cause of the flight failures and trace it back to the point of identifying the production motors that needed modification was made possible by the expanded research following the recommendations of the 1959 DoD Ad Hoc Committee. The enhanced support of the NASA starting in 1963 was also an important factor.
6. The episode led the U. S. Air Force to establish a substantial in-house capability in the area of combustor instability, and related contracted research programs, based at the Air Force Rocket Propulsion Laboratory.

---

* The change in the aluminum resulted from a switch by the supplier of the powdered aluminum fuel ingredient to delivery from a different production plant, because of a fire in the original plant. The "new" aluminum powder had a different oxide coating that changed combustion. Quality of oxide coating on the aluminum particle is not covered in quality acceptance specifications, although it has been shown to be important in subsequent combustion research studies.

1.4 PRACTICAL NATURE OF THE COMBUSTION INSTABILITY PROBLEM

From the case histories cited above, it is evident that it is not only difficult to consistently avoid combustion instability, but also to predict its effect on a flight system. From the practical viewpoint, the problem must be addressed at all levels of system planning, management and development. Somewhere along the way in every motor development program, the decision is made (overtly or by constraints due to other decisions) whether oscillating behavior will, or will not, be tolerated. If it is not to be tolerated, then there should be some assessment of risk made in choice of propellants, charge design and motor design; and test motors should be so instrumented that oscillatory behavior will be detected. Even if no evidence of oscillatory behavior is observed, the issue should be reassessed before commitment to final design, and production specifications should reflect safeguards against emergence of the problem due to subsequent propellant and design variations made by production engineers who are not familiar with the risk. These issues will be discussed in more detail in Chapter 3 (see also Ref. 1.43), but it is important to stress here that the longer the delay in consideration of combustion instability during a development program, the more costly and difficult will be the remedy should the problem arise. This is so because of the progression of commitments to propellant and design that get made, the increasing cost of getting diagnostic measurements, and the high cost of going back to change propellants and design that have in other respects been accepted as "qualified".

It is usually delay in consideration of combustion instability that leads to decisions to "live with it" when it is found in a propulsion system. When commitments of propellant, design, cost and time schedule are far advanced, it may seem wiser to "harden the bird" to vibrations and other instability induced effects. Given the unfortunate circumstances, this decision may be the best one to make at that time, but the risk needs to be fully understood. In complex flight systems it is not easy to anticipate all the ways that effects like combustion-induced vibrations can interfere with operation, and it may be very costly to qualify the system for safe operation in the adverse environment. Further, monitoring and controlling the adverse environment becomes a continuing production control problem that usually reverts to management by production personnel who have minimal knowledge of the problem. On the other hand, there are instances (usually involving simple flight systems) where motors having significant oscillatory behavior have gone into production and service without any adverse effects. The decision to live with unstable combustion, as illustrated by the Minuteman system described earlier, is a very serious decision (as is the situation that forces that decision). From the viewpoint of the system manager, it is important to bring "instability specialists" into the planning early, on the

principle that an ounce of prevention is worth more than "a pound of cure". The same "clinical" attitude applies to early detection, which can greatly simplify the cure. If the goals of the present text are achieved, the level of understanding all along the sequence of planning, development and production will be enhanced, the population of specialists will be enlarged, and exploitation of available knowledge will be made easier. For this book, that is the "practical" goal. There is also a more fundamental goal of aiding the specialist to come to grips with a vast and diverse body of knowledge that is otherwise poorly documented in primitive and fragmented form in original articles in archival journals and obscure reports.

Ultimately, one may hope that enough will be known about the complex coupled flow and combustion processes to permit advance design for stable operation. If that goal is achieved and sustained, it will be a result of future scientific advances, full utilization of existing knowledge, and timely availability and utilization of qualified specialists in the subject.

CHAPTER
TWO

COMBUSTION CHAMBER PROCESSES

The action of a resonator when under the influence of a source of sound in unison with itself is a point of considerable delicacy and importance, and one on which there has been a good deal of confusion among acoustical writers, the author not excepted.

J. W. S. Rayleigh, 1878

2.1 INTRODUCTION

In this chapter, the elementary concepts mentioned in Section 1.2 are described more fully and concisely so that the reader can be prepared for more technical and rigorous later description if needed. Should the later descriptions be overly complex for the needs of some readers, this chapter will provide the necessary background for a qualitative understanding of the physical and combustion processes and the technical language needed for persons who have to deal with instability as peripheral to their main concerns.

Before becoming immersed in a discussion of the details of combustor processes, it is appropriate to recall the primary objective of the rocket motor. It is a device designed for high capacity conversion of stored chemical energy into thermal energy and then into directed mechanical energy. The conversion from chemical to thermal energy is accomplished by high pressure combustion of the propellant, while the mechanical energy is acquired by acceleration of the high pressure gases down the pressure gradient in the combustion chamber and nozzle channel. The combustion and flow systems are mutually interactive and it is this interaction that gives rise to the possibility of oscillatory behavior. It is these contributing processes and their interaction that will be described in the following.

2.2 NATURE AND DIVERSITY OF COMBUSTION

A solid propellant is a body of chemically reactive ingredients, which is prepared by any of several processes. Its composition and physical structure are required to be uniform on a macroscopic scale. Many are highly heterogeneous on

a microscopic scale (< 1 mm) (Fig. 2.1). Propellants are generally very poor heat conductors. Therefore, they can be heated rapidly to a surface temperature that leads to chemical reaction and flame at the surface, while remaining cool a few mm below the surface. Heating the surface rapidly to start burning is called "ignition" and is done by auxiliary devices in the rocket motor called igniters. During the ignition phase of a motor, the flame is spread over the charge surface and the pressure increases under the combined influence of the igniter and the ignited propellant. Some surfaces of the propellant charge are protected from heating by bonding to a non-burning "inhibitor" or to the motor case (Fig. 2.2). If all goes well, when the igniter is fired the pressure in the combustor rises to the desired value at a time when the exposed surface is fully enflamed and the igniter is just ending its output.
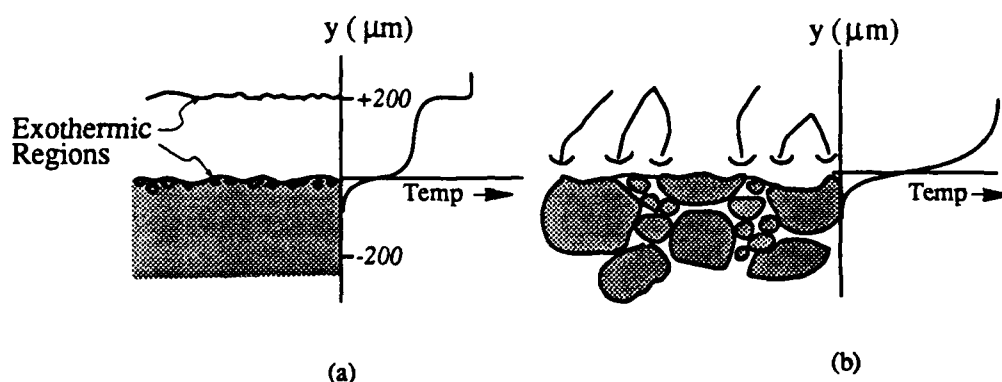
Fig. 2.1   Illustration of the propellant combustion zone and comparison of heterogenous and homogeneous propellants:
      (a) Homogeneous propellant, e.g., NC, NG, and
      (b) Compositie propellant, e.g., PBAN-AP.

At this point, the burning surface is moving inward into the solid at a velocity of order 10-2 m/sec. The vapors from the solid surface are around 600°C, and move away from the surface at roughly 1-10 m/sec. These vapors represent decomposition products of the propellant ingredients. Decomposition is usually (but not always) endothermal, with the heat for decomposition coming from energetic reactions in the vapor phase above the surface. The energy release is substantially complete in the vapor outflow within 1 mm of the solid surface. The details depend on the nature of the propellant and the environmental conditions (pressure, propellant initial temperature, influence of combustor flow conditions near the burning surface). Exothermic reactions may occur at more than one location in the · overall combustion layer, with those nearest the burning surface tending to influence burning surface regression rate most effectively because heat transfer to the surface is greater. Exothermic reactions sometimes occur in the burning surface and are particularly effective in determining the burning rate. Certain propellants are practically homogeneous (e.g., nitroglycerin-nitrocellulose pro-

pellants) and the combustion zone can be thought of as a sequence of reaction layers that may be viewed as successive planar flames (Fig. 2.1a). Other propellants are sufficiently heterogeneous so that the flame structure is affected by the need for lateral diffusion of vapor reactants so they can react with each other (Fig. 2.1b). Since diffusion occurs more rapidly when the scale of heterogeneity is small, the heat release is then closer to the surface and burning rate is higher. In analytical models, the geometrically complex nature of such combustion zones is generally modeled in a manner similar to the homogeneous propellants (i.e., a sequence of exothermic regions, planar flames). Then the position of each kind of flame is calculated as some kind of an average stand-off distance dependent on scale of heterogeneity (Fig. 2.1b).

- - - - - - - - - - Burning Surface
━━━━━━━━━━━ Inhibited Surface
━━━━━━━━━━━ Bonded to Case Liner
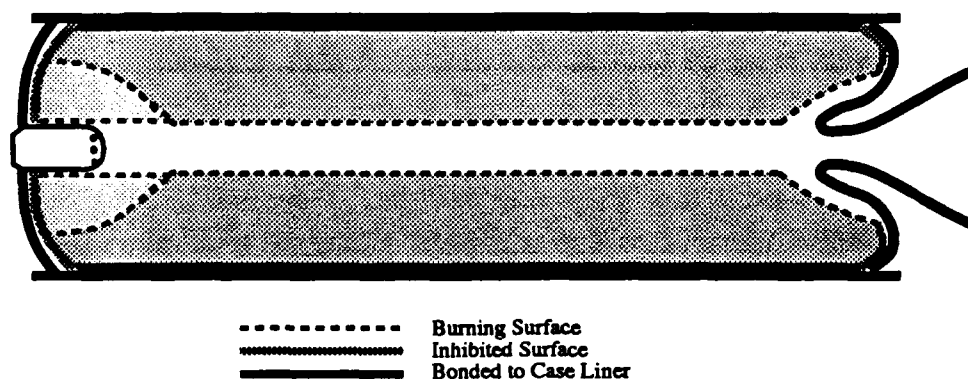
Fig. 2.2   Illustration of the arrangement of the ignitor and of exposed, inhibited, and bonded propellant surfaces.

We are concerned here with both steady and non-steady burning. For homogeneous propellants, "steady burning" means that the temperature profile in the combustion zone (and related composition profiles) remains invariant with time, and moves with the propellant surface as a wave of constant velocity into the propellant (the burning rate of the propellant). Although theory is good for understanding why some propellants have different burning rates than others, accurate data on burning rate is obtained from direct measurements on burning samples. Fig. 2.3 shows typical steady state burning rates for some homogeneous propellants, and shows how they depend on pressure and temperature. The steady state burning rate of an inhomogeneous propellant is defined only in terms of the rate of regression of an average surface, since the regression rate may vary from
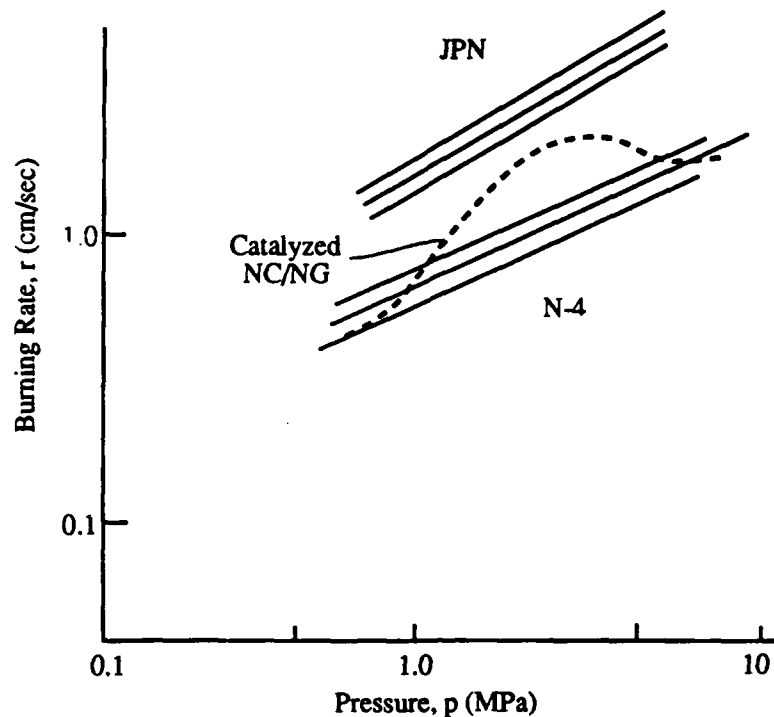
Fig. 2.3 Steady-state burning rates of homogeneous propellants.

place to place at any given moment (due to inhomogeneities). Fig. 2.4 shows a high magnification picture of a quenched surface of a composite propellant, from which it is evident that surface behavior is dependent on local composition and the associated flame complexes above the burning surface. While such propellants burn unevenly on the microscopic scale, the high burning rate sites are generally short-lived due to the disorder in the propellant microstructure. The surface remains flat on a macroscopic scale and the regression rate can be characterized in the same way as a homogeneous propellant when viewed on a distance scale larger than a few millimeters.

As one might suspect, propellants with low burning rate have relatively thick combustion zones and thermal waves in the solid, while high burning rate propellants have thin combustion zones and steep temperature gradients. High rates result from high pressure and/or temperature environments, fine particle sizes, high energy ingredients (high flame temperature), and use of catalysts that enhance near-surface exothermic reactions or move outer reactions closer to the surface. Some typical combustion zone dimensions are shown in Fig. 2.1. As a matter of perspective, it is helpful to note that the thickness of the steep part of the thermal wave in the solid is typically less than the diameter of oxidizer particles, and that an oxidizer particle is traversed by the burning surface in roughly 10^{-2} seconds (100 μm at 1 cm/sec).

Fig. 2.4   Burned surface of an AP-PBAN propellant quenched from 2.5 MPa
burning by rapid depressurization.

2.3 COMBUSTOR GAS FLOW FIELD

Under normal (steady) operation of an SRM, a reasonably steady pressure is
reached after ignition. In a simple interior geometry, gases leaving the lateral
burning surfaces of the propellant turn and flow toward the nozzle (Fig. 2.5a).
While this gas flow field changes during burn-away of the propellant at the cavity
walls, this change is slow compared to flow times in the combustor, so that
calculations of flow usually are based on steady flow theory. Because of the
increasing mass flow toward the nozzle end of the combustor, the velocity
increases with distance downstream from the forward end and there is a corre-
sponding drop off in pressure. The operating pressure is determined by a balance
between mass burning rate and mass discharge rate through the nozzle, $m_b = m_d$.
Calculation of equilibrium pressure thus requires determination of m_b by integra-
tion over the charge surface

$$m_b = \int_0^L \rho_p r \, dS_c = \int_0^L \rho_p r \, q \, dx \qquad (2.1)$$

where r is the burning rate of the propellant and S_c is the area of propellant charge burning area upstream of x. The rate, r, will vary with location (x) because the burning rate depends on pressure and other properties of the flow field. q is the perimeter of the burning surface at the station x, and ρ_p is the density of the solid propellant. For internal ballistic calculations, the flow field is usually calculated using a "one-dimensional" representation of the gas flow, implicit in the above equation (one-dimensional steady flow with mass addition (Ref. 2.1, 2.2)). However, a more rigorous analysis may be required for motors with very complicated interior geometry. Although rather approximate, the simple flow analyses seem to describe the features most important for predicting steady state motor performance. An example of the dependence of flow variables on axial location is shown in Fig. 2.5b.
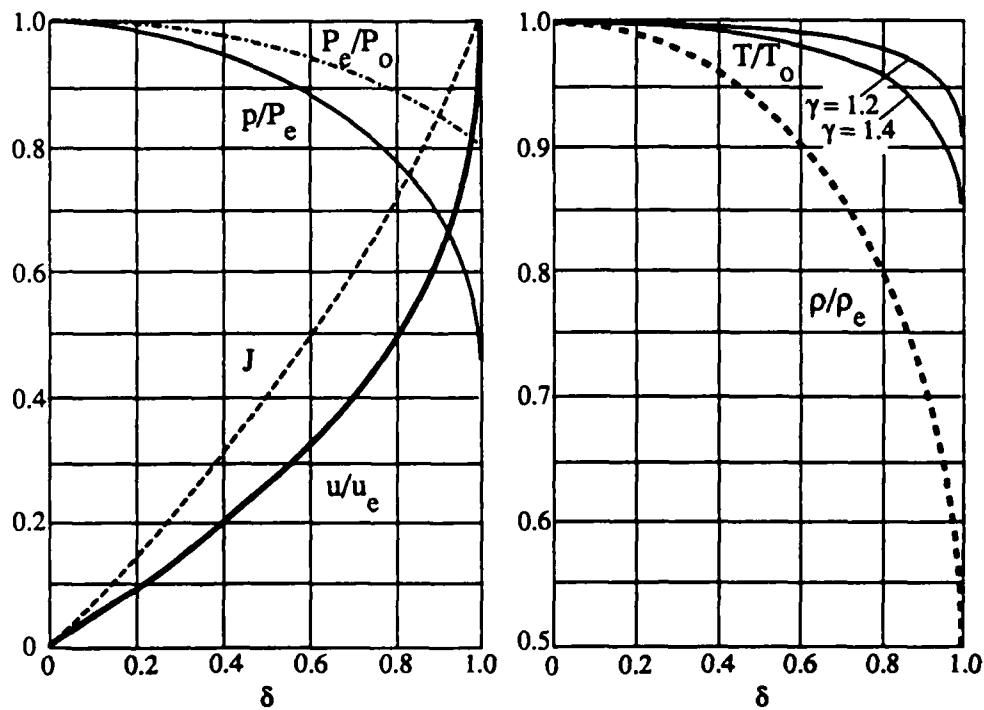
Fig. 2.5   Solution of the steady 1-D mass addition flow problem for geometries of uniform conduit cross-sectional area (from Ref. 2.1).

2.4 OSCILLATIONS

The most conspicuous aspect of combustor instability is the presence of periodic oscillations in pressure, which are accompanied by less easily measured oscillations in other variables of state of the gas (temperature, density, etc). In the simplest cases, these oscillations are the same (or nearly so) over the entire combustor volume, a behavior that is possible only at low frequencies of oscillation and ordinarily experienced only in low L* motors. At higher frequencies, the oscillations involve surging motions of the gas, with pressures in one part of the combustor peaking when the surging gas has come to rest at that location, and peaking later "at the other side of the cavity" when the surging motion has come to rest there. One can picture the moving gas as having momentum that produces a compression of the gas when the motion approaches a cavity wall. The resulting compression stops the motion and then sets the gas in motion in the opposite direction. This sets the stage for a compression on the opposite wall of the cavity. This is most easily visualized by the gas motions in a straight pipe with closed ends (Fig. 2.6). The surging motion is in the longitudinal direction of the pipe, and the frequency of oscillation is given by

$$f = \frac{n\,a}{2L}$$

where L is the length of the pipe, a is the velocity of sound in the gas, and 2L/a is the time for a pressure disturbance to travel the length of the tube and back. The

a) First Standing Mode   b) Second Standing Mode
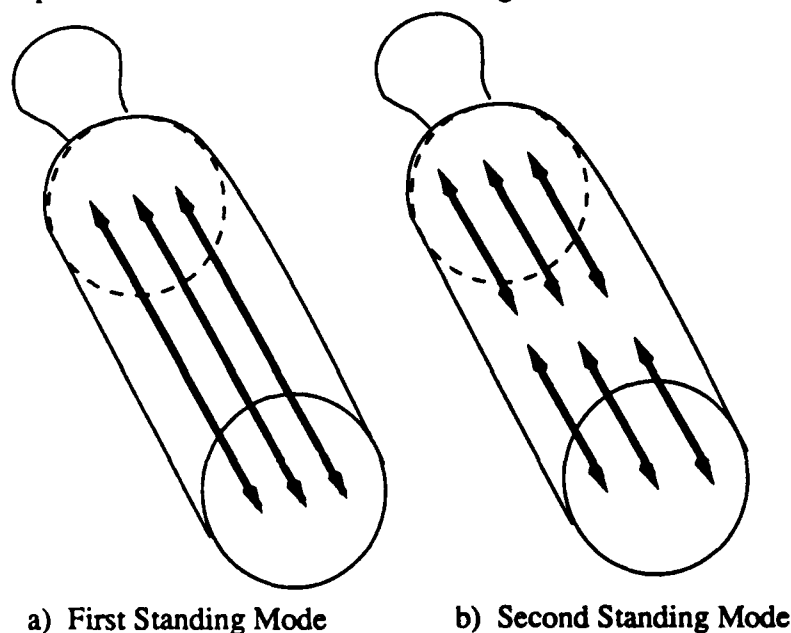
Fig. 2.6   Gas motion during longitudinal oscillations in a simple cavit geometry.

factor n is an integer and indicates the possibility that gas may be set in motion in different directions in different parts of the cavity at the same time. This is illustrated in Fig. 2.6b, which shows the motions for n = 2. In this case, the timing of the oscillation in the two halves of the cavity is such that the surging gases in the opposite halves of the column approach the midpoint of the cavity at the same time and "bounce off each other" much as if there were a wall there. Thus, in this "second mode", the pressure disturbance in each half makes a round trip of a half length of the column in a time 2(L/2)/a, with a frequency a/L. In the language of acoustics, this is the "second longitudinal mode" of the cavity and n is the mode number. It is not difficult to visualize that other modes with n > 2 can occur, or that similar oscillatory motions can occur in the crossways direction in the tube (transverse modes).

In practice, oscillations can occur in more than one mode at a time and change during burning of the propellant charge as the geometry of the cavity changes. This is illustrated in Fig. 2.7, which is a "modal" analysis of the oscillations in an actual motor, showing the amplitude and frequency vs time of various modes. The lowest frequency is the first longitudinal mode and the frequency remains constant because L doesn't change during burning. The high frequency corresponds to a transverse oscillation and the frequency decreases as burning progresses because

Fig. 2.7   Modal analysis "waterfall" of pressure oscillations during an unstable test firing.

the transverse cavity dimensions increase as burning progresses. The display of oscillation frequency and amplitude vs time for an oscillating motor (as in Fig. 2.7) is often called a "waterfall diagram".

The surging motions described above correspond to a special class of oscillatory behavior referred to as "standing acoustic modes". These relatively simple modes are the ones most commonly seen in motors and are often sufficient for qualitative description of more complex behavior. One 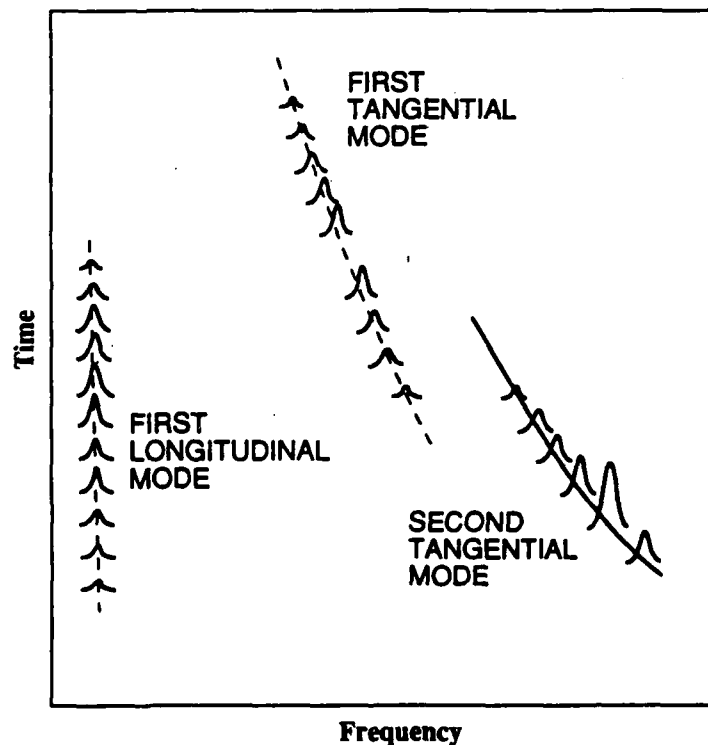further important insight that should be gained from the standing modes is the concept of "mode structure". This relates to the spatial distribution of the oscillatory behavior. Pressure oscillations in a first axial mode may be severe at the ends of the cavity, while there will be no oscillations at all midway between the ends. This is illustrated in Fig. 2.8, which shows the distribution of pressure amplitude with longitudinal position for three longitudinal modes. The locations of maximum amplitude are called "antinodes" and the locations of zero amplitude are called "nodes". Evidently one would not detect the presence of an oscillation with a pressure detector located at a nodal point. With longitudinal modes this is not usually a problem, because the pressure transducer is located on the forward cavity wall where pressure amplitude is a maximum. It is much more difficult to get a transducer at an antinode of a transverse mode (and be assured that the antinode doesn't wander away) (Fig. 2.9).

Relative to combustor instability problems, it should be noted that the acoustic mode structure determines the nature of the oscillatory environment at different locations of the burning surface. For a particular acoustic mode, some regions of the surface will be exposed to strong pressure oscillations, but relatively little oscillatory motion of the adjoining gas field (regions near pressure antinodes). At the same time at other locations on the burning surface (near pressure nodes) there will be relatively little pressure oscillation, but the gas oscillations parallel to the burning surface may be large (the pressure mode is a velocity antinode, as shown in Fig. 2.8). In solving stability problems, it is necessary to examine the response of combustion at each site on the burning surface to its own particular oscillatory flow environment, and the response at all the sites must be combined to determine the net effect of combustion on a given mode of oscillation. The procedures for this are described in Chapter 8. In Chapter 4, the nature of the combustion response to oscillations in the flow environment is described in a relatively elementary way, with more complete description in Chapter 5.

2.5 DYNAMIC COMBUSTION RESPONSE

When a quantity of solid propellant expands during conversion to gaseous combustion products in the combustion zone, it does work on the gas already in the combustor, causing the motion of the gas toward and out of the nozzle. Under normal conditions, this is a continuous process. A disturbance in gas evolution rate means a fluctuation in the rate of work on the gas field, which leads to a
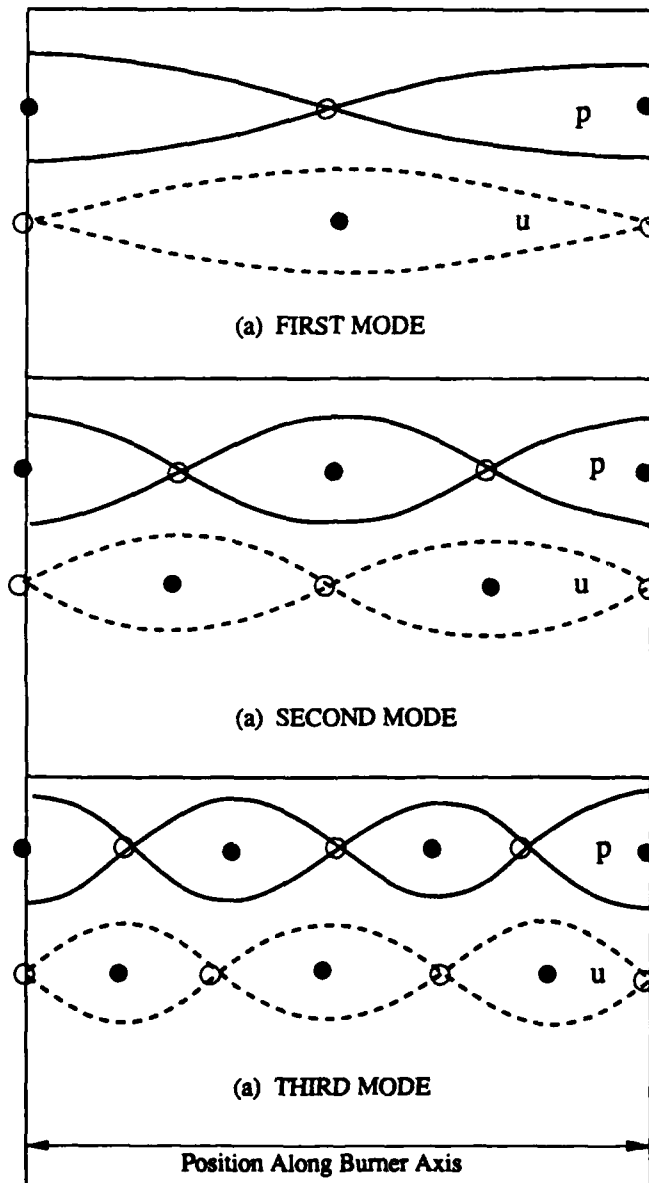
Fig. 2.8 Amplitude of oscillation vs location in the cavity for longitudinal
mode oscillations (a cylindrical cavity with closed ends is assumed in the
figure, and is a reasonable approximation for motors of simple geometry and
length to diameter ratio greater than 3 or 4). Open circles mark nodes at which
amplitude is zero; black circles are antinodes marking points of maximum
amplitude. p denotes the pressure distribution; u represents the particle velocity.

Fig. 2.9   Distribution of pressure and velocity amplitude for some transverse modes of a circular cylinder (curves of constant amplitude are shown).

disturbance having a definite disturbance of energy in the gas motion from the location of the combustion disturbance. Such a disturbance is typically manifested by a pressure wave emanating from the site of the combustion disturbance. The combustion zone over the entire burning surface is exposed to these propagating flow disturbances, and the combustion rate can be disturbed over a large part of the burning surface when flow disturbances are present. In short, a flow disturbance can stimulate a combustion disturbance, which can reinforce the flow disturbances. This is called the "dynamic combustion response", and is the heart of the combustion instability problem. Understanding the practical problem requires that one know the nature of the flow disturbances that occur in the region of the combustor where concentrated reaction occurs (usually near the propellant surface), and also know how the combustion responds to these flow disturbances. Aside from a general comment on the nature of the combustion-flow interaction, the following will explain the phenomenon by an example involving relatively simple interaction. The general comment is a three-part one: 1) the flow disturbances can be very complex and can be dependent on location in the combustor,

2) the combustion response is very complex and dependent on the nature of the local flow disturbance, and 3) the state of knowledge of both the flow disturbance field and the combustion response is still rather primitive. Understanding is somewhat better for the special case of combustion response to pressure waves that are perpendicularly incident on the combustion zone, and that special case will be used here to describe concepts of dynamic combustion response.

If one views the combustion zone and flow field as one-dimensional, with a well-defined outer boundary (Fig. 2.10), then the work done by the combustion zone on a perpendicularly incident pressure wave that is produced by a cavity oscillation is commonly related in acoustic theory to the ratio of the oscillation of velocity outward from the combustion zone to the oscillation in pressure experienced by the combustion zone.

$$A_b \equiv \gamma \frac{u'/\bar{a}}{p'/\bar{p}} \qquad (2.2)$$

p' is the oscillation in pressure about its mean value $\bar{p}$, and u' is the oscillation in velocity about its mean value $\bar{u}$. The ratio of specific heats, γ, is included in the definition of A_b in "anticipation" of convenience in later analyses. A_b is referred to as the specific acoustic admittance of the combustion zone. In the classical

HOMOGENEOUS SOLID   **FLAME**   **GAS MOTION PERPENDICULAR TO SURFACE**   **MEAN FLOW**

Fig. 2.10   Combustion Flow interaction for a one-dimensional system.
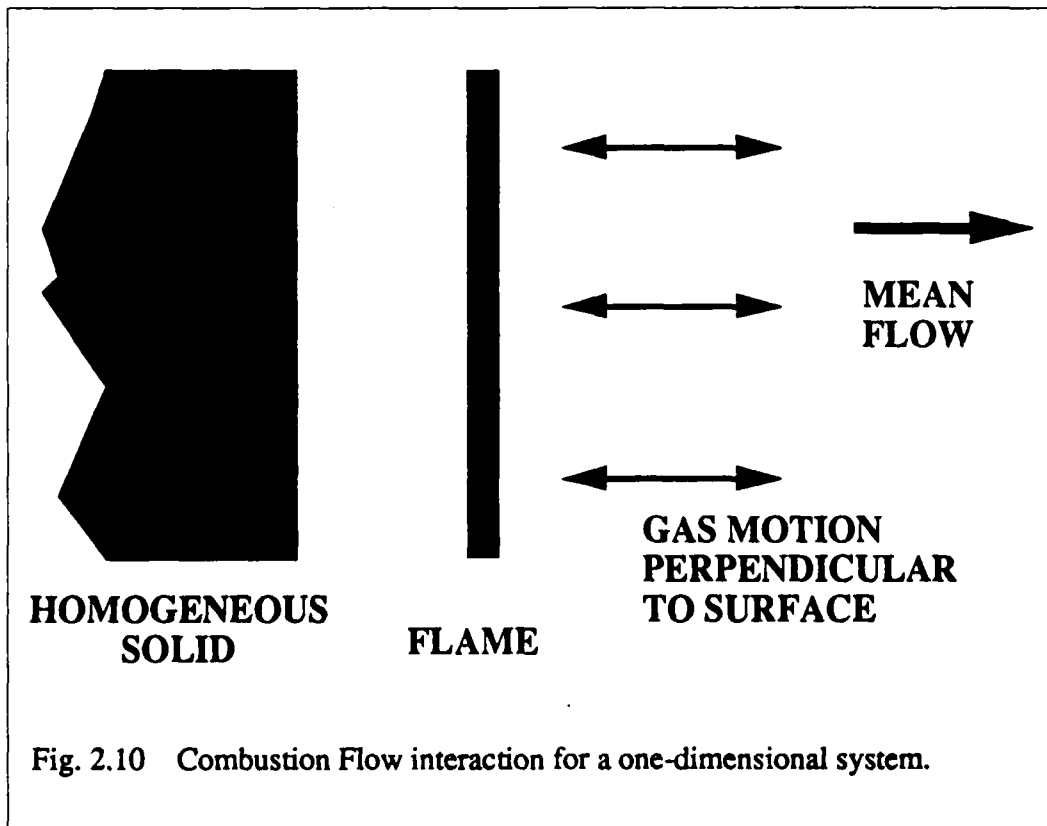
acoustic analyses of combustor stability, the admittance is a boundary condition for solution of the equations for the cavity oscillations. For the present purposes, we are looking at the region on the combustion zone side of the admittance surface, and it is desirable to relate A_b to other properties of the oscillating combustion zone. By expressing the mass conservation equation in small perturbation form,

$$m = \rho u = (\bar{\rho} + \rho')(\bar{u} + u') = \bar{m} + m'$$ (2.3)

where ρ', u' and m' are small oscillations about the mean values $\bar{\rho}$, $\bar{u}$, and $\bar{m}$. The perturbation terms must (to first order of approximation) satisfy the equation

$$\frac{m'}{\bar{m}} = \frac{\rho'}{\bar{\rho}} + \frac{u'}{\bar{u}} = \frac{\rho'}{\bar{\rho}} + \frac{u'}{\bar{a}} \frac{1}{M_b}$$ (2.4)

(all variables will be used here as referring to conditions at the outside edge of the combustion zone, with velocities perpendicular to the surface; M_b is the mean Mach number there)   If a mass response function, R_p, is defined as

$$R_p = \gamma \frac{(m'/\bar{m})}{(p'/\bar{p})}$$ (2.5)

then Eq. 2.2, 2.4 and 2.5 can be combined to give the admittance function

$$A_b = R_p - \frac{(\rho'/\bar{\rho})}{(p'/\bar{p})}$$ (2.6)

and if a perfect gas law $p = \rho R T/\mu$ is assumed, this can be written

$$A_b = R_p + \frac{(T'/\bar{T})}{(p'/\bar{p})} - \frac{(\mu'/\bar{\mu})}{(p'/\bar{p})} - 1$$ (2.7)

where T' is the temperature oscillation at the "admittance" surface, and μ' is the oscillation in molecular weight.

This expression gives some idea of what must be known in order to connect the response of the combustion zone to an incident pressure oscillation, p'. Keep in mind that p', T', μ', and R_p (the relative oscillation in mass rate) are oscillating quantities that do not necessarily oscillate in phase with each other. Since it has thus far been extremely difficult to measure R_p, T', or μ' oscillations, A_b is usually determined by either analytical modeling of the dynamic response of the combustion zone for R_p, $T'/\bar{T}$, and $\mu'/\bar{\mu}$ or by experimental estimate of A_b from its effect on combustor pressure oscillations. The problem of analytical modeling is discussed in Chapter 5, and the experimental methods for measuring A_b involving combustor oscillation are discussed in Chapter 11. Also mentioned there are some relatively recent efforts to measure the oscillations u' directly.

Looking further at Eq. 2.7, it is usually assumed that the term $(T'/T)/(p'/\bar{p})$ is divided into two parts

$$\frac{(T'/T)}{(p'/\bar{p})} = \frac{\gamma - 1}{\gamma} + \frac{(\Delta T'/T)}{(p'/\bar{p})} \tag{2.8}$$

where $(\gamma-1)/\gamma$ is a portion of the oscillation corresponding to isentropic relations of T to p and

$$\frac{(\Delta T'/\bar{T})}{(p'/\bar{p})}$$

is the part of the real oscillation different from the isentropic part. Then Eq. 2.7 becomes

$$A_b = R_p - \frac{1}{\gamma} + \frac{(\Delta T'/\bar{T})}{(p'/\bar{p})} - \frac{(\mu'/\bar{\mu})}{(p'/\bar{p})} \tag{2.9}$$

The terms involving $\Delta T'$ and μ' are not usually rigorously modeled in analyses (μ' is usually neglected without acknowledgment), and different models give different results. However, R_p is ordinarily the dominant term, and is the object of many analytical models (Ref. 2.2-2.4). Examples of such results are shown in Fig. 2.11, where R_p is shown as a function of frequency for different values of two principal parameters in the model.

In Fig. 2.11, the two parts of the figure show the "real" and "imaginary" parts of R_p, a terminology that reflects the fact that complex variables were used to represent the oscillating quantities. The real part corresponds to the magnitude of the component of the mass oscillation that is in phase with pressure, and the imaginary part indicates the magnitude of the component 90 out of phase with pressure. Stability analyses show that in most situations the component in phase with pressure is the part responsible for driving of the oscillation (See Chapter 8).

Looking at Fig. 2.11, the abscissa is a non-dimensional frequency

$$\Omega \equiv \frac{\alpha \omega}{\bar{r}^2} = \left(\frac{2\pi\alpha}{\bar{r}^2}\right) f \tag{2.10}$$

where $\alpha/\bar{r}^2$ is the thermal diffusivity of the solid propellant divided by the square of the mean burning rate of the propellant ($2\pi\alpha/\bar{r}^2$ is typically of order 10^{-2} sec). In Fig. 2.11a, the value of $R_p^{(r)}$ increases with frequency to a maximum around 1000 Hz and drops off at higher frequency. The parameters A and B have physical meaning in the analytical models (e.g., A is related to the activation energy of the surface decomposition reaction), but the values cannot be determined unambiguously, and are usually chosen to yield the best fit with experimentally determined values of $R_p^{(r)}$, as illustrated in Fig. 2.12. The primary value of analytical models
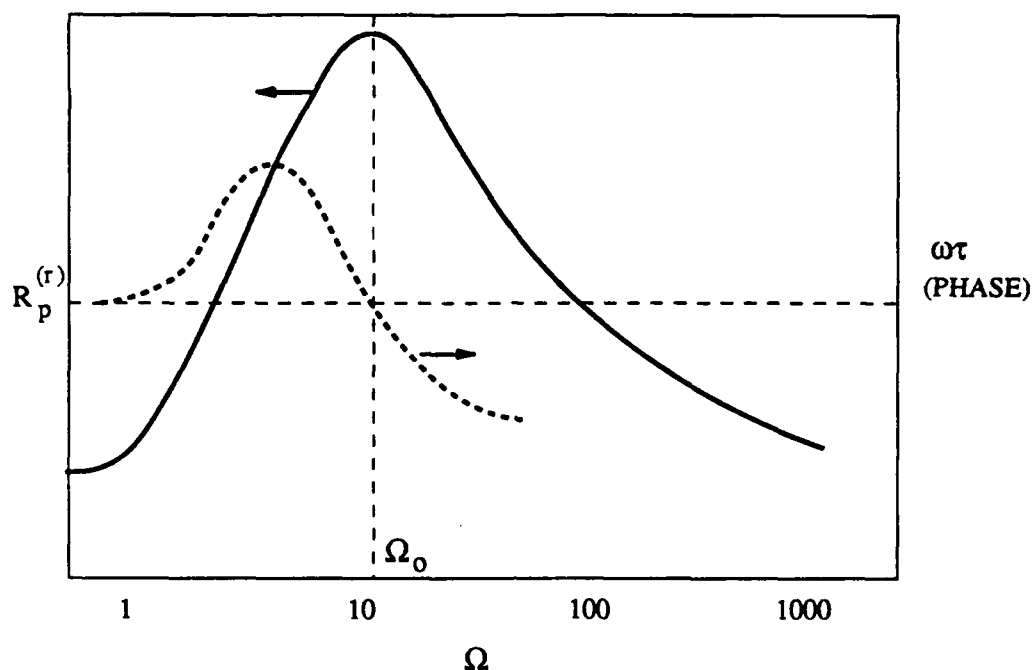
Fig. 2.11   Dependence of pressure-coupled response R on nondimensional
frequency and modal parameters A and B (See Ref. 2.2).

has been to a) better understand dynamic combustion response, b) provide an
extrapolation formula for experimental data, and c) help in understanding scaling
laws (taking into consideration also that frequency is inversely proportional to
dimensions). From the form of the response function curves, it is evident that there
is a frequency range in which stability is more likely in the sense that $R_p^{(r)}$ and
hence, A_b and acoustic driving tend to be large. The figures also show that the
frequency range in question is strongly dependent on mean burning rate through
the dependence of Ω on $\bar{r}$. As will be seen in Chapter 5, analytical modeling of
combustion response is still under development, with limited capability to encom-
pass the wide range of propellant behavior encountered in practice. The measured
response function trends are found to be dependent on propellant variables and
flow environment variables whose roles are not encompassed in the models.
These are areas of ongoing research, and there is much more information available
than implied above. However, the elementary analyses serve the present purpose
of illustrating the manner in which combustion responds to flow disturbances and
amplifies these disturbances. In the next section, the consequence of this behavior
is examined in the context of the combustor environment.

2.6 COMBUSTOR STABILITY

In the preceding sections the nature of the oscillatory motions of the gas in the combustor cavity has been described in a qualitative way, and the concept of responsiveness of the combustion to the flow disturbances has been introduced. Since disturbed combustion can produce flow disturbances and flow disturbances can cause combustion disturbances, one may anticipate that the combined disturbances might, under some conditions, reinforce each other and produce growing disturbances. The particular conditions are those under which the combustion-generated flow disturbances are suitably phased to reinforce the initiating flow disturbances, and the sources of damping of flow disturbances are not too high. Because of multiple reflections of pressure waves, the disturbances are ordinarily periodic and tend to occur in the less heavily damped natural cavity modes (whichever ones are more strongly reinforced by combustion response and less heavily damped by viscous and radiative loss of oscillatory energy). When the combustion reinforcement of a particular mode is stronger than the damping of the oscillation, the oscillations will grow with time, and the mode is said to be unstable. As the amplitude of oscillation increases, the combustion reinforcement
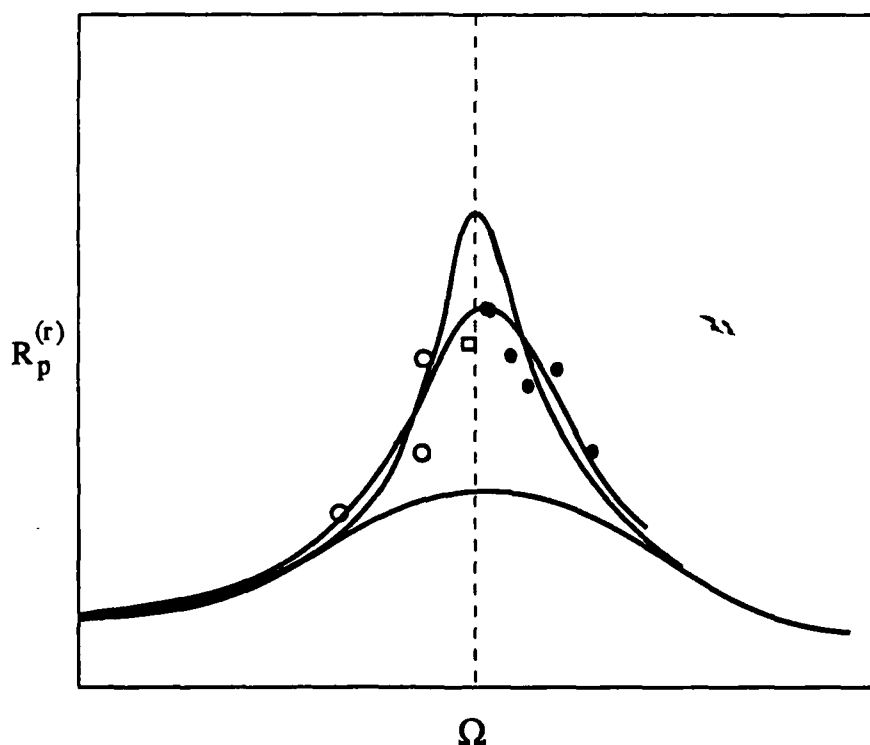
Fig. 2.12 Comparison of experimentally determined values of R with theoretical curves.

increases as does the damping. In the usual case, the excess of combustion reinforcement over damping grows with amplitude, so the amplitude increases at an increasing rate (Fig. 2.13) and very large amplitudes can be reached.

To understand unstable behavior better, it is helpful to describe the behavior in terms of energy in the oscillation of a mode of interest. Addressing a specific geometry and mean flow situation corresponding to a particular time during burning of the propellant charge, the oscillatory motion of a specific mode at a specific amplitude can be characterized by a specific energy of the oscillation, E. The combustion response to the oscillation contributes energy to the oscillations at a rate designated by $\dot{E}_c$, and damping processes dissipate energy at a rate $\dot{E}_d$ where

$$\dot{E}_c + \dot{E}_d = \frac{dE}{dt} \qquad (2.11)$$

For the sake of description, assume for the moment that E may have any value (which would depend on previous conditions), and consider how $\dot{E}_c$ and $\dot{E}_d$ would depend on E. At moderate amplitudes of oscillation (as indicated by the value of E), $\dot{E}_c$ and $\dot{E}_d$ are typically proportional to E, so that $\dot{E}_c$ and $\dot{E}_d$ vs E are typified by the straight lines in Fig. 2.14 (this corresponds to a response function independent of amplitude, and similar linear dependence of damping forces on amplitude). In the illustration in this figure, $\dot{E}_c$ is shown as larger than $\dot{E}_d$, which means that (since $\dot{E}_d$ is negative) dE/dt > 0, i.e., the oscillations are growing as in Fig. 2.13. Further, dE/dt is larger for large E, corresponding to more rapid growth of oscillations at large amplitude.
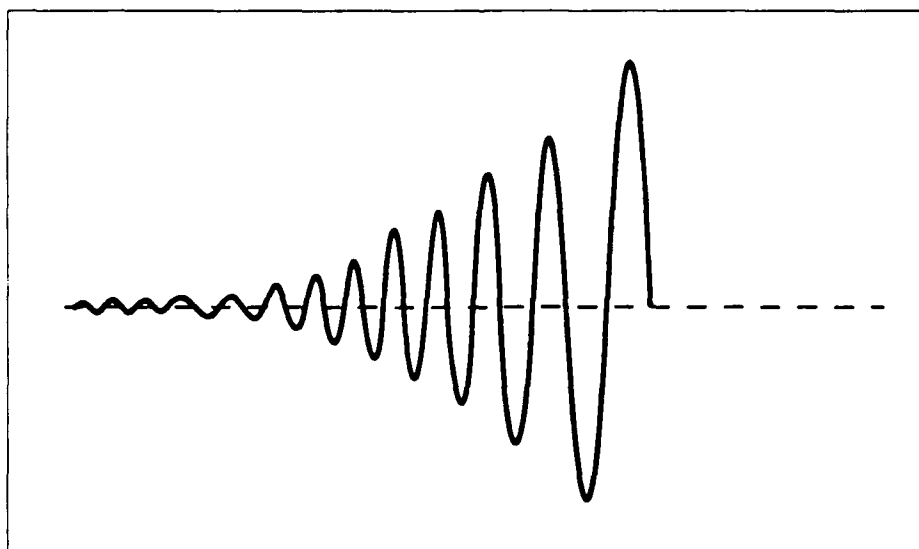
Fig. 2.13   Example of divergent oscillations due to excess of combustion reinforcement over damping.
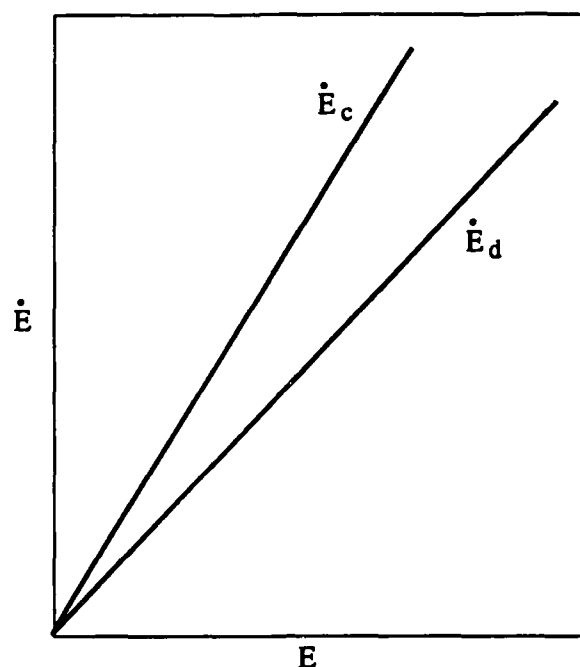
Fig. 2.14 Illustration of stability argument by comparison of combustion energy gains and energy losses to flow oscillations (the ordinate is oscillation energy change per second, shown as a function of oscillation energy level). Example is for linear system; with $\dot{E}_c > - \dot{E}_d$, unstable.

Under different conditions the $\dot{E}_c$ curve may be below the $- \dot{E}_d$ curve; under such conditions E would decrease, or, in the absence of oscillations, none would develop. This would correspond to stable conditions. During the burning of a specific motor, conditions may change from stable to unstable and/or the reverse, so oscillations in a particular mode may develop and sustain only during a certain part of the burning period (Fig. 2.7). Modifications in design would be aimed at causing the $\dot{E}_c$ curve in Fig. 2.14 to be below $-\dot{E}_d$ for all times during burning, under all normal operating conditions of the motor. The problem of stability analysis involves quantitative evaluation of the values of $\dot{E}_c$ and $\dot{E}_d$ for all times during burning of the motor, for all modes of oscillation, over all operating conditions of the motor (e.g., temperature). To the extent that the curves in Fig. 2.14 are straight lines, it is sufficient to show that the slope of the $\dot{E}_c$ curve is lower than the slope of the $- \dot{E}_d$ curve at E = 0 for all conditions. This generally is not a very easy thing to do, because the calculations are tedious, the conditions to be considered are numerous, and the input data on combustion response and damping are only poorly known. However, the analyses are extremely useful for estimating the conditions most likely to yield oscillatory behavior, what mode(s) might be unstable, and how sensitive stability is to relevant design and propellant variables. Such information is helpful in guiding test work, and in design to avoid or correct instability. These are issues discussed at length in later chapters.

The foregoing discussion was designed to help the novice understand why oscillations may occur. The description corresponds closely to a concept related to "linear" stability theory. This is reflected in the linear dependence of $\dot{E}_c$ and $\dot{E}_d$ on E, and goes back to the use of linearized forms of governing conservation equations, which are applicable only at small amplitudes of oscillation. There are important aspects of observed combustor instabilities that cannot be described by linear theory, which are explained qualitatively here, and examined in more detail in later chapters. The five qualitative aspects of observed nonlinear behavior that are most conspicuous are:

a) At large oscillation amplitudes, the mean burning rate is often modified (with corresponding changes in mean pressure as noted in Fig. 1.5).

b) At large amplitudes the oscillations level off, indicating that $\dot{E}_c$ and $\dot{E}_d$ become equal at some value of E (Fig. 2.15a).

c) In some systems, $\dot{E}_c < -\dot{E}_d$ at low amplitude (low E), but oscillations will grow if they are stimulated independently at large amplitude (meaning that $\dot{E}_c$ becomes larger than $-\dot{E}_d$ at large values of E (Fig. 2.15b).

d) Under certain conditions, the oscillations develop into shock-like waves that do not behave like any combination of the simple cavity modes that are observed at low amplitudes (Fig. 2.16).

e) In some cases, the excitation of oscillations involves conversion of mean flow energy to oscillations by action of viscous forces (e.g., via vortex shedding behavior) rather than by, or in addition to, combustion oscillations (Ref. 2.5).

Of the above aspects of large amplitude behavior, item a) does not ordinarily contribute directly to the growth or decay of oscillations, but (b-e) do contribute, and will be discussed in detail in Chapters 8 and 10. The behavior in (b) (amplitude limiting) is illustrated in Fig. 2.15a in terms of dE/dt dependence on E. The combustion contribution to dE/dt ceases to be proportional to E at large E, and at some value of E, $\dot{E}_c$ becomes less than $-\dot{E}_d$. This indicates that oscillations would stop growing at some limiting amplitude, and change thereafter only as the dE/dt vs E curves change with changing combustor geometry and mean flow field. If this type of nonlinearity did not come into play, oscillations would grow to destructive amplitude in most episodes of instability.

The type of nonlinearity in c) above is often involved in longitudinal mode instability, and was described by an example in Chapter 1. In terms of the dE/dt vs E diagram, the slope of the $\dot{E}_c$ curve is lower than the slope of the $\dot{E}_d$ curve at low amplitude (Fig. 2.15b), but at intermediate amplitude, $\dot{E}_c$ becomes larger than $\dot{E}_d$. Then, growing oscillations can occur if they are started at large enough amplitude by (for example) discharge of debris through the nozzle. Such a system
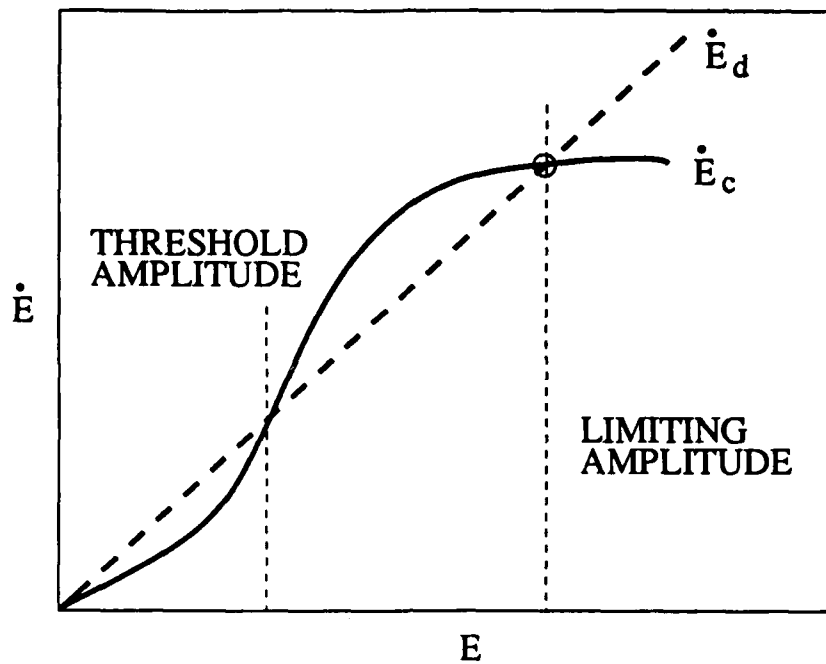
(a) Trends of $\dot{E}_c$ and $\dot{E}_d$ leading to a limiting amplitude.
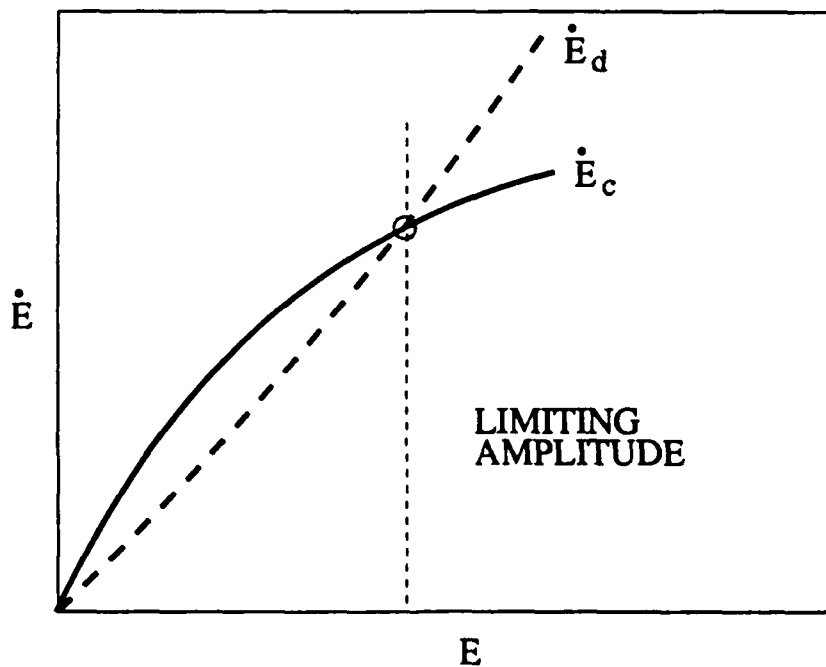
(b) Trends of $\dot{E}_c$ and $\dot{E}_d$ yielding stability to small amplitudes, but growing oscillations if the system is pulsed to large amplitude.

Fig. 2.15   Energy balance argument of Fig. 2.14 extended to nonlinear domain.

is "linearly stable", and may appear in tests to be stable until some spurious condition leads to instability. One of the objects of ongoing research is to identify the nonlinear processes that give rise to this kind of instability (Ref. 2.6, 2.7). In addition, methods of artificially pulsing suspect systems have been used to determine the presence of a nonlinearly unstable condition and to obtain such behavior for study (Ref. 2.8-2.11). Understanding of this type of behavior has been impeded by its complexity and its dependence on the whole combustor flow field (and the resulting high cost of experimental research).

The sharp wave front behavior (Fig. 2.16) referred to in e) is often manifested during the pulsed instability described above. The presence of such behavior is characteristic of nonlinear behavior, and implies that the behavior cannot be fully described on the basis of linearized analyses and simple cavity mode oscillations. Considerable study has been devoted recently to development of analyses that would explain the instability threshold, wave shape and limiting wave shape and amplitude. However, from the practical viewpoint, the problem is to avoid this type of instability, either by avoiding pulses, or by assuring a threshold so high that otherwise tolerable flow disturbances would correspond to less than threshold level. The detailed discussion in Chapter 10 includes this subject.

6.9 MPa

7.25 MPa

t →
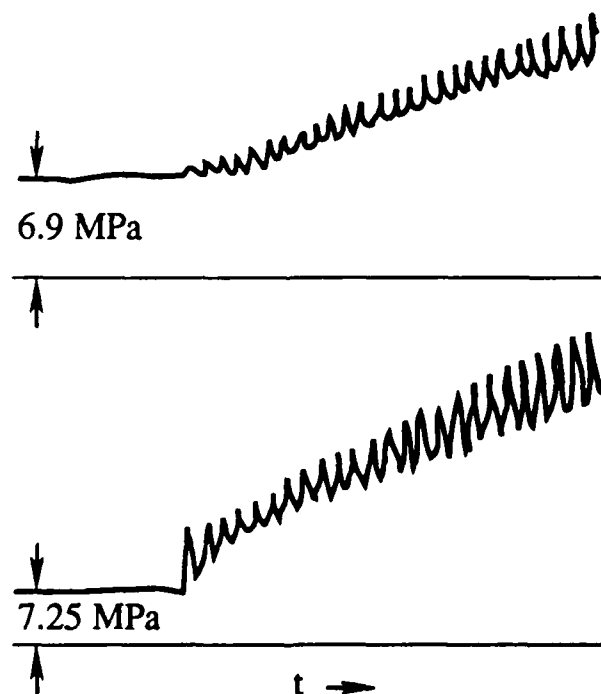
Fig. 2.16   Sketch of oscillations resulting from sharp-fronted waves.

2.7 CLASSES OF COMBUSTOR INSTABILITY

The designer is always in need of some simple rules to use in dealing with problems, and combustion instability is no exception. While nature is not very cooperative in this matter where combustion instability is involved, past experience has shown that instability behavior and causative conditions are strongly dependent on oscillation frequency. Following the lead of an earlier effort (Ref. 2.12, 2.13), instabilities are classified below into three frequency ranges and the unique features of instability in each range are described. This description should prove useful provided the reader recognizes that there is nothing fundamentally distinguished by frequency alone, and the instability characteristics cannot be classified uniquely by frequency. With this proviso, one might classify instabilities as low, intermediate, and high frequency. In this categorization,

1. Low Frequency Instability is in the range of 10 - 400 Hz, is observed mostly in large motors, usually in longitudinal modes, and usually with aluminized propellants. Below about 200 Hz, oscillations have been nearly sinusoidal. Vortex processes are sometimes an important contributor to the oscillations, especially in segmented motors and in configurations where the mean flow experiences abrupt velocity changes along the flow path to the nozzle. Two phase flow damping can be relatively low in this low frequency range, and is strongly dependent on the size of $Al_2 O_3$ droplets formed during combustion of the aluminum ingredient.

2. Intermediate Frequency Instability. This includes behavior typical of frequencies from about 200 Hz to about 1500 Hz, and typically involves longitudinal modes of oscillation with either aluminized or nonaluminized propellants (instances with aluminized propellants are usually below 800 Hz). This is the set of conditions under which pulsed instabilities and sharp-fronted wave forms are most likely to be found. However, oscillations may start from low amplitude. The amplitude can become very large, and is often manifested as strong vibrations in the rest of the flight system. The fact that the gas oscillations are in a direction parallel with the mean flow and to much of the propellant burning surface appears to be a major factor in the characteristics of this type of instability.

3. High Frequency Instability. This includes behavior in the frequency range above 1500 Hz, and usually corresponds to transverse mode oscillations (except in laboratory burners). Frequencies as high as 60,000 Hz have been recorded. The main problem is with tangential mode oscillations in motors with diameters of 0.4 meters or less. Because of two phase damping, HFI rarely occurs with aluminized propellants. Instability seems to depend primarily on pressure-coupled combustion response, which can be characterized in laboratory scale firings. Because of the complex cross-sectional shapes used for many propellant charges, the acoustic

modes and their stability are difficult to calculate, but change in cross sectional geometry is often an effective way of suppressing HFI.

Other ways of classifying instability include pulsed vs nonpulsed, velocity coupled vs pressure coupled, nonlinear vs linear, vortex driven vs combustion driven, with or without mean pressure rise, or classification by acoustic mode. Since no classification method serves all needs, and each overlaps the others in some measure, it is not useful to dwell on classification except as a qualitative introduction to the subject. Table 2.1 summarizes some of the above descriptive classification categories as they pertain to the LFI, IFI, HFI classification system. It should be understood that the cross-categorizations represent trends rather than rules.

SUMMARY

In this chapter, the physical processes that lead to combustion instability are described in qualitative terms, and some commentary on the state of knowledge is provided. This description may help the nonspecialist to understand the problem and communicate with the specialist. The chapter ends with a classification of combustor instabilities according to frequency of oscillation, and relates three frequency ranges with other features of behavior, design, and propellant. The physical concepts introduced here will be developed in full detail in later chapters.

Table 2.1 Some Rash Generalizations
about Trends of Combustor Instability

	LFI	IFI	HFI
Frequency	0 -400	200-1500	1500-20,000
Mode	Longitudinal, Bulk	Longitudinal	Transverse
Coupling	Pressure, "Velocity"	Pressure, "Velocity"	Pressure
Propellant*	Aluminized, (Nonaluminized?)	Aluminized, Nonaluminized	Nonaluminized
Spontaneous or Pulsed	Spontaneous	Spontaneous or Pulsed	Spontaneous
Severeity	Mild, except in some bulk mode cases	Mild to Severe, (Severe in pulsed instability)	Mild to Severe
Mean Rate Rise**	Mild	Mild-Strong	Strong
Coupling to Vehicle	Strong	Strong	Mild-Strong

*   Some propellants are never unstable. Aluminized propellants are stable in
    HFI because of two phase flow damping.

** Strongly dependent on severity of oscillation, strong with low burning rate
    propellants.

THREE

GUIDANCE IN MISSILE SYSTEM AND MOTOR DESIGN

In matters of this kind practice is usually in advance of theory; and many generations of practical men have brought the organ-pipe to a high degree of excellence

J. W. S. Rayleigh, 1878

3.1 INTRODUCTION - THE RISK

Combustor instability is a complex phenomenon, the control of which is not usually susceptible to quantitative design. Since it is encountered in only a minority of development programs, the first reaction of many design teams is to gamble that there will be no problem (a gamble often taken without explicit decision, but rather by doing very little in the way of avoidance measures). Choices of charge geometry and propellant are made to meet other design criteria. Even if an early decision is made to act to avoid combustor instability, the design criteria are so qualitative in nature that they may be ignored in the trade-offs for other more clearly defined competitive design requirements. Until the prediction of combustor stability is on a more quantitative footing, the treatment of the problem in development programs will probably continue to be a secondary consideration unless it is encountered as an unacceptable reality during developmental testing. In hindsight, it is clear that this is a bad policy, as encounters in testing (e.g., full scale static firings or flights) or later in operational service can require very costly remedial measures, or degradation of system performance. However, it is less clear what measures should be taken early in development, and it is the purpose of this chapter to offer some guidance on this question

The presence of a combustor instability problem in a development program ordinarily becomes evident during developmental testing, and in cases of severe oscillations, remedial measures are sought at that time. Detection early in the program provides a better opportunity for remedial measures. As in the examples in Chapter 1 and Ref. 3.1, detection or remedial efforts later in the program can be

very costly. In this regard, cases of less severe oscillation are sometimes deemed tolerable and go into service. However, cases that appear to be innocuous sometimes are found to cause unacceptable functioning of other vehicle systems (usually, but not always, as a result of associated vibrations). Such problems may not be manifested until well into a production program, when some changes in the vehicle or in the propulsion system lead to either greater sensitivity to vibration or a change in the nature of the combustor oscillations. Such episodes have been traced to changes in suppliers of vehicle components (vibration specifications rarely encompass vibration environments induced by combustor oscillations). Other episodes have been traced to changes in suppliers of propellant ingredients, or to minor changes in charge configuration made to solve production problems. Obviously, encounters with unacceptable combustor instability-induced problems during a production program can be very costly, causing production delays and uncertainty regarding the adequacy of previous production or even rejection of products. Given the potential cost of instability problems after production has begun, it is important to eliminate the problem during development. For the program in which a calculated risk of instability problems remains at the start of the production program, special measures should be taken to fully assess and contain the problem.

3.2 HOW MUCH DOES THE DESIGN-DEVELOPMENT ENGINEER KNOW?

Developing and implementing a strategy for avoiding combustor instability-related problems is not one of the requirements that automatically appears on the program manager's "check list", and most propulsion system engineers and propellant chemists have only a superficial knowledge of the problem. An awareness of this situation is thus the first prerequisite of a strategy for avoidance. The accumulated knowledge is, by now, sufficient for strategy planning, but the intimidating body of literature rarely addresses this subject. The balance of this chapter will address this subject in a manner aimed at serving program managers. It will, hopefully, also provide a lead-in for motor designers and and propellant chemists to other parts of the report that may be useful to them.

3.3 CONSIDERATIONS EARLY IN DEVELOPMENT PROGRAM

During a development program, a progressive process of analysis and design decisions occurs, guided by the preliminary performance goals and cost-safety constraints. The further this process goes, the more limited are the options for avoidance of instability problems without reversal of previous design and propellant choices and program commitments. If instability is detected late in a

development program, the level of commitment to design and the pressures of time and cost may lead to that unhappy decision to "live with instability" in the final system. Under such "tardy circumstances" this may be the appropriate decision. However, this represents an absence or failure of early strategy. Further, it carries with it the responsibility to develop an instability management program throughout flight qualification, production, and service. Since almost no development program has ever accepted that responsibility, the record shows primarily the episodes where the failure to do so caused major program problems. Early strategy to address the instability problem can lead to avoidance of major program problems and match the instability considerations to the particular program.

The first priority in a planning strategy is:

a)   a preliminary determination of the risk of instability with the propellants and designs under consideration,

b)   a judgement regarding the cost of modification and testing in the event instability is encountered, and

c)   a determination of the sensitivity of the flight vehicle to instability-induced malfunction.

Regarding a), there are combinations of designs and propellants that pose low risk of instability in some motor sizes and configurations, some combinations that pose high risk, and some combinations that are quite unpredictable. The degree of sophistication of the instability-avoidance aspects of the program should be estimated early in program planning, as soon as motor configuration and propellant type has been narrowed down. A program manager would do well to call in a combustion instability specialist with both fundamental and development program experience to assist in risk evaluation and commensurate program planning.

Regarding b) above (cost of empirical remedy of instability problems), it may happen in a "small motor" development program that motor fabrication and testing costs are low enough so that any instability problems can best be corrected by direct evaluation (using full scale motor firings) of judicious changes in propellant, charge configuration, or oscillation damping devices. It may even be practical to assess the margins of stability by pulse testing or testing with other destabilizing modifications. In such a development program, planning strategy would be aimed more at early detection and remedy, and less at complicated stability analyses and prevention. On the other hand, some programs involve motors that are very costly to produce and test. In such a program, much more reliance should be put on evaluation of stability characteristics of propellants (laboratory scale tests) and analytical-computational prediction of combustor stability (the government sometimes requires bidders for development contracts to indicate what testing and analysis will be proposed). Evidently, the strategy for dealing with a combustion instability risk may be quite different, depending on the cost of motor testing.

Regarding c) above (susceptibility of the flight system to impairment of function by combustor instability), there are simple systems in which the effect of instability

can be forecast and the seriousness assessed. That assessment may indicate that instability would produce no unacceptable adverse system performance (rarely true if instability is severe). This would be a basis for a somewhat "relaxed" attitude regarding combustor instability. In more complex propulsion and flight systems, an advance assessment of adverse effects of combustion instability may be prohibitively difficult. In such a system, it would be advisable to devote more attention to the combustion instability problem. The consequences of failure to address this situation can lead either to flight problems or to the necessity to "harden the bird" (detailed design and construction to function in the adverse vibration environment). Either alternative is a costly alternative to a timely and successful program for prevention of instability earlier in the development program.

The foregoing considerations (of risk of instability, potential complexity of corrective measures, and vulnerability of the flight system to instability-induced malfunction) are basic to a strategy for the problem. From these considerations it may be decided that instability is an unlikely problem, an easily fixable problem, or a problem with minimal adverse effects, or any combination of these. Such conclusions typically lead to subsequent neglect of the problem, with reasonable justification. On the other hand, a less optimistic preliminary judgement should lead to further strategy for containment of the problem. The balance of this chapter will address some of the technical aspects of combustor instability in the general terms needed for strategy planning.

3.4 DESIGN AND PROPELLANT CONSIDERATIONS

There are many combinations of motor-charge design and propellant composition for which combustor instability has never been observed. Indeed, there are some types of propellant that seem to be immune to instability, such as those using potassium perchlorate or ammonium nitrate as oxidizer. It is also observed that propellants containing more than about 10% aluminum powder as a fuel ingredient are rarely or never unstable in small rocket motors. On the other hand, there are some propellants that can cause instability in all size motors. Unfortunately, these differences are not usually fully understood. Further, there seems to be a tendency for the stable propellants to be ones of rather low performance (i.e., low Isp, as with AN and KP propellants). While there is no way to reduce this complex problem down to simple generalizations without risk of real-life exceptions to the generalizations, strategy planning has to be based on general trends and recognition of risk. It is in this context that some general qualitative trends are described here.

Instabilities ordinarily occur in the lower frequency transverse modes and longitudinal modes of the combustor cavity. In large motors, these modes correspond to relatively low oscillation frequencies. A cavity with a characteristic lateral dimension (L) of 1 meter will have a first transverse mode frequency (f) of roughly

$$f = a/2L = (1200 \text{ m/sec})/2 \times 1 \text{ m}$$

$$= 600 \text{ Hz}$$

and a first longitudinal mode frequency of perhaps 1/3 to 1/10 this value. The dynamic response of most propellants is very different in this low frequency range than at higher frequencies, and the damping characteristics of the propellant reaction products can also be strongly frequency dependent. One profound consequence of this is the failure of small scale tests to evaluate the stability of full scale motors. Another consequence is a rather significant difference in stability trends in large and small motors. Based on experience, large motors are less prone to combustion instability. In very large motors, such as the Titan IIIC and Space Shuttle booster motors, this is probably due to low dynamic response of the combustion at the low characteristic frequencies. In somewhat smaller sizes (but still large), stability is suppressed by damping processes associated with the condensed phase Al_2O_3 reaction products typical of such motors. However, combustion response to flow oscillations can be significant at frequencies above about 200 Hz (characteristic dimensions less than approximately 3 m) and episodes of unstable combustion become more common (and sometimes critically dependent on the damping characteristics of the Al_2O_3 products, as in one of the examples in Chapter 1).* Since the higher frequency transverse modes benefit more from the two-phase flow damping than do axial modes, the large motor instabilities tend to be more often observed in longitudinal modes. This is particularly true of booster motors, which have high length-to-diameter ratios (and aluminized propellants).

In the frequency range 600-1800 Hz corresponding to characteristic dimensions of 1 m to 1/3 m, there is strong competition between combustion response and two-phase flow damping. The system is strongly driven and strongly damped. Stability is relatively less predictable because very substantial uncertainties in both combustion response and damping can easily make the difference between a prediction of stable or unstable conditions. In short, stability depends on the difference of two large effects, neither of which is well determined. With aluminized propellants the trend is to increasing stability as mode frequencies go up. Propellants with 15% of aluminum rarely exhibit oscillations in motors at frequencies higher than above 1500 Hz (characteristic dimension 0.4 m). Thus, tactical rocket motors with aluminized propellants rarely, if ever, show unstable combustion in transverse modes, but are sometimes unstable in lower frequency longitudinal modes.

In applications using nonaluminized propellants, the trends imposed by two-phase flow damping (increased damping and stability at higher frequency) are absent. Since nonaluminized propellants have seen little use in large motors, there

---

* These trends do not apply to the bulk-mode oscillations that sometimes occur in low L* motors at frequencies of 10-200 Hz (see Chapter 8).

is little basis for generalization regarding stability. However, nonaluminized propellants are often preferred in tactical rocket motors, and the dimensions of such motors are typically in the range below 0.3 m (diameter) and 3 m (length). This corresponds to frequencies greater than 2000 Hz (transverse mode) and 200 Hz (longitudinal mode). Instabilities are encountered in both transverse and longitudinal modes in such motors, most often in the transverse modes. There are a wide variety of propellants used in these applications, and all those in common use are capable of producing instability.

Control of instability with "smokeless" propellants is accomplished by a variety of methods that are discussed in Chapter 14. For the program planner, it is important to note that there is a relatively high risk of combustion instability in motors of the size used in tactical rockets using propellants selected to minimize condensed phase products. It is also important to note that high frequency transverse mode oscillations are not generally resolved by routine static test instrumentation, so that their presence may go undetected in development programs unless it produces other detectable manifestations, such as the mean pressure shifts noted in Fig. 1.5. Reference may be made to Chapter 13 for information on measurements. As noted earlier, delay in recognition of an instability problem makes correction much more costly and/or difficult. Because of the relatively high risk of instability with smokeless propellants, the program planner would do well to seek guidance of a specialist before settling on a propellant or charge design, and when designing static test hardware and choosing static test instrumentation.

3.5 DESIGN TRADE-OFFS

Design of rocket motors is a process involving a careful balancing of many competing factors. High performance calls for high energy propellants, light motor cases, and acceptable reliability and safety. High energy propellants are generally more prone to combustion instability than others, and lightweight motors are more vulnerable to instability-induced damage. Similarly, smokeless propellants that are so desirable in some tactical applications are particularly susceptible to combustion instability because of low damping. Many propellant charge geometries that are particularly desirable in terms of either ease of production or attainment of desired ballistic performance are relatively more susceptible to combustion instability. High burning rate propellants are (in theory, and sometimes in practice) more susceptible, especially in high frequency modes. These trends reflect areas where design for attainment of stable performance can be in conflict with other demands on design or propellant, and extra effort may be needed to meet all requirements. Unfortunately, these design trade-offs have not been formalized in simple terms because the trends are not consistent over the range of propellants, designs and operating conditions of interest, and the more detailed trends have not been established. The program planner needs to be aware that his designers are

confronted with possible compromise and complication in design, testing and performance to achieve stable combustion.

3.6 MEASUREMENTS DURING TESTING

It was noted above that measurement of oscillations calls for special attention to detectors. The past record shows that there is an extraordinary resistance to incorporation of such instrumentation in test programs. There seem to be several reasons of which program planners should be aware:

a) nonrecognition of need,
b) unfamiliarity with methods,
c) unavailability of instrumentation,
d) failure to provide appropriate fixtures in test hardware (e.g., for mounting high frequency response transducers), and
e) fear that transducer or its fixture may be the cause of a motor case failure during a test.

The instrumentation problem is discussed in more detail in Chapter 14. For the purpose of this chapter, it is sufficient that the program manager understand that there are many practical reasons why occurrence of oscillations may not be detected, but the failure to do so can lead to tardy recognition of a problem, and the by now familiar penalties of a tardy remedial program or "live with it" decision.

SUMMARY

This chapter is intended to give some insight into the impact of combustion instability on motor design and missile system development. The content is addressed primarily to readers who are concerned with planning strategy for a development program. It is noted that propulsion system designers and propellant chemists are rarely knowledgeable concerning combustion instability, and that some overt management effort may be required to assure timely consideration of the problem. It is noted that the problem should be addressed and solved early in the development program in order to avoid very costly encounters later. The relative likelihood of instability-related problems is described in terms of the type of missile system, size of motor, and type of propellant. Some comments are made regarding measurements of oscillations during development testing, comments addressed to program planners and managers. Nearly everything in this chapter is treated elsewhere in the book in more detail, and the designer will generally find such treatments more useful. The program planner will find further guidance also in Ref. 3.1, and both planner and designer will find help on design and testing in Ref. 3.2 and 3.3.

CHAPTER
FOUR

FUNDAMENTALS OF PROPELLANT COMBUSTION

False facts are highly injurious to the progress of science, for they often endure long; but false views, if supported by some evidence, do little harm, for everyone takes delight proving their falseness.

Charles Darwin

4.1 INTRODUCTION

Combustion of solid propellants for rockets has been a topic of vigorous research since the early 1940s, with significant prior work in connection with guns. The research has become increasingly sophisticated since about 1955, and particularly since 1960, because of the growing role of rocket propulsion in military and space applications, and because of concurrent advances in combustion science and experimental methods. The complexity of the propellant combustion process and its diversity among the many propellant systems in use have prevented any definitive quantitative understanding, and research tends to be either a search for qualitative understanding or a quantitative experimental characterization of global combustion trends, such as mean burning rate as a function of pressure, propellant bulk temperature, and ingredient variation. Measurements of global combustion behavior provide both design data and trends that realistic combustion theory must be able to correlate. As was noted earlier, direct measurement of details of the combustion process is usually precluded by difficulties with a hostile measurement environment and the microscopic scale of the key combustion regions. Given this situation, one must anticipate that understanding of oscillatory combustion rests on a complicated combination of information about propellant combustion involving: a) analyses that are chronically oversimplified, b) thermal decomposition measurements of unknown relevance to combustion, and c) observations of global combustion behavior that reveal little direct information about combustion mechanisms. Some insight into this situation can

be obtained from a recent book on solid propellant combustion (Ref. 4.1).

In the present book, it is necessary to have a reasonable understanding of the nature of the combustion process (and its diversity) in order to address the oscillatory combustion problem realistically, and the objective of this chapter is to provide that understanding in a way designed to reflect the particular needs of this book. The section headings indicate the approach, from a description of the propellants themselves to a description of how the individual ingredients behave at elevated temperatures, to a discussion of what is known about the combustion process, and a description of strategies for analytical modeling of steady state and oscillating combustion. Chapter 5 presents the analytical models, and Chapter 7 describes models of the combustion-flow interaction.

4.2 NATURE OF PROPELLANTS AND INGREDIENTS

Solid propellants must meet an extremely diverse set of requirements, of which combustion behavior is only one. As a result, any discussion of the state of knowledge of combustion behavior draws from a pool of past work that was heavily constrained by consideration primarily of propellant ingredient combinations and formulations that qualify relative to the many requirements other than combustion behavior. Among those constraining requirements, it is necessary that propellants be energetic but safe, strong but processable, highly combustible but resistant to unintentional ignition. The outcome of such considerations is that propellants are typically materials with relatively hard, rubbery consistency, poor heat conductors, homogeneous "in the large" but often heterogeneous on the 1-1000 micrometer scale. The heterogeneity ordinarily reflects the combinations of an oxidizer and a fuel. The oxidizer is usually a crystalline solid in powder form, and the fuel is usually a polymeric material, which serves also as a "binder" and provides the mechanical integrity of the mixture. Depending on the relative importance of safety and propulsion performance, the binder may be either a synthetic rubber-like material or an energetic material (e.g., nitrocellulose) with an energetic plasticizer (e.g., nitroglycerine). In some applications, the high energy binder is used without the oxidizer, resulting in a homogeneous propellant. In many cases, an appreciable amount of metal powder (usually aluminum) is used as a fuel ingredient. Some of the oxidizers that are used are perchlorate salts (ammonium, potassium, lithium), ammonium nitrate, and nitramine salts (HMX, RDX). Of these, AP and HMX are most common. Propellants with "rubber" binders require a high oxidizer content in order to achieve maximum propulsion performance (e.g., 90%), a requirement that is in conflict with requirements for processability, mechanical strength and low sensitivity of the propellant. Rubber-binder propellants typically have 10-20% binder. The overall stoichiometry is normally fuel-rich, a property that reduces the tendency for erosion of exposed motor components (but can leave the exhaust capable of

combustion in air). The particle size of ingredients is adjusted within limits to control the burning rate of the propellant, but is usually carefully blended to permit effective "packing" in the matrix to yield the highest solids content compatible with acceptable mechanical properties (in the product and during mixing). For these reasons, the particle size distribution is already significantly constrained and, thus, is not fully available for control of combustion behavior.

In combination with the subject matter in Chapter 2, the foregoing can provide some insight into the nature of propellants and complexity of combustion to be expected. However, it should be noted that propellant ingredients differ drastically in their response to the temperature encountered in the combustion zone, and that a good understanding of the combustion requires an understanding of the thermal response of all the major ingredients. This topic is addressed in the following, where it will be noted that the same problems that plague measurement of propellant combustion zone processes are still present, but to a lesser degree, in characterizing the behavior of the individual ingredients.

4.3 INGREDIENT DECOMPOSITION AND SELF-DEFLAGRATION

Background. From the standpoint of decomposition characteristics, propellant ingredients range from metal particles that don't decompose to hydrocarbon binder and some oxidizers that decomposes endothermally, to energetic binders and oxidizers that decompose exothermally and usually self-deflagrate under some conditions. These differences in decomposition characteristics strongly influence the role that each ingredient plays in propellant combustion. It is not feasible to summarize the large body of pertinent literature on ingredient decomposition here, but some understanding of ingredient behavior is essential to understanding and modeling combustion, and in deciding what decomposition data are relevant to combustion.

Decomposition behavior of propellant ingredients has been studied for a variety of reasons, such as safety of processing and storage, hazard in fire environments, and evaluation of catalysts and stabilizers. It is not yet clear how much of the results of such studies are relevant to propellant combustion processes, although such results are often used as guidance in propellant formulation studies. The uncertainty regarding relevance is due primarily to the low temperatures of decomposition studies compared to propellant surface temperatures. A difference is 50 - 100 °C, which is very large when studying complex chemical reactions governed by rate laws with exponential temperature dependence. High temperature experiments are very difficult, precisely because the reaction rates are so high. Controlled heating and quantitative time-resolved measurement is so difficult that little in the way of high temperature data is available. Much of our current understanding of ingredient decomposition rests on the low temperature

decomposition results, or back-inference from global observations of self-deflagration and propellant combustion.

One useful experiment for showing qualitative features of ingredient decomposition at moderate temperatures is the differential thermal analysis (DTA) method. In this experiment, a test sample is heated by conduction from an electrically heated sample holder, and the endo- or exothermicity is observed by its effect of sample temperature, measured by a thermocouple. Temperature is programmed upward at a pre-chosen rate (e.g., 10 to 100 °C/min). Excursions in sample temperature due to sample response to heating are recognized by using a second sample holder with an inert sample and a second thermocouple. The second sample holder is in the same heater environment as the first one. The thermocouples are connected in opposition to each other, so that the net output indicates the difference in temperature of the control sample and the test sample. The experiment requires that the heating rate be kept low so that all parts of the two sample holders will be in thermal equilibrium except for the small difference due to test sample response. The test sample decomposes over a period of many minutes, and is ordinarily completely decomposed (or vaporized) by the time the temperature reaches 450-500°C (typical for tests on ammonium perchlorate). Exothermic samples must be sufficiently dilute to avoid runaway self-heating. Otherwise, rapid evolution of gases disrupts the sample and effectively terminates the test. The sample holder is heated in an inert atmosphere when atmospheric effects are of concern. Very little experimentation with propellant ingredients has been done at pressures above one atmosphere.

Figure 4.1 shows a typical DTA record from a test on ammonium perchlorate. From this and other tests, it is known that AP decomposes slowly by dissociative sublimation at temperatures of 220-242°C and experiences an endothermic crystal phase change at 242°C . At higher temperature, more complex exothermic decomposition occurs. DTA tests typically show double maxima in the exotherm, centering on 370 and 490°C . Details are dependent on experimental methods, and the reason for the double peak is not unambiguously established. Other decomposition experiments (e.g., involving analysis of gas evolved during heating) help to clarify what is happening in decomposition experiments (e.g., it is generally agreed that AP decomposes by dissociative sublimation, decomposition of the $HClO_4$ product, and successive reactions that oxidize the primary NH_3 product. Since the secondary reactions are likely to be in the gas phase, their progress depends on pressure, dilution by other gases, presence of container walls, and temperature-time history in the reaction volume. The only ingredient experiment with AP where these conditions approximate those in a propellant combustion zone is in self-deflagration of pure AP samples (Ref. 4.2, 4.3).

In varying degree according to the specific ingredient under consideration, it is appropriate to regard the usual decomposition experiments only as a starting point for any postulate regarding how decompositon proceeds during combustion,

keeping in mind that most of the reaction that takes place during combustion (including most of the transformation from solid to gas) occurs at temperatures much higher than in the controlled decomposition experiments (Ref. 4.4, 4.5). With this mental reservation as a guide, the following is a description of ingredient decomposition with emphasis on what is, or is not, known about high temperature decomposition.

Crystalline Oxidizers. In most propellants, 40-90% of the mass is in the form of crystalline particles of oxidizer. The more chemically stable of these (e.g., potassium perchlorate and ammonium nitrate) decompose endothermally, will not deflagrate on their own at rocket motor pressures, and are little used because their propellants yield relatively low specific impulse. Interestingly enough, these propellants have also not exhibited oscillatory combustion. Table 4.1 shows estimates of significant tempertures for response of various ingredients. The melting temperature of AN is about ___ °C (KP apparently decomposes without melting). Decomposition starts at about ____ °C for KP and _____ °C for AN in DTA tests. It is generally believed that the surface o f a burning propellant AN is molten, raising the possibility of liquid phase mixing with other ingredients (or flow over their surface). The primary decomposition step of AN is apparently to _____ and _____. There is little data on surface temperature during burning. The decomposing surface of KP in the combustion of propellants is apparently dry, with the primary decomposition step being to _____ and _____ vapor. A molten decompositon product (KCl) is sometimes left on the KP surface during some decomposition experiments. A variety of exothermic oxidizers have been considered for propellants. The most common is AP, which was discussed as an illustrative example earlier. The nitramines (particularly HMX) have also been used extensively. These materials are "energetic", will self-deflagrate, and the nitramines are sensitive and detonatable. The decomposition characteristics are summarized in Table 4.1. It was long believed that AP decomposed by dissociative sublimation, as observed in many controlled heating experiments (where AP deposited out on cold surfaces of low pressure reactors). Exothermic steps were thus assumed to occur in the gas phase, with the surface efflux being NH_3 and $HClO_4$. Early investigators found that AP would self-deflagrate at elevated pressure, but continued to argue that deflagration was supported by an $HClO_4$-NH_3 flame. Studies in the 1960s showed that at usual rocket motor pressures above 2MPa (and below about 10 MPa), AP deflagrated with a frothy surface (Ref. 4.2). It was also noted that the observed burning rates were hard to explain in terms of exothermic reactions in the gas phase only (Ref. 4.6), and it is now argued that roughly 50% of the heat release occurs in a decomposing liquid surface layer. The temperature of this layer has been estimated to be around 600 °C(Ref. 4.7), well above the temperatures of conventional controlled decomposition experiments. The details of this complex high tempera-

ture decomposition process are still matters of speculation, as is the even more exotic decomposition behavior observed at higher pressures (15 - 30 MPa, Ref. 4.8). Dissociative sublimation may be the relevant process in low pressure propellant combustion. In fact, the low pressure limit for self-deflagration may be due to "loss of" the surface liquid and its exothermic steps as pressure decreases (Re. 4.9). The total heat release by self-deflagration is low by propellant standards, while the self-deflagration rate is comparable to propellant rates (at 7 MPa), suggesting that a significant part of the heat release is at the surface; rate is observed to drop off rapidly with decreasing pressure, consistent with an interpretation that the portion of heat release at the surface decreases with pressure (corresponding to decreasing surface temperature). It may be that the low pressure deflagration limit is due to decrease of the surface temperature to an as yet unproven AP melting temperature and shut down of all exothermic surface reaction. Important to later discussion is the point that, whatever the cause of the low pressure limit, it is much higher when the initial (bulk) sample temperature is low (Ref. 4.__). This further illustrates the marginality of the self-deflagration, reflecting a "marginality" of the heat balance resulting from the low final flame temperature of AP (estimated to be only 1400 °C for ambient sample temperature.

The details of AP decomposition and self-deflagration have been pursued in detail here because there is far more information pertaining to AP than any other oxidizer, and because the results demonstrate the limitations of controlled heating decomposition experiments in determining decomposition behavior in combustion waves. Thus, it is not clear where one should obtain the kinetic and transport properties that are called for in analytical models of propellant combustion, and the reader should anticipate that such properties as activation energies, molecular weights and diffusion coefficients in analytical models may often be treated as undetermined parameters, with values chosen to yield best correlation of global combustion characteristics such as burning rate. This is common practice in combustion science, where measurement of global combustion behavior is often easier to do than is measurement of more fundamental aspects of the process. It is also appropriate to note that validity of this approach rests on the relevance of the particular analytical model to the real combustion process.

Returning to the other energetic oxidizer, the DTAs for HMX and RDX are shown in Fig. 4.2. Decomposition proceeds at a low rate prior to melting. The melt endotherm is evident in the DTA (~ 220 °C for HMX, 200 °C for RDX). Decomposition is already proceeding slowly at these temperatures, and the width of the melt endotherm is deemed by some investigators to reflect something more complicated than mere phase change. The melting endotherm is followed immediately by an exotherm for RDX and, in controlled heating experiments, the sample size and dilution must be chosen to prevent abrupt consumption of the sample due to self heating (i.e., loss of control of sample temperature). The exotherm for HMX occurs at higher temperature, around 275 °C . Details of the exotherm are generally a function of experimental technique, test pressure, heat-

ing rate, sample particle size, etc. Methods have been devised to calculate order and activation energy of decomposition reactions from the thermal analysis tests such as DTA, DSC and TGA,* but the results for HMX and RDX depend upon method and experimental variables. Perhaps more significant, the test samples are ordinarily fully consumed long before reaching the temperature deemed to prevail on the surface of a burning sample, and the decomposition rates are such that during deflagration very little reaction would occur in the short time spent in the combustion wave at those temperatures experienced in controlled decomposition tests. Thus it is uncertain whether decomposition data obtained in controlled heating experiments is relevant to combustion. The results do indicate that a decomposing melt would be expected on a burning surface.

Both HMX and RDX are nearly stoichiometric in composition, in the sense that most of the carbon and hydrogen atoms are oxidized to CO_2 and H_2O in the final deflagration reaction products. The energy release is correspondingly high, and HMX and RDX self deflagrate over a wide range of conditions, with flame temperatures around ____ ^oC (compared to around 1400^oC for AP). The self-deflagration rates are about 1.2 cm/sec at 7 MPa (HMX), as compared to a value for AP of about 0.7 cm/sec. HMX and RDX burn with an exothermic reaction zone in, and immediately above the surface that leads to temperatures around ____ ^oC, with a second flame that stands far enough from the surface (Fig. 4.3) to have relatively little effect on self-deflagration rate (a behavior to be noted below also for double base NC/NG propellants). The surface temperatures of deflagrating HMX and RDX appear to be lower than those of AP in spite of their higher self-deflagration rate, indicating that they decompose relatively easily. The melt layer on the surface is relatively more thick than for AP, raising the possibility of some liquid phase mixing with fuel melts in a propellant situation.

Binders. Propellants are held together by plastic-like binder materials, which are the connected part of the propellant matrix. Binders are also the fuel ingredient. They range in practice from hydrocarbon polymers, such as PBAN and HTPB, to polymers with energetic plasticizers, such as ____ and ____, to energetic polymers or colloids, such as NC/NG ("double base" binders). Propellants with energetic binders typically have a lower volumetric loading of oxidizer because the binder has more oxygen content, and because energetic binders are usually less suitable to high solids content from the standpoint of processing, mechanical properties, and hazard.   The typical hydrocarbon elastomeric binders decompose endothermally in controlled heating experiments in the temperature range ____ to ____ ^oC. There seems to have been very little study of the vapor species that result under rocket motor-like conditions. It is recognized that the initial mode of decomposition of a polymer molecule will involve bond-

---

* DTA means "differential thermal analysis", DSC means "differential scanning calorimetry", and TGA means "thermal gravimetric analysis", which is time-resolved weight measurement during heating.

breaking in the polymer backbone in some polymers (e.g., _____), and breaking of bonds to pendant groups in other polymers (e.g., _____). In the controlled heating experiments, most of the hydrocarbon polymers soften to viscous "melts" in the _____ to _____ °C range and bubble at from _____ to _____ °C, with this temperature differing significantly for different polymers. In slow heating experiments, most of the test sample is decomposed by the time the temperature reaches ____ °C (a sample DTA curve is shown in Fig. 4.4). The semi-liquid surface is observed also in combustion experiments, and residual evidence of a melt remains on the surface of propellant samples quenched from high pressure burning. In combustion modeling, it would be useful if the binder response to heating could be characterized by a one-step irreversible conversion to vapor products according to an Arhenius rate law. The available information suggests that pressure is more complicated, and that a search for appropriate values of activation energy and pre-exponential factors for the rate law is of limited meaning.

Of the energetic binders, the nitrocellulose-nitroglycerin system has been the most studied. This energetic binder has been used as a monopropellant for the last 100 years, first as a gun propellant and then as the first satisfactory rocket propellant. At the molecular level it consists of two ingredients, NC and NG. In decomposition of the colloid, NG apparently evaporates in the ____ to ____ range, and NC decomposition becomes important at ____ °C.

Decomposition of NC is reported to start with rupture of $O-NO_2$ bonds, and the activation energies obtained in some experiments are consistent with this. However, the initial reactions are in the condensed phase, as are some subsequent steps, and the rate of conversion to gas depends on this complex sequence of reactions and evaporation. When NG or other plasticizers are present, the reacting surface layer includes the evaporating plasticizer and the surface thus is a complex mixture of ingredients and intermediate products in a solution or froth. The NC decomposition is autocatalytic and exothermic, with its rate often strongly affected by additives used to either inhibit the autocatalytic reaction (for storage stability) or enhance reaction rates at elevated temperature to increase burning rate. During self-deflagration, the surface regression rate of different double base formulations are found to linearly dependent on the heat of reaction (Fig. 4.5), which can be varied by changing NC/NG ratio or by changing the degree of nitration of the NC. This correlation is believed to be due to the dominance of exothermicity of the reactions in the condensed phase-melt-foam layer, and the effect of composition variables on these exothermic reactions. Indeed, considerable success has also been achieved in modification of burning rate by catalysts

that are thought to affect these reactions. The surface temperatures of self-deflagrating double base formulations are reported to be 320-400o C, with considerable uncertainty associated with the absence of a well defined and unambiguously located surface due to gas formation "in" the condensed phase. Temperatures determined by thermocouples traversed by the combustion zone show a very steep temperature rise (Fig. 4.6) to about ___o C in the gas phase, indicating exothermic gas phase reaction. After a further, more gradual temperature rise, a second steep temperature rise occurs to a final temperature of ___ to ___o C. The second steep temperature rise corresponds to a flame that is readily visible in experiments below 1.0 MPa. In fact, the flame stand-off distance is sometimes reported as a function of pressure (Fig. 4.7). While a large part of the heat of reaction is released in this stand-off flame, it is too distanct from the surface to be a dominant factor in heat flow to the solid preheat region, except possibly through its effect on reaction rate in the primary exothermic region. However, the stand-off flame may be important to the transient combustion response, and to combustion of other ingredients when the propellant is used as a binder in composite propellants.

Metals. The principal metal ingredient in current propellants is aluminum powder. While there is no decomposition or deflagration to relate to the present section title, it is important to note that most metals don't vaporize at the temperatures of the propellant burning surface, posing the questions of how the metal particles get away from the burning surface and where they burn. Since the particles emerge at the burning surface from a binder-surrounded matrix location, they are often in an adherent binder melt. It is observed that metal particles concentrate to some extent on the surface (as do other additives, such as particulate burning rate catalysts). Aluminum particles are resistant to ignition because of a refractory Al2O3 coating on the particles. Combustion ordinarily takes place after detachment from the surface, often as agglomerates of large numbers of particles that were concentrated on the burning surface. Details will be discussed in the next section, but it should be kept in mind that metals (and all nonvolatile ingredients or intermediate reaction products) experience a complex concentration-agglomeration-sometimes ignition process on the burning surface that is strongly dependent on other propellant variables and on pressure. This process is responsive in its own unique way to flow oscillations and associated oscillations in other combustion zone processes.

4.4 GENERAL FEATURES OF PROPELLANT COMBUSTION

In preparation for discussion of oscillatory combustion, it is necessary to first understand the nature of the combustion zone and processes that oscillate. Adopting the view of small perturbation theory, we may look upon the combustion as a

process oscillating about its mean state, which is the steady state part of a transient solution of a nonsteady problem. From the discussion of ingredient decomposition and self-deflagration, we can anticipate that the combustion zone can be very complex for heterogeneous propellants, that the nature of the combustion will be very different with different ingredient combinations, and that the details (both physical and chemical) will be only qualitatively known and difficult to measure. On the other hand, this has not stopped efforts to model the combustion behavior analytically, both steady and nonsteady. While such modeling may at times seem futile, given the degree of oversimplification necessary, it is an essential part of development of physical insight, provides a basis for ordering and interpreting experimental results, and provides a necessary part of any model of the overall combustion behavior that determines whether oscillations will or will not occur and how they may grow.

The goal of this section is to provide some perspective on what the combustion zone is. We may start with a one-dimensional view as in Fig. 4.8., and then examine what processes (one-dimensional or otherwise) may be going on in each region of the one-dimensional picture. For convenience, the regions will be chosen as follows (Fig. 4.8), with more detailed description following a preliminary identification.

1. A thermal induction region where reactants are heated by conduction, but where significant chemical reaction is not present.
2. A second thermal induction region where chemical reactions are important but no disruption of the microstructure has yet occurred.
3. A region where liquification or vaporization of some ingredients causes breakdown of the heterogeneous microstruction, and an opportunity for diffusion of ingredients and/or intermediate decomposition products.
4. A "surface", below which most of the material is condensed phase, and above which most of the material is vapor phase.
5. A primary gas phase induction zone, in which exothermic reaction is delayed for some propellants) while ingredient mixing occurs and build-up of free radical concentration sets the stage for Region 6 flames. For some propellants (double base, some nitramine) this region involves a continuation of Region 3 exothermic reactions.
6. A primary gas phase flame (or flamelets) that is closely coupled to the underlying regions by virtue of its proximity and heat release. Such a flame is viewed as yielding intermediate reaction products capable of further reaction (homogeneous propellant), or as consuming some portion of reactants that have already mixed (heterogeneous propellants).
7. In the case of homogeneous propellants, there is usually a further chemical induction region prior to a secondary flame. With a

heterogeneous propellant, this region may instead consist of a myriad of diffusion-controller oxidizer-fuel flamelets, and may at the same time have chemical induction processes leading to secondary monopropellant flames if the diffusion or reaction of adjoining ingredient vapor flows is slow.

8. It is customary to specify a secondary exothermic flame, which is clearly evident in the case of most homogeneous propellants. With heterogeneous propellants (as implied in (7)), there are usually exothermic reactions extending well above the primary flame, which may or may not appear as a well-defined secondary flame, depending on the rate of diffusive mixing of ingredient vapors and the chemistry of their interaction.

9. Finally, relatively nonvolatile ingredients, such as metals, may remain substantially unvaporized at the secondary flame, and burn as a cloud of individual particles (droplets) while moving outward in the product flow.

Region 1 is the leading front of the thermal wave, in which heat conduction is the primary process. For propellants with very fine ingredient particles, the propellant may behave as a homogeneous material. For particle sizes larger than 50 μm, the heat flow is probably significantly three-dimensional, especially when the thermal properties of the solids are widely different (as they usually are). The heat-up may also involve crystal phase transitions and thermal properties that are temperature-dependent. These considerations may be important in determining the non-one-dimensional features of overlying regions, but are rarely considered in analytical models.

Region 2 is similar to Region 2 in the sense that physical degradation has not proceeded to the point of facilitating diffusion of ingredients, but differs from Region 1 in the presence of chemical reactions. In a homogeneous propellant, this would correspond to beginning of decomposition, and the processes involved may sometimes be the ones affected by burning rate catalysts. In a heterogeneous propellant, this region may have either interfacial reactions between ingredients, or beginning decomposition of the less stable ingredients. In many one-dimensional models this region encompasses all of the condensed phase reactions because those models do not allow a Region 3 for bubble formation or diffusion of ingredients in the condensed phase.

Region 3 is intended to encompass a variety of complex situations that are acknowledged to be important but usually neglected or represented artificially in analytical models. These are processes associated with phase change to liquid and/or gas. The energetics of such processes are often included in models as either homogeneous or surface heat absorption (phase change) or release (reaction). Analytical models rarely address the three-dimensional realities of growing bubbles; interfacial reactions between "melting" ingredients; subsurface decom-

position of one ingredient in the matrix of another, more thermally stable ingredient; or interdiffusion of one molten reactant into another. There are practical situations where one might expect each of these processes to be important. Some examples are the following:

1. AP-hydrocarbon binder propellants exhibit burning down the contact surfaces between oxidizer and binder when burning at pressures near or below one atmosphere, resulting in a Region 3 consisting of solid oxidizer, solid binder, penetrated by exothermally reacting interfaces in which as yet undetermined ingredient interaction-reaction processes release heat. At higher pressure the interface seems to be nonreactive, the binder exhibits a melt surface, and the AP self-deflagrates.
2. Various theories for combustion of HMX-HC binder propellants have been proposed, one of which (Ref. 4.___) has individual HMX particles burning ahead of the unreacted matrix, such that Region 3 would have a population of exothermic sites moving sporadically inward with hot gas and flow. Another source suggests (Ref. 4.___) that the HMX and the binder melt and mix on the surface and burn as a homogeneous surface layer, in which case Region 3 would be a melt-mixing region with possible bubble formulation. The apparently contradictory descriptions are probably related to real differences in behavior over the range of formulations and test pressures used.
3. Double base (NC/NG) propellants are usually relatively homogeneous, but the "leading edge" of the reaction wave quickly generates gaseous products, and Region 3 is an exothermic layer commonly called the "foam" zone (Ref. 4.___, 4.___). The undecomposed material softens to a viscous fluid, presumably populated by growing microbubbles. Near the surface, continued degradation of the melt is reported to leave a concentration of carbonaceous solid residue, which figures in arguments on how catalysts change burning rate (Ref. 4.___).

This diversity of behavior in Region 3 is belabored here because its importance to combustion behavior is widely acknowledged, but rarely embraced realistically in analytical models of combustion (partly because it would greatly complicate analyses, and partly because the processes are so difficult to measure that good guidance for modeling is lacking). Region 4 is ideally defined as the "burning surface", the interface between condensed and gas phase. In a one-dimensional model it is a plane that can be characterized by a single temperature and regression rate. Combustion models ordinarily treat the combustion zone as made up of a condensed phase region and a gas phase region, with appropriate (but different) conservation equations for each region. Boundary conditions are matched at the

"surface". this gives the surface a singular role in the analysis, and measured or calculated surface temperatures are conspicuous in discussions of theory. From the comments about Region 3, it is evident that the "surface" is almost never a plane with uniform state. Even the self-deflagration of a pure ammonium perchlorate crystal does not give a uniform planar surface (Fig. 4.9a), and surfaces of propellants are notable for their complex structure soon after they are extinguished and have time to release bubbles and settle down before freezing (Fig. 4.9b, c). It may be anticipated that the surface complexity implied by Region 3 will remain neglected in analytical models (especially nonsteady models), but notable efforts have been made to deal with specific aspects of such "non-ideal" behavior (Ref. 4.__ to 4.__) in cases where representation of such complications was considered crucial to useful modeling.

The nature of Region 5 is strongly dependent on the kind of propellant. With double base propellant (and pure HMX) this is a thin region in which continued exothermic reaction occurs (Fig. 4.6), effectively supplying heat to the underlying regions. In these systems, the temperature that is reached represents about 50-6% of the total heat release. The reaction products of this region are sufficiently stable so that further heat release is delayed to a more remote Region 8 of the combustion zone.

With AP propellants, Region 5 is an induction region of low heat release. Over areas of AP, this is a stand-off region (Fig. 4.10) for the AP monopropellant flame,* and is so thin (10 - 20 5m, Ref. 4.__, 4.__) that it has not been directly observed. Over and near areas of surface binder, Region 5 is a mixing region for oxidizer and fuel, a stand-off region for the O-F flame. Thus, with AP propellants, Region 5 is one of low heat release, culminating in AP and O-F flamelets. Being a thin region over a convoluted surface, it is not particularly visible.

Region 6 is defined here to accommodate the near-surface flames that occur with AP propellants. Over areas of AP, this corresponds to the AP self-deflagration flame noted above and described in Section 4.3. This region also accommodates primary O-F flamelets noted above (Fig. 4.10) that consume the oxidizer and fuel vapors that have mixed in Region 5. These flamelets are the leading edge of more extended diffusion flamelets in the mixing region remaining beyond Region 6. They are distinct from the extended flame in that they represent a near-surface concentrated combustion of oxidizer and fuel vapors premixed without reaction in Region 5. In addition, the primary flamelets in Region 6 are the flame holders for the more extended outer diffusion flamelets in Region 7, and their presence, position and heat release depend on a delicate balance of diffusion of species and heat, and of reaction kinetics for the oxidizer-fuel mixture.

The primary O-F flamelets described above may be important with other

* The AP flamelet may be absent at low pressures, or with very small AP particles.

heterogeneous systems, such as potassium perchlorate oxidized systems, but detailed studies are lacking. Current nitramine composite systems differ in that O-F vapor mixing does not set the stage for exothermic flamelets (because the nitramines are already stoichiometric).

Region 7 is a chemical induction region for many propellants, such as double base and some nitramine composite propellants. The region contains decomposition products such as NO, H2, CO and CO2, which eventually react to N2CO, CO2 and H2O in an outer flame (Region 8). The thickness of Region 7 for these propellants is strongly pressure-dependent (Fig. 4.3). The temperature is roughly ___o C. Because of this induction region, the high temperature outer flame does not contribute strongly to propellant burning rate. However, the pressure dependence of chemical induction processes probably makes the outer flame contribution more important at higher pressure, resulting in a relatively high dependence of steady state burning rate on pressure for those types of propellants. As will be seen later, this pressure dependence is a factor in the dynamic response to oscillations, but not the decisive contribution one might first suspect.

In composite propellants, Region 7 is one of continued diffusion of oxidizer and fuel vapors. Unlike the underlying regions, the temperature here is high enough to yield chemical reaction rates that are high compared to the diffusion rates. As a result, the reactions are concentrated in the mixing boundaries between microscopic outward moving oxidizer and fuel flows from the heterogeneous surface, yielding flamelets in these microscopic mixing fans (Fig. 4.10). Region 7 is thus populated by microscopic O-F flamelets, anchored to the primary flamelets in Region 6. The height of this region is dependent on the size of the heterogeneous surface elements (and corresponding mixing lengths in the diffusion field). In the case of AP propellants, the substantial heat release in these O-F flamelets and the moderate distance from the surface lead to a significant contribution to burning rate, larger when particle size is small. The pressure dependence of this contribution to burning rate is relatively low, because the diffusion-limited flamelet height is relatively insensitive to pressure. In the case of nitramine composite propellants, the O-F reaction is not energetic and, consequently, contributes little to heat flow to the surface and to the burning rate. In addition, the nitramine product flow may consist of only intermediate reaction products and Region 7 may still be a chemical induction zone followed by a high temperature secondary flame in Region 8. Details depend strongly on nitramine particle size, pressure, and type of binder.

Metal ingredients become fully inflamed in Region 7 with AP propellants, but are probably not yet up to speed with the gas flow and are still largely unburned. With double-base and nitramine propellants, complete inflamation of accumulations of aluminum is often delayed until entry into the high temperature of Region 8.

Region 8 is assigned here to the relatively concentrated stand-off flame fol-

lowing chemical induction and non-exothermic mixing in Region 7. The chemical induction-secondary flame process is moderately well understood in double base propellant combustion (Ref. 4.___, 4.___) and nitramine self-deflagration (Ref. 4.___), but its nature is more diverse and less well characterized for nitramine composite propellants because of the involvement of both surface and gas phase mixing of ingredients and product flows (Ref. 4.___, 4.___). However, it is clear that a stand-off secondary flame, similar to that with double base propellants, occurs with some nitramine composite propellants under some conditions (Ref. 4.___). This implies that the binder vapors can mix with the primary or intermediate vapor products of the nitramine without forming the diffusion flamelets characteristic of AP composites. The secondary flame in such cases is more nearly a pre-mixed, planar flame in Region 8.

Region 9 is defined here to accommodate the continued combustion on non-volatile reactants, such as metals, and intermediate products, such as carbon, that survive Regions 3 - 8 unreacted. In some propellants, a significant part of the heat release occurs in an extended region, which can include the entire volume of a small or low pressure motor. This is highly dependent on the details of the concentration-agglomeration of the reactants in Regions 3 and 4 (Ref. 4.___), processes that determine size of the slow-burning agglomerates in Region 9. It is also important to realize that the reaction products of aluminum combustion are Al2O3 droplets, which may constitute up to 40% of the reaction products. This can be the dominant source of damping of gas oscillations.

From the foregoing, it is evident that the character of the combustion zone can be quite different with different combinations of ingredients, particle sizes, and pressure of the combustion environment. Detailed understanding of the combustion processes is only qualitative and not well catalogued. Qualitative aspects are fairly well understood for double base propellants and AP composite propellants. The description presented above, in the context of Fig. 4.8, is contrived to fit a one-dimensional picture, partly as a means to address a complex and diverse array of substantially sequential processes, and partly to provide the framework for the one-dimensional models that are used to analyze combustion. It is important to understand that the gas flow in the combustion of a motor is not one-dimensional (sometimes the flow is modeled one-dimensionally, but, when it is, the dimension chosen is perpendicular to the dimension pictured in the combustion zone in Fig. 4.8). In other words, the combustor flow is usually parallel to the burning surface and may exert a shearing effect on a combustion zone such as that pictured in Fig. 4.8 - 4.10. This gives rise to the burning rate enhancement known as "erosive burning" in steady state and implies that the combustion zone is not the same under sheared flow conditions as it is when flow is simply outward from the surface. In oscillatory combustion, one should expect two kinds of effects from parallel flow:

a) The combustion zone that is oscillatory differs according to the mean

flow situation (and hence the location in the combustor and time during charge burning).

b) The gas oscillations will normally involve components of motion parallel to the burning surface so that the combustion zone experiences three-dimensional oscillations (the nature of which depend on location in the combustor and on the acoustic mode of the oscillation).

This situation will be addressed at length in this book, but it should be recognized at the outset that we are examining the interaction between a very complex combustion process and a very complex gas motion. Only if one understands the complexity of the real processes can one understand the degree of, or reason for, simplification used in analytical models, or recognize the limitations in their use and the needs for better experimentations, analysis and theory.

Binders. Propellants are held together by plastic-like binder materials, which are the connected part of the propellant matrix. Binders are also the fuel ingredient. They range in practice from hydrocarbon polymers, such as PBAN and HTPB, to polymers with energetic plasticizers, such as _____ and _____, to energetic polymers or colloids, such as NC/NG ("double base" binders). Propellants with energetic binders typically have a lower volumetric loading of oxidizer because the binder has more oxygen content, and because energetic binders are usually less suitable to high solids content from the standpoint of processing, mechanical properties, and hazard. The typical hydrocarbon elastomeric binders decompose endothermally in controlled heating experiments in the temperature range _____ to _____o C. There seems to have been very little study of the vapor species that result under rocket motor-like conditions. It is recognized that the initial mode of decomposition of a polymer molecule will involve bond-breaking in the polymer backbone in some polymers (e.g., _____), and breaking of bonds to pendant groups in other polymers (e.g., _____). In the controlled heating experiments, most of the hydrocarbon polymers soften to viscous "melts" in the _____ to _____o C range and bubble at from _____ to _____o C, with this temperature differing significantly for different polymers. In slow heating experiments, most of the test sample is decomposed by the time the temperature reaches ___o C (a sample DTA curve is shown in Fig. ___). The semi-liquid surface is observed also in combustion experiments, and residual evidence of a melt remains on the surface of propellant samples quenched from high pressure burning. In combustion modeling, it would be useful if the binder response to heating could be characterized by a one-step irreversible conversion to vapor products according to an Arhenius rate law. The available information suggests that pressure is more complicated, and that a search for appropriate values of activation energy and pre-exponential factor(s)??? for the rate law is of limited meaning.

Of the energetic binders, the nitrocellulose-nitroglycerin system has been the most studied. This energetic binder has been used as a monopropellant for the last

100 years, first as a gun propellant and then as the first satisfactory rocket propellant. At the molecular level it consists of two ingredients, NC and NG. In decomposition of the colloid, NG apparently evaporates in the ____ to ____o C range, and NC decomposition becomes important at ____o C.

Decomposition of NC is reported to start with rupture of O-NO2 bonds, and the activation energies obtained in some experiments are consistent with this. However, the initial reactions are in the condensed phase, as are some subsequent steps, and the rate of conversion to gas depends on this complex sequence of reactions and evaporation. When NG or other plasticizers are present, the reacting surface layer includes the evaporating plasticizer and the surface thus is a complex mixture of ingredients and intermediate products in a solution or froth. The NC decomposition is autocatalytic and exothermic, with its rate often strongly affected by additives used to either inhibit the autocatalytic reaction (for storage stability) or enhance reaction rates at elevated temperature to increase burning rate. During self-deflagration, the surface regression rate of different double base formulations are found to linearly dependent on the heat of reaction (Fig. ___), which can be varied by changing NC/NG ratio or by changing the degree of nitration of the NC. This correlation is believed to be due to the dominance of exothermicity of the reactions in the condensed phase-melt-foam layer, and the effect of composition variables on these exothermic reactions. Indeed, considerable success has also been achieved in modification of burning rate by catalysts that are thought to affect these reactions. The surface temperatures of self-deflagrating double base formulations are reported to be 320-400o C, with considerable uncertainty associated with the absence of a well defined and unambiguously located surface due to gas formation "in" the condensed phase. Temperatures determined by thermocouples traversed by the combustion zone show a very steep temperature rise (Fig. ____) to about ___o C in the gas phase, indicating exothermic gas phase reaction. After a further, more gradual temperature rise, a second steep temperature rise occurs to a final temperature of ___ to ___o C. The second steep temperature rise corresponds to a flame that is readily visible in experiments below 1.0 MPa. In fact, the flame stand-off distance is sometimes reported as a function of pressure (Fig. ___). While a large part of the heat of reaction is released in this stand-off flame, it is too distant from the surface to be a dominant factor in heat flow to the solid preheat region, except possibly through its effect on reaction rate in the primary exothermic region. However, the stand-off flame may be important to the transient combustion response, and to combustion of other ingredients when the propellant is used as a binder in composite propellants.

Metals. The principal metal ingredient in current propellants is aluminum powder. While there is no decomposition or decomposition(???) to relate to the present section title, it is important to note that most metals don't vaporize at the

temperatures of the propellant burning surface, posing the question of how the metal particles get away from the burning surface, and where do they burn? Since the particles emerge at the burning surface from a binder surrounding matrix location, they are in an often adherent binder melt. It is observed that metal particles concentrate to some extent on the surface (as do other additives, such as particulate burning rate catalysts). Aluminum particles are resistant to ignition because of a refractory Al2O3 coating on the particles. Combustion ordinarily takes place after detachment from the surface, often as agglomerates of large numbers of particles that were concentrated on the burning surface. Details will be discussed in the next section, but it should be kept in mind that metals (and all nonvolatile ingredients or intermediate reaction products) experience a complex concentration-agglomeration-sometimes ignition process on the burning surface that is strongly dependent on other propellant variables and on pressure. This process is responsive in its own unique way to flow oscillations and associated oscillations in other combustion zone processes.

4.5 GENERAL NATURE OF THE DYNAMIC RESPONSE OF COMBUSTION

When the stability problem can be posed as one of wave behavior in a combustion gas flow field with combustion concentrated at the propellant burning surface, one then seeks to determine how the concentrated combustion is affected by the gas oscillations. In a simple combustion like an end burning "T-Burner" (Fig. ____), the flow oscillations usually take the form of perpendicularly incident plane pressure waves reflecting from the burning surface, a situation that corresponds to simple one-dimensional motion. If the incident pressure wave is characterized by the amplitude of the pressure oscillation at the burning surface, then it is customary to define a "pressure coupled combustion response", R_p, which is

$$R_p = \gamma \frac{(m'/\bar{m})}{(p'/\bar{p})} \tag{4.1}$$

where m' and p' are mass and pressure oscillations about their mean values $\bar{m}$ and $\bar{p}$. It is assumed in the definition that m and p are sinusoidal oscillations, and found from both experiment and theory that m' (and hence R_p) depend on frequency of the pressure oscillation, p'. In addition, the oscillation m' is not generally in phase with p', a property that figures very strongly in the question of whether the combustion oscillation amplifies the pressure wave or not. Further, the phase is also frequency-dependent, so the response function R_p must contain information about amplitude and phase of m relative to p, both of which depend on frequency. The argument is easily express graphically as in Fig. ____a. The

figure shows a pressure wave that is reflecting from the burning surface, accompanied by a secondary pressure wave, induced by the fluctuation in mass rate from the surface. This secondary wave simply superimposes on the reflection of the incoming wave, strengthening it and shifting its phase. In stability analyses it is shown that the extent of strengthening of the pressure oscillation is determined by the component of the combustion-generated wave that is in phase with the primary (incident) wave (Fig. ___b), which explains why both the magnitude and phase of the combustion response are important. These conventions are represented formally by writing m' and p' as oscillating quantities, with

$$p' = P \cos \omega t$$
$$m' = M \cos \omega(t + \tau) \tag{4.2}$$

where τ is the time lead of m' relative to p', and $\omega\tau$ is the phase lead (which can be a lag, as in Fig. ___). Using a trigonometric identity, m' can be written as the sum of two sinusoidal components, one of which is in phase with pressure, and one 90 degrees out of phase

$$m' = M \cos \omega t \cos \omega\tau - M \sin \omega t \sin \omega\tau \tag{4. 3}$$

(see Fig. ___b). In stability analyses it is usually the in-phase (first) term above that contributes to amplification of the pressure wave (or suppression, depending on the value of τ). In stability analyses, the mass oscillation is usually represented by a complex variable

$$m' = M e^{i(\omega t + \theta)} = M[\cos(\omega t + \theta) + i \sin(\omega t + \theta)] \tag{4.4}$$

such that the real part (first term) is the component 90o out of phase with pressure. In that notation, Rp is the ratio of two complex variables, and is thus itself a complex variable with in-phase and out-of-phase components. It is intuitively evident that a large magnitude for Rp corresponds to the potential for strong amplification of pressure waves, especially if < is near zero so that the combustion oscillation is nearly in phase with the pressure. Under these conditions, when the pressure "pushes" on the combustion zone, the combustion zone "pushes back," producing a compression wave stronger than would be the case for a purely rigid reflecting surface. In practice, accurate stability analyses require that Rp of the propellant in question be known quantitatively as a function of mean pressure, oscillation frequency, and even condition of the mean flow field vs location on the charge burning surface. Then the contribution of each part of the burning surface must be determined and a summation of such contributions must be determined and a summation of such contributions must be made over the whole surface. For the end burning T-Burner mentioned above, this summation is easy because conditions are the same over the whole burning surface. T-Burners

were designed with this in mind, and are used to measure Rp (a subject that will be discussed more fully in Section ___).

The foregoing description of "combustion response" was designed to help the physical insight of the more casual reader, introduce some language concerning oscillatory behavior, and to lead the less casual reader into more complete treatment of the combustion response phenomenon in later sections. It is appropriate to close with two important points regarding the state of knowledge of combustion response. The first point is that neither theory or experiments provides us with values of Rp that are accurate enough for reliable stability analyses. The second point is that Rp is usually not a sufficient description of how the combustion responds to the complicated range of steady and oscillatory flow conditions present in the different locations in any one rocket motor.

———

Figure _____a

Sketch of an incident pressure wave reflected from a burning surface (shown for an instant in time). The dotted line shows a combustion-generated pressure wave is caused by the pressure fluctuation, that reinforces the original wave. Note that the combustion response wave (in the example) lags the original perturbing wave by a time, , distance, C, and phase, f.

Figure _____b

Sketch of part a on a larger vertical (pressure) scale. In addition to the combustion-generated wave, the dotted lines show the components of that wave in
phase with the incident pressure wave and 90o out of phase. In wave-mode instabilities it is the in-phase component that amplifies the incident pressure wave. When the oscillations are described by complex variables, this is the "real" part of the complex pressure variable.

4.6 DYNAMIC COMBUSTION RESPONSE

During steady state burning, a propellant establishes its own combustion zone structure. This structure is known to be dependent on pressure and gas flow environment because the mean burning rate depends on those "environmental" variables. Thus, it would be no surprise if the burning rate were found to oscillate if the pressure or flow environment were to oscillate. In fact, one might calculate the burning rate oscillations from pressure oscillations using the known dependence of burning rate on pressure (e.g., strand burning rate data). This would work at low frequency (e.g., 1 Hz), but one should not expect the burning rate to follow this dependence at high frequencies because the combustion zone cannot follow rapid changes imposed upon it from the outside. This can be understood by reference to Fig. 4.___, which shows the temperature profiles in the solid corresponding to two different burning rates (corresponding, for example, to two different pressures). If the propellant were burning at the higher rate, it would have a higher surface temperature (necessary for the higher pyrolysis rate), and a thinner heated layer. If the pressure were reduced very rapidly to a value corresponding to the lower rate in Fig. 4.___, the surface layer would initially react too rapidly for the new, lower pressure, until the surface cooled down to the new lower temperature corresponding to the lower pressure. During this time, the rest of the thermal profile would have to adjust to the new steady state profile, which has a higher heat content than the thinner high rate profile. The details of how this thermal accommodation comes about depend on how the heat supply (gas phase flame and surface reactions) is behaving during the transient (a large, rapid pressure drop will quench most propellants). During combustion instability, the oscillations in flow environment are so rapid that the details of transient response of the combustion zone become very important, and steady state rate dependences become relatively unimportant. As one might expect, the combustion zone oscillations then become functions of frequency which can be described only if the details of the transient behavior are considered. The result may be oscillations in mass flow rate, temperature, density and molecular weight in the outflow from the combustion zone. In the case of heterogeneous propellants, the response of different ingredients (e.g., AP, binder and aluminum) to oscillations in environmental variables will generally be different, resulting in very complex (interactive) oscillations that may include even oscillations in the complex surface geometry of the heterogeneous solid. The details of this complex oscillatory behavior are an object of ongoing study. For the present, we will address primarily the "global" consequences as viewed from the surface-averaged global response that produces combustor oscillations.

The Concept of Combustion Response Functions. We will consider first how one would represent the effect of pressure oscillations on the mass burning rate, because it is this aspect of the combustion response to combustor oscillations that is usually most important, and most fully studied. This will be an elaboration on the description in Section 2.5.

When the pressure oscillations of a particular frequency develop in a combustor, the pressure oscillations can be represented by

$$\frac{\hat{p}}{\bar{p}} = P e^{\alpha t} \cos \omega t = \left[P e^{\alpha t} e^{i \omega t} \right]^r \qquad (4.5)$$

where P is the amplitude of oscillation at some arbitrary time taken as $t = 0$, $e^{\alpha t}$ describes the rate of growth of amplitude of oscillations; and ω is the oscillation frequency in radians/sec ($\omega = 2$ f). The expression on the right is the description of the oscillation in complex variable notation, where the superscript "r" designates the real part. Complex variable notation is introduced here because it facilitates representation and analysis of oscillating quantities.

Under the influence of a pressure oscillation described by Eq. (4.___), the mass burning rate is observed from theory and experiment to oscillate according to

$$\frac{\hat{m}_b}{\bar{m}} = M e^{\alpha t} \cos \omega(t + \tau) = \left[M e^{\alpha t} e^{i \omega (t+\tau)} \right]^r \qquad (4.6)$$

$M e^{\alpha t}$ is the amplitude of oscillation, and $\omega\tau$ is the phase lead of the mass rate oscillations relative to the pressure oscillations. In the small perturbation theory for combustion response, $e^{\alpha t}$ is the same in both Eq. (4.___) and Eq. 4.___), and M/P is independent of time or amplitude, but depends on frequency, as does the phase lead $\omega\tau$.   can be expressed (using a trigonometric identity for $\cos\omega(t+\tau)$ as the sum of a component of the oscillation in phase with pressure and a component of the oscillation out of phase with pressure (with phase lead of /2 radians)

$$\frac{\hat{m}_b}{\bar{m}} = M e^{\alpha t} (\cos \omega\tau \cos \omega t - \sin \omega\tau \sin \omega t)$$
$$= \left[M e^{\alpha t} e^{i \omega (t+\tau)} \right]^r \qquad (4.7)$$

This can be written

$$\frac{\hat{m}_b}{\bar{m}} = RP e^{\alpha t} (\cos \omega\tau \cos \omega t - \sin \omega\tau \sin \omega t)$$
$$= R \cos \omega\tau \frac{\hat{p}}{\bar{p}}(t) + R \sin \omega\tau \frac{\hat{p}}{\bar{p}}(t - \frac{\pi}{2}) \qquad (4.8)$$

The quantity "R" is

$$R \equiv \frac{M}{P} \qquad (4.9)$$

The quantities R and $\omega\tau$ describe the relation of the sinusoidal mass burning rate oscillations to the pressure oscillations, and depend on frequency of oscillation, propellant composition, and the aspects of the combustion environment that affect the steady state combustion zone (e.g., mean pressure, propellant temperature). $R\cos\omega\tau$ is the ratio of the amplitude of the component of burning rate in phase with pressure to the amplitude of the pressure oscillation, and $R\sin\omega\tau$ is the ratio of the amplitudes for the out-of-phase component of $\dot{m}_b/\bar{m}$. These quantities, R, $\omega\tau$, $R\cos\omega\tau$ and $R\sin\omega\tau$ are the objects of many experimental investigations (Ref. 4.___, 4._____) and analytical studies (Ref. 4.___, 4.___, 4.____). For analytical convenience, the analyses are carried out in complex variable notation that leads to a complex "response function"

$$\Re = \Re^r + i\,\Re^r \tag{4.10}$$

in which

$$\Re^r = R\cos\omega\tau$$
$$\Re^i = R\sin\omega\tau \tag{4.11}$$

$\Re$ is a vector in the complex variable plane as in Fig. 4.___, in which Eq. (4.___) to (4.____) apply and hence

$$R = \sqrt{(\Re^r)^2 + (\Re^i)^2}$$
$$\omega\tau = \tan^{-1}\frac{\Re^i}{\Re^r} \tag{4.12}$$

The concept of the response function is better visualized by reference to Fig. ___. This shows a pressure coupled response function based on a specific analytical model (Ref. 4.___). The solid curve is the magnitude of burning rate response to pressure oscillations, i.e., R = M/P. The abscissa is a nondimensional frequency

$$\Omega = \frac{\kappa\omega}{\bar{r}^2} \tag{4.13}$$

The curve indicates that burning rate response increases with frequency up to a frequency = ____, and then drops off at higher frequency. The low frequency limit is the response that would be obtained if the burning rate followed the steady state dependence on pressure. The broken line in Fig. 4.____ shows the dependence of the phase, $\omega\tau$, of the burning rate oscillation on frequency. T ε low frequency limit is zero, as one would expect for steady state response. The phase increases (phase lead) with increasing frequency and then drops off through zero at the frequency for which R is a maximum. At still higher frequency the burning rate

oscillations lag the pressure oscillations (the details of these curves differ appreciably as a function of propellant formulation and as a function of parameters in analytical models). In combustor stability analyses, it is usually the product $R \cos \omega \tau$ (the real part of $\mathfrak{R}$, $\mathfrak{R}^r$) that determines the stability. This quantity can evidently be calculated as a function of or frequency from R and $\omega \tau$ in Fig. 4.___, and is shown as a dotted line in the figure. From the figure, it is evident that $R \cos \omega \tau$ is high over an appreciable range of frequency, giving a high probability that a combustor will have natural cavity modes with frequencies in this high response range that may exhibit combustion-driven oscillations.

Other Combustion Responses. The concept of a response function was developed in some detail in the foregoing in terms of the response of the mass burning rate to pressure oscillations. It is important at this point to recognize that there is more to the dynamic combustion response than simply mass rate oscillations induced by pressure oscillations. It was noted in Section 2.5 that oscillations in gas density, temperature and molecular weight in the outflow from the combustion zone will also affect the outflow velocity and hence the combustion zone admittance. In addition, oscillation in these properties of the outflow may be induced by attributes of the combustor gas oscillations other than (or in addition to) pressure (e.g., "shearing" oscillatory motions parallel to the burning surface). Each of these responses may be characterized by a response function. In addition, with heterogeneous propellants, the burning surface may be made up of different areas that consist of different ingredients that exhibit different dynamic responses. Thus, there are response functions for mass rate, temperature, and molecular weight reflecting responses to pressure oscillations, shearing gas oscillations, turbulence oscillations and radiation oscillations, all of which may sometimes have to be classified according to the local sites on the burning surface. In current literature, the symbol $\mathfrak{R}$ usually refers to mass rate oscillations; and a subscript p usually refers to response to pressure oscillations, a subscript v usually refers to response to a component of combustor gas oscillations parallel to the burning surface. As stability analyses become more detailed, a double subscript may be used as $\mathfrak{R}_{m,p}$, to designate pressure coupled mass burning rate response, etc. The response function theory is currently in a state of evolution, based on new understanding of both combustion zone structure and of the mean and oscillatory gas motions in the region of the combustor where the combustion zone is located. These subjects will be developed more fully in later chapters.

Some experimental results have led to speculations that combustion may be spontaneously oscillatory, either independent, or only weakly dependent on gas oscillations in the combustor. The evidence for this is primarily in increased tendency for combustor oscillations at rather specific frequencies (which usually are dependent on pressure). The same kind of behavior would be expected if the response functions were more peaked than in Fig. 4._____, so that fully spontaneous self oscillation could only be demonstrated by observation of the oscillations

in the absence of flow oscillations. To date, this does not appear to have been done except with samples consisting of dry-pressed mixtures of ammonium perchlorate and aluminum (Ref. 4.___, 4.___). Such behavior is predicted by one dimensional response function models under certain extreme conditions. Some authors, led by speculations about spontaneous oscillations, have postulated that this may be due to periodic variation in properties of the propellant in layers parallel to the burning surface, and have analyzed the corresponding combustion behavior. However, spontaneous oscillations remain to be demonstrated (with the exceptions noted above), as has the layered composition that was proposed to explain them. The nearest thing to spontaneous oscillatory behavior in combustion that has been reported for a propellant appears to be the "preferred frequency" oscillations reported in Ref. 4.____ for a double base propellant containing a powdered aluminum-magnesium alloy as a fuel additive. The combustion of the metal in this propellant apparently tended to be periodic as in the case of AP-AL tests noted above. It was noted in Ref. 4.___ that ith any propellant tested to date, spontaneous oscillatory behavior, if it occurs at all, would tend to be randomly phased over the burning surface, and that the coherent oscillations necessary to produce combustor oscillations would require some degree of responsiveness of the combustion to combustor oscillations.

FIVE

ANALYTICAL MODELING OF COMBUSTOR FLOW

Newton's derivation of the velocity of sound was an achievement of genius. His calculated value, however, was about 20 per cent lower than the experimentally derived estimates. Having learned these experimental values, Newton decided to make further assumptions that would take care of the discrepancy. How did Newton arrive at the numerical values for his assumptions? He had no factual basis for them; he did not have data to show that air contained 10 per cent water vapor; he could not have known that particles of air were solid. These were unknown parameters. Though Westfall bluntly states that making these assumptions was 'nothing short of deliberate fraud'; my opinion is that making mathematical approximations in an intractible problem is actually the best that can be done to show that a theory is feasible at all.

Alexander Kohn, 1986 (from False Prophets)

5.1 INTRODUCTION

This chapter provides a detailed mathematical description of the environment inside a rocket motor combustion chamber during periods of organized pressure fluctuations. At least as much past effort has gone into the construction of mathematical models as has been expended on experimentation with combustion instability. This is because it is vitally important to have an organizing framework available for the interpretation of complex empirical observations. The procedures for construction of such a framework will be undertaken herein. In this process we will identify numerous flow problems that must be treated in depth individually for later assembly into a complete system description of the time-dependent behavior of a rocket internal gas flow.

The principal goal of mathematical modeling of the type presented in this chapter is to illuminate the physical and chemical origins of the combustion instability problem. The main application for such models is in the correlation and interpretation of experimental findings. A goal that has not yet been fully attained is a general analytical model capable of a predictive as well as an interpretive function. The material to be covered provides the framework within which such models can be assembled. Later chapters are devoted to more detailed treatment of specific parts of the combustion instability analysis.

It will be necessary to address both steady and unsteady features of the flow field, since the latter cannot be properly analyzed without an adequate representation of the steady-flow field upon which it is superimposed. Therefore, considerable attention will be paid to a proper treatment of the mean flow and its coupling to various oscillatory phenomena. The composite system problem thus posed must be among the most difficult yet addressed in contemporary fluid mechanics.

This difficulty comes from the need to treat many interacting physical and chemical phenomena simultaneously. We must mathematically represent:

- Time-dependent release of chemical energy in a combustion zone of finite size.
- Heat-transfer effects across at least two phases (*eg* solid to gas).
- Viscous, compressible, time-dependent (possibly turbulent) flow bridging the region of heat release and the main combustion chamber volume.
- Complex chamber boundaries changing in size and shape with time.
- Multi-phase gas flow containing solid or liquid particles of transient size and shape.
- Multiple sources or sinks of energy capable of exciting or damping natural unsteady gas motions of several types.

Since the present state of understanding has been built on approximate methods of analysis, much of the discussion in this chapter will follow the classical approach. However, recent advances in development of reliable computational algorithms for solving complex internal flow problems will likely lead eventually to the routine application of such tools in combustion instability problems. Even if such numerical tools were available now and were economically practical, there is much to be gained by a study of the approximate solutions. The physical insight that accompanies a thorough understanding of these results is a great benefit in constructing and interpreting more complete and accurate numerical solutions. Obviously, such insight is also necessary in the interpretation of experimental findings and in the formulation of practical corrective procedures.

The material in this chapter is built upon the efforts of many investigators. No attempt is made either to follow precisely the approach of any one school of thought or to treat the material in historical order. Rather, the authors have followed their own biases in selecting and presenting the material in as logical and accessible a form as possible. Reference will be made continually to an extensive list of previous works for the benefit of those interested in tracing the origins of the ideas and techniques employed herein

Plan for Chapter 5

The main goal of this chapter is construction of an organizing framework for the analysis of rocket motor combustion instability by means of an interlocking set of flow field models. The topics that will be addressed are:

1. Formulation of governing gas-phase equations
2. Linearization of equations using perturbation methods
3. Steady-state combustion chamber flow field solutions
4. Small-amplitude unsteady (acoustic) solutions
5. Effects of chamber geometry on simple unsteady solutions
6. Superposition of simple solutions for representation of more complex gas motions such as steep-fronted traveling waves

The resulting basic analytical formulations will be used singly and in combination in later chapters as the basis for detailed discussions of oscillatory behavior of solid rocket motors.

A qualitative description of several major flow field elements is first undertaken to establish the set of models needed to handle the composite mean/ unsteady-flow problem. All basic physical assumptions and their limitations are assessed. Areas demanding further study are identified in this process.

A useful simplifying step is the separation of the analysis into steady and time-dependent parts. This is based on the observation that fluctuations often appear as small perturbations on an otherwise steady mean flow field. The nature of the oscillatory behavior, especially its tendency to grow or decay, is influenced directly by the mean flow on which it is superimposed. Most of the coupling mechanisms that provide the path by which driving energy flows into a growing pressure wave are tied to the mean chamber flow. It is therefore necessary to pay particular attention to modeling of the steady-flow component.

Effects related to the mean flow are introduced by means of a set of example formulations each progressively encompassing more realistic representations of the geometry and boundary conditions. This is followed by a detailed formulation of the basic oscillatory combustion problem itself. The complex processes in the combustion zone are reduced to a time-dependent boundary condition at the propellant surface. Other boundary conditions such as those at inert chamber surfaces and in the nozzle entrance are also considered. Consideration is given to incorporation of turbulent flow effects.

Attention is directed to several energy sources and sinks which, taken as a system, determine the stability of a given rocket motor. In addition to the classical pressure-coupled energy transfer between wave motions and the combustion process, one must account for the possibility of velocity coupling effects in which the oscillatory motion of the gas particles generates a coupling effect. Some such effects are shown to be inherently nonlinear, and care must be taken in their representation in a linearized formulation. It is also necessary to incorporate interactions with natural instabilities of the chamber flow field. Regions of strongly sheared flow are subject to hydrodynamic instability or periodic "vortex shedding" that may couple with the acoustics of the motor chamber.

In this chapter emphasis is placed on traditional analytical methods such as acoustical modal analysis, Fourier series expansions, and perturbation methods since numerical assaults based on modern computational fluid dynamics have not yet reached a stage of development sufficient for their routine use even in the mean flow calculations. This situation will surely change as Class VII (Cray, etc.) computer access becomes more readily available to workers in combustion instability and as appropriate numerical procedures and modeling approaches are further developed. A special section is devoted to a discussion of the requirements for such future numerical investigations.

5.2 DESCRIPTION OF COMBUSTOR FLOW

This section presents a qualitative description of the flow field in a generalized rocket combustor. Its purpose is to highlight several elements of the field that will be treated as separate analytical models. It describes the nature of each basic element of the flow field and the relationships between them. This somewhat arbitrary separation into regimes of flow represents a strategy to break the extremely complex fluid dynamics formulation into more readily treatable elements. There are dangers inherent in this separation process. It is emphasized throughout this chapter that interactions between each regime are quite extensive, even to the point of rendering some widely accepted concepts as highly suspect. Areas requiring further work or special interpretation are identified.

General Description of a Rocket Motor Flow Field

The flow field inside a burning solid propellant grain can be described in terms of zones as illustrated in the several parts of Figure 5.1. The main volume of the burning port will usually be referred to as the "chamber". It will be shown later that, except in unusual situations and in the vicinity of the high-speed part c^f the nozzle entrance and expansion flow, the steady part of this field is essentially incompressible in nature.
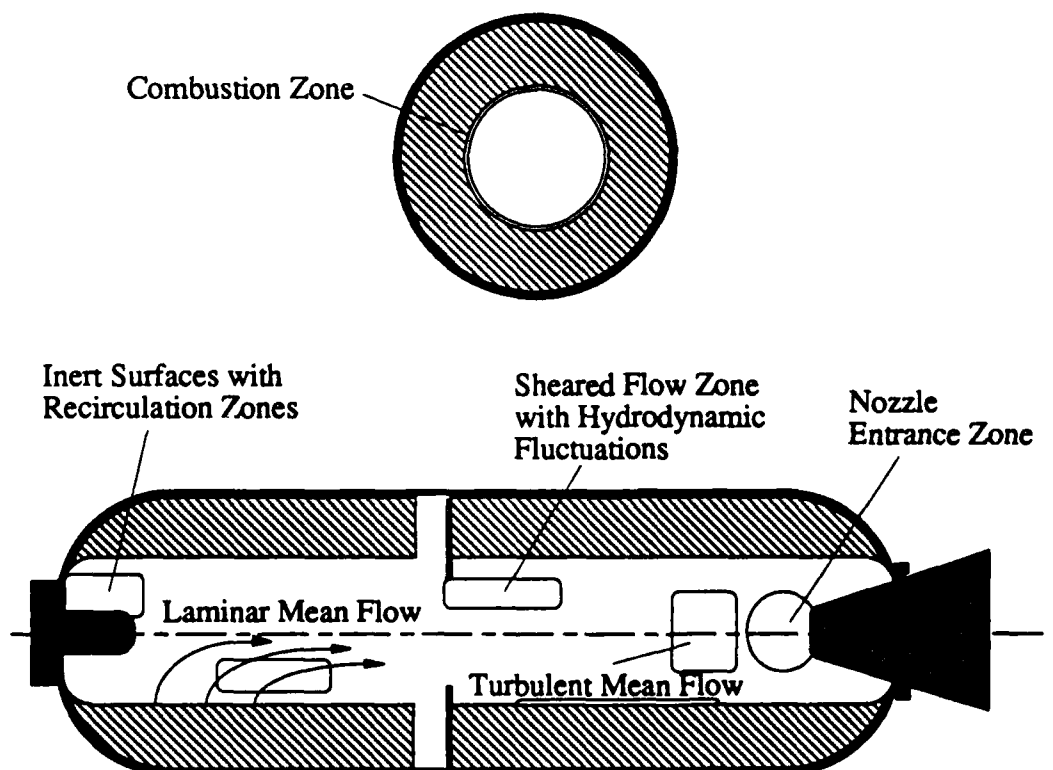

Figure 5.1 Definition of Flow Zones in Rocket Motor Combustion Chamber

In many cases the steady-flow component is also laminar within a significant portion of the volume. In motors with a sufficiently long combustion chamber or with sufficiently small port-to-throat area ratio the flow becomes fully turbulent as it approaches the nozzle end of the channel. The location and geometry of the transition zone depends critically on the motor grain configuration and the propellent burning-rate. The turbulent fluctuations themselves may affect the nature of the combustion processes locally in the form of "erosive burning." They may also affect the response of the burning surface to organized pressure fluctuations.

Gas flow is generated at the surface of the burning propellant in the combustion zone as described in Chapter 2. As already discussed, in many cases this zone can be assumed to have negligible thickness compared to the other dimensions of the chamber. The combustion region consists of a very complex set of interacting physical processes dominated by release of chemical energy and rapid changes of phase. Although usually neglected in mathematical models of the type described earlier, viscous flow effects can play an important role in this zone. For example, the viscous "no-slip" condition, requiring that the gas evolved in the combustion process enters the chamber in a direction perpendicular to the instantaneous solid surface, can affect both the steady and unsteady fields. The shear stresses give rise to several important phenomena such as the "flow-turning" effects, which must be accounted for instability calculations. The need to treat the multi-dimensional, compressible, viscous behavior of the gas flow in the burning zone is a controversial subject that will be discussed in more detail later. Another aspect of this zone that has not received adequate attention is the behavior of solid particulate material evolved in the combustion of metallic propellant additives and their interaction with the other physical and chemical processes present in the combustion zone.

A boundary region that is often neglected in internal ballistics and stability calculations is that located at nonburning surfaces such as exposed chamber walls. Of special concern are surfaces that protrude into the main flow field or form cavities or depressions in the flow channel. These can be sites of sheared mean flow, which may give rise to hydrodynamic flow instabilities that can modify the overall unsteady energy balance of the system. This is a well-known mechanism for transfer of energy from a mean flow into a superposed acoustic field. It has only recently been incorporated into the treatment of unsteady rocket flows.

Intersections between slots or conocyls in the propellant grain itself or rapid changes in the burning port cross-sectional area can also generate local free shear layers. Regions of highly sheared flow are inherently unstable and tend to produce organized large-scale vortex structures. Such vortices usually grow rapidly in both size and strength in the downstream direction and are often strongly coupled to the chamber acoustic field. There may be "pairing" of adjacent vortices and an eventual breakdown of the organized structures with an associated contribution to the turbulent characteristics of the flow stream. Vortices some-

times directly affect the acoustic energy balance as volume quadrupole sources as in the classical jet noise phenomenon (Flandro 1986; Lighthill 1952), or may release significant acoustic energy via the more powerful dipole mechanism (Flandro 1986; Rockwell 1982) as they interact with downstream obstacles, solid boundaries or chamber surfaces such as the nozzle entrance. Vortices may also interact locally with elastic features at the chamber boundaries resulting in flutter or other flow-induced vibrations. These motions may in turn couple to the chamber acoustic field to form yet another path by which energy is transferred from the mean flow into acoustic fluctuations.

Recirculation regions can be formed in the parts of the chamber bounded by solid walls where adverse pressure gradients may arise. As suggested in Figure 5.1, the volume behind a submerged nozzle is especially likely to exhibit recirculation vortices. These flow patterns can have significant influence on the local heat-transfer and must be accounted for in surface insulation design. They may also influence the oscillatory behavior of the system, but such possibilities have not been explored in depth.

Finally, the gas flow must exit the chamber through one or more choked nozzles. The flow field in the approach to the nozzle entrance is dominated by compressibility effects. The influence of this part of the chamber on the overall unsteady energy balance requires special attention.

Clearly, an integrated study of the complete chamber flow field is required if these many fluid and chemical phenomena are to be linked in a system analysis of time-dependent rocket operation. The major goal of this chapter is to construct an appropriate analytical framework describing these interlocking features of the gas flow. Later chapters will address the detailed analyses necessary to build a complete system model.

Formulation of the Rocket Motor Internal Flow Problem

The fundamental equations governing the flow of combustion gases in a rocket chamber are now described. These follow standard practice in fluid dynamics and are based on a continuum field description of the gas. For the present, only the gas phase will be displayed in detail. Effects of two-phase mixtures involving the interactions of solid particles produced in the combustion process with the gas flow will be included symbolically for later elaboration.

The combustion products will be modeled as an ideal gas although this may be inappropriate in parts of the problem dominated by release of chemical energy. The compressible Navier-Stokes equations will be used to represent the gas dynamics, but full use will be made of boundary-layer approximations and other simplifications where appropriate. As in any gas dynamic modeling problem, it is necessary to make frequent (but judicious) use of approximations in order to make progress (see the quotation at the beginning of the chapter). A main goal of the following material is to provide justification for these approximations as they appear in the analysis. Emphasis is placed on modeling of the chamber gas flow

itself. No attempt will be made to carry along the complete set of relationships representing chemistry and multiphase flow effects. Inclusion of these important elements will be accomplished latei as the details are gradually elaborated using the basic formulation as the framework for the analysis.

With the above considerations in mind, we set out to formulate the fluid mechanics of the rocket motor flow problem. Here, and in all subsequent discussions, full use is made of vector notation to keep the presentation as concise as possible. A detailed table of the nomenclature will be found at the end of the chapter. For the most part, standard fluid mechanics notation will be used. Bold-faced type indicates vector quantities. Steady or slowly changing components will be represented by capital letters; oscillatory quantities will be written in lower case. It will be necessary to distinguish between several types of oscillatory flow components. Thus, special symbols will be introduced as required. For instance

numerical superscript $\mathbf{u}^{(1)}$ denotes oscillations of any type of order indicated by the number in parentheses

prime $\mathbf{u}'$ denotes acoustic (compressible, irrotational) fluctuations

tilde $\tilde{\mathbf{u}}$ denotes hydrodynamic (incompressible, rotational) fluctuations

It is always useful to employ dimensionless variables in the general formulation of the problem. This is done for several reasons. Of greatest importance is the emphasis that it places on similarity parameters such as Mach number and Reynolds number that appear naturally in the analysis. Their presence greatly assists in the process of assessing appropriateness of simplifying assumptions for the several flow regimes. A set of dimensionless variables is now defined that fits the needs of the general combustion instability problem. It will be necessary to justify these definitions and to modify several of them in later chapters to accommodate more complex situations. For now, it is sufficient to use the following:

$$r = \frac{r^*}{L} \qquad t = \frac{\bar{a}}{L}t^* \qquad \rho = \frac{\rho^*}{\bar{\rho}}$$

$$u = \frac{u^*}{\bar{a}} \qquad P = \frac{P^*}{\bar{P}} \qquad T = \frac{T^*}{\bar{T}} \qquad (5.1)$$

where overbars indicate reference values of the principal thermodynamic variables (dimensional) defined at a convenient point in the combustion chamber (at the forward .d stagnation point, for example), and stars denote the dimensional variables. L is a convenient reference length such as the radius, R or length, L of the combustion chamber. Velocities are normalized with respect to the speed of sound $\bar{a}$ since it is anticipated that fluctuations of the acoustic type will be of primary interest. It is important to understand at the outset that other types of oscillatory behavior may appear. Both hydrodynamic and thermal fluctuations may accompany and interact with the acoustic waves. We will see later that it is absolutely necessary that these other time-dependent effects be accounted for if the system boundary condtions are to be properly accommodated.

The basic formulation is based on the standard equations for the time-depend-

ent motion of a compressible, viscous gas. Conservation of mass, momentum, and energy require that

$$
\begin{cases}
\dfrac{\partial \rho}{\partial t} = - \nabla \cdot \rho \mathbf{u} \\[2mm]
\rho \dfrac{D\mathbf{u}}{Dt} = - \dfrac{1}{\gamma}\nabla p + \mathbf{F} + \dfrac{1}{R_e}\left[\dfrac{4}{3}\nabla(\nabla \cdot \mathbf{u}) - \nabla \times \nabla \times \mathbf{u}\right] \\[2mm]
\rho \dfrac{DT}{Dt} = \dfrac{(\gamma - 1)}{\gamma}\dfrac{DP}{Dt} + \mathbf{F} \cdot \mathbf{u} + \dfrac{1}{R_e P_r}\nabla^2 T + \phi \\[2mm]
P = \rho T,
\end{cases}
\tag{5.2}
$$

where $\mathbf{F}$ is any reaction force. For example, $\mathbf{F}$ will be used later to represent the force exerted on the gas by a superimposed cloud of solid or liquid particles to account for metallic oxide particulates formed in the combustion process. ϕ is the energy dissipation function. R_e is a Reynolds number based on L and the reference chamber speed of sound. P_r is the Prandtl number.

The fourth equation represents an appropriate constitutive relationship between the several thermodynamic variables. To fix ideas, the ideal gas equation of state is displayed here although there are cases in which its use might be inappropriate. For example, it might be necessary to adjust for the effect of particulate matter in a two-phase gas flow on the gas constant. Heat-transfer and combustion heat release are displayed only symbolically at this point in the analysis. The full compressible Navier-Stokes viscous effect and corresponding dissipation terms in the energy equation are not written out in detail in equations 5.2. In fact, they are seldom used in combustion instability analyses since the inviscid assumption is invoked in the vast majority of cases. We will have cause later to question such assumptions, and a careful assessment of the role of viscous effects will be made. Also, the symbolic form of the total acceleration

$$
\frac{D\mathbf{u}}{Dt} = \frac{\partial \mathbf{u}}{\partial t} + \mathbf{u} \cdot \nabla \mathbf{u}
\tag{5.3}
$$

will often be used in the momentum equation for simplicity. It must be remembered that the general form

$$
\frac{D\mathbf{u}}{Dt} = \frac{\partial \mathbf{u}}{\partial t} + \nabla\left(\frac{\mathbf{u} \cdot \mathbf{u}}{2}\right) - \mathbf{u} \times \nabla \times \mathbf{u}
\tag{5.4}
$$

must be substituted if the coordinate system required in evaluations is other than a simple cartesian one.

Other fundamental fluid flow equations may also be necessary later. For example, the angular momentum equation and the second law of thermodynamics will be invoked in special situations where they are needed.

Separation of Steady and Unsteady-flow Components

A simplifying step that is often employed in the analysis of the rocket motor internal ballistics is separation of the flow into steady and unsteady parts. It is convenient to assume that presence of oscillations in no way affects the mean (steady) flow field. Many early analyses also neglected the direct influence of the mean gas stream on the unsteady part of the flow. Neither of these assumptions is appropriate, as we shall demonstrate from both experimental data and from the fundamental analyses.

However, it is useful to treat the steady and unsteady problems as distinct *coupled* elements of the complete description of the flow field. Thus we shall write for the velocity vector at any point in the motor chamber

$$u = U + u' \qquad (5.5)$$

where U is the steady or "mean" flow. Primed quantities represent superimposed fluctuations. This scheme quickly breaks down as more detail or effects of nonlinearities are introduced into the analysis. For example U may contain sheared zones that can produce time-dependent hydrodynamic instability or vortex shedding. Similarly, there may be circumstances in which interactions between parts of the unsteady field may contribute to the overall steady-flow. For example, in certain cases intense fluctuations can generate steady zonal secondary flows known as "acoustic streaming". Despite such complexities the separation implied by (5.5) is very useful in breaking the analysis into digestible pieces. This method is demonstrated in the next section in determining the steady rocket flowfield.

It may be surprising to find a rather complete treatment of the *mean flow* problem in a text devoted to time-dependent gas motions. However, we will show that a detailed knowledge of the mean flow is an essential prerequisite for a successful assault upon the time-dependent flow problem. Also, study of the mean flow will allow us to point out many of the pitfalls and theoretical limitations that will become even more important in the combustion instability calculations.

5.3 MODELING OF THE STEADY FLOW FIELD

Many rocket motor gas flow analyses used in motor design are based on the assumption of a one-dimensional flow. This is adequate in most cases for layout of the basic propellent charge geometry and for motor performance estimates. A simple one-dimensional approximation for the steady-flow in the motor chamber is not adequate if precise information about the motor combustion stability characteristics is needed (Culick 1966). Stability computations require detailed knowledge of the dynamics the internal flow since the fluctuating energy gains and balances are very sensitive to its geometry. We need detailed streamline information and velocity distributions as will become apparent in Section 5.4.

At the time of writing, there exist no universally accepted and proven methods for representing the three-dimensional internal flow field in a rocket. Several computational m~ ⎽ds show promise in generating the required information, but they are quite sp . :ed in nature and expensive to use. Until more work has been accomplishⳑ ⹁ this area, resort will be made to approximate solutions. However, simple approximations are of great value as a means for gaining physical insight, and for verifying more detailed numerical results. Several simple models of considerable utility in representing the steady-flow are constructed in this section. In this process, the approach needed for generating a detailed three-dimensional mean flow model will become apparent.

The steady, compressible, axiall᷍ symmetric flow of an ideal gas is governed by the equations des ⹁ibed in the previous section. Inserting (5.5) into the continuity, momentume equations yields the basic mean flow formulation. In dimensional form,

$$\nabla \cdot \rho \mathbf{U} = 0 \tag{5.6}$$

$$\nabla \frac{\mathbf{U} \cdot \mathbf{U}}{2} - \mathbf{U} \times \nabla \times \mathbf{U} = - \frac{\nabla P}{\rho} + \nu \nabla^2 \mathbf{U} \tag{5.7}$$

where ν is the kinematic viscosity coefficient, $\nu = \mu/\rho$. Since there are no general solutions for this set, it is necessary either to make additional simplifications or to resort to purely numerical strategies. An additional assumption that the effects of viscosity are everywhere negligible is routinely made in rocket motor analyses. This assumption will be carefully examined since its time-dependent analog will be shown to be of crucial importance in the combustions instability problem. If valid, it greatly simplifies the problem by making it unnecessary to utilize the energy equation explicitly since the latter collapses to the familiar isentropic flow relationship. It is also often assumed that the mean flow is incompressible. This is valid everywhere but in the nozzle entrance region or in the aft part of a very long motor grain or in tactical motors with small port-to-throat ratios. In the vast majority of situations, the mean flow Mach number in the motor port is everywhere less than, say, $M_b = 0.2$ and use of an incompressible formulation is completely justified.

Before proceeding, it is appropriate to discuss the prevalent feeling that viscous forces are unimportant in the rocket chamber mean flow. A feature of the flow is that gases evolved in the burning process must leave the propellant in a direction perpendicular to the local orientation of the surface. This is the familiar "no-slip condition" that is invoked as a boundary condition on solid surfaces in viscous flow situations. In other words, viscous forces must be present to justify the normal flow boundary condition. However, unlike the usual hardwall boundary-layer case, the transport of mass from the burning propellant results in convection of the vorticity generated by viscosity at the burning surface into the chamber. Therefore the usual diffusive mechanism that leads to thin boundary-layers is of secondary importance. The effective "boundary-layer" thickness can be of the order of the chamber reference length L. Since associated viscous forces are proportional to the normal gradient of the axial velocity vector, they may

indeed be negligible under certain conditions to be discussed. However, this simplification has often been generalized to the extent that important modeling errors have resulted. In the examples presented in this section, careful attention will be paid to convection and diffusion of vorticity produced at the propellant surface. This will provide useful guidance for our later study of the time-dependent part of the chamber flow.

Figure 5.2 illustrates several boundary configurations that must be treated in rocket motor mean flow analysis. Whether or not viscous forces are negligible depends entirely on the geometry of the flow chamber. Figure 5.2a illustrates conditions at the burning surface of a tubular rocket grain. Vorticity generated at the burning surface is immediately convected to completely fill the chamber volume. Thus the normal velocity gradient and hence the shear stresses are small and viscous forces may be ignored. Figure 5.2b shows a case involving a chamber with a head-end propellant web. In this situation, the gas flow from the sidewall does not penetrate as deeply into the chamber volume, and a highly sheared flow results. Clearly, viscous forces may not be negligible in this case. Figure 5.2c is a reminder that viscous effects are not negligible at non-burning parts of the chamber boundary.

Based on the observations of the last paragraph neglect of viscous effects may appear admissible at least outside of boundary-layers in the immediate vicinity of the propellant and inert bounding surfaces. We will now investigate this situation with great care, because an analogous but even more complex set of questions will arise later in treatment of the unsteady problem. Important hints for handling the fluctuating case will be found in our study of the steady-flow.

As in the analogous external aerodynamics problem, it is often useful to separate the treatment of the viscous and inviscid regions of the flow. The resulting flow models must be carefully matched together at a later stage. The reader should keep carefully in mind the need to treat similar questions in the time-dependent problems that we must address later.

One-Dimensional Mean Flow Approximations

Much rocket motor design is based on the assumption that the flow is one-dimensional. That is, only axial variations in flow speed and properties are important. This is a familiar approach that is elaborated in text books on gasdynamics (Anderson 1982; Liepmann and Roshko 1957; Shapiro 1953). Most of the information is garnered from a simple mass balance for the chamber. In control volume form, the steady mass and momentum balances are conveniently expressed as

$$\int_S \rho U \cdot n dS = 0 \qquad (5.8)$$

$$\int_S \rho U U \cdot n \, dS = \sum F \qquad (5.9)$$

where the surface integrals are over a control volume bounding the gas within the
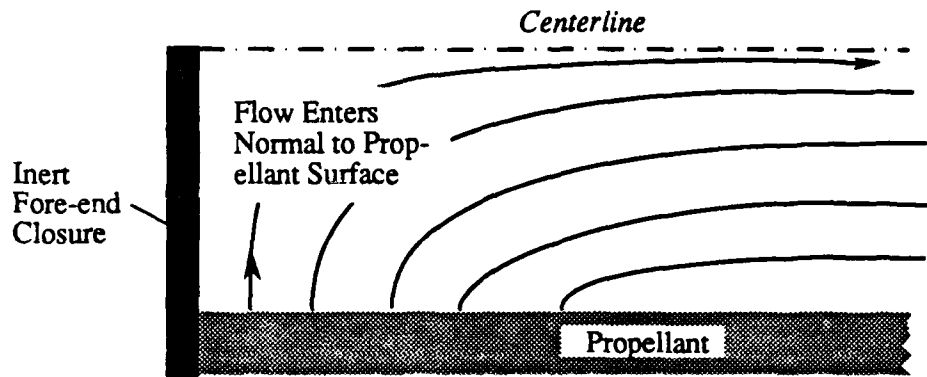
(a) Flow from sidewall only. Vorticity
spreads throughout chamber
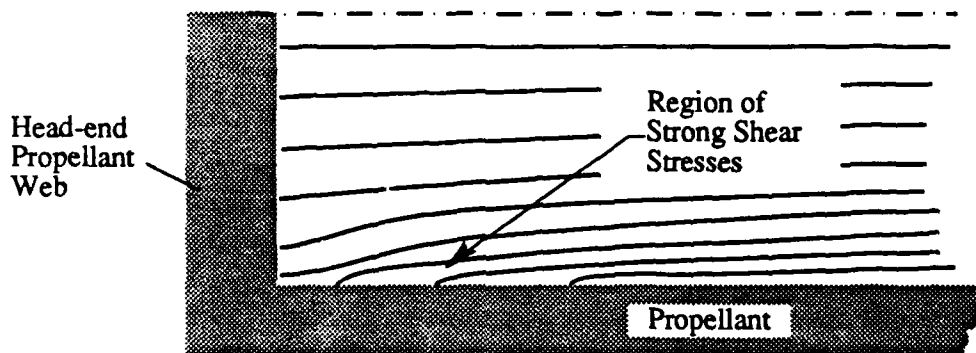
(b) Effect of head-end web. Vorticity is entrapped
within narrow region near side burning surface.

(c) Inert sidewall. Vorticity is generated within
and confined to a thin boundary layer at wall.

Figure 5.2 - Effects of Boundary Conditions on Mean Flow Features

chamber. The mass balance gives

$$\rho_p \, r \, C \, dz = \rho \, A \frac{dU}{dz} + \rho \, U \frac{dA}{dz} + A \, U \frac{d\rho}{dz} \tag{5.10}$$

where the three derivative terms express the effects of acceleration, duct cross-sectional area, and density changes. The term on the left represent the mass flux into the control volume due to generat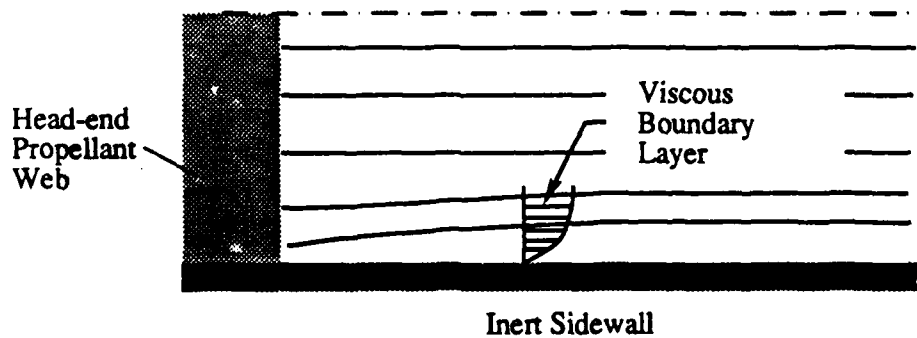ion of gases in the combustion process, r is the burning-rate (length per unit time) of the propellant, ρ_p is the propellant density, and $C(z)$ is the circumference of the duct.

For the simplest case of a cylindrical duct with constant cross-section and incompressible flow, this expression is easily solved to give the axial velocity variation along the burning port. Assuming the origin is located on an inert surface, the result is

$$\frac{U}{v_b} = 2 \frac{z}{R} \tag{5.11}$$

where R is the chamber radius and

$$v_b = \frac{\rho_p}{\rho} r$$

is the normal gas inflow velocity at the burning surface. Thus the flow velocity increases linearly along the duct. The pressure variation is found by using the momentum equation (which is equivalent to Bernoulli's equation in the present case of steady, incompressible, irrotational flow) with the simple result

$$\frac{p}{\bar{P}} = 1 - 2 \frac{\rho}{\bar{P}} \left(v_b \frac{z}{R} \right)^2 = 1 - 2\gamma \left(M_b \frac{z}{R} \right)^2 \tag{5.12}$$

showing that the pressure variation is a quadratic function of axial position and mean flow Mach number at the burning surface. $\bar{P}$ is the head-end stagnation pressure. Except in unusual situations (eg. low port-to-throat or very high burning-rates), mean pressure, density, and temperature changes in the burning port are negligible. Figure 5.3 shows typical pressure variations indicating the sensitivity to the mean flow Mach number. For a Mach number of 0.001, the mean pressure decreases by only about 3% from its value at the head-end in a distance 25 times the motor diameter. On this basis, $\bar{P}$ (as well as $\bar{T}$ and $\bar{\rho}$) will often be taken as constant in later analyses. That is, the mean rocket motor flow is adequately represented as an incompressible fluid as already assumed. This is the result of the low value of M_b, which is typically in the range

$$10^{-3} < M_b < 10^{-2} \tag{5.13}$$

and the axial pressure variation depends on the square of the mean flow Mach number.

Axisymmetric Mean Flow Solutions

To further investigate the consequences of neglect of viscous effects, we will analyze several examples of flow in axially symmetric motors. Considerable
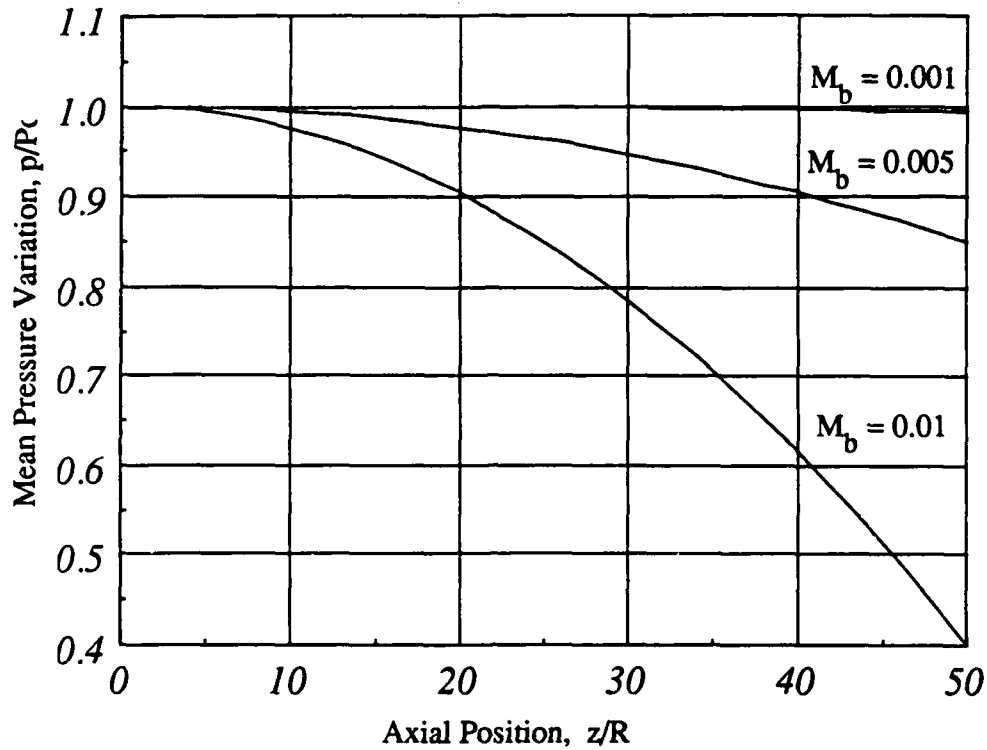
Fig. 5.3 Effect of Injection Mach Number on Axial Pressure Distribution
(One-D Flow Solution, Equation 6.12, $\gamma = 1.2$)

detail is presented, since crucial decisions regarding the unsteady-flow modeling will depend on a thorough understanding of the mean flow.

Later considerations will make it clear that a one-dimensional mean flow model is not generally an adequate representation for use in combustion instability analyses. Let us now consider a more realistic geometric situation such as that illustrated in Figure 2a. The parts of the mean flow in which viscous stresses are small are governed by

$$\nabla \cdot \rho U = 0 \tag{5.14}$$

$$\nabla \frac{U \cdot U}{2} - U \times \nabla \times U = - \frac{\nabla p}{\rho} \tag{5.15}$$

where

$$U = U_r e_r + U_z e_z$$

is the mean flow velocity vector, and the density will be assumed constant as discussed earlier. The continuity equation is automatically satisfied if one introduces the stream-function, ψ, such that the velocity components are given by

$$U_r = - \frac{1}{r} \frac{\partial \psi}{\partial z}, \qquad U_z = \frac{1}{r} \frac{\partial \psi}{\partial r} \tag{5.16}$$

It is useful to eliminate the pressure gradient from the momentum equation by taking the curl of each side. Equation (5.15) is then converted to *vorticity form*, and it provides information on the behavior of this important fluid property (the appendix contains a brief review of the physical meaning of the vorticity vector in the sense we need it for understanding rocket flows). The result is

$$\nabla \times (\mathbf{U} \times \mathbf{\Omega}) = 0 \qquad (5.17)$$

and due to the assumption of axisymmetric flow, the vorticity , $\mathbf{\Omega} = \nabla \times \mathbf{U}$, has only one non-zero component, the azimuthal part given by

$$\mathbf{\Omega} = \Omega \mathbf{e}_\theta = \left(\frac{\partial U_r}{\partial z} - \frac{\partial U_z}{\partial r} \right) \mathbf{e}_\theta \qquad (5.18)$$

Writing this expression and 5.17 in terms of the stream function one finds

$$\frac{\partial \psi}{\partial r} \frac{\partial \Omega}{\partial z} - r \frac{\partial \psi}{\partial z} \frac{\partial}{\partial r} \left(\frac{\Omega}{r} \right) = 0 \qquad (5.19)$$

$$\frac{\partial^2 \psi}{\partial r^2} - \frac{1}{r} \frac{\partial \psi}{\partial r} + \frac{\partial^2 \psi}{\partial z^2} = - r \, \Omega \qquad (5.20)$$

Equations 5.19 and 5.20 along with the necessary boundary conditions can be solved for the vorticity amplitude and the stream function. Once these are available, the details of the flow field can be established by use of the stream-function relationships 5.16 (to determine the velocity distribution) and the momentum equation 5.15 (to be solved for the pressure distribution).

To emphasize the importance of vorticity transport, two special cases will now be examined. The results will aid us in making critical decisions regarding the time-dependent flow formulation. Each of these solutions has been used extensively in combustion instability calculations.

In the first case, it is assumed that vorticity is zero everywhere within the chamber. This is a plausible condition since viscous forces are justifiably assumed to be negligible. The second case assumes that vorticity is generated at the boundary and must be accounted for as it is convected through the chamber. It will be seen that this will make possible a solution with more realistic boundary conditions than in the simpler first case. Physical arguments will be used to determine which of the two approaches is the more realistic. It will be important later to establish in a similar fashion how analogous time-dependent vorticity transport affects rocket combustion stability.

Irrotational Axisymmetric Solution

On the basis of the inviscid flow assumption, no vorticity can be created within the chamber (in the absence of externally applied force fields) and it is plausible that none is generated within the combustion zone or at the porous boundary through which flow enters the chamber. It will be necessary later to carefully assess this assumption by examining realistic flow field models appro-

priate in the combustion zone or boundary regions. Under these conditions, equation (5.19) is obviously exactly satisfied, and the stream function is determined from the linear, homogeneous equation

$$\frac{\partial^2 \psi}{\partial r^2} - \frac{1}{r}\frac{\partial \psi}{\partial r} + \frac{\partial^2 \psi}{\partial z^2} = 0 \cdot \qquad (5.21)$$

The boundary conditions to be satisfied are:
  Normal influx velocity at burning surface:

$$\frac{1}{r}\frac{\partial \psi}{\partial z} = v_b \quad (r = R, z) \qquad (5.22)$$

No flow through head-end closure:

$$\frac{1}{r}\frac{\partial \psi}{\partial r} = 0 \quad (r, z = 0) \qquad (5.23)$$

Note that it is unnecessary to impose a symmetry condition since this has already been accomplished in the definition of the stream function (equations 5.16)). The boundary-value problem for the stream function is easily solved by standard techniques with the result

$$\psi = \frac{v_b}{R} z r^2 \qquad (5.24)$$

and the two velocity components are

$$U_r = -v_b \frac{r}{R}, \quad U_z = 2v_b \frac{z}{R}. \qquad (5.25)$$

Again, the linear variation of the axial velocity with axial position appears, in agreement with the one-dimensional analysis. The pressure distribution is found by integrating the momentum equation (5.15); the result is the familiar irrotational form of Bernoulli's equation. Pressure varies through the chamber according to

$$\frac{p}{\bar{p}} = 1 - 2\left(\frac{\rho}{\bar{p}}\right)\left(v_b \frac{z}{R}\right)^2 = 1 - 2\gamma M_b^2 \left(\frac{z}{R}\right)^2 \qquad (5.26)$$

The radial variation is very small and is neglected in 5.25. As already discussed, the axial variation is also negligible for typical (small) values of surface mean flow Mach number.

Figure 5.4 shows streamline plots for this solution. This axisymmetric flow has been used frequently in rocket stability analyses because of its great simplicity. Its main defect is plainly evident in the behavior of the streamlines near the burning surface. Since vorticity has been set to zero, it is not appropriate to invoke the no-slip condition at the boundary. Thus, the axial velocity component is not zero at the surface. If one imagines that the burning surface is analogous to a porous plate through which gas is injected into the chamber, then the flow should enter radially and generation of vorticity in the injection process is implied. Cold-flow simulations verify this view of the flow field, and experiments with actual flow in window-equipped combustors show that the flow enters without an axial component. Significance of errors generated in subsequent analyses by inattention to these discrepancies will be addrssed presently. It will be found that there is an important (and controversial) time-dependent analog to the situation that has arisen here.

Note: Velocity vector has an axial component at the propellant surface. In any real gas, the parallel component must be zero at the boundary.
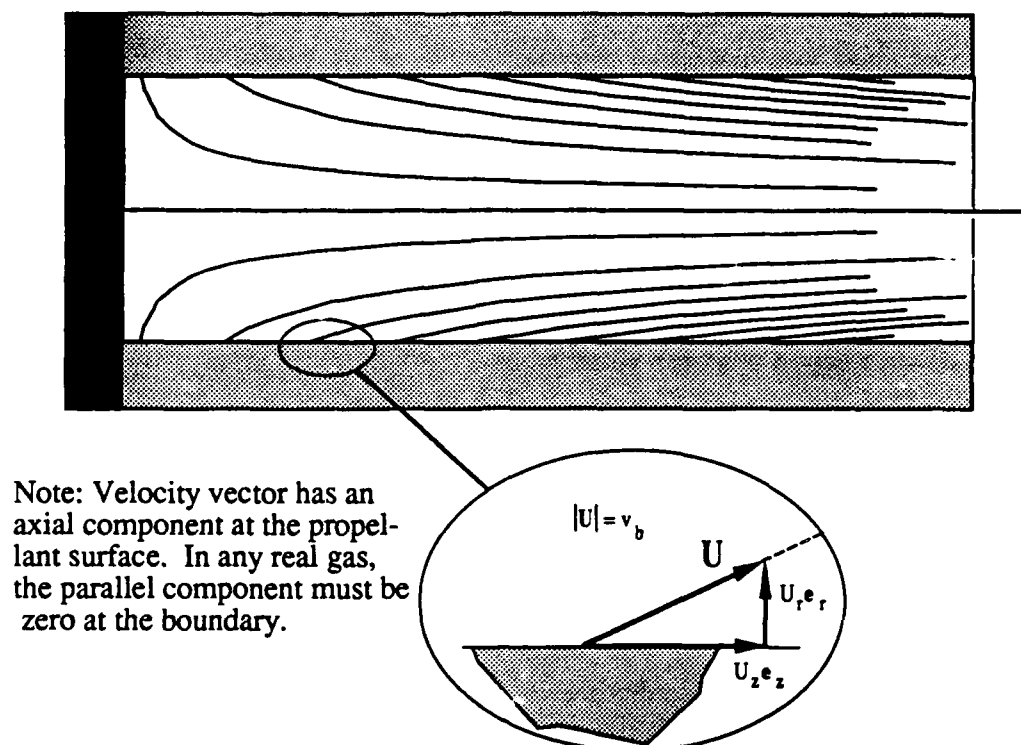
Fig. 5.4 Streamlines for Irrotational Axisymmetric Flow

Inclusion of the Effects of Convective Vorticity Transport

Culick (Culick 1966) devised an improved axisymmetric mean flow model that eliminates the deficiencies arising from neglect of viscous forces. Since the arguments on which this model is based are central to later discussions, a complete description is given. Emphasis is on the approximations invoked and on the physical interpretations of the results.

This mean flow model, often referred to as the "Culick velocity profile" has been verified experimentally both in cold-flow experiments and in numerical solutions of the flow field equations. In light of these findings, some investigators have interpreted the results as indicating that viscous forces need not be treated explicitly in rocket motor flow analyses. In fact, the more realistic boundary condition at the burning surface, *requires* that viscous effects be accounted for. Important decisions in modeling of instability effects hinge on the validity of this generalization.

Again assuming an incompressible, axially symmetric flow, but insisting that the velocity vector be normal to the burning surface, the field is governed by the vorticity equation, which links the stream function and the magnitude of the vorticity, and the momentum equation as expressed in equations 5.19 and 20. Only azimuthal vorticity is involved because of the assumption of axial symmetry as expressed in 5.18. However, the magnitude of the vorticity and its distribution

in the chamber is unknown and must be determined as part of the solution. The
boundary conditions now include a requirement that flow enters radially. Solu-
tions must be found such that

1. $\dfrac{\partial \psi}{\partial r} = 0$ $(r = R, z)$ (Gas enters radially)   (5.27)

2. $\dfrac{1}{r}\dfrac{\partial \psi}{\partial z} = v_b$ $(r = R, z)$ (Constant normal velocity)   (5.28)

3. $\dfrac{\partial \psi}{\partial r} = 0$ $(r, z = 0)$ (Axial velocity zero at head-end)   (5.29)

4. $\dfrac{\partial \psi}{\partial z} = 0$ $(r = 0, z)$ (Symmetry about the z-axis)   (5.30)

Notice that no provision is made for invoking the no-slip condition at the head-
end inert boundary. That is, *effects of viscosity are only accounted for in the
combustion process* (implicitly, by insisting on normal mass influx). No account
is taken of viscous forces in the body of the fluid or in boundary-layers at inert
surfaces. The latter effects are not usually important, although there can be local
flow separation due to the radial adverse pressure gradient near the centerline at
the head-end closure. These may affect local heat-transfer and erosion patterns.
Also, no account is taken of possible turbulent transition of the flow.

The momentum equation yields vital information regarding the relationship
between the vorticity and the stream function. Manipulation of equation 5.19
shows that

$$\frac{\dfrac{\partial \psi}{\partial r}}{\dfrac{\partial \psi}{\partial z}} = \frac{\dfrac{\partial}{\partial r}\left(\dfrac{\Omega}{r}\right)}{\dfrac{\partial}{\partial z}\left(\dfrac{\Omega}{r}\right)} ,$$ (5.31)

which indicates that the stream-function must be proportional to the magnitude of
the vorticity divided by the radius. Thus in order that no vorticity is generated
within the chamber it is necessary that

$$\frac{\Omega}{r} \sim \psi.$$

Equation 5.20 can now be written as a linear differential equation for the stream
function

$$\frac{\partial^2 \psi}{\partial r^2} - \frac{1}{r}\frac{\partial \psi}{\partial r} + \frac{\partial^2 \psi}{\partial z^2} + C^2 r^2 \psi = 0,$$ (5.32)

and the solution can be determined by classical techniques. Note that 5.32
contains the additional constant, C (the constant of proportionality in the relation-
ship between vorticity and stream function) which must be determined by satis-
faction of the boundary conditions. That is, there is a special vorticity magnitude
required for a given surface injection velocity v_b, which can only be determined
in the process of solving the differential equation (5. 32). The latter is now in
linear form, and conventional methods of solution apply. For example, separation

of variables (inserting $y = f(r)Z(z)$) yields the equivalent ordinary equations:

$$\begin{cases} Z'' \pm k^2 Z = 0 \\ f'' - \dfrac{f'}{r} + C^2 r^2 f = \pm k^2 f . \end{cases} \tag{5.33}$$

The only appropriate solution for the axial function $Z(z)$ is one that is linear in z since its derivative must be constant at any point on the injection boundary (condition 5.28). This is consistent with uniform mass addition as a function of axial position as required by a constant value of normal mass influx. Thus the separation constant k is zero, and the dependence on r is governed by

$$f'' - \frac{f'}{r} + C^2 r^2 f = 0 . \tag{5.34}$$

This is a standard form of Bessel's equation. Solutions are Bessel functions of the first kind of order 1/2 such that

$$f = r \left[C_1 J_{\frac{1}{2}}\left(\frac{Cr^2}{2}\right) + C_2 J_{-\frac{1}{2}}\left(\frac{Cr^2}{2}\right) \right] . \tag{5.35}$$

This in turn can be expressed in terms of trigonometric functions by means of the identities

$$J_{\frac{1}{2}}(x) = \sqrt{\frac{2}{\pi x}} \sin(x), \qquad J_{-\frac{1}{2}}(x) = \sqrt{\frac{2}{\pi x}} \cos(x), \tag{5.36}$$

with the result that $f(r)$ becomes

$$f = A \sin\left(\frac{Cr^2}{2}\right) + B \cos\left(\frac{Cr^2}{2}\right), \tag{5.37}$$

where A and B are constants of integration still to be determined. To satisfy the remaining boundary conditions, it is necessary that $B = 0$ for an axially symmetric flow (condition 5.30) and in order to satisfy the no-slip condition at $r = R$ (condition 5.27), it is required that

$$\cos\left(\frac{Cr^2}{2}\right) = 0 , \tag{5.38}$$

which establishes the eigenvalue C. Acceptable values are

$$C = (2n + 1)\frac{\pi}{R^2} \qquad (n = 0, 1, 2 \ldots), \tag{5.39}$$

but only the case $n = 0$ is physically interesting. The other values correspond to flow fields with surfaces of zero radial flow located between the axis and wall. They also involve negative axial velocity components that would require reverse flow in annular zones in the chamber. Thus, the only physically realistic solution is

$$\psi = v_b R z \sin\left(\frac{\pi}{2}\left(\frac{r}{R}\right)^2\right), \tag{5.40}$$

where the constant of integration A has been set to match the injection velocity at the burning surface (condition 5.28). Thus the velocity components are

$$
\left\{
\begin{array}{l}
U_r = -v_b \dfrac{R}{r} \sin\left(\dfrac{\pi}{2}\left(\dfrac{r}{R}\right)^2\right) \\[4mm]
U_z = \pi\, v_b \dfrac{z}{R} \cos\left(\dfrac{\pi}{2}\left(\dfrac{r}{R}\right)^2\right),
\end{array}
\right.
$$

(5.41)

(5.42)

and the corresponding vorticity distribution is

$$
\Omega = \pi^2 \frac{v_b}{R}\frac{r}{R}\frac{z}{R} \sin\left(\frac{\pi}{2}\left(\frac{r}{R}\right)^2\right).
$$

(5.43)

Figures 5.5 and 5.6 show the radial and axial velocity profiles described by equations 5.41 and 5.42. Figure 5.7 shows the streamline pattern. Data taken by Dunlap (Dunlap, Wiloughby, and Hermsen 1974) in an elegant cold-flow experiment agree with these results very closely; there is no question that effects of vorticity are important. Significant errors in stability calculations result if the less realistic flow field results are employed.

Dimensionless Variables in the Mean Flow Solutions

It is useful to examine the solutions we have just constructed from the standpoint of dimensionless variables. We have deliberately written out all the results using *dimensional* variables to emphasize the natural way in which dimensionless forms appear in the solutions. The results for the velocity components in equations 5.41 and 5.42 show this clearly. Notice that the chamber radius appears everywhere there is a physical length involved. Thus the ratios r/R and z/R are the natural way to express the position in the solutions. Similarly, the injection velocity occurs everywhere a velocity is needed, so the ratios

$$
\frac{U_r}{v_b} \quad \text{and} \quad \frac{U_z}{v_b}
$$

are the natural way to describe velocities. Thus for the mean flow problem as we have solved it, velocities are made dimensionless by dividing by v_b and lengths by the only available length parameter, the chamber radius R. Note, however, that we earlier decided to use the speed of sound as the reference velocity in our calculations to emphasize effects of compressibility. This requires only a slight modification in the present situation. Thus, if we make equations 5.41 and 5.42 dimensionless using speed of sound and chamber radius, the result is

$$
\left\{
\begin{array}{l}
U_r = -\dfrac{M_b}{r}\sin\left(\dfrac{\pi}{2}r^2\right) \\[4mm]
U_z = \pi\, M_b\, z \cos\left(\dfrac{\pi}{2}r^2\right),
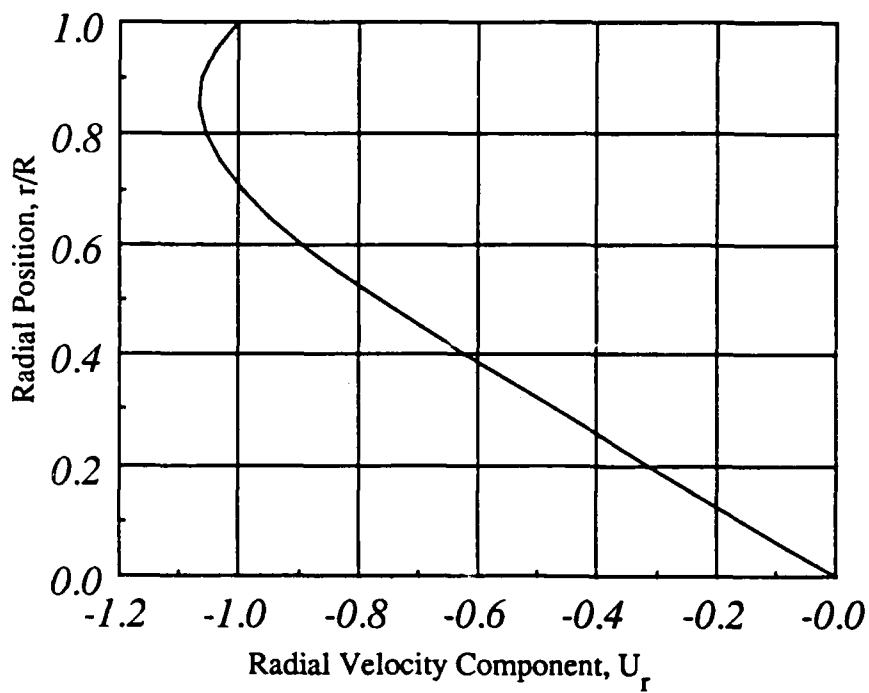\end{array}
\right.
$$

(5.44)
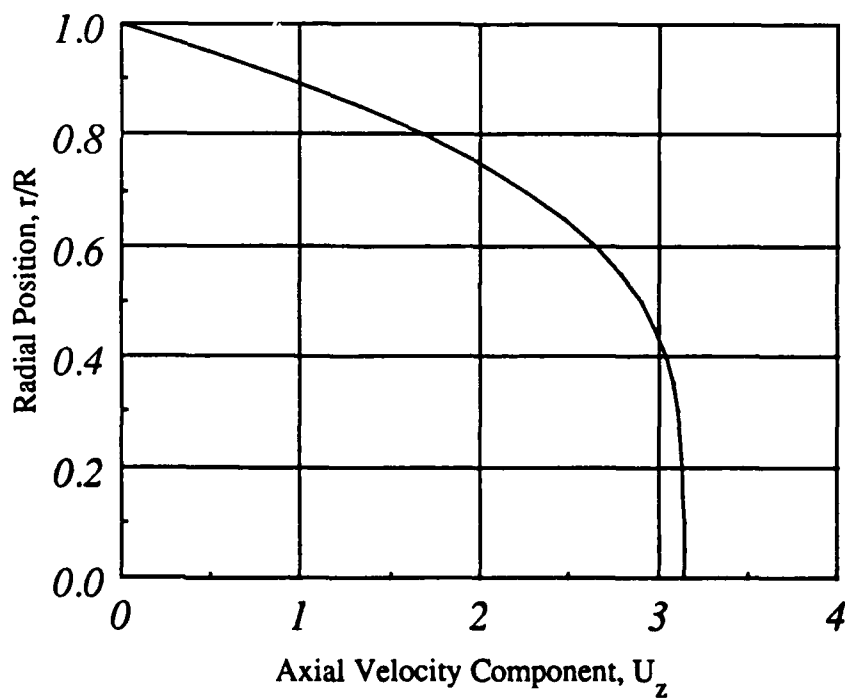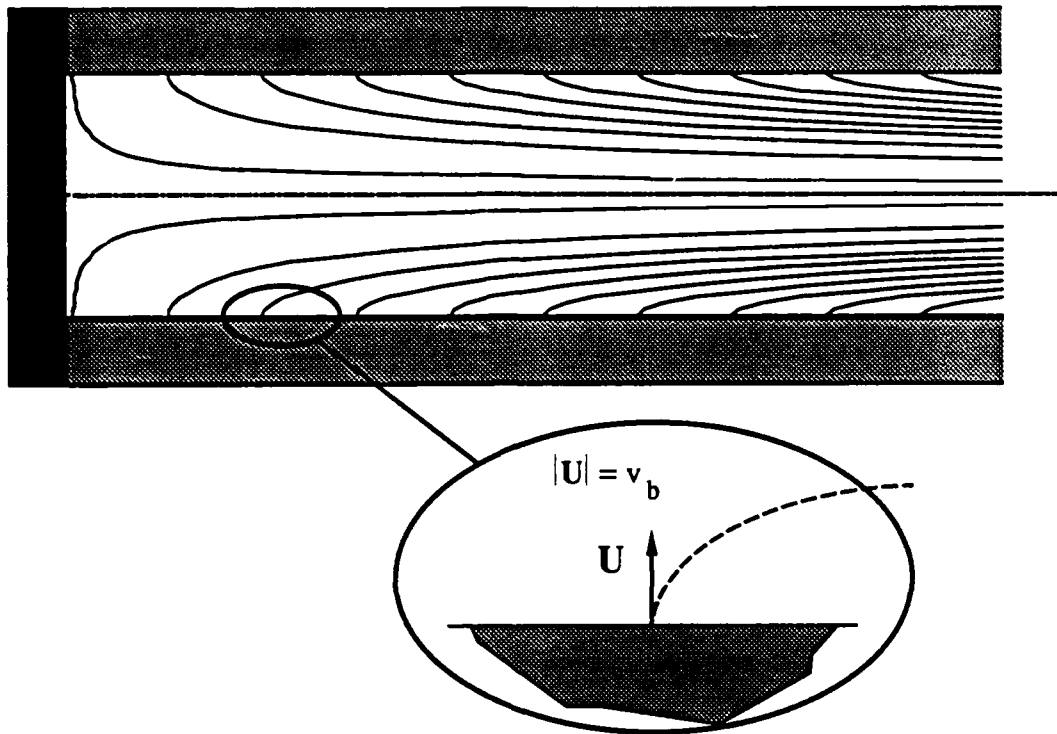
Fig. 5.5 Radial Velocity Component vs Radial Position

Fig 5.6 Axial Velocity Component vs Radial Position at z/R = 1

Note: Velocity vector is perpendicular
to the burning surface as required by
the no-slip boundary condition

Fig. 5.7 Streamlines for Rotational Axisymmetric Flow

where the mean flow Mach number,

$$M_b = \frac{v_b}{\bar{a}}$$

(5.45a)

is the main scaling parameter that sets the size of the mean flow effects relative to other features of the motor chamber flow field yet to be investigated.

If we had retained the viscous terms in the momentum equation, another dimensionless group including the coefficient of viscosity would have appeared. In the steady case, using v_b and R as scaling variables for velocity and length, this group is the injection Reynolds number

$$R_s = \frac{\rho v_b R}{\mu} = \frac{v_b R}{\nu}$$

(5.45b)

which governs the importance of viscous stresses. Thus in the momentum equation 5.7 if U is normalized by v_b and lengths by R, the dimensionless form becomes,

$$\nabla \frac{U \cdot U}{2} - U \times \nabla \times U = - R \frac{\nabla P}{v_b^2} + \frac{1}{R_s} \nabla^2 U$$

(5.46)

where the inverse of the injection Reynolds number appears in its natural place with the viscous stress term. It should now be clear, that in order to ignore the direct effects of viscosity, we have implied the limiting case

$$R_s \to \infty$$

and we must now ask what happens in reality, since a large Reynolds number suggests that turbulent flow effects could be important.

Limitations of the Inviscid Solutions

The results for flow in a cylindrical chamber do not account for the possibility of turbulent vorticity transport. Some recent work (Beddini 1986; Dunlap, et al. 1987) has been accomplished in determining the effects of turbulence on the mean flow characteristics in long tubular grains. Both extensive cold-flow measurements and numerical treatment of the problem using turbulent flow models such as the (k-ε) were utilized. The work of Beddini is based on the use of a full Reynolds stress turbulent flow model. He shows that high levels of turbulence can exist while the mean flow distribution maintains its laminar form as given by equations 5.44. If the chamber is sufficiently long (or if the port-to-throat ratio is very small), a transition in the flow profile to the turbulent form takes place at a very large value of a Reynolds number based on axial distance from the head-end rather than chamber radius.

The relationship between turbulent fluctuations in the gas flow and the propellant burning-rate has been of great concern in rocket motor design. There have been nearly as many studies of steady "erosive burning" and related topics as there have been investigations of combustion instability. The interactions be-

tween turbulent fluctuations and acoustic oscillations have also been the focus of much worry in terms of stability implications. This is a topic we will return at a more appropriate point. We will find the approximate "laminar" mean flow solutions will suffice for the vast majority of situations we will encounter in assessing motor combustion stability. We will concentrate on cases in which the chamber length is not too large and the assumption of laminar mean flow is justified. We will, however, return to the question of direct interaction between turbulent and acoustic fluctuations. Some recent fascinating experimental data will provide much food for thought (Brown, et al, 1986). It will become apparent that much still remains to be learned in understanding these features of combustion instability.

5.4 MODELING OF UNSTEADY FLOW OF COMBUSTION GASES

There is nearly universal agreement in the literature on the fundamental mathematical description of the rocket motor gas flow as we have described it in previous sections. It is at this point that crucial decisions must be made in constructing time-dependent solutions of these equations. It is remarkable how the complexity increases at this stage. The difficulties we encountered in the steady counterpart of the problem in the last section are compounded when oscillatory behavior must be modeled. Not only are nonlinear convective effects of potential importance, but the influence of the reactive combustion processes at the propellant surface must be accounted for.

The resulting nonlinear differential equations cannot be solved directly using classical methods of analysis. Computational procedures such as finite-difference or finite-element methods have apparently not yet matured to the degree needed for routine use for the problem; several attempts to introduce such methods have not been fully successful.

Application of simplifying assumptions such as were used to produce the steady-flow results described in Section 5.3 is the accepted method for generating time-dependent solutions. This section will focus on application of *perturbation techniques* as a means for constructing a solvable time-dependent rocket flow problem.

It is not merely "solvability" that we seek. It is crucial that the physical content of the results can be readily extracted in any calculation. There is a great need to produce results that are useful in interpreting experimental data. Numerical solutions often seem to produce additional experimental data (of a different sort) rather than improved understanding of the physical processes. The approach that we use must emphasize the sometimes subtle interactions between the physical variables chosen to describe the motor flow system. We must attempt to develop a window into the many complex interactions which comprise the combustion instability problem. The resulting analytical framework must not only promote physical understanding but must also provide a means for useful quantitative estimates. The tool of choice for this purpose is the asymptotic perturbation

method, which has been a cornerstone of combustion stability research. Perturbation methods exploit the fact that the oscillatory components of the gas motion often have small amplitude relative to the steady parts. This is obviously the case in the earliest stages of a growing disturbance. That is, at the "stability boundary". It is this part of the problem that has received by far the most attention in the literature because it allows *linearization* of the problem. Virtually all accepted combustion instability models are founded on linearized analysis. Chapter 9 will describe the computational algorithm (the Standard Stability Program, SSP) based on the analysis. As we shall see, linearization greatly simplifies both the relationships between key variables and the computational task of estimating their values.

The relative smallness of the fluctuations is utilized in a formal expansion procedure to construct an approximate solution by allowing only the most important interactions to be retained at any desired level of precision. The linearized solutions represent the lowest order or "first-order" of precision. In principle, perturbation methods allow one to construct corrections to the linearized results to what ever degree of accuracy is required. As we shall see, this may not always be a practical undertaking if truly nonlinear features must be addressed. Methods for attacking the difficult and important nonlinear part of combustion instability problem will be the subject of an entire chapter (Chapter 10). We will see that several of the most important practical features of combustion instability are *symptoms of its inherent nonlinearity.*

Many investigators think of the perturbation approach as merely a method for "linearization" of the problem. Indeed, achievement of a linear representation in a given situation is often all that is required in resolution of a problem. Actually, perturbation methods can lead to far more than that. Asymptotic perturbation expansions also provide a convenient tool for investigating the nonlinear behavior of a system in an approximate and often practical way. By "practical" we mean that it can be easily used to correlate, interpret, and clarify the meaning of experimental data. Nonlinear solutions generated in this manner sometimes have the disadvantage of being algebraically complex. Nevertheless, at the present time, they provide a significantly better view of the physical content of the problem than one can generate by reliance on a purely numerical attack. They are also quite cost effective in that they do not require the number-crunching capability of a Class VII computer. In recent years they have been largely ignored because of the attention focused on numerical methods made possible by the rapid development and accessibility of large-scale computational facilities. There is evidence that analytical tools such as perturbation techniques are being used more extensively as analysts confront the inherent limitations of purely computational problem solving approaches.

Application of Perturbation Methods

From a practical standpoint, perturbation methods give us the necessary tools and insights both to construct meaningful experiments and to approach the solution of real combustion instability problems as they occur in the field. Application of special methods such as the perturbation approach are intended to give us the greatest possible return for our analytical investment. A mathematical instrument of such great power should be part of every propulsion engineer's tool kit. Unfortunately, standard college programs, including most graduate curricula, do not now contain coverage of these important methods. Thus for completeness we include this short tutorial; it can be skipped by those already familiar with perturbation methods.

The mathematically inclined reader will note a certain lack of rigor both in the following discussions and the application of perturbation techniques throughout the text. In fact, perturbation methods as they are employed in practice are often based on *ad hoc* assumptions that are justified simply because they have been found to work in numerous cases! That is, they produce results that agree with experimental findings. They are not always backed by a complete and rigorous set of axioms and proofs of existence, although there has been gradual acceptance as an established branch of engineering mathematics (Nayfeh 1973). The reader interested in a more detailed treatment of the more formal aspects of asymptotic expansion methods should consult the References (Cole 1968; Jeffrey and Kawahara 1982; Nayfeh 1973; Van Dyke 1964).

Perturbation methods capitalize on the relative smallness (or largeness) of key parameters in the formulation. Classical applications of this idea are exemplified by the *supersonic small disturbance* and *slender body* theories wherein the small deflection of the fluid particles in a direction normal to the main stream direction allows great simplification of the governing equations. Corrections for compressibility effects in subsonic flows are readily made by using the Mach number as a small parameter. This leads to the familiar *Prandtl-Glauert transformation*, which allows the problem to be solved essentially as an incompressible one (Anderson 1982; Liepmann and Roshko 1957).

Another key example is the classical *laminar boundary-layer theory*, which utilizes the inverse of the Reynolds number (assumed large) as a perturbation parameter. The latter problem provided Prandtl (Schlichting 1979; Stewartson 1964; Van Dyke 1964) the inspiration for a special perturbation approach that has evolved over the years into the "singular perturbation" method. In this case, dropping of higher-order terms (as one does in a straightforward perturbation series expansion) lowers the *order* of the differential equation making it impossible to satisfy all of the boundary conditions. It is then necessary to introduce coordinate transformations that allow treatment of the problem in two (or more) regions. Solutions for each region must be *matched* at an appropriately defined interface between them to yield a complete solution to the problem. We will have

occasion in the following several chapters to utilize this and many other classical perturbation methods in arriving at the various solutions needed in the combustion instability problem.

In the following several subsections we will present simple examples to show how perturbation techniques are to be used in the material to follow. We will also introduce the principal perturbation parameters and the scaling techniques needed to properly approach practical problems of interest in oscillatory combustion.

The Perturbation Expansion Process

Let us begin by demonstrating by means of a simple example how the method works. We will then apply this approach to increasingly more complex and realistic situations as they are needed in our formulation of the complete combustion instability model. The reader will see in the presentation of these results one of the principal benefits of the perturbation method. Improvements and corrections in previous work can be made *iteratively* without the need to start over from thebeginning. You will see the history of combustion instability research unfolding (in simplified form) as we develop the theory in perturbation series form.

Suppose we have a physical variable, say thepressure, p*, with a time-dependent part that is characterized by its small amplitude. The pressure as shown, could be expressed in any standard system of units such as *psi, lbf/ft²*, or *pascals*. If the time-dependent part is oscillatory, then the composite pressure, the sum of the steady and unsteady parts, can be written as

$$p^* = \bar{P} + p' = \bar{P} + A f(r) \cos(\omega t) \qquad (5.47)$$

where $\bar{P}$ is the mean part and A is the amplitude of the fluctuating part p' in which we are interested. The pressure fluctuation may also depend on position as represented by the factor f(r) which is taken to be of the order of unity. For example, in a simple one-dimensional acoustic wave we will find f(x) = cos(kx) which clearly varies between -1 and 1 depending on location x. The magnitude of the fluctuation at a given point is entirely determined by the amplitude A. It is natural to express the pressure field in dimensionless form by dividing by a convenient reference pressure, say $\bar{P}$. Then the composite pressure field is

$$p = \frac{\bar{P} + Af(r)\cos(\omega t)}{\bar{P}} = 1 + \frac{A}{\bar{P}} f(r)\cos(\omega t) \qquad (5.48)$$

Suppose further that A is small compared to $\bar{P}$. To stress the smallness of the resulting reference parameter, wewrite

$$\varepsilon \equiv \frac{A}{\bar{P}}, \qquad (5.49)$$

and we often state that $p' = \varepsilon f(r)\cos(\omega t)$ is "of the order e", where is a very small number. ε is often referred to as a "gauge" parameter and is always intimately connected to the physics of the problem. In this example it is just the ratio of amplitude of the pressure fluctuation to the mean chamber pressure.

Terms that are similar in size to these we describe as of "first-order in ε ". We will soon show that accompanying such a pressure fluctuation there are fluctuations of velocity, density, temperature, entropy, etc. that are all also of order ε if they are properly nondimensionalized.

The essence of the perturbation method is that all parts of the problem that can be represented by functions whose magnitudes are the same size, say of the order of ε, can be grouped together and isolated in an algebraic sense from elements of the problem that lie in a different size range. Suppose that there is another contribution to the pressure with a dimensionless amplitude that happens to be proportional to the square of e. We would describe this term as being of "second-order in ε". Clearly, if e is a small number, then ε^2 is considerably smaller and can be thought of as belonging to a different hierarchy of terms characterized by their powers of ε.

We say a function f is of the order of some gauge function g according to the following definitions. Symbolically this is expressed as either $f = O(g)$ or $f = o(g)$. These statements are both read as "function f is of the order of g". The distinction between the large and small "oh" order symbols is usually not important in combustion instability analysis, but for completeness, the definitions are:

$$f = O(g) \quad \text{if} \quad \lim_{g \to 0} (f) = \text{Constant}, \tag{5.50}$$

$$f = o(g) \quad \text{if} \quad \lim_{g \to 0} (f) = 0 . \tag{5.51}$$

The small "oh" order provides a slightly more restrictive or *sharper* definition that is important in some applications. See the references (Nayfeh 1973; Van Dyke 1964) for a more complete description of the differences. We will use the less restrictive large order symbol in our analyses. Thus, when we say for example that "the function f is of order ε, we mean $f = O(\varepsilon)$ as defined in equation 5.50.

The basic idea of perturbation theory is that any function can be decomposed, or *expanded*, into a series of simpler functions. Symbolically, one might write

$$F(r,t) = g_0 f_0(r,t) + g_1 f_1(r,t) + g_2 f_2(r,t) + O(g_4), \tag{5.52}$$

where the functions $g_n(\varepsilon)$ are a set of gauge functions based on an important small parameter ε showing up in the particular physical situation that gives rise to $F(r,t)$. A set of gauge functions that is used almost to the exclusion of any other in combustion stability calculations is the set of integer powers of ε. Thus we propose to use the "asymptotic sequence"

$$g_n(\varepsilon) = 1, \varepsilon, \varepsilon^2, \varepsilon^3, \dots \varepsilon^n \qquad n = 0, 1, 2 \dots \tag{5.53}$$

as our basic expansion procedure. Then we would write function F as

$$F(r,t,\varepsilon) = f_0(r,t) + \varepsilon f_1(r,t) + \varepsilon^2 f_2(r,t) + O(\varepsilon^3), \tag{5.54}$$

where it convenient to think of ε as a variable. That is, the proposed expansion holds for any value of ε within some prescribed range. There are, of course, many

other ways in which we could form a set of gauge functions in terms of the small parameter ε. For instance, there is no reason why we could not use fractional powers of ε. In fact, there are problems that *require* the use of more complicated gauge functions, representing a finer distinction between orders of magnitude. A situation that arises frequently is the need to introduce gauge functions incorporating the natural logarithm of ε.

Practioners in perturbation methods learn to recognize the signals that indicate the need to use something more complex than the simple sequence of functions given in equation 5.53. This is a subject that is beyond the scope of the present discussion and the needs of our particular application. Interested readers are invited to pursue such questions in more depth in one of excellent texts on perturbation methods (Nayfeh 1973; Van Dyke 1964). To the knowledge of the authors, there are no important problems in combustion instability that are not properly represented by a simple series expansion in integral powers of ε.

Notice that in a limiting process where ε becomes arbitrarily small, that each successively higher-order term approaches zero *faster* than the one preceding it. That is, using our definition for the order symbol,

$$F(r,t,\varepsilon) = f_0(r,t) + \varepsilon f_1(r,t) + \varepsilon^2 f_2(r,t) + O(\varepsilon^3) \qquad (5.55)$$

Thus, we can think of *truncating* the series by ignoring terms beyond a certain order in e. For instance, in a linearized problem we might write

$$F(r,t,\varepsilon) = f_0(r,t) + \varepsilon f_1(r,t) + \text{higher order terms in } \varepsilon, \qquad (5.56)$$

which implies that knowledge of the "zeroth" order part, $f_0(r, t)$, and the "first-order" part of the solution, $f_1(r, t)$, yields an adequate representation for the actual function $F(r, t, \varepsilon)$.

This idea works in a great many situations. The reason that it works is that while nature is inherently nonlinear, the departure from linearity is often small in certain practical situations, and we can sometimes exploit this fact by neglecting the complete nonlinear representation. If the linearized solution does not predict a crucial feature of the system behavior, this is almost always a signal that we are neglecting something involving nonlinearity. This is often the case when the amplitude in an oscillatory motion can no longer be considered small. Thus, we might devise a solution that works perfectly well as long as ε is less than, say, 0.05, but that clearly becomes less appropriate when ε approaches 0.5. Means for handling this situation are contained in the expansion strategy. The key often lies simply in the willingness to grapple with the algebraic problems posed by carrying more terms in the series expansion. For instance, instead of truncating the pressure series at $O(\varepsilon)$,

$$p = 1 + \varepsilon p_1$$

we might instead decide to carry second-order terms so that

$$p = 1 + \varepsilon p_1 + \varepsilon^2 p_2$$

This example illustrates the need for a notation geared to keeping track of a variety of estimates for any given variable. It is obviously desirable to use the same notation for the basic variable with modifications to indicate which order of magnitude is being discussed. Thus, if we are describing the pressure, it is necessary to denote which component in the perturbation series is under examination. A useful notation is the use of either subscripts as in the examples just given or superscripts. A common notation is

$$p = 1 + \varepsilon p^{(1)} + \varepsilon^2 p^{(2)} + \ldots \qquad (5.57)$$

where a one refers to first-order in ε, a two to second-order, and so on. Both of these schemes will be found in the literature. The reader should become familiar enough with both notations to freely translate between them. The superscript notation is somewhat more flexible, and we will tend to use it in preference to the subscript form especially as higher-order corrections become important in nonlinear analyses later on.

We will see that inserting such an assumed series into the governing differential equations allows us to write the originally nonlinear problem as a set of coupled linear problems. These can then be solved sequentially, because at each order of precision, the set of equations depend only on functions of lower order. Thus, once we have solved the problem to first-order in ε, then the second-order set of equations is complete and can be solved in turn. This procedure can, in principle, be carried out to arbitrarily high degree. A practical difficulty arises, however, in that the algebraic complexity increases astronomically as higher-order corrections are attempted. Thus, it is rare to find perturbation solutions carried beyond first- or second-order accuracy. There are some notable examples in other fields. In combustion instability calculations, there have been very few attempts to incorporate terms beyond the second order. Recent work has shown that it is necessary to go at least to the third-order to accommodate some important phenomena such as triggering or mean pressure shifts in nonlinear combustion instability. These will be the subject of Chapter 10.

A few investigators have recently begun to use the computer in a unique way to aid in implementing perturbation expansions (Van Dyke 1975). There are symbolic computer programs such as MACSYMA, MAPLE, Scratchpad, RE-DUCE, MATHEMATICA, and SMP that carry out the routine algebra that makes higher-order expansions difficult to construct by hand (Wolfram 1988). These are now available on a variety of small computers as well as large mainframes. The expansions can be determined to any arbitrary degree limited only by computer memory and stored in algebraic form. The results can then be combined with those from other parts of the problem as needed in generating an accurate solution to the problem. This method has many advantages over numerical integration of the differential equations, not the least of which is the avoidance of numerical stability difficulties that are the nemesis of finite-difference and finite-element methods. This approach is in its infancy, but shows much promise as an elegant means for utilizing the tremendous power of the digital computer in solving practical engineering problems.

Scaling Parameters for Perturbation Solutions

We have already taken most of the important steps in the "scaling" of the problem. In the formulation process and in the steady-flow examples we have carried out earlier in this chapter, the important scaling variables appeared almost automatically as we identified appropriate dimensionless quantities. For example, in the derivation of the mean flow model for a cylindrical motor port geometry, we deliberately carried out the solution without first putting the governing equations in dimensionless form. The final results made clear the proper choices for dimensionless parameters. Although not shown explicitly, two important limiting processes were needed to arrive at the final results. These were:

1. The Mach number at the burning surface is very small: $M_b \rightarrow 0$ (5.58)

2. The surface Reynolds number is very large: $R_s \rightarrow \infty$ (5.59)

By choosing the special ranges of values indicated by these limiting statements, we achieve great simplification in the equations. The first limit indicates that the effects of *compressibility* may be ignored or treated as a very small correction. The second limit indicates that the regions affected by viscosity can be regarded as of small extent compared to the chamber dimensions. This is the standard boundary-layer concept. It is implied that if we apply the resulting governing equations outside of these regions we can, in effect, ignore the viscous stresses.

In following discussions we will need to adopt a somewhat broader view of these two interpretations especially when time-dependent flow effects are of interest. In particular we will find that boundary-layer concepts usually do not apply to either steady or fluctuating gas motions inside a rocket motor except at inert boundaries. We already have some evidence for this in our mean flow solutions. Notice that it was necessary to invoke the *no-slip* condition at the burning surface in order to arrive at a valid representation of the flow, but viscous forces within the entire body of the gas flow could be neglected. The effects of convection from the injected gas are so overwhelming that viscous stresses are relatively unimportant in the mean flow situation. It will be interesting to see if this same behavior applies in the time-dependent problem. We will investigate the possible existence of an "acoustic boundary-layer" in which viscous forces dominate the fluctuating velocities near the burning surface. The proper choice and interpretation of scaling or "similarity" parameters will be a crucial part of this investigation.

Modeling of the Time-Dependent Velocity Field

Let us now consider what is required to treat small-amplitude oscillatory motions of the type described in detail in the introductory chapters. We can

utilize much of what we have already learned in the steady-flow analyses and proceed by analogy. For example, it is appropriate to assume that the mean flow Mach number is very small and the Reynolds number is large. If we also assume that oscillatory motions represent a small correction to the mean flow, that is that their amplitudes are much smaller than the mean flow velocity magnitudes, then we can construct a simple analysis based on perturbation ideas. From now on, applying what we have learned in earlier examples, it is clearly beneficial to use appropriate dimensionless variables *because they emphasize what is being assumed about the relative magnitude of each quantity.* Consider the velocity vector **u'** representing an oscillatory motion of the gas particles. Experiments show that such oscillations can be identified with acoustic wave motions; we are clearly dealing with a phenomenon governed by the compressibility of the gases. The appropriate scaling parameter is therefore the speed of sound in the gas. So we are led to make u' dimensionless by dividing by the speed of sound as we did in setting up the conservation equations (equations 5.2). The velocity fluctuation can be written as a product of three parts: an amplitude function, a geometrical function, and a time dependence. Thus, put

$$\mathbf{u'} = \varepsilon \ \mathbf{q}(r) \ e^{Kt}, \tag{5.60}$$

where e is the dimensionless amplitude of the oscillation. q(x, y, z), a vector with magnitude of the order of one, represents the spatial distribution of the fluctuations. The exponential function represents the time dependence.

This is similar to what we did earlier in the pressure example, but the spatial part is a vector to represent the vector nature of the velocity. The vector function **q** is often associated with the "mode shape" of the perturbation if a wave motion is involved. For example, if we were dealing with an axial acoustic wave in the x-direction, $\mathbf{q} = \sin(kx)\mathbf{i}$ would be an appropriate description of the spatial characteristics or shape of the disturbance.

The exponential term displays the time dependence. This simple model of the wave motion will be used frequently in our analyses. We have yet to demonstrate that it represents an actual solution to the governing equations, but this will be established in Section 5.5. Note that the argument of the exponential, K, can be complex, that is it consists of a real and imaginary part such that

$$K = \alpha + i\omega. \tag{5.61}$$

Thus, remembering the important identity,

$$e^{i\omega t} = \cos(\omega t) + i \sin(\omega t), \tag{5.62}$$

we see that the exponential time dependence contains not only a description of the periodic behavior of the wave, but also an exponential growth or decay. One of the principal goals of instability theory is to determine α, the real part of K, which governs the tendency of the system to grow. The exponential term in equation 5.60 can be written as the product

$$e^{Kt} = e^{\alpha t} [\cos(\omega t) + i \sin(\omega t)] \tag{5.63}$$

The dimensionless quantity ε is clearly to be interpreted as a Mach number representing the relative amplitude of the waves, since it is the dimensional amplitude, with the units of velocity, divided by the speed of sound. It will later be shown that this is the same parameter we used in describing the pressure perturbation in the previous example. In its present guise it can be treated as a very small Mach number. That is, we will assume the limiting process

$$\varepsilon \rightarrow 0. \tag{5.64}$$

Since, as we shall demonstrate, pressure, density and temperature fluctuations are directly related to the velocity fluctuations, then ε also represents the amplitude of oscillations of the thermodynamic gas properties. In most classical analyses, e is introduced as the oscillatory pressure amplitude as done earlier, but the definition used here is the most natural and useful interpretation. Hence, we will use it throughout the remainder of the text.

It will also be apparent from earlier discussions pertaining to the experimental description of combustion instability that ε cannot always be assumed to be constant. It usually changes with time on the scale of the motor burning time, but the changes occur quite slowly compared to the rapid variations in flow properties associated with the oscillations. However, there are situations where it might change rapidly during motor operation, and may grow to large amplitude. In order to deal with the latter situation in a realistic way, we will find it necessary to treat nonlinear features of the problem. That is, if e has anything but a very small magnitude and if it changes rapidly with time, then the importance of nonlinearity is definitely indicated, and we must find a way to extend the analysis to quantify these effects. In the following subsections we will describe the manner in which this will be done. We will also demonstrate the manner in which the important steady-flow effects are to be included. Clearly, it is necessary to account for possible interactions between the steady and unsteady parts of the flow field. The emphasis will be on finding a clear path through the algebraic forest that is now rapidly and unavoidably growing before us.

Inclusion of Mean Flow Interactions

A second important scaling parameter has made its presence known. It is the mean flow Mach number M_b. In Section 5.2, we described the benefit of separating the steady and unsteady parts of the flow field. Clearly, if the steady flow is represented as an amplitude multiplying a spatial distribution then upon normalizing with the speed of sound, the mean flow Mach number, M_b, appears in a manner analogous to that giving rise to the dimensionless amplitude e in the time-dependent part. Thus the composite flow can be represented as

$$u = M_b U + \varepsilon u' \tag{5.65}$$

In many cases we will treat M_b as a second perturbation parameter in order to exploit the fact that it is often a small number within the combustion chamber.

The classical theory of combustion instability is built upon the limiting process

$$\lim_{\varepsilon, M_b \to 0} \left(\frac{\varepsilon}{M_b} \right) = 0. \tag{5.66}$$

in which both ε and M_b go to zero with ε approaching zero *faster* than M_b. This suggests that we use double perturbation series. Although it is seldom described this way in the literature, it is useful to show this in a formal way. We propose that the combustion instability problem be represented by the series expansions

$$\begin{cases} p = 1 + \varepsilon p^{(1)} + \varepsilon^2 p^{(2)} + O(\varepsilon^3) \\ \rho = 1 + \varepsilon \rho^{(1)} + \varepsilon^2 \rho^{(2)} + O(\varepsilon^3) \\ T = 1 + \varepsilon T^{(1)} + \varepsilon^2 T^{(2)} + O(\varepsilon^3) \\ u = M_b U + \varepsilon u^{(1)} + \varepsilon^2 u^{(2)} + O(\varepsilon^3) \end{cases} \tag{5.67}$$

in which the wave amplitude perturbation series is imbedded within a mean flow Mach number perturbation series. That is, each of the functions in the wave amplitude expansions in equations 5.67 can be further expanded using the mean flow Mach number as the perturbation parameter. For example, we can write
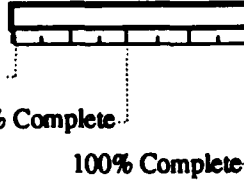
$$\begin{cases} p^{(1)} = p^{(10)} + M_b p^{(11)} + M_b^2 p^{(12)} + O(M_b^3) \\ u^{(1)} = u^{(10)} + M_b u^{(11)} + M_b^2 u^{(12)} + O(M_b^3) \end{cases} \tag{5.68}$$

Table 5.1 shows estimates of the extent to which each of the terms in this double series have been evaluated at the time of writing and to what physical effects each term is apparently related. Most work has concentrated on the linear parts of the problem (terms of $O(\varepsilon, M_b)$); considerably less attention has been devoted to nonlinear effects and to the influence of mean flow compressibility (terms of $O(\varepsilon^2, M_b)$, $O(\varepsilon, M_b^2)$ and higher).

Convective Acceleration Effects - A Demonstration of Expansion Procedures

An important way in which the mean flow affects the growth or decay of waves is through convective acceleration effects. That is, if the wave motions are superimposed on the average flow through the chamber then we must account for the convection of acoustic energy from the burning surface through the chamber and into the nozzle. The appropriate scaling parameter is clearly the mean flow Mach number. This is now demonstrated by expanding the convective acceleration term. This will show the basic algebraic procedure needed in implementing the perturbation expansion process. If readers unfamiliar with the perturbation method will follow through the details of this example, they will have seen all the basic elements of the method as they will be used throughout the remainder of the text and as they have been used to generate all of the classical combustion stability theory.

TABLE 5.1
Effects of Solution Order in Wave Amplitude and Mean Mach Number

Order in Wave Amplitude, ε	Order in Mean Flow Mach Number, M_b		
	$O(1)$	$O(M_b)$	$O\left(M_b^2\right)$
$O(1)$	(No Flow)	Linearized Incompressible Mean Flow	Compressibility Corrections to Mean Flow
$O(\varepsilon)$	Classical Acoustic Waves in a gas at rest	**CLASSICAL COMBUSTION INSTABILITY** (Linear Acoustics; pressure coupling)	High-Speed Mean Flow Corrections to Linear Acoustics
$O(\varepsilon^2)$	Wave Steepening from Nonisentropic Effects and Mode Coupling	Wave Steepening, Mode Coupling, Amplitude Limiting	Wave Steepening, Mode Coupling, Comp. Flow Corrections to Amplitude Limiting
$O(\varepsilon^3)$	Wave Steepening from Nonisentropic Effects and Mode Coupling	Wave Steepening, Triggering, Multiple Limit Amplitudes	Compressible Mean Flow Corrections to Triggering Points and Limit Amplitudes

Note: Bars Show an Estimate of the State of Completion of the Theoretical Treatment of the Combustion Stability Analysis to the Indicated Level of Approximation.

No Theory Available

50% Complete

100% Complete

This example will emphasize the manner in which the mean flow interacts with oscillatory parts of the gas motion. Consider the convective acceleration term in the momentum equation

$$a_{convection} = u \cdot \nabla u \qquad (5.69)$$

As it stands, this is clearly an example of a nonlinear influence, since it involves the product of a key variable, the velocity, with its own derivative. That is, the *square* of the velocity amplitude is introduced. Only if a variable appears alone without being raised to a power, multiplied by itself or a derivative of itself, or in a transcendental function can it be seen by inspection to enter the problem in a linear fashion.

What is needed now is application of the formal procedure that takes advantage of the smallness of each of the two perturbation parameters we have introduced to this point, the wave amplitude, ε, and the mean flow Mach number M_b. Inserting the proposed expansion yields

$$u \cdot \nabla u = (M_b U + \varepsilon u^{(1)} + \varepsilon^2 u^{(2)} + \dots) \cdot \nabla(M_b U + \varepsilon u^{(1)} + \varepsilon^2 u^{(2)} + \dots) =$$

$$= M_b^2 U \cdot \nabla U + M_b \begin{bmatrix} \varepsilon(U \cdot \nabla u^{(1)} + u^{(1)} \cdot \nabla U) + \\ + \varepsilon^2(U \cdot \nabla u^{(2)} + u^{(1)} \cdot \nabla u^{(1)} + u^{(2)} \cdot \nabla U) + \\ + O(\varepsilon^3) \end{bmatrix} \qquad (5.70)$$

$$+ O(\varepsilon M_b^2)$$

where we have collected terms according to their orders in M_b and ε. Since the mean flow plays a fundamental role, we must retain terms of at least first-order in if a useful theory is to emerge.

The classical combustion instability theory carries terms to *first-order* in both the Mach number M_b and the wave amplitude ε. Thus, the convective acceleration term to be included in the standard formulation must be written as

$$a_{convection} = M_b \left[\varepsilon(U \cdot \nabla u^{(1)} + u^{(1)} \cdot \nabla U) \right] + O(M_b \varepsilon^2, M_b^2 \varepsilon) \qquad (5.71)$$

where all terms of order higher than the product of mean flow Mach number and the wave amplitude are neglected. In most combustion stability analysis only linear terms in M_b have been retained. A few have carried out corrections for higher powers in ε, but usually only to the second-order (Flandro 1982; Flandro 1980).

Incidentally, as we have indicated before, the formula used here for convective acceleration is the *symbolic* form. If a coordinate system other than a cartesian system is used, for example cylindrical coordinates would be appropriate for a cylindrically perforated propellant grain, it is necessary to use the complete form as given in equation 5.4. Thus, to first-order in both wave amplitude and mean flow Mach number, the convective acceleration is

$$a_{\text{convection}} = \varepsilon M_b \left[\nabla (U \cdot u^{(1)}) - u^{(1)} \times \nabla \times U - U \times \nabla \times u^{(1)} \right]$$
$$+ O(M_b \varepsilon^2, M_b^2 \varepsilon) \tag{5.72}$$

a result valid for any coordinate system. Notice that both mean and oscillatory vorticity are brought into play. This illustrates the complex way in which the mean flow and the superimposed waves can interact *even though we have reduced the interaction to its simplest form.* The effects of vorticity related to the flow oscillations are usually ignored; this produces important errors.

We will incorporate convective acceleration results into the general analysis in the next chapter. Other major interactions between the acoustic field and the mean flow occurs in the combustion zone. One of these interactions is the principle source of energy driving combustion instability and will be very carefully analyzed.

There are other interactions in which the mean flow field plays an important role as described briefly later in this chapter together with additional scaling or "similarity" parameters needed in their mathematical description. For example, it has been found that in regions of the mean flow where there are steep velocity gradients, that is, where the flow is "highly sheared", the shear layers thus formed are subject to what is called "hydrodynamic instability". Such shear layers may give rise to vortex shedding. These periodic flow structures can in turn interact with the acoustic field, and may in some cases represent an additional source of acoustic energy. More detailed discussions of these other mean flow effects will be given at appropriate points in later chapters.

Expansion of the Conservation Equations

If the double perturbation expansions (5.67-5.68) are inserted into the continuity, momentum, energy, and state equations (5.2), one finds that the original (nonlinear) equations are decomposed into a sets of linear time-dependent equations. The expansions to first-order in the mean flow Mach number to various order of wave amplitude are shown in Tables 5.2-5.4. Notice the rapid increase in algebraic complexity as higher-order effects are retained. This is the main reason there has been very little use of perturbation methods in solving nonlinear problems. Examination of the sets of equations will show that they are linked in the direction of increasing ε. That is, each set depends on the solutions from the preceding ones. Thus, in principle, they can be solved in succession. The algebraic benefits of linearization are quickly reduced as higher-order corrections are attempted. Nevertheless, the construction of solutions in symbolic form provides many advantages, not the least of which is the retention of the algebraic relationships between the controlling variables. Dependence of results on key parameters can be studied in detail without full numerical evaluation. This is a feature that is lost in pure numericalanalyses in which the solution appears as a black-box out of which streams the numerical results. Even though use of

TABLE 5.2
First-Order Time-Dependent Gas Phase Equations

$$\frac{\partial \rho^{(1)}}{\partial t} = - \nabla \cdot \mathbf{u}^{(1)} - M_b \nabla \cdot \rho^{(1)} \mathbf{U} \tag{5.73}$$

$$\frac{\partial \mathbf{u}^{(1)}}{\partial t} = - \frac{\nabla p^{(1)}}{\gamma} - M_b \left[\mathbf{u}^{(1)} \cdot \nabla \mathbf{U} + \mathbf{U} \cdot \nabla \mathbf{u}^{(1)} \right] + \mathbf{F}^{(1)} + \delta^2 \nabla^2 \mathbf{u}^{(1)} \tag{5.74}$$

$$\frac{\partial T^{(1)}}{\partial t} = \frac{(\gamma - 1)}{\gamma} \left[\frac{\partial p^{(1)}}{\partial t} + M_b \mathbf{U} \cdot \nabla p^{(1)} \right] - M_b \mathbf{U} \cdot \nabla T^{(1)} +$$

$$+ M_b \mathbf{U} \cdot \mathbf{F}^{(1)} + \phi^{(1)} + \frac{\delta^2}{P_r} \nabla^2 T^{(1)} \tag{5.75}$$

$$p^{(1)} = T^{(1)} + \rho^{(1)} \tag{5.76}$$

NOTE: δ^2 is the inverse of the Reynolds number based on characteristic length L and the speed of sound:

$$\delta \equiv \sqrt{\frac{\nu}{\overline{a} L}}$$

TABLE 5.3
Second-Order Time-Dependent Gas Phase Equations

$$\frac{\partial \rho^{(2)}}{\partial t} = - \nabla \cdot \mathbf{u}^{(2)} - \nabla \cdot \rho^{(1)} \mathbf{u}^{(1)} - M_b \nabla \cdot \rho^{(2)} \mathbf{U} \tag{5.77}$$

$$\frac{\partial \mathbf{u}^{(2)}}{\partial t} = - \frac{\nabla p^{(2)}}{\gamma} - M_b \left[\begin{array}{l} \mathbf{u}^{(2)} \cdot \nabla \mathbf{U} + \mathbf{U} \cdot \nabla \mathbf{u}^{(2)} + \\ \rho^{(1)} (\mathbf{u}^{(1)} \cdot \nabla \mathbf{U} + \mathbf{U} \cdot \nabla \mathbf{u}^{(1)}) \end{array} \right] +$$

$$- \rho^{(1)} \frac{\partial \mathbf{u}^{(1)}}{\partial t} - \mathbf{u}^{(1)} \cdot \nabla \mathbf{u}^{(1)} + \mathbf{F}^{(2)} + \delta^2 \nabla^2 \mathbf{u}^{(2)} \tag{5.78}$$

$$\frac{\partial T^{(2)}}{\partial t} = - M_b \left[\rho^{(1)} \mathbf{U} \cdot \nabla T^{(1)} + \mathbf{U} \cdot \nabla T^{(2)} \right] - \rho^{(1)} \frac{\partial T^{(1)}}{\partial t}$$

$$- \mathbf{u}^{(1)} \cdot \nabla T^{(1)} + \frac{(\gamma - 1)}{\gamma} \left[\begin{array}{l} \frac{\partial p^{(2)}}{\partial t} + M_b \mathbf{U} \cdot \nabla p^{(2)} + \\ \mathbf{u}^{(1)} \cdot \nabla p^{(1)} \end{array} \right] +$$

$$+ \phi^{(2)} + \frac{\delta^2}{P_r} \nabla^2 T^{(2)} + M_b \mathbf{U} \cdot \mathbf{F}^{(2)} + \mathbf{u}^{(1)} \cdot \mathbf{F}^{(1)} \tag{5.79}$$

$$p^{(2)} = T^{(2)} + T^{(1)} \rho^{(1)} + \rho^{(2)} \tag{5.80}$$

TABLE 5.4
Third-Order Time-Dependent Gas Phase Equations

$$\frac{\partial \rho^{(3)}}{\partial t} = -\nabla \cdot \mathbf{u}^{(3)} - \nabla \cdot \rho^{(1)}\mathbf{u}^{(2)} - \nabla \cdot \rho^{(2)}\mathbf{u}^{(1)} \tag{5.81}$$

$$- M_b \nabla \cdot \rho^{(3)}\mathbf{U}$$

$$\frac{\partial \mathbf{u}^{(3)}}{\partial t} = -\frac{\nabla p^{(3)}}{\gamma} - M_b \begin{bmatrix} \mathbf{u}^{(3)} \cdot \nabla \mathbf{U} + \mathbf{U} \cdot \nabla \mathbf{u}^{(3)} \cdot \\ \rho^{(1)}(\mathbf{u}^{(2)} \quad \nabla \mathbf{U} + \mathbf{U} \cdot \nabla \mathbf{u}^{(2)}) \end{bmatrix} +$$

$$- M_b \left[\rho^{(2)}(\mathbf{u}^{(1)} \cdot \nabla \mathbf{U} + \mathbf{U} \cdot \nabla \mathbf{u}^{(1)}) \right] -$$

$$- \mathbf{u}^{(2)} \cdot \nabla \mathbf{u}^{(1)} - \mathbf{u}^{(1)} \cdot \nabla \mathbf{u}^{(2)} - \tag{5.82}$$

$$- \rho^{(1)}\frac{\partial \mathbf{u}^{(2)}}{\partial t} - \rho^{(2)}\frac{\partial \mathbf{u}^{(1)}}{\partial t} + \mathbf{F}^{(3)} + \delta^2 \nabla^2 \mathbf{u}^{(3)}$$

$$\frac{\partial T^{(3)}}{\partial t} = -M_b \begin{bmatrix} \rho^{(2)}\mathbf{U} \cdot \nabla T^{(1)} + \rho^{(1)}\mathbf{U} \cdot \nabla T^{(2)} \\ + \mathbf{U} \cdot \nabla T^{(3)} \end{bmatrix} - \rho^{(1)}\mathbf{u}^{(1)} \cdot \nabla T^{(1)} +$$

$$- \rho^{(1)}\frac{\partial T^{(2)}}{\partial t} - \rho^{(2)}\frac{\partial T^{(1)}}{\partial t} - \mathbf{u}^{(2)} \cdot \nabla T^{(1)} - \mathbf{u}^{(1)} \cdot \nabla T^{(2)} +$$

$$+ \frac{(\gamma - 1)}{\gamma} \begin{bmatrix} \frac{\partial p^{(3)}}{\partial t} + M_b \mathbf{U} \cdot \nabla p^{(3)} + \\ \mathbf{u}^{(1)} \cdot \nabla p^{(2)} + \mathbf{u}^{(2)} \cdot \nabla p^{(1)} \end{bmatrix} + \tag{5.83}$$

$$+ M_b \mathbf{U} \cdot \mathbf{F}^{(3)} + \mathbf{u}^{(1)} \cdot \mathbf{F}^{(2)} + \mathbf{u}^{(2)} \cdot \mathbf{F}^{(1)} + \phi^{(3)} + \frac{\delta^2}{P_r}\nabla^2 T^{(3)}$$

$$p^{(3)} = T^{(3)} + T^{(2)}\rho^{(1)} + T^{(1)}\rho^{(2)} + \rho^{(3)} \tag{5.84}$$

Note: The force vector term representing the effect of particulate material in the flow and the dissipation function has also been expanded in these equations as:

$$\mathbf{F} = \varepsilon \mathbf{F}^{(1)} + \varepsilon^2 \mathbf{F}^{(2)} + \varepsilon^3 \mathbf{F}^{(3)} + \dots \tag{5.85}$$

$$\phi = \varepsilon \phi^{(1)} + \varepsilon^2 \phi^{(2)} + \varepsilon^3 \phi^{(3)} + \dots \tag{5.86}$$

perturbation expansions entails considerable algebraic complexity, there is a distinct benefit in being able to examine the dependence of a solution on the physical parameters.

The First-Order Inviscid Time-Dependent Flow Problem

We are now in a position to examine the central problem of combustion instability in more detail. For reasons discussed in several contexts already, the viscous terms in the momentum equation can be dropped with the understanding that corrections may be introduced at a later stage. For similar reasons one can ignore the dissipation, viscosity and heat-transfer terms in the energy equation. To keep the problem as simple as possible at this stage, we will also assume that there are no body forces or forces due to two-phase gas/particle interactions. These also will be brought in later. With these assumptions, equations (5.73-5.76) become

$$\frac{\partial \rho^{(1)}}{\partial t} = - \nabla \cdot u^{(1)} - M_b \nabla \cdot \rho^{(1)} U \tag{5.87}$$

$$\frac{\partial u^{(1)}}{\partial t} = - \frac{\nabla p^{(1)}}{\gamma} - M_b \left[u^{(1)} \cdot \nabla U + U \cdot \nabla u^{(1)} \right] \tag{5.88}$$

$$\frac{\partial T^{(1)}}{\partial t} = \frac{(\gamma - 1)}{\gamma} \left[\frac{\partial p^{(1)}}{\partial t} + M_b U \cdot \nabla p^{(1)} \right] - M_b U \cdot \nabla T^{(1)} \tag{5.89}$$

$$p^{(1)} = T^{(1)} + \rho^{(1)}. \tag{5.90}$$

Notice that the energy equation (6.89) is particularly simple and can be immediately integrated with the result

$$T^{(1)} = \frac{(\gamma - 1)}{\gamma} p^{(1)}. \tag{5.91}$$

This is the familiar isentropic relationship as we might have anticipated. To check this, just remember that in dimensional form, the isentropic relationship between temperature and pressure can be written as

$$\frac{T}{\overline{T}} = \left(\frac{p}{\overline{P}} \right)^{\frac{\gamma - 1}{\gamma}}. \tag{5.92}$$

Inserting the expansions for T and p, we find

$$1 + \varepsilon T^{(1)} + \ldots = (1 + \varepsilon p^{(1)} + \ldots)^{\frac{\gamma - 1}{\gamma}}, \tag{5.93}$$

and using the binomial theorem to further expand the exponential term,

$$1 + \varepsilon T^{(1)} + \ldots = 1 + \varepsilon \left(\frac{\gamma - 1}{\gamma} \right) p^{(1)} + \ldots . \tag{5.94}$$

Therefore, 5.91 is the correct way to state that the system is isentropic to the first-order in perturbation amplitude. The binomial expansion will be used many times

throughout the analysis. Since dissipation and heat-transfer have been removed from the problem then entropy is conserved and special relationships between the thermodynamic variables apply. If we eliminate the temperature from 5.91 by use of the equation of state, 5.90, we obtain the isentropic relationship between density and pressure (to first-order in ϵ):

$$p^{(1)} = \gamma \rho^{(1)}. \qquad (5.95)$$

This can then be used to replace the density in the continuity equation with the pressure. Thus, the original set of four equations reduces to the pair

$$\frac{\partial p^{(1)}}{\partial t} + \gamma \nabla \cdot \mathbf{u}^{(1)} = -M_b \nabla \cdot p^{(1)} \mathbf{U} \qquad (5.96)$$

$$\frac{\partial \mathbf{u}^{(1)}}{\partial t} + \frac{\nabla p^{(1)}}{\gamma} = -M_b \left[\mathbf{u}^{(1)} \cdot \nabla \mathbf{U} + \mathbf{U} \cdot \nabla \mathbf{u}^{(1)} \right] \qquad (5.97)$$

These are the equations that are often used as the starting point for combustion instability calculations. The standard stability computer algorithms are based on solutions of these equations. Reviews of the method of solution and application of the results are the subject of Chapter 8.

5.5 SOLUTIONS FOR CLOSED CHAMBERS: ACOUSTIC MODES

It is helpful at this juncture to apply the perturbation approach we have just described to demonstrate some important features of time-dependent gas motions in a rocket chamber in their simplest form. The connection between combustion instability and the acoustic characteristics will be clarified, and means for estimation of possible frequencies of oscillation will be discussed.

Derivation of the Acoustic Wave Equation

Let us now examine a special limiting case of the perturbed first-order time-dependent problem as described by equations 5.96 and 5.97. Assume that M_b is exactly zero (no mean flow) and that the chamber boundaries are rigid. In this case the governing equations reduce to

$$\frac{\partial p^{(1)}}{\partial t} + \gamma \nabla \cdot \mathbf{u}^{(1)} = 0 \qquad (5.98)$$

$$\frac{\partial \mathbf{u}^{(1)}}{\partial t} + \frac{\nabla p^{(1)}}{\gamma} = 0, \qquad (5.99)$$

and we can eliminate either $p^{(1)}$ or $\mathbf{u}^{(1)}$ between the two equations to yield a single differential equation describing the remaining variable. The choice we make here as to which variable to use as the operational one is mainly a matter of convenience. The equations will be simpler if the scalar $p^{(1)}$ is chosen over the vector $\mathbf{u}^{(1)}$.

The final results are not affected by this decision.

There is an alternative approach that is sometimes used that takes advantage of the fact that the velocity perturbation is irrotational. That is

$$\nabla \times \mathbf{u}^{(1)} = 0 \qquad (5.100)$$

because there are no viscous stresses or nonconservative body or surface forces acting on the gas. This allows one to use the scalar potential function

$$\mathbf{u}^{(1)} = \nabla \Phi^{(1)}, \qquad (5.101)$$

which automatically satisfies the irrotationality condition.

If we choose to eliminate the velocity, we proceed by taking the time derivative of the continuity equation and subtracting from it γ times the divergence of the momentum equation as shown:

$$\frac{\partial}{\partial t}\left(\frac{\partial p^{(1)}}{\partial t} + \gamma \nabla \cdot \mathbf{u}^{(1)}\right) = \frac{\partial^2 p^{(1)}}{\partial t^2} + \gamma \nabla \cdot \frac{\partial}{\partial t}\mathbf{u}^{(1)} = 0 \qquad (5.102)$$

$$-\gamma \nabla \cdot \left(\frac{\partial \mathbf{u}^{(1)}}{\partial t} + \frac{\nabla p^{(1)}}{\gamma}\right) = -\gamma \nabla \cdot \frac{\partial \mathbf{u}^{(1)}}{\partial t} - \nabla^2 p^{(1)} = 0 \qquad (5.103)$$

$$\frac{\partial^2 p^{(1)}}{\partial t^2} - \nabla^2 p^{(1)} = 0. \qquad (5.104)$$

Notice that the term involving velocity is the same in both equations so it is eliminated by subtraction. The result is a second-order partial differential equation for the pressure as shown in 5.104. This is the acoustic wave equation describing pressure oscillations in the chamber. Note that once $p^{(1)}$ has been solved for, the velocity fluctuation is also known by direct time integration of the momentum equation written as

$$\frac{\partial \mathbf{u}^{(1)}}{\partial t} = -\frac{\nabla p^{(1)}}{\gamma}. \qquad (5.105)$$

If one chooses the velocity as the primary variable, it is useful to first replace it in terms of its equivalent velocity potential as already described. The governing equations become

$$\frac{\partial p^{(1)}}{\partial t} + \gamma \nabla^2 \Phi^{(1)} = 0 \qquad (5.106)$$

$$\frac{\partial \nabla \Phi^{(1)}}{\partial t} + \frac{\nabla p^{(1)}}{\gamma} = 0, \qquad (5.107)$$

where the Laplacian operator ∇^2 appears, since, by definition

$$\nabla \cdot \nabla \Phi^{(1)} = \nabla^2 \Phi^{(1)}. \qquad (5.108)$$

Again, the two equations can be combined in such a way that pressure is eliminated. By taking γ^{-1} times the gradient of the continuity equation and subtracting

the time derivative of the momentum equation, we find the wave equation

$$\nabla^2 \Phi^{(1)} - \frac{\partial^2 \Phi^{(1)}}{\partial t^2} = 0 \tag{5.109}$$

in terms of the scalar velocity potential. Similar wave equations can be derived for temperature and density fluctuations, but since relationships between these variables are already known, then there is nothing to be gained by this additional step. For instance, pressure/temperature and pressure/density are linearly related by the simple expressions derived earlier (equations 5.91 and 5.95).

Observe that the mathematical form of the governing differential equation is exactly the same in terms of pressure and the potential function. Had we decided to work with the velocity vector itself, the result would have been a vector wave equation, which could be written as three scalar equations of the same type we have already found.

Acoustic Rigid-Wall Boundary Conditions

The rigid chamber statement is equivalent to requiring that there is no flow through the boundaries so that very simple boundary conditions apply. This observation gives us an opportunity to introduce the very important subject of boundary conditions in the simplest form possible. This will be a topic of much concern as the effects of combustion and evolution of combustion gases at the boundary are brought into the problem.

In the rigid boundary case we neglect all effects of viscosity and elasticity of the chamber walls. Thus solutions must satisfy the condition that the normal velocity component at the wall is zero; no flow can pass through the boundary. There is no limitation on the *parallel* components since there is no viscosity, and hence no *no-slip* condition to satisfy. Thus all that is required is that

$$\mathbf{n} \cdot \mathbf{u}^{(1)} = 0 \qquad \text{at chamber boundaries,} \tag{5.110}$$

where $\mathbf{n}$ is a unit vector normal to the boundary at any point. By convention this will be taken positive outward from the cavity. Thus the potential function must satisfy the boundary condition

$$\mathbf{n} \cdot \nabla \Phi^{(1)} = 0 \qquad \text{at chamber boundaries.} \tag{5.111}$$

Using the momentum equation, we can easily find the corresponding condition on the pressure fluctuation. Thus

$$\mathbf{n} \cdot \nabla p^{(1)} = 0 \qquad \text{at chamber boundaries} \tag{5.112}$$

holds everywhere in the chamber since if the normal component of the velocity vector must vanish at the boundary, then its time derivative must also be zero.

Since time is involved in the problem, we must also give some thought to the need for *initial* conditions. However, as will become evident shortly, the solutions we will find most interesting represent periodic motions. Thus the time

origin is arbitrary and since the motion repeats periodically, no initial conditions, other than some statement about the amplitude of the oscillations at a given reference time, will be needed.

Solution for Unperturbed Acoustic Waves

The combination of the differential equation and boundary conditions gives rise to a complete boundary-value problem that can now be solved. It will be useful to demonstrate the acoustic wave solutions by working out the details for several representative chamber geometries. It is important to understand that closed-form solutions even for this very simple problem can only be found for special boundary shapes. These are known as "conformable shapes" that fit one of the standard orthogonal coordinate systems. Thus it is quite easy to find solutions for rectangular, cylindrical, or spheroidal chambers. The cylinder solution in three-dimensional form is of greatest interest since it closely fits the geometry of many actual solid rocket motor ports. Other solutions, such as those for ellipsoidal or spherical chambers, are also occasionally useful in practical applications.

Note that the final step of defining the *shape* of the chamber completes the formulation and sets the functional form of the solutions. The solution process can be carried out using classical mathematical methods in terms of tabulated functions only for very simple chamber geometries. Since actual rocket chambers are seldom simple shapes of the type we will use in the examples, one must ask how to proceed in the actual case. The problem then becomes a numerical one, and we will briefly describe, in a later paragraph, the current methods for handling practical situations involving complex motor port shapes.

Let us now work out solutions for some useful geometries. The reader with a background in advanced engineering mathematics can skim this section since it deals with very familiar mathematical ideas such as *eigenvalues* and *eigenfunctions*.

We will use only one of the many available methods for dealing with boundary-value problems. Operational methods such as Fourier and Laplace transforms and Green's function methods are very powerful tools, but they are not needed at the present stage. Application of the latter method will be introduced in Chapter 8.

One-Dimensional Axial Acoustic Modes

This geometry represents one that closely approximates that of many actual combustion instability situations. Axial modes are often of greatest importance because they involve the lowest frequencies of oscillation (assuming a chamber length to diameter ratio greater than unity). Also, with modern aluminized propellants they are often the only modes that can be driven since the aluminum oxide smoke tends to damp the higher frequency transverse waves. We will see

presently that it is almost always the case that the low order oscillations are important in practice because they require less energy to excite and are usually more lightly damped. Thus, they are more likely to grow to measurable amplitudes.

Figure 5.8 shows the assumed geometry. It is clear that choice of the chamber length L as the length scale for the problem is appropriate, so the length is shown as unity in the figure. All other lengths are scaled proportionately. It is assumed that the chamber cross-section A is uniform (it need not be a circular section). Otherwise the motion would be multi-dimensional. The only spatial variable needed in the solution is the axial position. For convenience we measure it from the left end as shown. Also notice that the gas flow is everywhere parallel to the sidewalls, so the end-wall boundary condition is only one required.
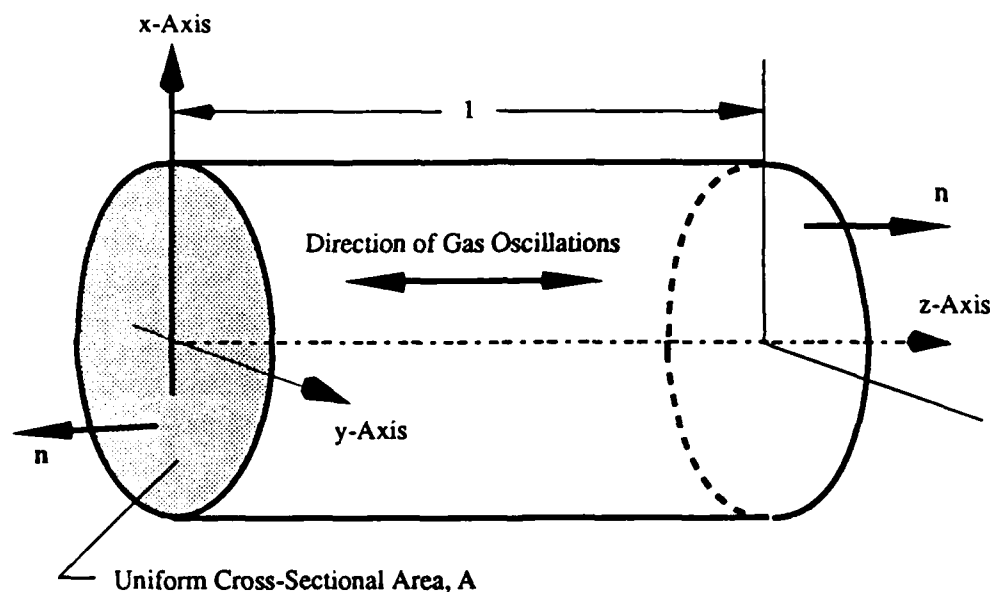
Fig. 5.8 Coordinate System for Analysis of Axial Acoustic Oscillations

The mathematical problem reduces to

$$\frac{\partial^2 p^{(1)}}{\partial z^2} - \frac{\partial^2 p^{(1)}}{\partial t^2} = 0 \qquad (5.113)$$

$$\frac{\partial p^{(1)}}{\partial z} = 0 \qquad \text{at } z = 0, 1. \qquad (5.114)$$

This is a linear problem, so any of the classical methods can be used. For example, *separation of variables* is appropriate. One can write the solution as the product of two functions each representing one of the two independent variables,

t and z. Thus, put

$$p^{(1)} = T(t)Z(z) \qquad (5.115)$$

and substitute this into the differential equation and the boundary condition. It is now seen that the terms in z and those in t can be collected on opposite sides of the equation. We can write

$$\frac{T''}{T} = \frac{Z''}{Z}, \qquad (5.116)$$

where primes indicate derivatives with respect to the argument of the function. Thus, T" represents the second derivative with respect to time of function T.
The equality evidently cannot hold for arbitrary t and z unless the two collections of terms are each equal to the same *constant*. That is

$$\frac{T''}{T} = \frac{Z''}{Z} = \pm K^2, \qquad (5.117)$$

where K is often referred to as the "separation constant". It is squared so that any sign ambiguity can be avoided. Also, it is treated as a real number for our present purposes. We use physical reasoning to choose one of three possibilities:

$$K^2 = \begin{cases} \text{Negative Const.} \\ 0 \\ \text{Positive Const.} \end{cases} \qquad (5.118)$$

Obviously the third choice would yield an exponential solution in time. This is not physically appropriate in our isolated system since there is neither a source of energy present nor a damping mechanism to lead to a decaying solution. The null value must also be rejected since it would imply a motion linearly increasing or decreasing with time. The only possible choice is that K^2 is negative so that

$$T'' + K^2 T = 0, \qquad (5.119)$$

and the temporal part of the solution can be written as a harmonic function:

$$T = a \cos(K t) + b \sin(K t). \qquad (5.120)$$

Since the time origin is arbitrary, it is acceptable to put a = 0 (or b = 0). We still do not know what the value of K is, but it is clearly a measure of the *frequency* of oscillation. The boundary conditions will determine its possible magnitudes. To show this we now attempt to solve for the spatial dependence, which must be governed by

$$Z'' + K^2 Z = 0. \qquad (5.121)$$

Again, we recognize this as the harmonic oscillator equation with the solution

$$Z = c \cos(K z) + d \sin(K z) \qquad (5.122)$$

To satisfy the boundary condition at the left end it is necessary that

$$\frac{\partial Z}{\partial z} = K(-c \sin(K z) + d \cos(K z)) = 0 \text{ at } z = 0 \qquad (5.123)$$

Putting $d = 0$ satisfies this requirement. At the right end, $z = 1$, we must have

$$\sin (K z) = 0 \qquad \text{at } z = 1, \tag{5.124}$$

since putting $c = 0$ would leave us with a "trivial" (or non-) solution! This can only be satisfied if we limit the values of K to the special values:

$$K = n\pi \qquad (n = 1, 2, 3 \dots). \tag{5.125}$$

These are often referred to as the *eigenvalues* or *characteristic* values of the problem. They form a sequence of numbers, which since they came from the spatial boundary condition are sometimes called the "wavenumbers" of the problem. They are dimensionless since we have written the problem from the beginning in dimensionless form. It is worth pointing out the great benefit of working in dimensionless form. We have just achieved a solution that is valid for *all* cases of one-dimensional acoustic motion in a hard-walled chamber. When we convert to dimensional form, the actual system dimensions and other parameters needed in a specific case enter the result. Observe that for the choice of dimensionless variables we have made, the wavenumbers and the frequencies are identical; this can be a real convenience. It is only when we convert to dimensional form that are different. Thus in dimensional form the wave numbers are

$$k_n = \frac{K}{L} = \frac{n\pi}{L}, \tag{5.126}$$

which have dimensions of inverse length.

In dimensional form, the time dependence is written, for example, as $\cos(\omega t)$; thus the circular frequencies (rad/sec) must be

$$\omega_n = \frac{\bar{a}K}{L} = \frac{n\pi\bar{a}}{L} \tag{5.127}$$

and the frequencies in cycles per unit time (cycles per second, or Hz if the speed of sound is given, say, in m/s and L is in meters) are

$$f_n = \frac{\omega_n}{2\pi} = \frac{n\bar{a}}{2L} \qquad n = 1, 2, 3 \dots \tag{5.128}$$

Notice that the frequencies are integral multiples of the fundamental ($n = 1$). Thus the third mode ($n=3$) has a frequency three times that of the fundamental, and so on. This is such a common situation in acoustics that it is often anticipated that frequencies will appear as integral multiples. That this is *not* always the case will become apparent when we consider transverse oscillations in a cylindrical chamber.

It is important to notice the effect of chamber sound speed and length on the frequencies as shown in equations 5.127 or 5.128. Frequency is of very great importance in combustion instability since driving and damping mechanisms are usually highly frequency dependent. Knowledge of the frequency characteristics of the time-dependent propellant acoustic response is often crucial in solving instability problems. Associated with each frequency is a *mode shape* which describes the spatial characteristics of the motion. If we write the final form of the solution for the pressure as

$$p^{(1)} = \underbrace{\cos(Kz)}_{\text{Mode Shape}} \cos(Kt) \tag{5.129}$$

the mode shape for a given wave number is the $\cos(K\,z)$ factor. Figure 5.9 shows plots of the pressure mode shapes for the first five modes. Notice that the largest pressure amplitudes occurs at the ends of the chamber. For the fundamental mode $(n = 1)$, the amplitudes are out of phase by 180° at the chamber ends. That is, when $p^{(1)}$ is positive at the left end, it is negative at the right end. This is true of all odd-numbered modes. For even modes $(n = 2, 4,$ etc.$)$, the pressure amplitude is in phase at each end. That is, the pressure reaches is maximum positive (or negative) value at the same instant at each end. Such maxima occur at points we will refer to as the pressure *antinodes*.
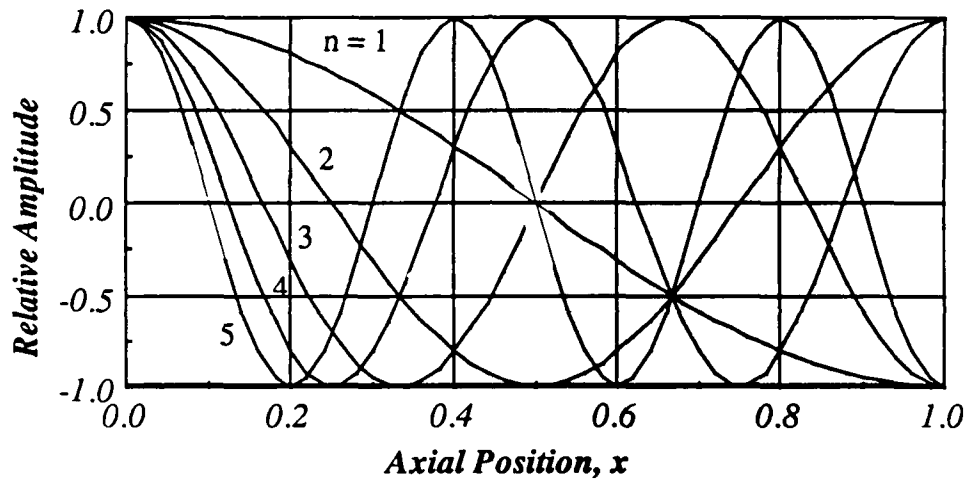
Fig. 5.9 PressureMode Shapes for the First Five Axial Acoustic Modes

Also notice that there are points where the pressure fluctuation is always zero. These are referred to as the pressure *nodes*. The fundamental mode has a single node, which is located at the chamber midpoint. Higher-order modes have a number of nodes equal to the mode integer. Thus the fifth mode has five nodes distributed uniformly along the chamber as shown in Figure 5.9. The actual pressure amplitude depends on the time as shown by the sinusoidal time dependence. Figure 5.10 shows how the amplitude varies with time for the fundamental mode. A wave motion of the type illustrated is referred to as a "standing-wave" since the nodal points are fixed. We will pay more attention to the distinction between traveling and standing-waveforms later. For now it is sufficient to say that a single traveling-wave component would not satisfy the boundary conditions of the axial-mode problem. A standing-wave can be decomposed into a pair of traveling-waves, each progressing in opposite directions. A traveling-wave can be represented by a system of standing-waves. This is a fact that has often been
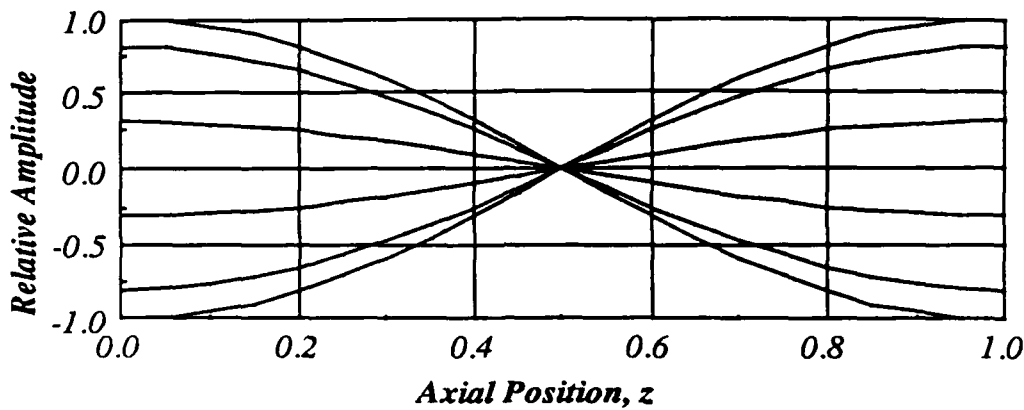
Fig. 5.10 First Longitudinal Mode Amplitude at Several Times

missed in rocket motor analysis, especially in cases where steep-fronted traveling-waves are involved.

Now that the pressure pattern is known, it is easy to determine the corresponding gas velocity. Of course one could solve for the velocity potential directly using exactly the method just used to get the pressure and then determine the velocity vector using equation 5.101. This is unnecessary and repetitious. The main result would just be to verify the frequency eigenvalues. The velocity can be directly determined by using the momentum equation. Thus integrating 5.105,

$$u^{(1)} = - \int \frac{\nabla p^{(1)}}{\gamma} dt = - \frac{1}{\gamma} \left\{ \frac{d}{dz} \cos (Kz) k \right\} \int \cos (Kt) dt \qquad (5.130)$$

and for standing axial waves we find

$$u^{(1)} = \frac{k}{\gamma} \underbrace{\sin (Kz)}_{\text{Mode Shape}} \sin (Kt) \qquad (5.131)$$

This result shows that the velocity fluctuation is out of phase with the pressure by $\pi/2$ radians (90°). The unit vector **k**, which points in a direction parallel to the z-axis, emphasizes the vector nature of the velocity. This is, of course not needed in the one-dimensional case, but we display it because three-dimensional forms will be needed later. Also notice the change in mode shape brought about by taking the gradient of the pressure. Figure 5.11 shows the velocity mode shapes for several modes. Observe that the velocity nodes lie at the chamber ends as required by the boundary condition that the normal velocity go to zero at the walls. It is also important to see that the fundamental does not have a velocity node within the chamber; its antinode is at the midpoint. That is, the velocity amplitude is largest at the center of the chamber. Velocity nodes within the volume appear as higher-order modes are considered. The second mode (n=2) has a single node at the chamber midpoint and so on.

The presence of the ratio of specific heats, γ, in the dimensionless solution for the velocity may seem puzzling, so let's check it against the classical acoustic results by rewriting our results in dimensional form. The dimensional pressure

and velocity can be written as

$$p = \bar{P} + \varepsilon \bar{P} \cos (Kz) \cos (Kt)$$

$$u = \frac{\varepsilon \bar{a}}{\gamma} \sin (Kz) \sin (Kt) k$$

(5.132)

The ratio of fluctuating pressure and velocity amplitudes is

$$\frac{|p'|}{|u|} = \frac{\varepsilon \bar{P}}{\frac{\varepsilon \bar{a}}{\gamma}} = \frac{\gamma \bar{P}}{\bar{a}} = \bar{\rho} \bar{a}$$

(5.133)

where the isentropic relationship

$$\bar{a} = \sqrt{\frac{\gamma \bar{P}}{\bar{\rho}}}$$

(5.134)

for the speed of sound has been used. Equation 5.133 is a familiar result in linear acoustics (Kinsler, Frey et al. 1982; Morse and Ingard 1968; Pierce 1981). The combination $\bar{\rho} \bar{a}$ is often referred to as the *characteristic acoustic impedance* or sometimes the *acoustic resistance* in the acoustics literature. From the acoustician's viewpoint, $\bar{\rho} \bar{a}$ has greater physical significance as a characteristic property of the gas than either the density or speed of sound taken individually.

Although the one-dimensional or "plane-wave" acoustics example just presented is very simple, it should be taken very seriously. It presents in the simplest form possible many of the concepts from acoustics that are needed in understanding the combustion instability problem.
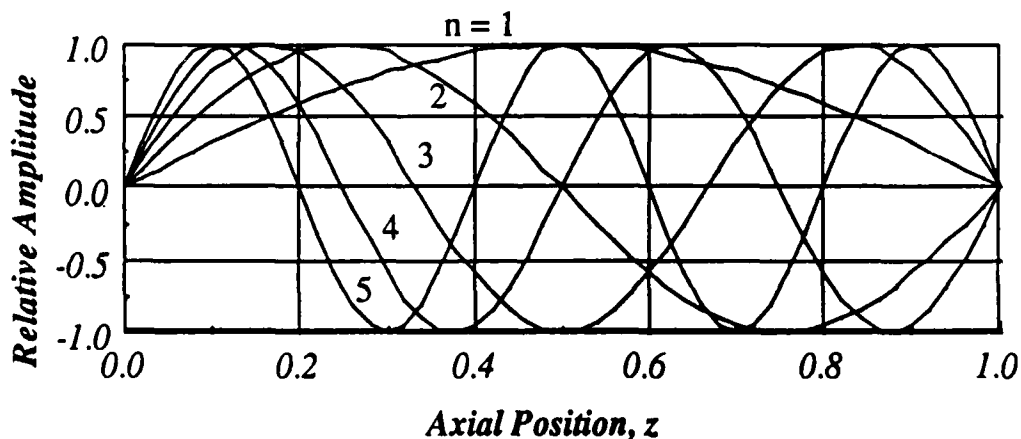
Fig. 5.11 Velocity Mode Shapes for the First Five Axial Acoustic Modes

Three-Dimensional Modes in a Rectangular Chamber

A rectangular cavity is a geometry occasionally of interest in rocket motor acoustics. Figure 5.12 shows such a cavity. It could, for example, represent a rectangular slot within a propellant grain. To determine three-dimensional solutions for rectangular volumes enclosed on all sides by rigid walls, it is necessary only to superimpose three axial solutions based on the one that was
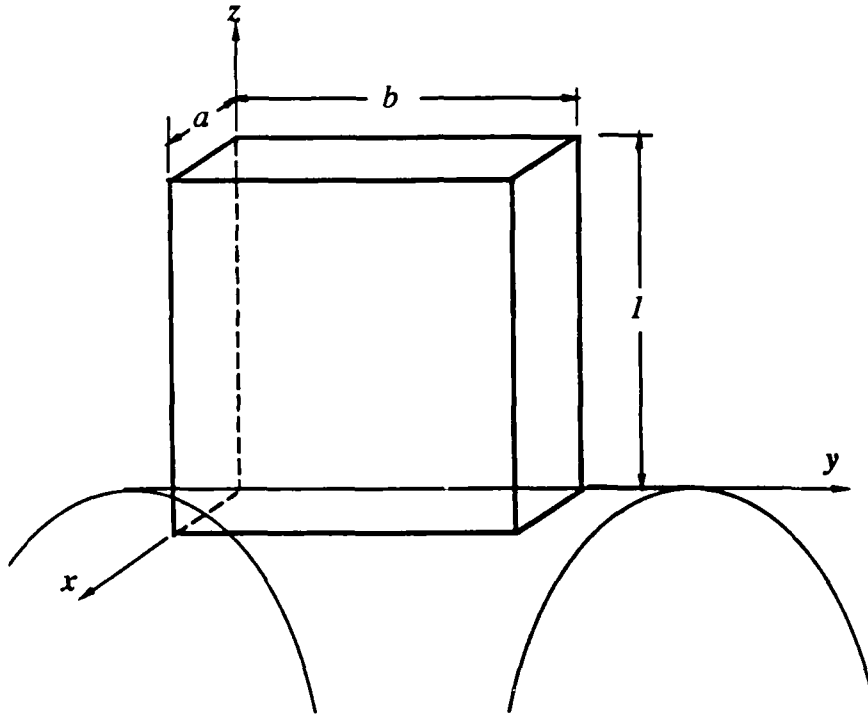
Fig. 5.12 Rectangular Cavity

carried out in the previous subsection. Thus one can write (the details of the calculation are left as an exercise for the reader; separation of variables can be used, but four functions are needed):

$$p^{(1)} = \cos(K_x x) \cos(K_y y) \cos(K_z z) \cos(Kt + \psi),$$ (5.135)

where we have introduced an arbitrary phase angle ψ to express the fact that the time origin is arbitrary at this point. Note that there are now three eigenvalues in the solution:

$$K_x = \frac{l\pi}{a}, \quad K_y = \frac{m\pi}{b}, \quad K_z = n\pi \qquad l, m, n = 0, 1, 2, 3 \dots,$$ (5.136)

and the corresponding frequencies are

$$K = \sqrt{K_x^2 + K_y^2 + K_z^2}.$$ (5.137)

Notice also that we now allow zero values for the mode integers where this would have been inappropriate in the corresponding one-dimensional solution. Modes are identified by specifying a set of mode integers. For example the (0,0,1) mode corresponds exactly to the one dimensional axial-mode we studied in the previous example (with gas motions in the z-direction).

As indicated in Figure 5.12, we have used the cavity length in the z-direction as the reference length. Thus a and b are the ratios of its physical x and y dimensions to its depth in the z-direction. Either of the other two choices for reference length would work as well.

The assumption of harmonic oscillations is appropriate in the class of problems we are dealing with; it is not necessary to treat the time dependence as formally as we did in the first example. It is often assumed that the time dependence is sinusoidal. Thus, the solution for a three-dimensional problem is

$$p^{(1)} = f(x,y,z)e^{Kt} .$$ (5.138)

Then the resulting differential equation giving the spatial characteristics of the problem is referred to as the Helmholtz equation. We will often utilize this approach in later chapters. We will employ the exponential form of the time solution in which the imaginary part of the eigenvalue corresponds to the frequency of oscillation, while the real part governs the growth or decay of the wave system.

Transverse Modes in a Circular Cylinder

Let us now consider the more complex three-dimensional problem of wave motions in a right circular cylinder as shown in Figure 5.13. In this case, we will choose the chamber radius as the length scale to emphasize the transverse gas motions. The need for cylindrical coordinates is clearly indicated. If instead we tried to use a cartesian system we would find the application of the boundary conditions would be greatly complicated. Assuming sinusoidal time dependence, the problem to solve is the Helmholtz equation and hard-wall boundary condition

$$\begin{cases} \nabla^2 f + K^2 f = 0 \\ \mathbf{n} \cdot \nabla f = 0 \text{ on boundaries} \end{cases}$$ (5.139)

as we have established in detail already, and for convenience we have assumed exponential time dependence as in equation 5.138.

Again, separation of variables would appear to be the simplest route to the solution. Assuming the solution is the product of functions

$$f = R(r)\Theta(\theta)Z(z),$$ (5.140)

it is necessary that

$$\frac{1}{rR}\frac{\partial}{\partial r}\left(r\frac{\partial R}{\partial r}\right) + \frac{1}{r^2\Theta}\frac{\partial^2\Theta}{\partial\theta^2} + \frac{1}{Z}\frac{\partial^2 Z}{\partial z^2} = -K^2 .$$ (5.141)
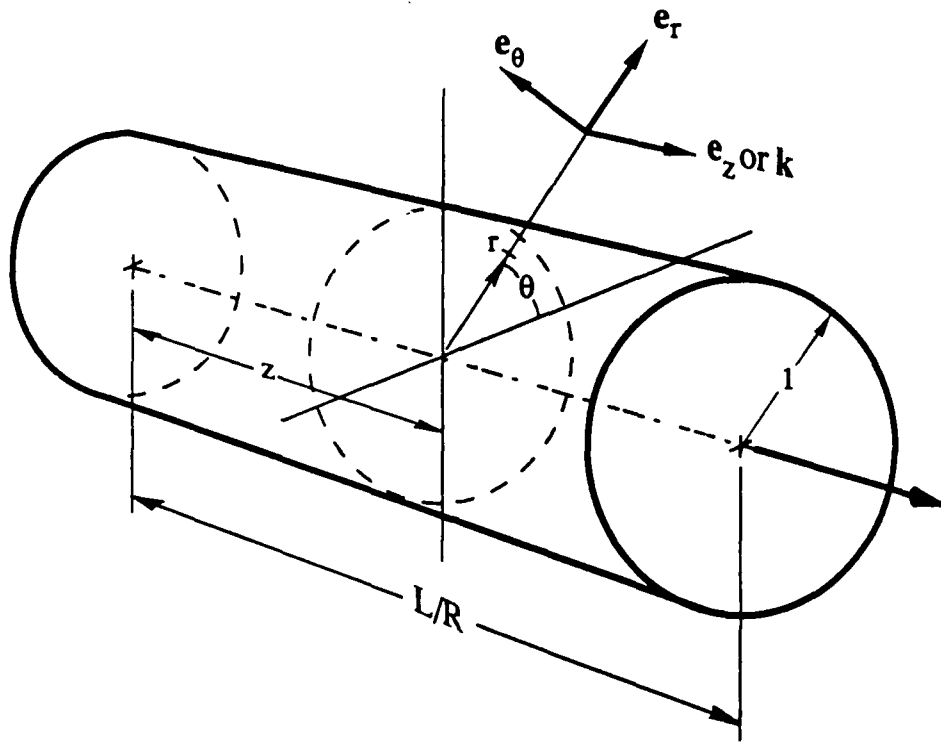
Fig. 5.13 Cylindrical Coordinate System and Unit Vectors

where there are now three separation constants to deal with. As before, physical reasoning must be used to pick the correct signs. The azimuthal behavior must be such that the angular dependence is not multivalued. That is, the solution must be periodic in angle θ. Thus the dependence on angle is of the form

$$\Theta = e^{\pm i\,m\,\theta} \qquad m = 0, 1, 2, \ldots \tag{5.142}$$

where m must be an integer. The axial part of the motion is handled just as it was when we considered it in the axial problem. Accounting for the fact that chamber radius is now the scaling length, one finds

$$Z = \cos{(k_1 z)} \tag{5.143}$$

where

$$k_1 = \frac{l\,\pi\,R}{L} \qquad l = 0, 1, 2 \ldots \tag{5.144}$$

This leaves the radial separation constant to be determined. Note that we are now confronted with a somewhat more complicated ordinary differential equation for the dependence on radial position. Equation 6.141 becomes

$$\frac{\partial^2 R}{\partial r^2} + \frac{1}{r}\frac{\partial R}{\partial r} + (k_{mn}^2 - \frac{m^2}{r^2})R = 0, \tag{5.145}$$

which will be recognized as Bessel's equation of integer order with solutions of the form

$$R = A J_m(k_{mn} r) + B Y_m(k_{mn} r) \qquad (5.146)$$

We must reject the solution Y_m (Bessel function of the second kind) by putting B = 0, since its retention would imply an infinite-amplitude at the axis of the chamber.   Thus only solutions of the first kind, J_m, are physically appropriate. Figure 6.14 illustrates the shapes of some of the Bessel functions.
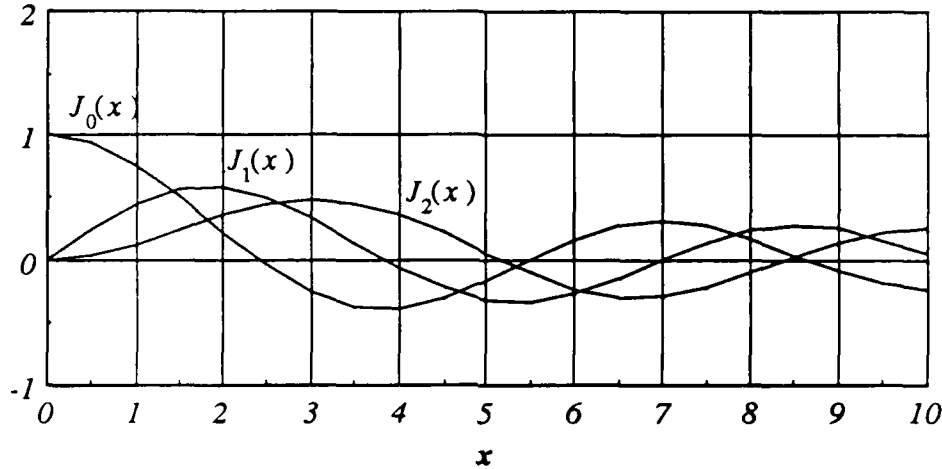
Fig. 5.14 Bessel Functions of the First Kind, $J_m(x)$

In order to satisfy the boundary condition that the normal component of the pressure gradient go to zero everywhere on the boundary (equivalent to making the normal velocity component zero at the boundary), it is necessary that

$$\frac{d}{dr} J_m(k_{mn} r) = 0 \qquad \text{at } r = 1 \qquad (5.147)$$

which provides the condition for extraction of the eigenvalues. Thus   must be the root of

$$J'_m(k_{mn}) = 0 \qquad (5.148)$$

Consideration of the separation constants leads to the relationship

$$K^2 = k_l^2 + k_{mn}^2 \qquad (5.149)$$

from which we find the formula for the frequencies:

$$\omega = \sqrt{k_l^2 + k_{mn}^2} \qquad (5.150)$$

Either traveling- or standing-wave solutions are possible. For example, we can write the final solution for the pressure as

$$p^{(1)} = J_m(k_{mn} r)\cos(k_l z)\cos(\omega t \pm m\theta) \qquad \text{Traveling Wave} \qquad (5.151)$$

or as

$$p^{(1)} = J_m(k_{mn} r)\cos(k_l z)\cos(m\theta)\cos(\omega t) \qquad \text{Standing Wave} \qquad (5.152)$$

The difference is made by which part of the azimuthal solution is used. In the traveling-wave case, sometimes described as the "spinning" solution, the pressure antinodes traverse the chamber in either the clockwise or counterclockwise direction (depending on which sign is used in equation 5.151). Figure 5.15 compares the pressure distributions for the standing and traveling forms for the fundamenta' transverse mode (l = 0, m = 1, n = 0). This is often described as the (0, 1, 0) tangential mode. This particular mode is the transverse oscillation most often encountered in practice (because it is subject to the least amount of damping and often the strongest driving effects). Either the standing or traveling form may appear, although experimental data is seldom sufficiently complete to determine which one is present. We will show later that the traveling form is probably more likely to be amplified, based on consideration of associated nonlinear damping effects.

The purely radial modes (0, 0, n) are seldom observed. Since their mode shapes involve the zeroth-order Bessel function, $J_0(k_{0n} r)$, they have a pressure antinode on the chamber axis (see Figure 5.13). A reason sometimes given for their scarcity in experimental data is that an energy source located near the axis would be needed to drive them strongly. Since the primary energy source is located at the burning surfaces, the tangential modes, (0, m, 0) are favored in transverse-mode solid rocket instability.

It is important to understand that in trying to identify modes in experimental data we may be dealing with combination modes in which both transverse and axial gas motions are present. It is unrealistic to expect a purely transverse wave in practice, since this would require gas motions parallel to the end-faces of the chamber. In reality viscous forces at the end-walls and in the nozzle entrance must be accounted for and the boundary conditions dictate that the velocity components parallel to the end-walls must vanish. The simplest way to account for this condition is to treat the waves as combination modes using the axial component to make the velocity zero at the port ends. There is considerable evidence that this is a likely form taken by transverse waves in cylindrical motors. The effect of the axial dependence on the frequency is not large, and in any event, uncertainties in speed of sound and chamber geometry also affect mode identifications. The experiments by Price (Price and Sofferis 1958) involving precise measurement of the grain shape in interrupted firings showed that finite-amplitude transverse oscillations have distinct axial burnback distributions as indicated by localized burning-rate increases. The results strongly suggested that combination transverse/axial-modes were present. The local burning-rate is affected by the oscillatory gas motion; this is another of the several nonlinear interactions that must be taken into account. Thus the extra surface regression in the central part of the bore may indicate that the amplitude distribution includes an axial component suggestive of an axial acousticmode. Figure 1.6 describes this effect.

An important practical feature of the transverse modes is that their oscillation frequencies are markedly higher than those of the axial-modes. Table 5.5 shows a few of the frequency eigenvalues (roots of 5.148). Thus they are often identified
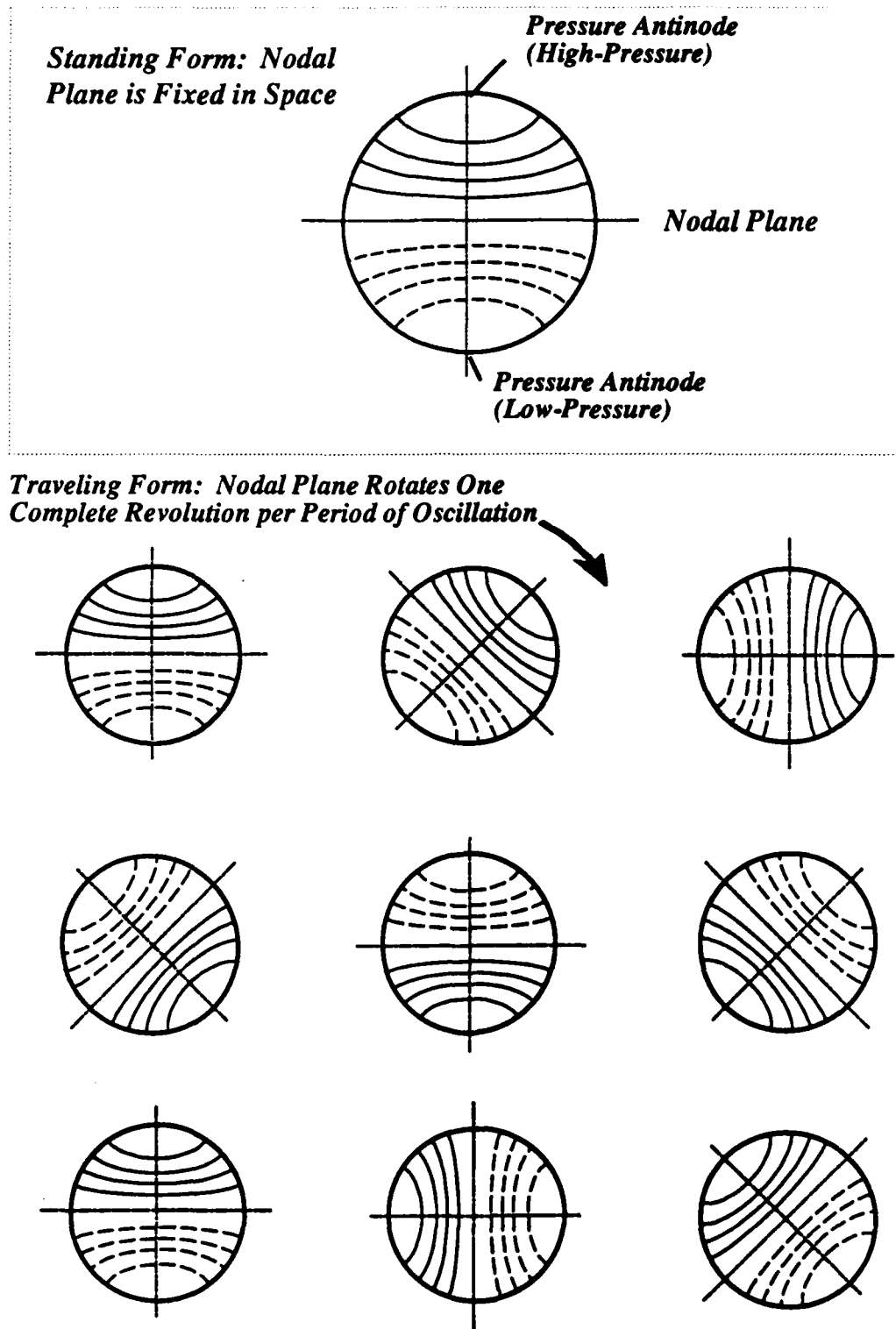
Fig. 5.15 First Tangential Mode, (0, 1, 0)

TABLE 5.5

Eigenvalues for Tangential Acoustic Modes in a Circular Cylinder

$$k_{mn}: \quad \text{Roots of } J'_m(k_{mn}r) = 0, \quad (r \to 1)$$

m	n				
	0	**1**	**2**	**3**	**4**
0	0	3.83171	7.01559	10.17347	13.32369
1	1.84118	5.33144	8.53632	11.70601	14.86359
2	3.05424	6.70613	9.96947	13.17037	16.34752
3	4.20119	8.01524	11.3459	14.58585	17.78875
4	5.31755	9.2824	12.6819	15.96411	19.19603
5	6.41562	10.51986	13.9872	17.31284	20.57551
6	7.50127	11.73494	15.2682	18.63744	21.93171
7	8.57784	12.93239	16.5294	19.94185	23.26805
8	9.64742	14.11552	17.774	21.22906	24.5872
9	10.71143	15.28674	19.0046	22.5014	25.89128
10	11.77088	16.44785	20.223	23.76072	27.18202

in the literature as "high-frequency" instabilities. They have often been the cause of the most troublesome forms of combustion instability, and are associated with catastrophic motor failures caused by unexpected changes in propellant burning-rate. In recent times they have not been considered important because modern propellants often contain aluminum powders or other stabilizing additives that promote stable burning. The precise way in which the additional damping arises is not completely understood, but may be related to two-phase gas effects since particulates can contribute damping in the higher-frequency oscillations. Later discussions will focus on the important practical question of additives and other devices for stabilizing combustion. Despite the current feeling that high-frequency instability is a problem of the past, transverse modes continue to play an important role, and often show up unexpectedly. In recent times this has happened in development of "clean" propellants. There is considerable practical interest in "low-smoke" and "no-smoke" propellants that have little or no aluminum or other metallic content. Such propellants are needed when contamination of vehicle surfaces in spaceflight applications or visibility of dense plumes in military applications must be considered. Transverse mode instability continues to plague development programs of this type. Unfortunately, there are many non-linear aspects of this phenomenon that have simply not been adequately resolved because rocket manufacturers have tended to believe that the use of aluminum eliminated the need for continued research.

Handling More Complex Geometries

The reader will now probably wonder how one can determine the acoustic frequencies and mode shapes for an actual rocket motor geometry. Since motor grain design usually involves combinations of slots, conocyls, and fins to achieve a desired thrust-time pattern, the result can be an acoustician's nightmare. In fact, this problem has only been partially solved by use of finite-element computer programs. The standard combustion stability code (Dudley and Waugh 1976) to be described in detail in Chapter 9 utilizes the NASTRAN finite-element program to approximate the mode-shapes and frequencies. This method works reasonably well, but requires an analyst experienced with the foibles of the program to produce reliable results.

There has been some success in using a scale model of the motor chamber to aid in determining the natural frequencies. The modes are excited by an acoustic driver placed at appropriate points. A good understanding of acoustic behavior is required in order to properly place the driver to excite modes of interest. A probe microphone is traversed through the chamber volume to map the three-dimensional fluctuating pressure distribution. Resonant conditions are readily detected by watching for peaks in the microphone response. Such peaks correspond to the natural or "normal" modes of the type we have described by mathematical means for simple chamber geometries. This method works fairly well for lower-order (hence lower frequency) modes, but it becomes a tedious process when high-frequency oscillations are of interest. Nodal points might be closely spaced and might move within the chamber is a traveling form is excited.

There is a real need for more complete computer software for accurate prediction of mode shapes and frequencies. Much art and experience is required at present to produce the needed information.

Superposition of Acoustic Modes

A feature of linear mathematical models is that two or more solutions of a given problem (differential equations plus boundary conditions) can be simply added together to represent more complex solutions. This is the basis for the solution of many classes of problems in engineering.

Another closely related topic is *spectral analysis* in which the Fourier transform method is applied to experimental data to determine the nature of its oscillatory constituents. That is, to determine the frequencies, amplitudes, and phase relationships of periodic components in the data. The idea here is that a time-dependent physical process can be described either in the *time domain* by giving its values as functions of time or in the *frequency domain* by specifying its amplitude and phase as functions of frequency. This is a subject of very great practical importance in the study of combustion instability because it is the principal method by which one determines from experimental evidence what modes of chamber oscillation are involved. This knowledge is essential in selection of corrective techniques or assessments of impact on system operation.

Although the gas oscillations in rockets are not, strictly speaking, acoustic waves, *it is almost a universal practice to associate them with the linear acoustic modes* of the combustion chamber. The basic concept is that the time-dependent part of the flow can be broken down into one or more acoustic components that, on the basis of their near-linearity, are essentially independent of one another. It is sometimes possible to determine what acoustic mode or modes of oscillation are most likely present by simple inspection of the data. One uses simple acoustics models of the type we have studied in making modal configuration estimates. It is quite easy to make errors in this process because the frequencies present in the actual data are not likely to correspond precisely to the theoretical acoustic modes. There are so many combination modes available that it is almost always possible to find one (or more) that will match the data. Unfortunately, one seldom has access to mode shape data. In other words, it is almost always data from one or two transducers, usually pressure transducers, placed at inappropriate (but accessible) locations in the chamber. Thus, it is only the frequency content that can be analyzed. It requires data from multiple transducers located strategically in the combustion chamber to make proper modal determinations. It often happens that an important oscillation is not picked up in the data analysis because the transducer was located near a node of the particular waveform involved. This has been a frequent problem with high-frequency transverse modes. The most logical location for a pressure transducer (from the instrumentation engineers point of view) is at the centerline of the fore-end of the motor where there is ready access through the ignitor port. This places the instrumentation near the pressure node of the most prevalent and potentially damaging high-frequency acoustic modes; the attenuated signal is a good indication of the true severity of the oscillation only if the mode identification is correct.

Some experimenters have had moderate success in modal determination by analyzing data from multiple strain measurements. The gages are attached to the outer surface of the motor case and can give some indication of the local increases in pressure. Attenuation from the propellant grain, liner, and other motor structures makes it difficult to interpret and use such data. Other instrumentation techniques such as use of microwaves and so on are treated elsewhere in this text. Their use has not been overwhelmingly successful in the determination of the wave structure in motors with pressure oscillations.

In many experimental situations, the signal is so complex that numerical treatment is required to extract the information it contains. Dedicated instrumentation is widely available for this purpose in the form of spectrum analyzers of various types. Many investigators, however, prefer to analyze data by means of specialized computer programs because this gives them more control of the process. This is especially important in cases where low-level signals are present that must be separated from more vigorous oscillatory content. No attempt will be made here to treat these important applications of modal superposition theory. Standard reference books on Fourier transform and spectral methods (Brigham 1974; Nussbaumer 1982; Press, Flannery et al. 1986) should be consulted for guidance in this area.

Representation of Wave Systems by Superposition of Acoustic Modes

Although the acoustic modes represent solutions to the unperturbed time-dependent problem, they can as we have seen in the last few subsections be superimposed to represent more complex cases. We will have occasion to use this technique many times as we attempt to develop more comprehensive models for the combustion instability problem. Therefore, it is appropriate to end this chapter with a brief review of a few additional properties of such series solutions, which will be essential in applying this approach. These are standard advanced calculus results, and are summarized here only for completeness.

Since we will be examining problems in which the departure from linear acoustics behavior is small, it will often be appropriate to represent the solutions as linear superpostions of the acoustic modes. The method is analogous to the representation of a complex function by a Fourier series. Thus we will often assume expansions of the form

$$p^{(1)} = \sum_{n=1}^{\infty} A_n p'_n \qquad (5.153)$$

The p'_n are solutions of the unperturbed wave equation for, say, the pressure. Each subscript n represents one acoustic mode; hence, for three-dimensional problems, n stands for the three modal integers. The coefficients A_n are to be determined. To find these, we take advantage of the powerful *Sturm-Liouville theorem* which establishes the property of *orthogonality* of a set of characteristic solutions of a governing differential equation. The theorem, its proof, and discussions of its application can be found in better texts on advanced engineering mathematics [Wylie, 1975].

A central result of considerable utility is that solutions of the type of second-order, linear differential equations that arise in our analyses give rise to sets of orthogonal functions. The word *orthogonal* as used here is based on an analogy with vector spaces. For a simple example, the unit vectors we often employ to describe a three-dimensional space are mutually perpendicular, or orthogonal. The eigenfunctions (also often called the *eigenvectors*), such as p'_n, representing an infinite set of solutions to a differential equation can be thought of as a set of vectors describing a space of infinite dimension. Each of the "unit vectors" is mutually "perpendicular" in a sense that we will define. In a three-dimensional space, vectors are orthogonal if their scalar products are zero. If the scalar ("dot") product of any member of the set with itself is unity, then the set is said to be *orthonormal*. In a space of eigenvectors, the vectors are orthogonal if a special kind of scalar product vanishes for any pair of unique solutions. This scalar product is represented by the orthogonality integral of the form

$$\int_a^b w\, p'_n p'_m\, dx = 0 \qquad n \neq m \qquad (5.154)$$

where, depending on the form of the differential equation, a weight function w

must be included. The integral is over the domain of the problem. That is, since the differential equation describes some physical effect in a definite region with boundary conditions that must be satisfied at the limits of the domain, then the integral is over the corresponding region.

Instead of treating the general concept of orthogonality in more detail, it is sufficient for our purposes to state the results for examples of the kinds of systems we will confront. In most cases, the domain of interest will be bounded by the surfaces, both burning and inert, and by the nozzle entrance of the rocket chamber. In our problem the orthogonality relationship will take the form of a volume integral over the chamber

$$
\begin{cases}
\displaystyle\int_V \psi_\alpha \psi_\beta \, dV = 0 & \alpha \neq \beta \\[3mm]
\displaystyle\int_V \psi_\alpha \psi_\beta \, dV = E_\alpha^2 & \alpha = \beta,
\end{cases}
\tag{5.154}
$$

where the ψ_α are the solutions of the Helmholtz equation

$$
\nabla^2 \psi_\alpha + K_\alpha^2 \psi_\alpha = 0
\tag{5.155}
$$

This is just the wave equation after assuming the time dependence is harmonic (see the discussions concerning equation 5.138 and 5.139). In some cases, especially those involving traveling waves, a slightly more general form is required since the eigenfunctions of the Helmholtz equation are complex; that is, for convenience they contain both real and imaginary parts to automatically take account of the relative phase of the pressure distribution as a function of time and position. Thus, if complex eigenfunctions are needed, the orthogonality relationship

$$
\begin{cases}
\displaystyle\int_V \psi_\alpha^* \psi_\beta \, dV = 0 & \alpha \neq \beta \\[3mm]
\displaystyle\int_V \psi_\alpha^* \psi_\beta \, dV = E_\alpha^2 & \alpha = \beta
\end{cases}
\tag{5.156}
$$

is the one that will be needed. The stars indicate the complex conjugate of the function. That is, the same function with the sign of the imaginary part reversed.

To illustrate the practical application of equation 5.154 (or 5.156), let us apply it to the three chamber geometries we studied earlier is this section. The simplest is the one-dimensional axial wave. In that case the eigenfunctions are

$$
\psi_\alpha = \cos(K_\alpha z)
\tag{5.157}
$$

(see equation 5.129). Since the cross-section, A, of the chamber was assumed constant, the volume integral collapses to a simple integral over the length of the chamber:

$$
\int_V \psi_\alpha \psi_\beta \, dV = A \int_0^1 \cos(K_\alpha z) \cos(K_\beta z) \, dz
\tag{5.158}
$$

The integrals are easily evaluated using standard forms, and we find for axial

waves
$$\int_V \psi_\alpha \psi_\beta dV = \begin{cases} 0 & \alpha \neq \beta \\ \dfrac{A}{2} & \alpha = \beta . \end{cases} \tag{5.159}$$

For waves in a three-dimensional chamber describable by cartesian coordinates, the eigenfunctions are found from equation 5.135 to be

$$\psi_\alpha = \cos(K_l\, x)\cos(K_m\, y)\cos(K_n\, z), \tag{5.160}$$

where the there are now three modal integers (l, m, n) needed. Application of the orthogonality principal over a volume with sides of length a, b and c (such as the one illustrated in Figure 5.12) results in

$$\int_V \psi_\alpha \psi_\beta dV = \begin{cases} 0 & \alpha \neq \beta \\ \dfrac{abc}{6} & \alpha = \beta . \end{cases} \tag{5.161}$$

Notice that the result for $\alpha = \beta$ is a special constant often expressed as E_m^2 that is related to the kinetic energy residing in the wave system. We will examine this interpretation in Chapter 8 when the energy method is employed to solve the combustion instability boundary value problem. This constant is sometimes used to "normalize" the modes so that the orthogonality integral yields a value of unity for $\alpha = \beta$. It sometimes happens that two modes have the same eigenvalue (same natural frequency) making the straightforward application of 5.154 fail if it is applied to those modes. Such modes are referred to as degenerate modes. Complete discussions of the handling of this situation are given in standard texts. The excellent treatiseby Morse and Ingard [Morse, 1968] gives an especially lucid description. We do not require that level of detail in our treatement at this juncture.

For a three-dimensional wave motion in a cylindrical cavity, the eigenfunctions are found from equations 5.151 (traveling wave) and 5.152 (standing wave) to be

$$\psi_\alpha = \begin{cases} J_m(k_{mn}r)e^{im\theta}\cos(k_l z) & \text{traveling wave} & (5.162) \\ J_m(k_{mn}r)\cos(m\theta)\cos(k_l z) & \text{standing wave.} & (5.163) \end{cases}$$

The dependence on angle θ in the traveling wave is now written in exponential form to take advantage of the complex notation. For either case, the appropriate differential volume element is
$$dV = r\, dr\, d\theta\, dz \tag{5.164}$$

Since the standing wave can be described unambiguosly without the need for complex notation, then equation 5.154 is appropriate, and we find

$$\int_V \psi_\alpha \psi_\beta dV = \begin{cases} 0 & \alpha \neq \beta \\ E_\alpha^2 & \alpha = \beta \end{cases} \tag{5.165}$$

where

$$E_\alpha^2 = \int_0^{L/R} \int_0^{2\pi} \int_0^1 rJ_m^2(k_{mn}r)\cos^2(m\theta)\cos^2(k_1 z)dr\ d\theta\ dz \qquad (5.166)$$

Notice that the volume integral readily decomposes into a product of three ordinary integrals. Also note that each of these has precisely the form required by the Sturm-Liouville theorem. as we stated it in equation 5.154. The two trigonometric integrals are easily evaluated. The Bessel function integral is a little more complicated. Notice also that the radius, r shows up in the integral as the weight function. The final orthogonality result for standing cylindrical waves is

$$E_\alpha^2 = \frac{L\pi}{4R}\left(1 + \frac{\sin 2\pi l}{2\pi l}\right)J_m^2(k_{mn})\left(1 - \frac{m^2}{k_{mn}^2}\right) \qquad \begin{array}{c}\text{Standing}\\\text{Wave}\end{array} \qquad (5.167)$$

We proceed in like fashion for the traveling waves, but now equation 5.157 is the appropriate orthogonality relationship. The algebra is only slightly more complicated, and we find for the product of the eigenfunction with its complex conjugate

$$\psi_\alpha\psi_\beta^* = J_m^2(k_{mn}r)e^{i\theta}e^{-i\theta}\cos^2(k_1 z) = J_m^2(k_{mn}r)\cos^2(k_1 z) \qquad (5.168)$$

The same integrals used in the standing case appear and we find without difficulty that

$$E_\alpha^2 = \frac{L\pi}{2R}\left(1 + \frac{\sin 2\pi l}{2\pi l}\right)J_m^2(k_{mn})\left(1 - \frac{m^2}{k_{mn}^2}\right) \qquad \begin{array}{c}\text{Traveling}\\\text{Wave}\end{array} \qquad (5.169)$$

For the reader who is not mathematically inclined, the practical significance of the orthogonality results may not be readily apparent. Our interest in them is entirely practical. For example, they give us the means, in principle, to find the coefficients in a series representation such as that introduced in equation 5.153. This is the same approach used in evaluating the terms in a Fourier series; it is just the way that the Euler equations for the Fourier coefficients are found. For example, suppose that in a certain application, we find (after some algebra) that the solution for the pressure distribution, say, is some function G(x,y,z).

$$G(x,y,z) = \sum_{i=1}^{\infty} A_n\psi_n \qquad (5.170)$$

We need a way to find the values of the A_n in the series. Orthogonality gives us the means to do this. For example, suppose we wish to determine a particular coefficient, A_m. To isolate it, multiply 5.170 through by the corresponding eigenfunction and then integrate over the domain. The integral of the sum on the left side can be broken into the sum of integrals such that

$$\int_V \psi_m G(x,y,z)dV = \sum_{i=1}^{\infty} \int_V A_n \psi_n \psi_m dV \qquad (5.171)$$

Now orthogonality (equation 5.154) can be utilized to eliminate all terms on the right that have subscripts other than m. Thus the expression for any coeffcient in the series is

$$A_m = \frac{1}{E_m^2} \int_V \psi_m G(x,y,z)dV \qquad (5.172)$$

and, providing the integral on the right can be evaluated, then the required series representation can be completed. If complex eigenfunctions are appropriate (as in the case of a traveling wave) then the complex conjugate of ψ_m appears in equation 5.172 in the place of the normal eigenfunction. The basic mathematical tools just reviewed will be of great utility in treating the combustion instability system model in Chapter 8.

5.7 EFFECTS OF VORTICITY AND VISCOSITY

Several times in this chapter we have encountered the effects of vorticity or *rotation* of fluid elements. Since a clear understanding of the underlying physical ideas is essential in chapters to follow, this brief section is included for the benefit of readers who are not familiar with the background ideas. Emphasis is on the physical origins of vorticity and its relationship to viscous effects. Readers interested in more detailed discussions should consult any good text on fluid dynamics.

Much of the latter part of this chapter has been based on the assumption that the time-dependent flow in a rocket chamber resembles acoustic wave motions. These waves represent irrotational waves of compressibility. That is, effects of viscosity and rotationality have been completely ignored in our treatment of the time-dependent flow to this point in the book. Indeed, nearly all representations of the gas oscillations now in use to assess rocket combustion instability are based on this simplification. However, we found in section 5.3 that a realistic model for the steady flow requires that we account for the vorticity generated at the burning surface in the process of generation of the combustion gases. This vorticity plays a major role in controlling the mean velocity distribution. It is clearly plausible that similar effects could be important in the oscillating component of the flow. In later sections we will demonstrate in detail that this is the case. In fact, inclusion of vorticity transport leads to rational answers to questions related to velocity coupling, flow turning, and other effects used to correct the standard combustion instability models. These corrections attempt to account for vorticity effects, although this has not always been recognized by those responsible for the models.

Vorticity production is usually related to the action of viscous forces acting within the gas. The classical example is the generation of vorticity in the boundary layer of a fluid streaming along a wall. If a single fluid particle near the boundary is considered, one sees that the side closest to the wall must consist of a fluid layer moving more slowly than that on the side most distant from the wall. The fluid near the wall is retarded by viscous forces in such a way that the no-slip condition is satisfied. Thus the element posesses angular velocity. The angular velocity vector is perpendicular to the plane of the motion in this simple example, and it points along the instantaneous axis of spin. The shearing stresses caused by viscosity can be said to generate the rotation or vorticity. A measure of the spin is the curl of the velocity vector

$$\Omega = \nabla \times U \tag{5.173}$$

If the fluid particle were suddenly frozen so that it moved like a tiny rigid body, then its angular velocity of spin would be half the magnitude of the vorticity.

Vorticity generated in a boundary layer propagates into the outer reaches of the fluid by the process of diffusion if the boundary is a solid one. If the boundary is a source of gas such as a porous surface or a burning propellant, then vorticity generated near the surface is also propagated by convection. The vorticity always stays attached to the same fluid. Thus as gas moves away from the surface, it carries the vorticity it picked up by whatever surface processes acted on it. The vorticity may decay because of the continued action of viscosity. In most rocket analyses, the gas is assumed to be inviscid. This does not mean that there is no vorticity. We saw this situation in section 5.3. Unless we insist that the gas carries vorticity, then we cannot satisfy a realistic boundary condition at the burning surface. The appropriate boundary condition is that the the gases enter the chamber in a direction perpendicular to the burning surface. This is the no-slip boundary condition. Its origin is in the action of viscosity on particles of gas formed in the combustion process. No velocity component parallel to the surface is allowed. In modeling this effect, it is not necessary, at least in the steady flow problem, to account explicitly for viscous forces within the body of the gas. The Culick mean flow solution demonstrates this feature. Nevertheless, the gas carries azimuthal vorticity representing the spin induced as it enters the chamber.

Now consider the unsteady flow. Since we know from many experiments that the gas oscillations have characteristics like acoustic waves (the frequencies closely match those of the chamber acoustic modes) then it is natural to assume that they are acoustic waves. All analyses used in rocket stability calculations start with this assumption. Remember that acoustic waves are irrotational. That is, they represent gas motions that do not involve vorticity. Since viscous effects were not important in the mean flow problem, it is again natural to assume that they do not influence the unsteady flow. However, the unsteady motion must satisfy boundary conditions at surfaces analogous to those controlling the steady part. That is, the no-slip condition must be satisfied. There is great confusion associated with this part of the combustion instability problem. The literature is

replete with attempts to account for this discrepancy by "band-aid" fixes. For example, the so-called "flow-turning" correction [Culick, 1972] is intended to account for the momentum exchanges related to accounting for the transition from strictly normal gas oscillations at the surface into axial oscillations within the main volume of the chamber. Velocity coupling must also be mentioned in this regard. It is based on the idea that there is a parallel fluctuating velocity component in the vici ity of the combustion zone, the "cross-flow" velocity that is supposed to couple with the combustion processes. It is obvious that one needs detailed information concerning the actual velocity field near the burning surface to account for this properly. If the no-slip condition is satisfied, then the velocity field must clearly carry vorticity. A purely acoustic solution cannot be correct in the vicinity of burning surface. We will address this problem in detail in the next chapter. We will find much evidence, both analytical and experimental, that proves the importance of vorticity transport in the combustion instability problem.

5.8 SUMMARY

This chapter introduces some of the fundamentals of the mathematical modeling of the flow in a rocket chamber. The formulation of the governing equations, and the mathematical strategies for their solution are discussed in detail. Equations for the gas phase behavior are deduced to the third-order of accuracy, for use in later chapters. The need for a reliable mean flow model on which to build the time-dependent analysis is emphasized. The major influence of vorticity generation and transport in rocket flows is clearly shown in the steady flow problem. Later chapters will build on this insight to show that vorticity effects play an important role in the energy transfer from combustion processes into the wave motions in combustion instability.

Much of the mathematical jargon of the subject is carefully reviewed in this chapter with the intent to make its vast literature more accessible to users in the rocket industry. This is done by means of simple example problems. Emphasis is on acoustic waves since they play a central role in the accumulation of energy in unsteady wave motions in a rocket chamber.

The powerful method of superposition is demonstrated as a means to analyze complex unsteady features such as traveling shock-like waves often associated with combustion instability. Superposition of simpler solutions is allowed because of the linearization accomplished in the mathematical formulation.

Using the basic toolset assembled in this chapter we can undertake a systematic analysis of the rocket combustion instability problem. This amounts to adding mathematical descriptions of additional physical and chemical effects to the basic combined mean flow/acoustic wave system we have defined. An important topic introduced only in its simplest form in this chapter is the incorporation of the active boundary conditions at a propellant burning surface.

REFERENCES

Anderson, J. D. (1982). Modern Compressible Flow. New York, McGraw-Hill Book Company.

Beddini, R. A. (1986). "Injection-Induced Flows in Porous-Walled Ducts." AIAA J. 24 (12): 1766-1773.

Betchov, R. (1958). "Nonlinear Oscillations in a Column of Gas." Physics of Fluids. 1 (3): 205-212.

Brigham, E. O. (1974). The Fast Fourier Transform. Englewood Cliffs, NJ, Prentice-Hall.

Brownlee, W. G. (1964). "Nonlinear Axial Combustion Instability in Solid Propellant Motors." AIAA J. 2(2): 275-284.

Brownlee, W. G. and G. H. Kimball. (1966). "Shock Propagation in Solid-Propellant Rocket Combustors." AIAA J. 4(6): 1132-1134.

Chester, W. (1964). "Resonant Oscillations in Closed Tubes, J. Fluid Mechanics." J. Fluid Mechanics. 18: 44.

Chu, B. T. and S. J. Ying. (1963). "Thermally Driven Nonlinear Oscillations in a Pipe with Traveling Shock Waves, Physics of Fluids." Physics of Fluids. 6(6): 1625-1637.

Cole, J. D. (1968). Perturbation Methods in Applied Mechanics. Waltham, Massachusetts, Blaisdell Publishing Company.

Culick, F. E. C. (1966). "Rotational Axisymmetric Mean Flow and Damping of Acoustic Waves in a Solid Propellant Rocket." AIAA J. 4(8): 1462-1463.

Culick, F.E.C. (1972). "Interactions between the Flow Field, Combustion, and Wave Motions in Rocket Motors," Naval Weapons Center, TP 5349, June 1972.

Dickinson, L. A. (1962). "Command Initiation of Finite Wave Axial Combustion Instability in Solid Propellant Rocket Motors." ARS J. 32: 643-644.

Dudley, D. P. and R. D. Waugh. (1976). Standardized Stability Prediction Method for Solid Rocket Motors.

Morse, P. M. and K. U. Ingard. (1968). Theoretical Acoustics. New York, McGraw-Hill Book Company.

Myers, M. K. (1980). "On the Acoustic Boundary Condition in the Presence of Flow." J. Sound and Vibration. 71(3): 429-434.

Nayfeh, A. H. (1973). Perturbation Methods. New York, John Wiley & Sons.

Nayfeh, A. H., J. E. Kaiser and B. S. Shaker. (1974). "Effect of Mean Velocity Profile Shapes on Sound Transmission through Rectangular Ducts." J. Sound and Vibration. 34(3): 413-423.

Nayfeh, A. H., J. E. Kaiser and D. P. Telionis. (1975). "Acoustics of Aircraft Engine-Duct Systems." AIAA J. 13: 130-154.

Nussbaumer, H. J. (1982). Fast Fourier Transforms and Convolution Algorithms. New York, Springer-Verlag.

Pierce, A. (1981). Acoustics. New York, McGraw-Hill Book Company.

Press, W. H., B. P. Flannery, S. A. Teukolsky and W. T. Vetterling. (1986). Numerical Recipes: The Art of Scientific Computing. Cambridge, Cambridge University Press.

Price, E. W. and J. W. Sofferis. (1958). "Combustion Instability in Solid Propellant Rocket Motors." 28(No. 3): 190-192.

Ribner, H. S. (1957). "Reflection, Transmission and Amplification of Sound by a Moving Medium." J. Acoustical Society of America. 29: 435-441.

Riemann, B. (1953). On Propagation of Plane Air Waves of Finite Amplitude. The Collected Works of Bernhard Riemann. New York, Dover.

Rockwell, D. (1982). Oscillations of Impinging Shear Layers. AIAA Aerospace Sciences Meeting.

Schlichting, H. (1979). Boundary-Layer Theory. McGraw-Hill Series in Mechanical Engineering. New York, McGraw-Hill Book Company.

Shapiro, A. H. (1953). The Dynamics and Thermodynamics of Compressible Fluid Flows. New York, Ronald Press.

Dunlap, R. and e. al. (1974). "Flowfield in the Combustion Chamber of a Solid Propellant Rocket Motor." AIAA J. **12**(10):

Dunlap, R., G. A. Flandro, R. A. Beddini, R. S. Brown and H. McDonald. (1987). Internal Flow Field Study.

Flandro, G. A. (1982). "Energy Balance Analysis of Nonlinear Combustion Instability." J. Propulsion and Power. **1**(3): 210.

Flandro, G. A. (1986). "Vortex Driving Mechanisms in Oscillatory Rocket Flows." J. Propulsion and Power. **2**(3): 206-214.

Flandro, G. A. (1980). Stability Prediction for Solid Propellant Rocket Motors with High-Speed Mean Flow.

Ingard, K. U. (1959). "Influence of Fluid Motion Past a Plane Boundary on Sound Reflection, Absorption and Transmission." J. Acoustical Society of America. **31**: 1035-1036.

Jeffrey, A. and T. Kawahara. (1982). Asymptotic Methods in Nonlinear Wave Theory. Boston, Pitman Advanced Publishing Program.

Keller, J. B. (1955). "Reflection and Transmission of Sound by a Moving Medium." J. Acoustical Society of America. **27**(6): 1044-1047.

Kinsler, L. E., A. R. Frey, A. B. Coppens and J. V. Sanders. (1982). Fundamentals of Acoustics. New York, John Wiley & Sons.

Kirchhoff, G. (1877). Vorlesungen uber Mathematiche Physik: Mechanik. Leipzig, Teubner.

Liepmann, H. W. and A. Roshko. (1957). Elements of Gasdynamics. Galcit Aeronautical Series. John Wiley & Sons, Inc.

Lighthill, M. J. (1952). "On Sound Generated Aerodynamically." Proc. Royal Society, Series A. **231**:

Maslen, S. H. and F. K. Moore. (1956). "On Strong Transverse Waves Without Shocks in a Circular Cylinder." J. Aeronautical Sci. **23**: 583-593.

Miles, J. W. (1957). "On the Reflection of Sound at an Interface of Relative Motion." J. Acoustical Society of America. **29**: 226-228.

Sigman, R. K. (1985). "Boundary Condition for Rocket Motor Stability." AIAA J. 23(7): 1079-1085.

Sirignano, W. A. and L. Crocco. (1964). "A Shock Wave Model of Unstable Rocket Combustors." AIAA J. 2(July): 1285-1296.

Sotter, J. G. and G. A. Flandro. (1968). "Unstable Combustion in Rockets." Scientific American. 12(12):

Stewartson, K. (1964). The Theory of Laminar Boundary Layers in Compressible Fluids. Oxford, The Clarendon Press.

Temkin, S. (1967). Nonlinear Gas Oscillations in a Resonant Tube..

Van Dyke, M. (1964). Perturbation Methods in Fluid Mechanics. Applied Mathematics and Mechanics. New York and London, Academic Press.

Van Dyke, M. (1975). "Computer Extension of Perturbation Series in Fluid Mechanics." SIAM J. Appl. Mech. 28: 720-734.

Van Wylen, G. J. and R. E. Sonntag. (1978). Fundamentals of Classical Thermodynamics. New York, John Wylie & Sons.

Wolfram, S. (1988). Mathematica, A System for Doing Mathematics by Computer. Redwood City, CA, Addison-Wesley Publishing Co.

MODELING OF COMBUSTION DYNAMICS

*In spite of the considerable effort which has been made since 1960 in at-
tempts to elucidate the phenomena of combustion instability, it is evident ..
that many gaps exist in our base understanding of the phenomena.*

G.F.P. Trubridge, 1969

6.1 INTRODUCTION

The principal source of energy that drives oscillations in a solid rocket
chamber is the combustion process itself. This energy source is mitigated by the
effects of the associated flow of combustion gases and other loss effects that are
inherent in the flow channel and nozzle. The purpose of this chapter is to provide
both physical and mathematical descriptions of the mechanisms that generate
acoustic energy in the combustion zone of the propellant. Emphasis is on the
accepted models for these mechanisms, but the assumptions and approximations
on which they are based will be carefully scrutinized. Such a discussion cannot
be carried out without some mention of experimental means for verifying the
models and for providing a means to evaluate features that cannot be based on
rational analysis. A later chapter is devoted to detailed treatment of the state of
affairs in the experimental arena.

The first step is to provide a clear physical picture of the manner in which the
combustion process responds to acoustic pressure fluctuations. A simple energy
balance provides considerable insight. Using this simple model one can define
response functions or acoustic admittance functions that provide a bridge be-
tween the complex combustion effects and the chamber gas dynamics. Unfortu-
nately, there exists a bewildering array of different notations and interpretations
in the literature. We will attempt to clarify the relationships between the differ-
ent systems of notation. It is easy to show that all are variations on just one
theme. A comprehensive table is provided to ease the task of translating between
the myriad publications on the subject of combustion coupling.

The subject of modeling of time-dependent combustion processes is a controversial one. It is almost impossible to avoid using models that involve parameters that cannot be directly determined from known or measurable propellant or combustion gas properties. It is of course difficult to deal with combustion of solid propellants experimentally because the the combustion zone is extremely thin, the burning surface is anything but a smooth, homogeneous surface, and the chemical species and combustion dynamics are not readily susceptible to direct measurements. In modeling these effects, one must attempt to deal with heat transfer from and to the propellant surface, pyrolysis of the surface, diffusion of mass, and gas-phase chemical reactions. This is a very complicated analytical problem. Most models, although seemingly quite different in terms of handling of the chemistry and fluid mechanics, can be shown to contain the same basic information [Culick, 1968]. This is because the strongest influence in these models is the role played by heat transfer in controlling the response to pressure fluctuations. Gas phase effects apparently play a minor role unless the oscillation frequency is very high. Thus most models employ the *quasi-steady gas phase* assumption, which greatly simplifies the analysis.

Many models are based on a one-dimensional treatment of the mean flow field. This is, in fact, completely justifiable in the majority of applications. Concern about this assumption has led to much confusion. The major worry has to do with the role of gas oscillations *parallel* to the burning surface. Since the oscillating pressure field clearly interacts strongly with the combustion process, it seems entirely logical that the transverse acoustic velocity should produce some analogous effects. Indeed, experiments with burners involving propellant samples placed with their surfaces parallel to the local acoustic velocity show that there is a measurable effect of wave incidence. At the time of writing there are several research programs in progress aimed at elucidating this "velocity coupling" effect. Unfortunately, in the original hypothesis on which it is based, too much emphasis was placed on making it completely analogous to pressure coupling with little or no attention paid to the gas dynamics of the situation. Analogies to steady-state erosive burning were also drawn without detailed consideration of the fluid dynamics. One must define a "cross-flow velocity" related to the local acoustic fluctuations which plays a role analogous to the local pressure fluctuations. This leads to a velocity coupled response function analogous to the pressure coupling response. There has been much conjecture on the nature of this function but practically no serious attempt to relate it to the physics and chemistry of the problem. The reasons for this will become quite clear as we examine the details of the time-dependent combustion process. In fact, it will be easy to show that *there is no cross-flow velocity in the vicinity of the chemically reactive part of the combustion zone* (except for oscillations at very high frequencies outside the range of practical interest).

Velocity coupling will be carefully considered as we carry out the details of the pressure coupling modeling. Realistic assessements will be made of the actual geometry of the problem. This will set the stage for more detailed

analyses in later chapters after we have assembled important tools and flow field descriptions. We will also discuss findings from recent experimental programs employing cold-flow simulations of rocket flow effects. Of considerable interest is progress in computational fluid dynamic (CFD) modeling of the interactions between the gas oscillations and the burning zone. These results support many of the views expressed in this chapter concerning the true nature of velocity coupling and related topics.

Since turbulent fluctuations are obviously important in certain parts of the steady combustion problem, it seems logical to expect turbulent interactions with the organized acoustic oscillations in the chamber. There is some interesting current research in this potentially important area; we will review it and its implications in terms of combustion dynamics modeling.

6. 2 COUPLING OF WAVES WITH MEAN FLOW AND COMBUSTION

There are major differences between the simple acoustics problems we studied in Chapter 5 and the gas oscillations in a rocket. These are brought about by the coupling of the waves with the mean flow and with the combustion processes at the burning surfaces forming part of the chamber boundary. In this section we will attempt to identify all major characteristics of the acoustic coupling to combustion and flow by means of simple analyses. Emphasis will be on describing the various interacting phenomena in uncomplicated form.

In the treatment of any complex phenomenon such as combustion instability, it is of the utmost importance that simple physical models describing its main features be understood thoroughly before attempting to tackle the the actual problem with all of its physical, chemical, geometrical, and computational tangle. The reader must understand that several of the topics to be discussed represent controversial issues in which some basic questions have not been fully resolved. Some of the simple models to be used here to introduce the subject of coupling may conflict with views held by other researchers working in the field. In introducing coupling effects we must touch on concepts about which no consensus has been reached despite over three decades of study.

Boundary Conditions

First it is necessary to reopen the question of boundary conditions in order to set the stage for analysis of more realistic models of time-dependent rocket flow in sections to follow. The questions that we will raise in a brief and simple way here are probably the most difficult ones in combustion instability analysis. We will see that a confrontation with all of the complexities peculiar to the time-dependent operation of a rocket motor is unavoidable. In what follows, though, we will emphasize the physical nature of the phenomenon. We will seek to demonstrate the principal manner in which boundary processes provide a source of energy, which may in some cases supply energy to the wave motions within

the chamber. A major goal is to clarify these processes by showing the relationship to simple, well-established thermodynamic concepts. We will show that all such processes are encompassed by the First (with limitations dictated by the Second) Law of Thermodynamics. It will thus become clear that a *work/energy* approach to modeling of combustion instability effects is strongly motivated.

Let us first establish what we need from the mathematical standpoint. Then we will seek out the answers by physical arguments. At the end of Section 5. 4, we found the equations governing small-amplitude (linearized) oscillations for a rocket combustion chamber. We proceed just as we did for the special case of a hard-walled chamber without mean flow (Section 5.5), but we must retain the perturbations due to the injection of mass at the boundary represented by terms of $O(M_b)$ in 5.96 and 5.97. To display the complete problem that must be solved, first combine the two equations by eliminating the velocity perturbation between them just as we did for the acoustic case (see the procedure that led to equation 5.104.) The momentum balance (equation 5.97) can then be used to express the condition that must be satisfied by the pressure fluctuation at a the burning propellant surface or other bounding surfaces. Thus the boundary value problem that we must solve is

$$\nabla^2 p^{(1)} - \frac{\partial^2 p^{(1)}}{\partial t^2} = M_b \left\{ \nabla \cdot \left[U \frac{\partial p^{(1)}}{\partial t} + \gamma(u^{(1)} \cdot \nabla U + U \cdot \nabla u^{(1)}) \right] \right\} \qquad (6.1)$$

$$n \cdot \nabla p^{(1)} = - n \cdot \left\{ \gamma \frac{\partial u^{(1)}}{\partial t} + M_b \left[\gamma(u^{(1)} \cdot \nabla U + U \cdot \nabla u^{(1)}) \right] \right\} \qquad (6.2)$$

An entire chapter (Chapter 8) is devoted to the detailed treatment of this problem and a thorough discussion of the results. Its implementation in a practical computational tool is described in Chapter 9. What we need now is to understand what information must be assembled to make a realistic solution possible. Equation 6.2 gives considerable guidance in this regard. First observe the importance of knowledge of the mean flow geometry (as represented by the vector U) as we indicated in Section 5.3. There is mass generation at the surface because of the phase change from solid to gas, therefore we must also account for a *fluctuating velocity component* at the surface. Thus the normal component of $u^{(1)}$ is not zero on the boundary as it was in the hard-walled acoustics problem. The basic idea of *coupling* is that there is some relationship between $u^{(1)}$ and $p^{(1)}$ in the boundary zone involving complex chemical and physical interactions.

Coupling Mechanisms

By coupling mechanisms we mean interactions of the wave motions with the chamber environment that increase or decrease the energy they carry. If the fluctuating velocity of gases at the burning surface is affected by the pressure fluctuations, then it is clearly necessary to quantify this relationship in order to establish the right-hand side of equation 6.2 to state a complete boundary value

problem to represent the flow.

Since the most obvious source of energy to drive waves to higher amplitude is associated with the combustion processes at the propellant surface, we are compelled to model energy sources and sinks as boundary phenomena. A typical example of such an energy producing interaction is the classical *pressure coupling* that represents the cornerstone of classical combustion instability analyses. Direct measurements verify the importance of pressure coupling and it has been accepted as the fundamental energy source for oscillatory flow fields. What is needed is made clear by our boundary conditions as stated in equation 6.2. To complete this statement to enable us to solve for $p^{(1)}$, we must know the relationship between $p^{(1)}$ and $u^{(1)}$ at the burning surface.

It is not necessary at this point to be too specific about the mechanics of the boundary processes. It will be assumed that the combustion zone is a thin region at the propellant surface that can be modeled as a linear transfer function. A simple physical model serves to explain how this works: fluctuations in pressure invoke a fluctuating response in the burning rate. Thus, at the edge of the combustion zone, there is a fluctuating mass flow representing the response of the combustion and other chemical and physical processes to the pressure oscillations. This response *may be out of phase* with the input signal as one would expect in any real process. The main assumption is that the processes are adequately represented by a linear model. For example, we can describe the coupling in terms of a simple linear algebraic relationship such as

$$v^{(1)} = - \mathbf{n} \cdot \mathbf{u}^{(1)} = \Re p^{(1)} \tag{6.3}$$

$v^{(1)}$ is the fluctuating velocity component at the edge of the active zone induced by the presence of the oscillation $p^{(1)}$. It is related to the modification in mass flow rate from the burning zone due to the pressure sensitivity of the combustion processes.

An important geometrical condition pertains to all coupling effects. It is that, on the scale of the reaction zone, the burning rate response is a *normal velocity fluctuation*, a modification to the unperturbed acoustic velocity fluctuation. From the form of equation 6.2, it is clear that the factor of proportionality, often referred to as the *admittance function* or *response function* is of the order of the mean Mach number. That is,

$$\Re = O(M_b) \tag{6.4}$$

It is essential to establish that it is in the normal velocity correction that one finds the main source of driving energy in the combustion instability phenomenon. This is done in the following subsection.

It is convenient to utilize complex notation as we have found useful several times before. Thus we can easily allow for the phase lag or lead of the combustion response to the pressure by making $\Re$ a complex function:

$$\mathfrak{R} = \mathfrak{R}^{(r)} + i\mathfrak{R}^{(i)}. \tag{6.5}$$

This can be written in the form

$$\mathfrak{R} = |\mathfrak{R}|\cos \omega\tau + i|\mathfrak{R}|\sin \omega\tau, \tag{6.6}$$

where τ is the time lead between the combustion response $v^{(1)}$ and the input signal $p^{(1)}$. Assuming a sinusoidal signal with circular frequency ω,

$$p^{(1)} = |p^{(1)}|e^{i\omega t} = |p^{(1)}|\cos \omega t + i|p^{(1)}|\sin \omega t \tag{6.7}$$

where the vertical bars indicate the local amplitude of the fluctuation. Keep in mind that this amplitude is a function of the mode shape and thus changes with position in the chamber. The velocity fluctuation becomes

$$v^{(1)} = v^{(1)^{(r)}} + iv^{(1)^{(i)}} = |\mathfrak{R}||p^{(1)}|e^{i\omega(t+\tau)}, \tag{6.8}$$

and the combustion response leads or lags the pressure fluctuations depending on the real and imaginary parts of $\mathfrak{R}$. The lead time and response function amplitude are given by

$$|\mathfrak{R}| = \sqrt{(\mathfrak{R}^{(r)})^2 + (\mathfrak{R}^{(i)})^2}, \tag{6.9}$$

and

$$\tau = \tan^{-1}\left(\frac{\mathfrak{R}^{(i)}}{\mathfrak{R}^{(r)}}\right). \tag{6.10}$$

The formulation we have introduced here is the simplest and most direct way to incorporate complex coupling mechanisms.

Many definitions of coupling have been utilized in previous work. *Response function*, *admittance function*, and so on are all closely related descriptions of the same phenomenon. We will discuss the definitions more formally in a later section and attempt to link the many notations found in the literature. Following this an important task will be to perfom a detailed analysis of the time-dependent chemistry of the combustion zone that lies behind the coupling.

The coupling mechanism we have now introduced will referred to henceforth as *pressure coupling*. A linear one-to-one relationship between the pressure and the normal fluctuating velocity response is assumed to be known everywhere on the chamber boundaries (this must include propellant surfaces, inert surfaces, and the nozzle entrance area). It is often represented as a *property* of the propellant and is thus taken to be independent of position in the chamber. This is perhaps the least controversial aspect of pressure-coupled combustion instability. The vast majority of experimental studies of solid rocket instability have been aimed at verifying and quantifying this form of coupling.

Other coupling mechanisms are quite a bit more controversial. Of these, the *velocity coupling* issue remains clouded despite decades of study. A related

boundary effect is the *flow turning correction*, which has also been mentioned frequently in earlier chapters. Flow turning is not usually thought of as a coupling effect, but as will be demonstrated, it is closely related to velocity coupling. We will attempt in this section to clarify the relationships between the several types of coupling; an important task will be to demonstrate that some of these are attributes of the same phenomenon and should not be treated as independent mechanisms. Important errors in motor stability assessment may result if these items are treated carelessly. A common mistake is to correct twice for the same energy gain or loss. Another mistake is to treat three-dimensional effects as one-dimensional boundary phenomena. A worse mistake is to extrapolate one-dimensional results into 3-D calculations. We will soon find ourselves gazing into the the proverbial "can of worms". These difficult questions must be faced squarely if a practical grasp of the problem is to be achieved.

Fluctuations in Mass Flow Rate at the Propellant Surface

The first law of thermodynamics describes mechanisms for modifying the energy of a system. Energy flows into the acoustic wave structure in the chamber when there is a properly phased source of heat at the boundary (or within the chamber volume) or if mechanical work is done within the system or at the boundary. In the present situation we have assumed that all combustion energy release takes place in a thin boundary zone. This can be represented as a surface enclosing the acoustic chamber. All energy flux then takes the form of a time-dependent boundary process. Imagine a control volume encompassing the chamber proper with boundary surfaces at the edges of the combustion zone. This is an *open system* since mass crosses the boundary. In applying the first law, one must take account of the flux of energy in the form of heat and also the mechanical work exerted in the process of forcing mass across this boundary. This "flow work" includes both steady and unsteady contributions. It is the latter that is of interest here. Figure 6.1 shows an element of the surface of the control volume and describes the manner in which work is done on the chamber gases. Using a simple perturbation description, the energy flux is proportional to the familiar *PdV* work done in injecting an element of mass into the chamber. In a short time interval, the mass element moves distance *dy* into the chamber as shown. What work must be done in moving it against the pressure force dF? This is a question that we must answer in detail.

Consider first a very simple model of the time-dependent flow in the vicinity of the burning propellant. What we are about to describe is the very essence of the combustion instability problem. It has been expressed in many different ways during the past three decades by scores of investigators. We will attempt to demonstrate it in the simplest possible way by use of basic thermodynamic concepts.

Figure 6.1 shows a small control volume at the interface between the combustion zone and the chamber proper. As described in the last section, it is ap-
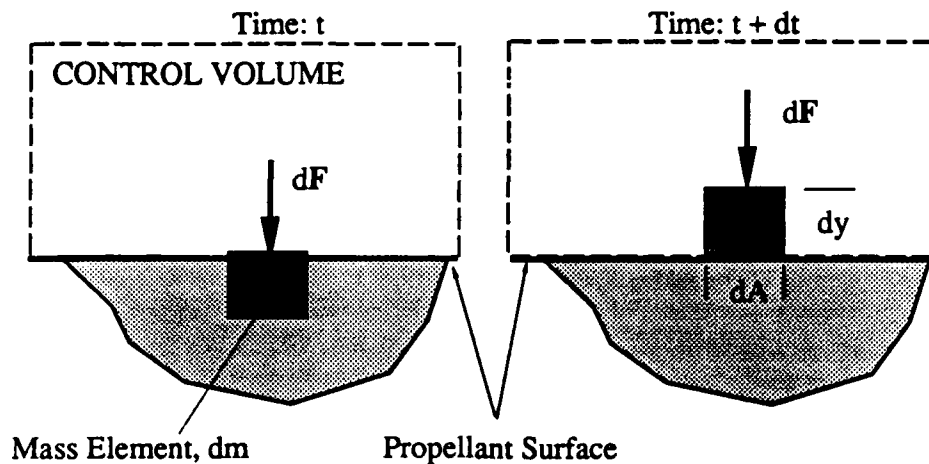
Fig. 6.1 Control Volume for Computing Flow Work

propriate to assume that the chamber fills the vast majority of the space within the motor. In this region many of the simplifying assumptions based on acoustic wave models are appropriate. The combustion zone, the region in which these simplifications do not hold, is quite thin relative to the chamber dimensions. Thus without great error, the outer surface of the combustion zone can be thought of as being simultaneously located at the actual solid boundary and the boundary of the flow port. This must be considered to be an *active* chamber boundary. It is, first of all, the source of the mean flow traversing the chamber. It is also a region that may be sensitive to variations in local gas properties. For example, the rate at which gas enters the chamber locally is clearly dependent on local changes in pressure. This is demonstrated by the well-known exponential steady-state burning law often expressed as

$$\bar{r} = B\bar{P}^n \qquad (6.11)$$

where $\bar{r}$ is the mean speed of regression (usually measured in inches or centimeters per second) or "burning rate" of the propellant surface. n is the "burning rate exponent", a number usually less than unity. It will be more convenient in our analysis to work with properties of the gas flow, so we note from application of the steady continuity equation to the mass element emerging into the control volume as shown in Figure 6.1 that

$$\text{Mass Flow Rate} = \rho_p dA\bar{r} = \rho dAv \qquad (6.12)$$

where v is the relative gas velocity at the surface. On the average, gas particles leave the surface in the normal direction because viscous forces (the no-slip condition) so require. Thus the burning law can be written in terms of the gas velocity as

$$v = \beta B\bar{P}^n \qquad (6.13)$$

where β is the ratio of the density of the solid to the local mean gas density.

$$\beta = \frac{\rho_p}{\rho} \tag{6.14}$$

β typically lies in the range $100 < \beta < 1000$.

Let us examine a time-dependent analog of this empirical formula (equation 6.11) based on the steady-state behavior. We will focus on the departure from steady flow represented by $p^{(1)}$ and the other perturbation flow properties that correspond to it. It is clear from 6.11 that when $p^{(1)}$ is not zero, there will be a *time-dependent* change in the burning rate. We write 6.11 in perturbed form by inserting the expansions for pressure and velocity, and separating the various orders of magnitude as usual. Retaining only terms to first order in the oscillation amplitude, and reverting to dimensionless form, 6.13 can be written as

$$M_b V + \varepsilon v^{(1)} + O(\varepsilon^2) = B'\left[1 + \varepsilon p^{(1)} + O(\varepsilon^2)\right]^n \tag{6.15}$$

where B' is a dimensionless constant of proportionality related to the original dimensional burning rate coefficient B in equation 6.11. This establishes that accompanying the change in burning rate there will be a change in the normal velocity entering the chamber. Expanding the right side of 6.15 by means of the binomial theorem, and focusing on the time-dependent part, it is apparent that

$$v^{(1)} = nB'p^{(1)} \tag{6.16}$$

This is precisely what we assumed earlier when we wrote equation 6.3. Thus at least for the linearized case the handling of the time-dependent boundary condition is consistent with the established empirical steady-state burning law. Since time-dependent effects are now involved, we must allow for phase relationships as we have already done in our definition of the surface response. For now, we are interested only in the physical implications of the relationship between variations in pressure and the response of the combustion zone in terms of the fluctuating mass flow rate.

Flow Work at the Boundary - The Source of Acoustic Energy

Consider a fluid element of area dA just emerging from the burning zone at time t into the chamber (Figure 6.1). In a short time dt, it moves a distance

$$dy = v\,dt = (M_b V + \varepsilon v^{(1)} + O(\varepsilon^2))dt \tag{6.17}$$

This motion is opposed by the pressure force $dF = |dF| = p\,dA$, and a differential amount of work

$$\delta W = dF\,dy = \left[1 + \varepsilon p^{(1)} + O(\varepsilon^2)\right]\left[M_b V + \varepsilon v^{(1)} + O(\varepsilon^2)\right]dA\,dt \tag{6.18}$$

is thus done on the gas. It is this form of pdV work, often referred to in classical thermodynamics texts as "flow work" [Van Wylen and Sonntag, 1978] that may

add (or delete) energy from that resident at a given instant within the chamber.

Expanding in the usual fashion, and collecting terms of like order, we find that the *rate* at which work is done per unit area on the gas in the chamber is

$$\frac{dw}{dt} = M_b V + \varepsilon \left[M_b V p^{(1)} + v^{(1)} \right] + \varepsilon^2 \left[M_b V p^{(2)} + p^{(1)} v^{(1)} + v^{(2)} \right] + O(\varepsilon^3)$$

(6.19)

Thus the rate of work consists of a steady term representing the energy flux supplied to the mean chamber flow by combustion energy release. The two first-order terms in fluctuating quantities are not very interesting because they do no *net* work (assuming a periodic oscillation) on the wave system. That is, their *time-average* is zero. The time-average of any function f(t) is defined as

$$\langle f(t) \rangle = \text{Time Average of } f(t) = \lim_{T \to \infty} \frac{1}{T} \int_0^T f(t)\, dt$$

(6.20)

Taking the time-average of the rate of work on the chamber, we find

$$\left\langle \frac{dw}{dt} \right\rangle = M_b V + \varepsilon^2 \left\langle M_b V p^{(2)} + p^{(1)} v^{(1)} + v^{(2)} \right\rangle + O(\varepsilon^3)$$

(6.21)

We will identify the second-order quadratic combination of the fluctuating quantities with work done on the wave system. Since we have no way to estimate the second-order pressure and velocity fluctuations at this time we will simply assume that they are unimportant. That is, we are attempting to construct a linearized model in which such quantities are neglible. The combination

$$\left\langle \frac{dw}{dt} \right\rangle = \varepsilon^2 \left\langle p^{(1)} v^{(1)} \right\rangle = \varepsilon^2 \left\langle \Re(p^{(1)})^2 \right\rangle$$

(6.22)

however, may exhibit a *net* flow of energy to the chamber wave structure since 6.22 is clearly not zero if the velocity fluctuation has a component in phase with the pressure. That is 6.22 is nonzero if the real part of $\Re$ is not zero. This is an important point and needs to be examined very carefully. A measure of the net energy flux is the time-average over many cycles of oscillation. Assuming harmonic oscillations as we have done before we can assume the pressure variation is $p^{(1)} = \cos kz \cos kt$ so that at a point near the chamber boundary it can be written as
$$p^{(1)} = |p^{(1)}| \cos kt$$
where the magnitude is a value in the range $-1 < |p^{(1)}| < 1$ for the dimensionless system we are using. Taking the time-average we find

$$\left\langle p^{(1)} v^{(1)} \right\rangle = \left\langle \Re(p^{(1)})^2 \right\rangle = \lim_{T \to \infty} \frac{1}{T} \int_0^T \Re |p^{(1)}|^2 \cos^2(k\,t)\,dt$$

(6.23)

$$= \Re |p^{(1)}|^2 \lim_{T \to \infty} \frac{1}{T} \left[\frac{t}{2} + \frac{\sin(2k\,t)}{4k} \right]_0^T = \frac{\Re |p^{(1)}|^2}{2}$$

As a last step we take the real part as always with the final result

$$\left\langle \frac{dw}{dt} \right\rangle_{WAVE} = \varepsilon^2 \frac{\Re^{(r)} \left| p^{(1)} \right|^2}{2} + \text{Terms of higher order} \qquad (6.24)$$

Notice that if the combustion zone is not "acoustically active", or if the boundary point in question lies on an inert surface, then the pressure and velocity near the surface are described by the simple acoustic solutions we have already found. That is $v^{(1)} = 0$. In this case, there is no net energy flux due to the oscillations. This is because the velocity and pressure are exactly 90 degrees out of phase near the surface (pressure antinode; velocity node). If, however, the normal velocity has some arbitrary phase relative to the pressure caused by boundary processes such as combustion or viscous effects then there is net work done on the wave system. This can be either a positive or negative effect. Tnat is, energy can either be added to the waves or removed from them. The sign depends entirely on the real part of the response (or admittance) function, $\Re^{(r)}$. If it is positive then the energy flux is positive and there is a flow of energy from the boundary into the wave structure. If it is negative, it represents a damping effect that tends to remove energy. Thus we have found one of the important rules governing dependence of combustion instability on the response of the burning surface to pressure fluctuations.

Much remains to be done in order that this rule can yield useful information concerning the stability characteristics of a given motor system. For one thing, all other gain and loss mechanisms of the same order must be analyzed so that a complete energy balance can be computed. This is the subject of Chapter 9.

Later we will seek to express this relationship in a more formal way and explore ways, both analytical and experimental, to determine the relationship between pressure and velocity interactions in the burning zone. Equation 6.16 is not sufficient for this purpose because it is simply as an empirical relationship based on steady-state experimental data. It does not contain the physics needed to account for the unsteady effects in the combustion zone. To see this, notice that it gives no information regarding the split into real and imaginary parts. That is, it does not provide information needed for dealing with time-dependent interactions. Only by performing carefully designed experiments or by analyzing the chemical and physical interactions in the burning zone can we determine the required response function information.

Additional Energy Considerations

One or two additional matters related to energy must be clarified. The reason for the need to retain work terms to second-order in the wave amplitude should be fairly obvious from the fact that energy effects are quadratic. A measure of the acoustic energy density in a region of space is given in dimensional form by

Kirchoff's time-honored expression [Kirchoff, 1877]

$$E' = \frac{1}{2}\overline{\rho}\, u' \cdot u' + \frac{1}{2}\frac{p'^2}{\overline{\rho}\,\overline{a}^2} \quad . \tag{6.25}$$

In dimensionless form and in the notation we have been using, this becomes

$$E = \frac{E'}{\overline{\rho}\,\overline{a}^2} = \varepsilon^2 \left[\frac{u^{(1)} \cdot u^{(1)}}{2} + \frac{p^{(1)^2}}{2\gamma^2} \right], \tag{6.26}$$

where energy density is made dimensionless quite naturally by dividing by $\overline{\rho}\,\overline{a}^2$, which has units of energy per unit volume. Although there is disagreement over the application of this result in situations like ours where there is a mean flow, it is still possible to see that the energy in the chamber is of second-order in wave amplitude. This matches up as it should with our pressure coupling work term which is also quadratic in ε.

Without working very hard we have now found two important pieces in an energy balance structure for analysis of motor chamber oscillations. Combining an expression such as 6.26 with the expression for the rate of work done by pressure coupling gives us the outline of a full energy balance for the system. What is needed is a proper statement of the First Law that links them together. It is worth a brief digression to bring the parts together. We will have occasion later to use the resulting tool in several different ways. An important one is in exploring nonlinear instability. The simplest application will be in finding an expression for the system linear growth rate. This is the basis for the combustion stability codes used in the rocket industry. The system is modeled as a container of oscillating gas particles. Appended to this container are a variety of interactions that are capable of changing the system energy. This system analysis approach is useful in that it allows us to organize our attack on the problem. It takes full advantage of linearization in that each loss or gain can be incorporated in the model by simple addition.

In order to utilize this approach we require the appropriate form of the First Law of thermodynamics. We will follow the acousticians method for deriving this by working with the mechanical form of the energy equation. Multiplying the momentum equation 5.99 by the oscillatory velocity vector yields

$$u^{(1)} \cdot \frac{\partial u^{(1)}}{\partial t} = - u^{(1)} \cdot \nabla \frac{p^{(1)}}{\gamma} = - \nabla \cdot (p^{(1)} u^{(1)}) + p^{(1)} \nabla \cdot u^{(1)}, \tag{6.27}$$

where a vector identity has been used on the right hand side. The divergence of the acoustic velocity is now removed by means of the continuity equation (equation 5.98). After a little rearranging, and remembering that

$$u^{(1)} \cdot \frac{\partial u^{(1)}}{\partial t} = \frac{\partial (u^{(1)} \cdot u^{(1)})}{2 \partial t} \tag{6.28}$$

and defining the vector *acoustic energy flux* or *acoustic intensity* as

$$I \equiv \frac{p^{(1)} u^{(1)}}{\gamma} , \tag{6.29}$$

we find the mechanical energy equation in the form

$$\frac{\partial}{\partial t}\left[\frac{u^{(1)} \cdot u^{(1)}}{2} + \frac{1}{2}\left(\frac{p^{(1)}}{\gamma} \right)^2 \right] = -\nabla \cdot I . \tag{6.30}$$

The combination of terms on the left will be recognized at the time-derivative of the acoustic energy density, so the final result is

$$\frac{\partial E}{\partial t} + \nabla \cdot I = 0 . \tag{6.31}$$

This expression is interesting, but its interpretation may not be completely clear at this point. Let us attempt to put it in conservation form to exhibit its physical content. We do this by integrating the equation over the volume of the rocket motor chamber. Then Gauss' theorem can be used to rewrite the volume integral of the divergence term as a surface integral over the control surface that encloses the chamber. One finds

$$\frac{\partial}{\partial t}\iiint_V E \, dV + \iint_S I \cdot n \, dS = 0, \tag{6.32}$$

which expresses the fact that the energy contained within the control volume is modified by the *flux of acoustic energy* through the surface of the control volume. Since this is the way one often starts in deriving the differential form of the conservation laws, then it appears that equation 6.31 does make an appropriate statement about the changes in system energy. We can use it now to see if it makes sense from the standpoint of our discussions on coupling at a burning boundary. Suppose we have a chamber represented by control volume V bounded by surface S part of which is a burning propellant surface of the type we have been trying to understand and the rest by nonreacting surfaces. On the propellant surface, the acoustic intensity, I is not zero because of the fluctuating velocity component in action there. Now evaluate the required normal component of I remembering that n is always an outward pointing normal unit vector. Use 6.30 at a point on the burning surface by inserting the coupling expression 6.3 with the result

$$\frac{\partial}{\partial t}\iiint_V E \, dV = \begin{array}{l} \text{Rate of Change of} \\ \text{Acoustic Energy in} \\ \text{Control Volume} \end{array} = \iint_{S_{burn}} \frac{\Re p^{(1)2}}{\gamma} \, dS \tag{6.33}$$

Suppose we desire to evaluate the surface integral for a specific case, say a longitudinal acoustic mode in a tubular chamber,

$$p^{(1)} = \cos(kz) e^{ikt} \tag{6.34}$$

where we have used the complex form in order to make use of the complex notation used in expressing the admittance function $\Re$. It is necessary to treat the square of the pressure fluctuation with care. It is quite easy to make a very serious error here, one that has invalidated many analyses in the past. It is a situation wherein products of variables with sinusoidal time dependence appear in the evaluations. This occurs both in the application of energy methods where we are dealing with quadratic combinations of the acoustic variables and in nonlinear problems (see equation sets (5.77-5.80) and (5.81-5.84) developed earlier for use in nonlinear analyses). It is tempting to write

$$p^{(1)^2} = \cos^2(kz)\, e^{i(2kt)} = \cos^2(kz)[\cos(2kt) + i\sin(2kt)], \qquad (6.35)$$

which would lead to erroneous results. When products of this sort are needed, its is necessary to express the components in *real* notation. After the multiplication is done it is correct to revert to *complex* form. Since we will be doing this fairly often in later developments, let us make use of the present situation to learn the proper procedure. Instead of the expression shown in 6.35, we must write

$$p^{(1)^2} = [\cos(kz)\cos(kt)][\cos(kz)\cos(kt)] = \cos^2(kz)\cos^2(kt) =$$
$$= \cos^2(kz)\tfrac{1}{2}[1 + \cos(2kt)] = \tfrac{1}{2}\cos^2(kz)[1 + e^{i(2kt)}], \qquad (6.36)$$

where all the necessary steps are shown. The reader interested in getting correct results in his own analyses should study the several manipulations and applications of trigonometric identities with great care. If we had carelessly used the incorrect result in 6.35, the time average of the real part of the right-hand side would be zero indicating that, on the average, no energy flows into the system from the reacting combustion zone. If 6.36 is used, we find that there is a modification of the system energy which depends on the distribution of the oscillating pressure relative to the burning surface. The real part is

$$\begin{array}{l}\text{Time-average Flux of}\\ \text{Acoustic Energy from}\\ \text{Combustion Zone}\end{array} = \frac{\Re^{(r)}}{2\gamma} \iint\limits_{Sburn} \cos^2(kz)\, dS \qquad (6.37)$$

This agrees with our previous assessment and shows not only that the real part of the admittance governs whether a loss or gain is involved, but also shows that the net energy flux depends on the mode shape and distribution of the burning surfaces on the
chamber boundary.   Again we note that there will be a positive flow of energy, that is a gain, only if the real part of the admittance function is positive.

In following chapters we will frequently find it useful to move from differential to integral forms of the governing equations. For instance, the energy balance expressed in simplified form in 6.32 is a powerful tool in accounting for the various energy loss and gain mechanisms affecting the system. Before it can

be of use to us in our assessment of system stability, it will be necessary to extend it by incorporating 1) mean flow effects, 2) pressure/velocity coupling effects, and 3) assorted linear loss/gain mechanisms such as the influence of the nozzle, two-phase flow effects due to solid particles immersed in the gas, and losses at inert boundaries.

The energy approach will prove to be a useful alternate tool in stability analysis; we will apply in formally in Chapter 8. There will be numerous uses for the basic ideas introduced in simple form in this subsection. A very substantial benefit comes from the fact that energy methods are based on *scalar* properties of the gas flow. The more direct approach requires a relatively painful confrontation with the various force, momentum, and velocity vectors that arise naturally in gas dynamics problems.

Effect of the Mean Flow on Coupling

The reader will notice that in our linearized treatment of coupling no influence of the mean flow seems to be present. This "just doesn't feel right" since the coupling is so strongly dependent on the mass flux generated in the combustion process. In fact, there is considerable controversy about the influence of the mean flow, and we would be remiss to pass too quickly over certain of these questions. In order that we do not ignore important directions for our expanding treatment of combustion instability, we will introduce two important example situations in the last two subsections of this chapter. These are intended to introduce some potentially important effects of the mean flow field. The first broadens our simplified approach to the fluid mechanics of rocket motors by bringing in some evaluation of the effects of viscous forces. In the second situation, we introduce the controversial subject of *velocity coupling*.

Before starting the special examples, a short general discussion on the proper representation of boundary conditions is in order. This will serve as an introduction to later detailed treatment of this important element of motor combustion stability. It should be quite apparent to the reader in view of the central role played by the coupling effects we have identified thus far that success or failure in our ability to either predict stability characteristics or to interpret experimental data hinges on proper representation of the boundary between the gases in the motor cavity and the combustion zone itself. This is obvious since the combustion zone is the origin of the energy driving both the steady and unsteady motions in the chamber flowfield.

Sigman (Ref .4238) applied some recent aeroacoustics results to the rocket motor problem. We will employ his findings as the outline for this introductory material. We will return several times to questions raised in his paper since these are crucial to the results of the analysis. Sigman demonstrates that simple coupling terms of the sort we have found (see equation 5. 169) do not properly represent the type of interactions between the flow and the combustion zone that we need to account for. The admittance form of 5. 169 is adequate for representation of interfaces that are fixed in space. For example, they properly represent interactions between acoustic waves and inert duct liners such as those often used to suppress oscillations in ducts and jet engine inlets. If however the boundary zone is bridged by a mean flow, as it is in the case we must handle, then there are additional elements that must be considered. In particular, we must pay close attention to the definition of the interface between the combustion zone and the chamber proper. Figure 5. 27 illustrates the difference between the classical fixed interface and the actual behavior that we must address.

Figure 5. 27(a) shows the combustion zone bounded by a fixed surface S_o located near the burning surface. This distance from the actual solid surface defines the thickness of the burning zone, which is often taken to be a length small compared to the reference length used to describe the acoustic cavity.

Figure 5. 27(b) illustrates the approach used in computing the acoustic modes of the chamber. The burning zone is
is replaced by a rigid media to allow us to use the rigid-walled boundaries needed in employing the standard acoustics results. Figure 5. 27(c) shows the combustion zone and motor chamber in quiescent conditions in which there is no time-dependent motion of the combustion gases. In this case, the boundary between the two regions is illustrated by two identical surfaces S and S_o. Finally, 5. 27(d) illustrates the situation we must actually deal with. In the presence of fluctuating flow disturbances the interface itself oscillates in response as the varying position of S indicates. S_o is then to be regarded as the time-averaged interface position which is what we have implied is the point we will apply the boundary conditions in the mathematical treatment of the problem. The point is, that if the latter approach is to be used, we must somehow account for the *motion* of the actual interface. The results are strongly dependent on the details of the mean flow in the vicinity of the combustion zone. This is a problem
that has been of great concern to duct acousticians (see References 4227,4240-4247).

Sigman (Ref. 4238) modified the duct acoustics results to fit the needs of the rocket motor problem. He found that in addition to the type of coupling we have already identified, there are two correction terms that must be considered. These result from a more rigorous handling of the combined steady and oscillating flow at a carefully defined interface between the combustion zone and the acoustic chamber. In particular, account is taken of motion of the interface in response to the gas oscillations and to the details of the mean flow velocity distribution in the vicinity of the interface.

Effects of Parallel Wave Incidence

Velocity coupling is thought to be invoked (References 4057-4059, 4064)when there is an acoustic velocity vector component *parallel* to the chamber boundary. Working by analogy, it would appear that the velocity fluctuations should affect the instantaneous burning rate in much the same fashion as pressure variations. For instance, velocity fluctuations might enhance the mixing of gas species in the combustion zone or affect the convective heat transfer to the solid phase by some time-dependent analog of the "erosive burning" effect noted in the steady state motor combustion, thus altering the time-dependent mass flow rate. The characteristics of such a velocity coupling can be illuminated by means of simple tools we have already constructed.

Consider a particular propellant for which measurements of instantaneous burning rate are available. It is clear that the apparent pressure coupled response should depend on the orientation of the wave motions to the burning surface. Figure 5. 28 depicts two orientations of special interest. In the first, waves impinge normally on the surface as assumed in most one-dimensional time-dependent combustion models. This is the basic pressure coupling situation in

which the burning rate is modified as a result of the pressure variations (and associated temperature fluctuations) and its effect on heat transfer into the propellant. Incidentally, the only reason pressure (unsteady of density fluctuations for instance) is selected as the wave descriptor is that it is the quantity representing the wave action most readily measured in an unstable motor, so it is natural to think of the pressure fluctuations as the waves themselves. As we have already seen, the wave is equally well described in terms of velocity, temperature, density, fluctuating mass flow, or entropy oscillations.

Now consider the effect of changing the direction of wave incidence by 90 degrees so that the unperturbed velocity fluctuations lie parallel to the chamber surface. If the boundary were inert, then the acoustic velocity would be felt right down to the boundary as shown in Fig. 5. 8. Of course this is not a realistic picture because of the natural effects of viscosity, which would cause the velocity to decay in the boundary zone in order that the no- slip condition is satisfied.

Assuming the simplest possible scenario in which there is no influence of the boundary on the acoustic velocity as already described, it is clear that the fluctuating pressure distribution is locally identical to what it was in the normally incident case. Thus, if we account for boundary processes by means of the simple pressure response function (equation 5.), the normal velocity fluctuation is precisely the same as before, that is

All of the discussion pertaining to energy flux in the normally incident case now also describes the parallel incidence case, but only if we neglect viscous effects or other interactions of the parallel velocity fluctuations with the combustion, mixing, and viscous processes in the boundary. Notice however, that since the velocity and pressure are directly related (eq. 5.), it is perfectly correct to describe the effect of the waves on the gas flow as a velocity coupling as we shall now do.

A Simple Demonstration of Velocity Coupling

Since the pressure and velocity fields are directly related (for example, equation   showed that

then there is no reason why we cannot describe the boundary effects in terms of velocity instead of pressure. In fact, one could define a "temperature coupling" and use it to describe the same boundary reactions. For instance, one might define

indicating that the normal velocity response, v' is related to the local parallel velocity fluctuations, u'. This statement is completely equivalent to our original response function definition because for a simple standing wave,

and we see that the velocity and pressure coupling response functions are related in this simple example case by

The important point is that either definition completely describes the physical

BULK MODE OSCILLATIONS AND L* INSTABILITY

Dr. Thiel had already tried a simpler injection system, rows of ordinary holes in a flat headplate. But with large chambers this did not work so well. Professor Beck of the Dresden College of Engineering had been working for about two years on the development of a circular slit injection nozzle. It was much easier to produce but so far we had succeeded in making it work properly only with small motors of less than 2000-pound thrust. With the 25-ton unit there were loud humming sounds of varying rhythms, a drop in performance, and serious vibrations of the chamber during test-bed running. We were therefore compelled, despite production difficulties, to continue for the time being with the eighteen-burner-cup chamber head.

Dr. Walter Dornberger, (1952)

7.1 INTRODUCTION

Under certain conditions, solid rocket motors and laboratory burners will exhibit spontaneous oscillations at low frequencies (5-500 Hz), in which the pressure rises and falls everywhere in phase in the combustor. Such low frequency oscillations have been called "bulk mode" or "nonacoustic" oscillations because they do not involve acoustic wave modes. This type of low frequency behavior provides a good route for introduction to the concepts of combustor stability because their are extensive test results from simple laboratory combustors, and a relatively simple analytical model of combustor behavior. In this chapter, the nature of the instability behavior will be described in qualitative terms with samples of experimental results from the literature. An approximate analytical model will be present that has been used widely, and the model will be used to forecast trends to be expected of experimental variables. These trends are compared with a specific set of experimental results from tests that would normally be expected to conform to the assumption in the analytical model. The comparison shows that the analysis is a useful tool for understanding the phenomenon, but not adequate to explain all the trends in experimental results in the literature, or even in the set of tests chosen for detailed examination. The reasons for the frequent disagreements between theory and experiment are discussed, and give some insight into the diversity of instability behavior and the remaining incomplete state of knowledge typical of the entire combustion instability problem.

situation. Notice, however, that our simple "velocity coupling" has some unexpected properties. While the pressure coupling could be interpreted as a local property of the propellant, the velocity coupling depends in a complex manner on *position* within the chamber. This, in fact, is one of the main attributes thought to characterize velocity coupling. Clearly, in this simple example, the same phenomenon is being described by either formulation, so there is no mysterious implication in the peculiar position dependence. For instance if we proceed without remembering that the coupling is really just simple pressure coupling in disguise, it might appear at first glance that there is acoustic driving by velocity coupling in the forward part of the chamber and acoustic damping by velocity coupling in the aft part. This is clearly an erroneous conclusion arising from a neglect of the relative phase and amplitude dependence of the parallel velocity itself on position in the chamber.

Figure 5. is a plot of the position dependence from equation . What is shown here is precisely the position dependence usually anticipated in velocity coupled response. Remember, though, that what we are describing is simple pressure coupling. In the present case either one or the other descriptions is perfectly correct. It is obviously inappropriate to use them simultaneously since they both represent the same coupling. Also, given a choice, one would obviously pick the pressure coupled model because of its inate simplicity. The

7.2 THE NATURE OF L* INSTABILITY

Bulk mode oscillations usually occur at low combustor pressures (< 2.5 MPa). Some confusion has arisen in the literature because the cause of the oscillations can involve an inherent instability in the propellant combustion (manifested even in a constant pressure combustor), or the oscillations can result from a responsiveness of combustion to pressure disturbances and a resulting dynamic instability of the combustion-combustor flow system.* The latter of these two situations manifests a clear dependence of oscillatory behavior on the ratio of combustor volume to vent throat area, called the L* of the combustor (Fig. 7.1).

Propellant

Nozzle

V

A
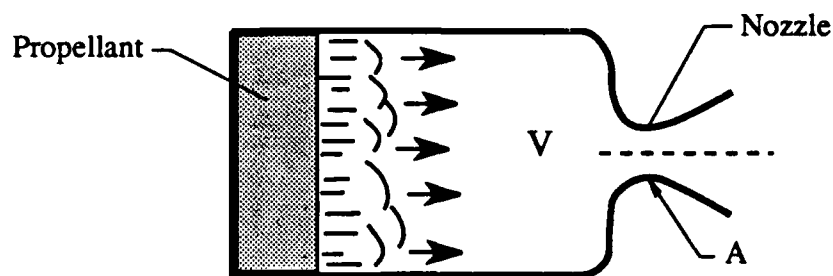
V = Cavity Gas Volume
A = Cross-Sectional Area of Nozzle Throat

Fig. 7.1 A Simple Combustor and Definition of L* (Sketch typifies
the arrangement of a laboratory L* burner)

Figure 7.2 shows some examples of combustor behavior in low L* tests as indicated by pressure measurement in the combustor. At very low L* the burning is intermittent, resulting in a series of "chuffs" (Fig. 3.2a) that may either terminate by permanent extinction, or may quench reignite and continue chuffs until the propellant is consumed. If burning away of propellant leads to sufficiently increased L* the chuffs may progress to the behavior shown in Fig. 7.2b and 7.2c typical of somewhat higher L*. Very little study has been made of chuffing behavior because it is complex and dependent on details of motor geometry and heat flow between propellant and hot motor components. Further, chuffing behavior represents an extreme manifestation of L* instability at very low L*, and designers are more concerned with more mild, but still unacceptable, instabilities at less extreme L*, as illustrated in Fig. 7.2b and 7.2c. Such behavior is relatively reproducible in careful tests on a given propellant, but the details

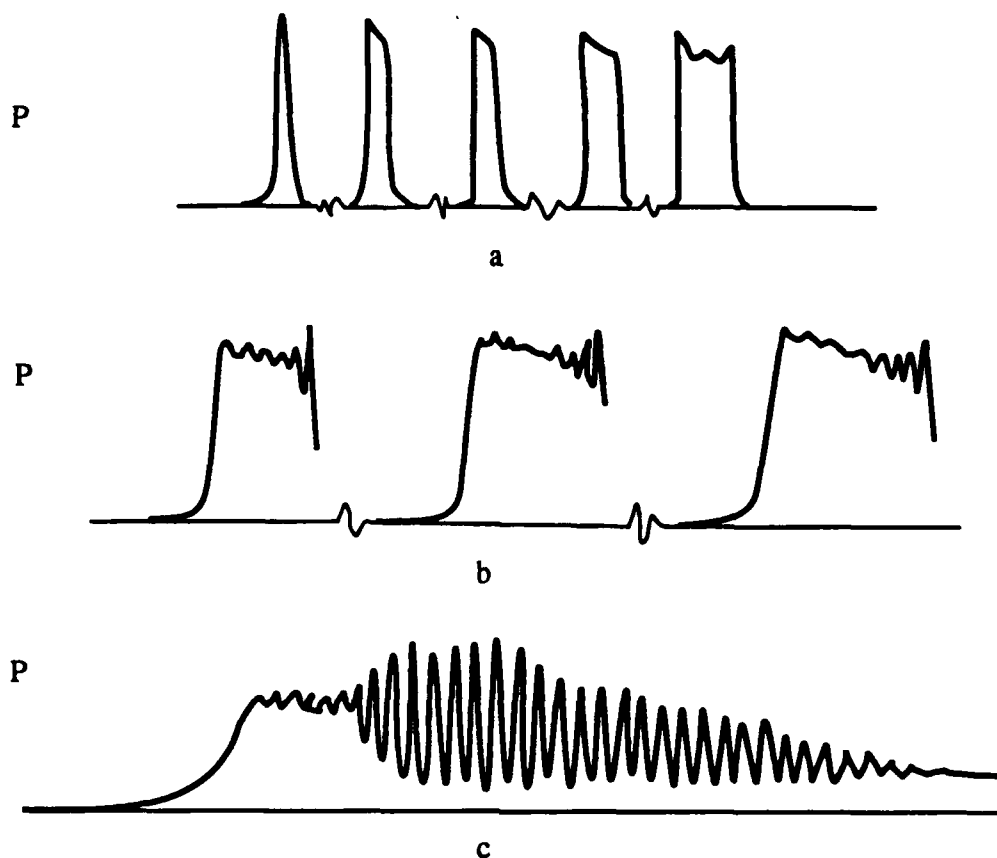* In many cases, oscillatory behavior shows evidence of something inbetween these extremes.

Fig. 7.2 Typical pressure-time histories during L* instability:
  a. Intermittent burning referred to as "chuffing". This behavior is the most extreme form of L* instability, and sometimes fails to reignite after the first self quench.
  b. Repeated burns with growing oscillations culminating in self quency and reignition (typically at higher L* than for chuffing).
  c. Continuous burn with growing oscillations that level off and decay as L* increases.

of behavior and conditions of occurrence (e.g., L* and pressure) are strongly dependent on propellant formulation (composition and particle size distribution). In tests yielding the behavior in Fig 7.2b, data reported usually involves frequency of oscillation and mean pressure along with estimates of L* for each successive "burn", based on initial geometry and calculated volume increase due to burnout of propellant. When the growth of oscillations is orderly, the growth rate is sometimes calculated for each burn. The growth rate (Fig. 7.3) is defined by α in the expression

$$P = P_0 e^{\alpha(t-t_0)}$$

(7.1)

where P_0 is the amplitude of pressure oscillation at some selected time, $t = t_0$, and P is the amplitude at any other time t. α is regarded as well defined only in

the relation

$$\ln\left(\frac{P}{P_0}\right) = \alpha t \qquad (7.2)$$

is a reasonably straight line (with slope α), a property characteristic of oscillations in "linear" systems.

At still higher L^*, the behavior in Fig. 7.2c may occur. Some investigators might regard the point of maximum amplitude as a time when $\alpha = 0$ (as per Eq. 7.2). which in acoustic instability would be viewed as a stability limit (in L^* and p) Other investigators regard the point where amplitude has decayed to some very small value as the stability limit. The differences involved here have not been fully argued, and such as argument would have to entrain nonlinear features that are unwelcome and inconsistent with the strategy behind use of eq. 7.2 Apparently no one has determined whether a test, started under conditions intermediate between these two "stability limits" would develop oscillations or not. In any case, the two limits may not involve much difference in L^*.

It was found in early studies (Ref. 1-3) that, for a given propellant, test conditions yielding oscillatory behavior at low L^* and/or low $\bar{p}$, and conditions yielding no oscillations could be separated by a stability limit, $\alpha = 0$, often of the form

$$L^* = C'(\bar{p})^{-2n} \qquad \text{(unstable at } L^* \text{ below this value)} \qquad (7.3)$$

where $\bar{p}$ is the mean pressure and n is the sensitivity of the mean burning rate to pressure

$$n \equiv \frac{\bar{p}}{\bar{r}} \frac{\partial \bar{r}}{\partial \bar{p}} = \frac{\partial \ln \bar{r}}{\partial \ln \bar{p}} \qquad (7.4)$$

This sensitivity is often assumed to be independent of $\bar{p}$, leading to the familiar burning rate "law"

$$\bar{r} = C(\bar{p})^n \qquad (7.5)$$

The result in Eq. (7.3), while probably not universally applicable, conveys a general observation that this type of instability is limited to low L^* and low pressure, with unstable behavior encountered at a given p when L^* is too low (a situation most likely to prevail early in burning in motors with high volumetric loading and low operating pressure, conditions sometimes encountered in "space" motors). The collected experimental results also indicate (e.g., Ref. 4-6) that the coefficient C' in Eq. (7.3) has a wide range of values depending on the propellant involved. In other words, some propellants are much more susceptible to low L^* instability than others.

The many experimental investigations of L^* instability (mostly in laboratory scale burners) are most notable for the diversity of choices of variables for
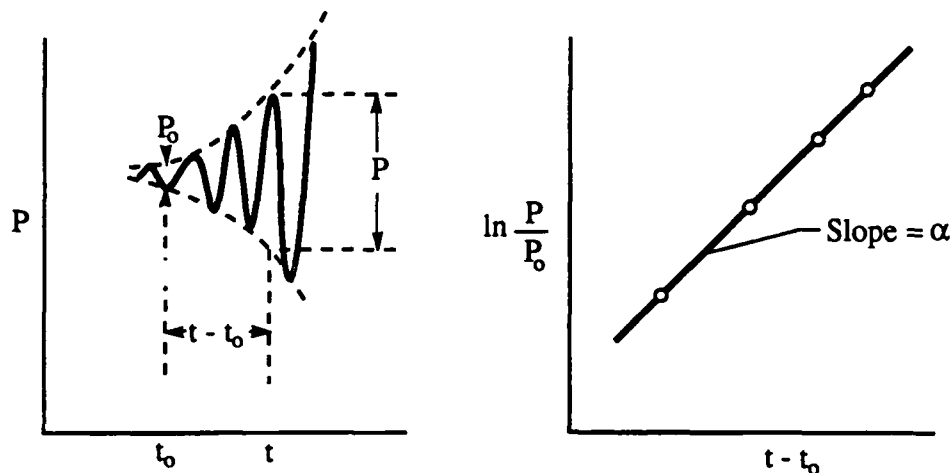
Fig. 7.3 Determination of Growth Rate of Oscillation

reporting results, and a corresponding difficulty of comparing results of different investigations or drawing generalizations. In order to understand the situation, it is helpful to start with an elementary analysis of the combustor stability. This can then be used to examine the significance of published experimental results, and to identify the more important unsolved aspects of the L* instability problem.

7.3 SIMPLIFIED STABILITY ANALYSIS

Description of Approach.

A stability analysis consists of application of appropriate conservation laws to a description of processes in the combustor-combustion system. It is generally advantageous (although not always realistic) to do independent analyses of the dynamic behavior of the propellant combustion and the combustor gas flow system. This is rationalized by an assumption that the combustion zone is thin (i.e., localized near the propellant surface), so that conditions in the rest of the combustor volume can be described without undue detail regarding gas composition and gas enthalpy. We will adopt this convention, but examine its implications later in the chapter. This later examination is called for because the thin combustion zone assumption is clearly less realistic in low pressure, low L* (short flushing time) combustors than in more conventional motors.

The simplifying assumptions that will be used initially for the combustor will reduce the consideration of conservation laws to consideration of conservation of mass. The combustion will be described as a dynamic response of mass influx at the burning surface to imposed pressure fluctuations. This "response function" is the subject of separate analysis in Chapter 5. The system analysis will describe the oscillatory behavior of the combustor with the response junction of the

propellant treated first as a parameter. Particular attention will then be given to prediction of stability limits such as the experimentally determined ones described in the last section. This will be followed by examination of the details of oscillatory behavior in the unstable domain as predicted by the analysis, including particularly the predictions arising from use of the QSHOD response function described in Chapter 5. In a later section a comparison will be made between these predictions and some typical experimental results. This will be followed by discussion of other published results and state of theory and of understanding of experin ental results.

Stability Analysis

In developing an analytical model, we will adopt two crucial assumptions about the combustor, one of which was mentioned above:

    a. The volume of the combustion region is small compared to the combustor volume;

    b. The combustor volume is small enough so that the contents are flushed out in a time that is short compared to the period of oscillation (the analysis will show this to be valid).

Under these conditions, the temperature of the gas in the combustor volume is spatially uniform at the flame temperature, which is essentially constant during a cycle of oscillation at the isobaric flame temperature of the propellant.*

Under these conditions, conservation of mass requires that

$$\frac{m_b}{\overline{m}} = \frac{m_a}{\overline{m}} + \frac{m_d}{\overline{m}} \tag{7.6}$$

where m_b, m_a, and m_d are the instantaneous (oscillating) values of mass burning rate mass accumulation rate, and mass discharge rate for the combustor and $\overline{m}$ is the mean flow rate (i.e., time average of m_b). Assuming the nozzle is short and has isentropic flow,

$$m_d = C_d A_t p = \left(\frac{\gamma\mu}{RT}\right)^{\frac{1}{2}} \left(\frac{2}{\gamma+1}\right)^{\frac{\gamma+1}{2(\gamma-1)}} A_t p$$

$$\frac{m_d}{\overline{m}} = \frac{C_d}{\overline{C}_d}\frac{p}{\overline{p}} = \left(\frac{\overline{T}}{T}\right)^{\frac{1}{2}} \frac{p}{\overline{p}}$$

where C_d is the isentropic nozzle discharge coefficient (defined by the equation). For isothermal combustor oscillations (assumption b, above), $\overline{T}/T$ and

* As noted in Chapter 5, the combustion response includes a small temperature oscillation, which will be neglected here.

$C_d/\overline{C}_d = 1$, and

$$\frac{m_d}{\overline{m}} = \frac{p}{\overline{p}} \qquad \text{(isothermal)} \qquad (7.7)$$

If it is assumed that the ratio of propellant density to gas density is large (e.g., > 10^3 and $p = \rho RT/\mu$, then the mass accumulation rate is

$$\frac{m_a}{\overline{m}} = \frac{1}{\overline{m}}\frac{d(\rho V)}{dt} = \frac{V}{\overline{m}}\frac{d\rho}{dt} = \frac{V}{\overline{m}}\frac{d(p\mu/RT)}{dt}$$

$$\frac{m_a}{\overline{m}} = \frac{V}{\overline{m}}\frac{\mu}{R\overline{T}}\frac{d\rho}{dt} = \frac{\overline{\rho}V}{\overline{m}}\frac{d(p/\overline{p})}{dt} = \tau_{ch}\frac{d(p/\overline{p})}{dt}$$

$$\frac{m_a}{\overline{m}} = \frac{\mu}{R\overline{T}\overline{C}_d}\frac{p}{\overline{p}}\frac{V}{A_t} = A'L^* \frac{d(p/\overline{p})}{dt} \qquad \text{(isothermal)} \qquad (7.8)$$

where τ_{ch} is the flushing time of the chamber $\dfrac{\overline{\rho}V}{\overline{m}}$ and A' is

$$A' = \frac{\mu}{R\overline{T}\overline{C}_d} = \left(\frac{\gamma\mu}{RT}\right)^{\frac{1}{2}}\left(\frac{2}{\gamma+1}\right)^{\frac{\gamma+1}{2(\gamma-1)}} \qquad (7.9)$$

Then the mass balance equation becomes

$$\frac{m_b}{\overline{m}} - \frac{p}{\overline{p}} = \tau_{ch}\frac{d(p/\overline{p})}{dt} = A'L^* \frac{d(p/\overline{p})}{dt} \qquad (7.10)$$

Now represent $p/\overline{p}$ and $m_b/\overline{m}$ in terms of *small perturbations* about the mean values,

$$\frac{p}{\overline{p}} = 1 + \frac{\hat{p}}{\overline{p}}; \quad \frac{m_b}{\overline{m}} = 1 + \frac{\hat{m}_b}{\overline{m}} \qquad (7.11)$$

Then the mass balance in terms of perturbations is

$$\frac{\hat{m}_b}{\overline{m}} - \frac{\hat{p}}{\overline{p}} = \tau_{ch}\frac{d(\hat{p}/\overline{p})}{dt} = A'L^* \frac{d(\hat{p}/\overline{p})}{dt} \qquad (7.12)$$

For completeness here, the description of the concept of combustion response to pressure oscillations presented in Chapter 4 and 5 will be repeated to show how $\hat{m}_b/\overline{m}$ is related to $\hat{p}/\overline{p}$. Thus, if $\hat{p}/\overline{p}$ is described by

$$\frac{\hat{p}}{\overline{p}} = Pe^{\alpha t}\cos \omega t = \text{Re}\left(Pe^{\alpha t}e^{i\omega t}\right) \qquad (7.13)$$

the burning rate oscillation can be represented as

$$\frac{\hat{m}_b}{\overline{m}} = Me^{\alpha t}\cos \omega(t+\tau) = \text{Re}\left(Me^{\alpha t}e^{i\omega(t+\tau)}\right) \qquad (7.14)$$

where P and M are amplitudes at some time chosen to be t = 0. "Re" ,means the real part of the complex form on the right. For small amplitudes M/P is

independent of time and amplitude; but depends on frequency of oscillations. τ is the time lead of $\dot{m}_b$ relative to $\dot{p}$, also dependent on frequency ($\omega\tau$ is the phase lead). The mass burning rate oscillation can be expressed as

$$\frac{\dot{m}_b}{\bar{m}} = Me^{\alpha t}(\cos \omega\tau \cos \omega t - \sin \omega\tau \sin \omega t) = Re\left(Me^{\alpha t}e^{i\omega(t+\tau)}\right) \quad (7.15)$$

which is the sum of a component in phase with pressure and a component out of phase with pressure. This can be written as

$$\frac{\dot{m}_b}{\bar{m}} = RPe^{\alpha t}(\cos \omega\tau \cos \omega t - \sin \omega\tau \sin \omega t) \quad (7.16)$$

where

$$R \equiv \frac{M}{P} \quad (7.17)$$

The quantities R and $\omega\tau$ are properties of the propellant combustion extensively studied both experimentally (Ref. 7.7) and by analyses (Ref. 7.8). For convenience, these analyses are carried out in complex variable notation that leads to a complex combustion response function,

$$\Re = \Re^r + i\,\Re^i \quad (7.18)$$

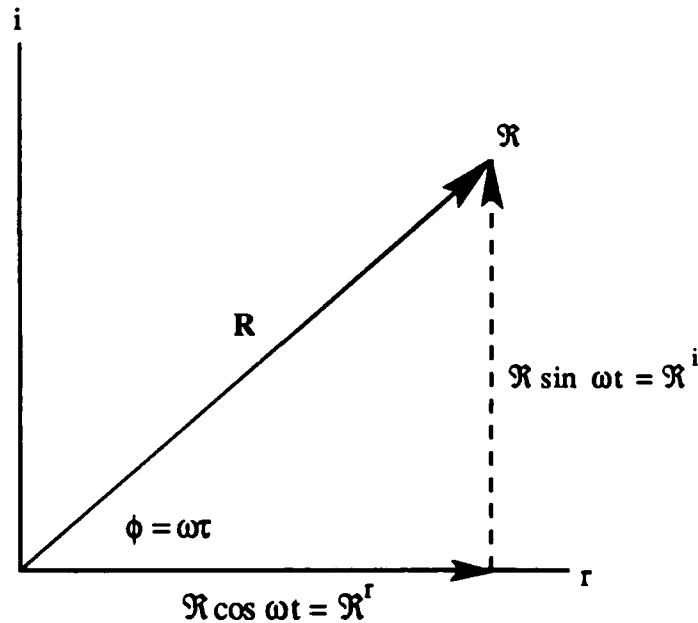represented by the sketch in Fig. 7.4., with real and imaginary parts of magnitude

Fig. 7.4 The Response Function Pictured as a Vector in The Complex Plane.

$$\mathfrak{R}^r = R \cos \omega\tau \qquad (7.19)$$

$$\mathfrak{R}^i = R \sin \omega\tau \qquad (7.20)$$

from which

$$R = \sqrt{\mathfrak{R}^{r^2} + \mathfrak{R}^{i^2}} \qquad (7.21)$$

$$\omega\tau = \tan^{-1}\left(\frac{\mathfrak{R}^i}{\mathfrak{R}^r}\right) \qquad (7.22)$$

Discussion of this dynamic combustion response was presented in Chapter 5; the quantities R and ωτ will be used at this point as though they were known functions of propellant, frequency of oscillation, and other combustion environmental variables, such as pressure (illustrated by an example in Fig. 7.5).
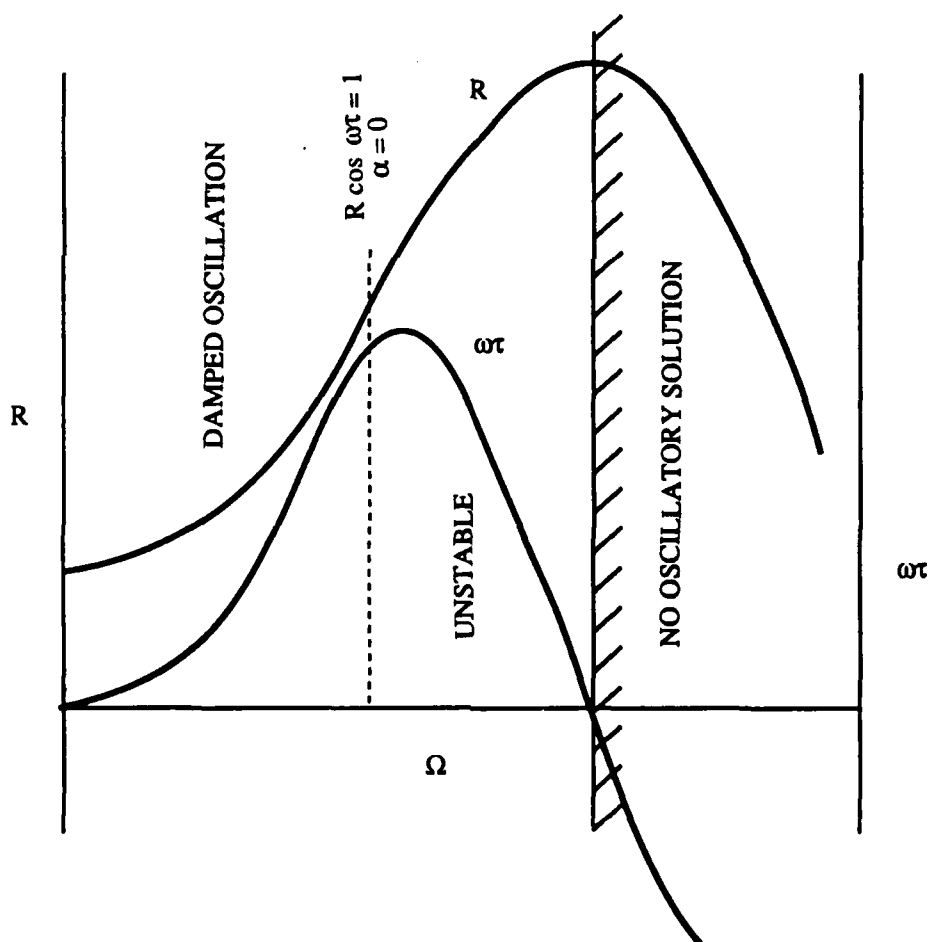

Fig. 7.5 Examples of Dependence of the Magnitude and Phase of the Response Function on the Nondimensional Frequency $\Omega = \kappa\omega/\bar{r}^2$. Bulk Mode Oscillations Do Not Occur in the Region Where Phase is Negative.

Thus returning to the mass balance equation (7.12) and assuming a solution of the form in Eq(7.13) and using (7.14) or (7.16),

$$M e^{\alpha t} \cos \omega(t + \tau) - P e^{\alpha t} \cos \omega t = \tau_{ch} P e^{\alpha t} (\alpha \cos \omega t - \omega \sin \omega t)$$

$$R(\cos \omega \tau \cos \omega t - \sin \omega \tau \sin \omega t) - \cos \omega t =$$

$$= \tau_{ch} e^{\alpha t} (\alpha \cos \omega t - \omega \sin \omega t)$$

$$\left(R \cos \omega \tau - \alpha \tau_{ch} - 1 \right) \cos \omega t + \left(\omega \tau_{ch} - R \sin \omega \tau \right) \sin \omega t = 0 \qquad (7.23)$$

which is identically equal to zero only if

$$R \cos \omega \tau = 1 + \alpha \tau_{ch} = 1 + \alpha A'L^* \qquad (7.24)$$

$$R \sin \omega \tau = \frac{\tau_{ch}}{\tau} \omega \tau = \frac{A'L^*}{\tau} \omega \tau \qquad \text{(positive)} \qquad (7.25)$$

Equations (7.24) and (7.25) will be referred to here as the "oscillator equations," which relate the chamber geometry variables L*, the propellant response variables R, τ, and the oscillation variables ω and α. A' contains the properties of the propellant reaction products, γ, μ and isobaric flame temperature (Eq. 7.9). R and τ are functions of frequency, propellant properties, mean pressure and ambient propellant temperature (and possible other mean flow variables in motors with complex internal mean flow field). It should be noted that Eq. (7.24) and (7.25) do not depend on any assumptions regarding the response function other than those implicit in Eq (7.16).

Oscillatory and Non-Oscillatory Domain

Equations (7.24) and (7.25) can be used in a variety of ways to

a. Determine conditions under which oscillatory solutions to Eq.(7.12) are possible;
b. Determine domains of growing oscillations (positive) and of decaying oscillations (α negative) and stability boundary ($\alpha = 0$);
c. Determine relations among oscillatory and geometrical variables;
d. Determine combustion response from oscillatory behavior (α and ω) of unstable tests.

Assuming for convenience (temporarily) that the combustion response can be represented as in Fig. 7.5, then Eq. (7.25) *does not have an oscillatory solution in the region of negative* $\omega \tau$ (shaded). This can be understood physically by reference to Fig.7.6. In the figure, oscillations in mass rate and pressure are shown. It is evident (considering a moment during the pressure cycle when $p = \bar{p}$) that the mass must oscillate with a phase lead in order for the pressure to "overshoot" $\bar{p}$.
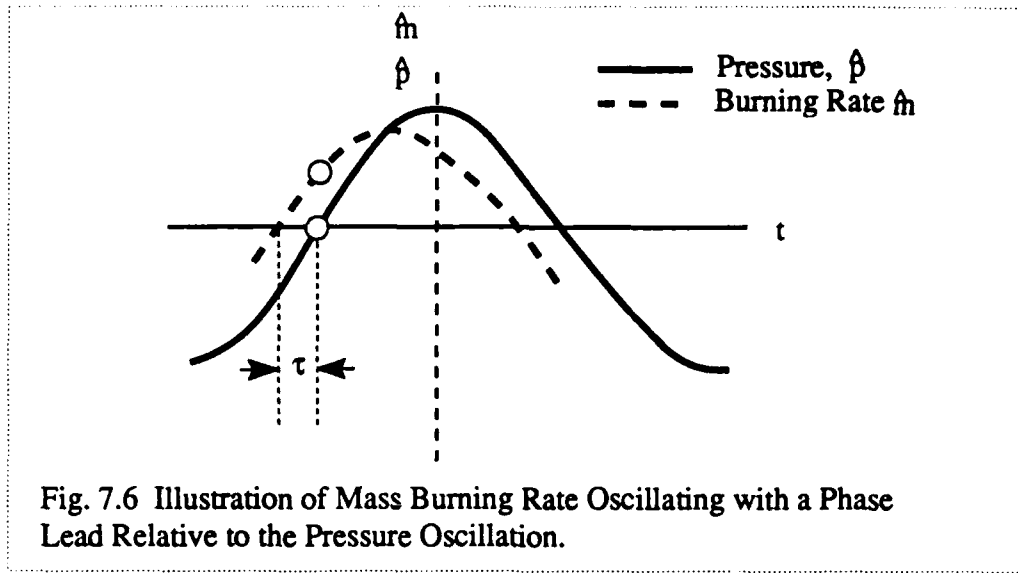
Fig. 7.6 Illustration of Mass Burning Rate Oscillating with a Phase Lead Relative to the Pressure Oscillation.

$$\omega\tau > 0 \qquad\qquad \text{(for oscillations)} \qquad\qquad (7.26a)$$

At some lower Ω there is a particular value for which Eq. (7.24) gives $\alpha = 0$

$$\left.\begin{array}{l} R\cos\omega\tau = 1 \\ \Omega = \Omega_0 \end{array}\right\} \quad\rightarrow\quad \alpha = 0 \qquad\qquad (7.26b)$$

Where the subscript 0 refers to the condition $\alpha = 0$. This is the stability limit, and corresponds to a definite point on a response function curve like that in Fig. 7.5 (more than one stability limit point is conceivable, depending on complexities of the response function). Note that if the response function ($\mathfrak{R}(\Omega)$) is pressure-dependent, the stability limit value of Ω will be pressure dependent, but will always correspond to $R\cos\omega\tau = 1$. This is illustrated in Fig. 7.7, which shows a family of response functions curves plotted as R vs $\omega\tau$. In this coordinate system, the stability limit is the $R\cos\omega\tau = 1$ curve shown in the figure. Unstable conditions are above this line stable conditions below.

The value of L* that gives neutral stability is given by Eq. (7.25) in the form

$$L^* = \frac{R\sin\omega\tau}{A'\omega} = \frac{\kappa}{A'\bar{r}^2}\frac{R\sin\omega\tau}{\Omega} \qquad\qquad (7.27)$$

$$L_0^* = \frac{\kappa}{A'\bar{r}^2}\frac{\sqrt{R_0^2 - 1}}{\Omega_0} \qquad (\alpha = 0) \qquad\qquad (7.28)$$

Thus the value of L* for the stability limit depends on pressure through the dependence on $\bar{r}$; *if the response function* $\mathfrak{R}(\Omega)$ *is independent of pressure,*

$$L_0^*(\bar{r}^{-2}) = \frac{\kappa}{A'} \frac{\sqrt{R_0^2 - 1}}{\Omega_0} = \text{constant} \qquad (7.29)$$

and $L_0^*(\bar{r}^{-2})$ has a definite value. Recalling the conventional form of $\bar{r}(\bar{p})$ as in Eq. (7.5), the result in Eq. (7.3) is obtained

$$L_0^* = C'(\bar{p})^{-2n} = \frac{\kappa}{C^2 A'} \frac{\sqrt{R_0^2 - 1}}{\Omega_0}(\bar{p})^{-2n} \qquad (7.30)$$

which is a line of slope -2n in the $\ln L^*$ vs $\ln p$ plane (as in Fig. 7.8). This line is often drawn as a straight line, which can be identified with assumptions in Eq.
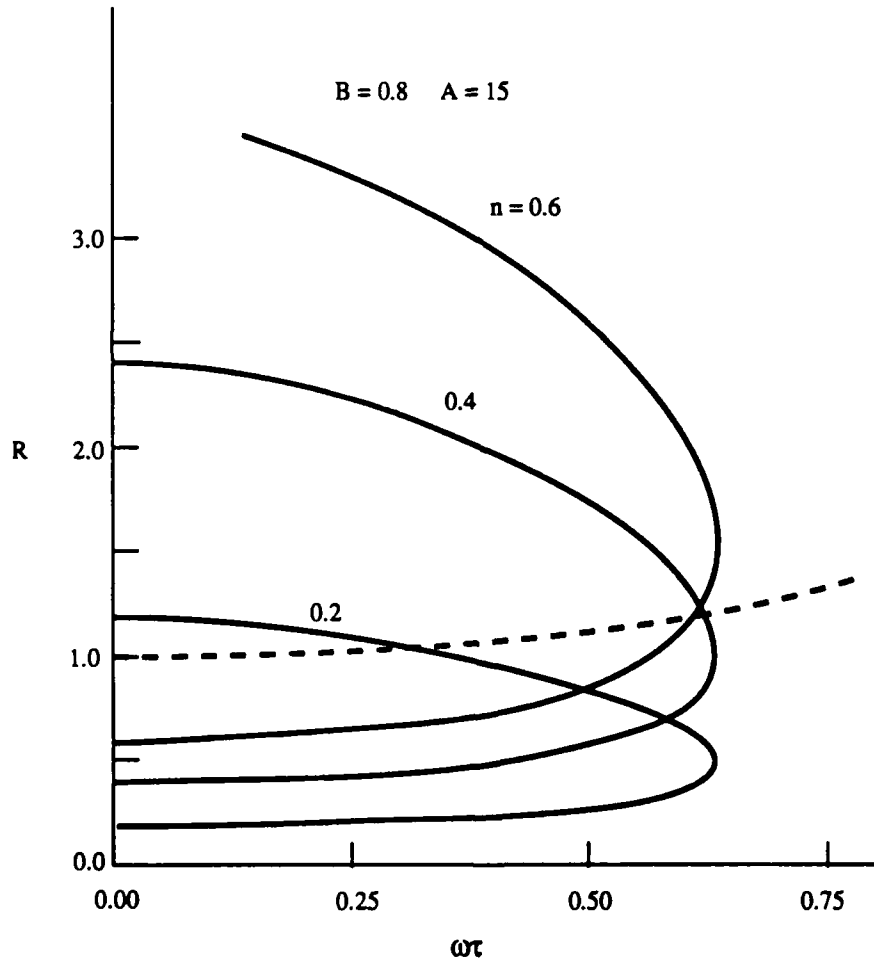
Fig. 7.7 Response function shown as magnitude R vs phase $\omega\tau$. Curves are shown for different values of the burning rate pressure exponent, n. The broken line is the stability limit R cos $\omega\tau$- 1. The curves were calculated from "QCHOD" theory with the model parameters A and B as indicated in the Figure. In this theory $\omega\tau$ vs Ω is the same for all of the curves, i.e., Ω is constant along ordinate lines.
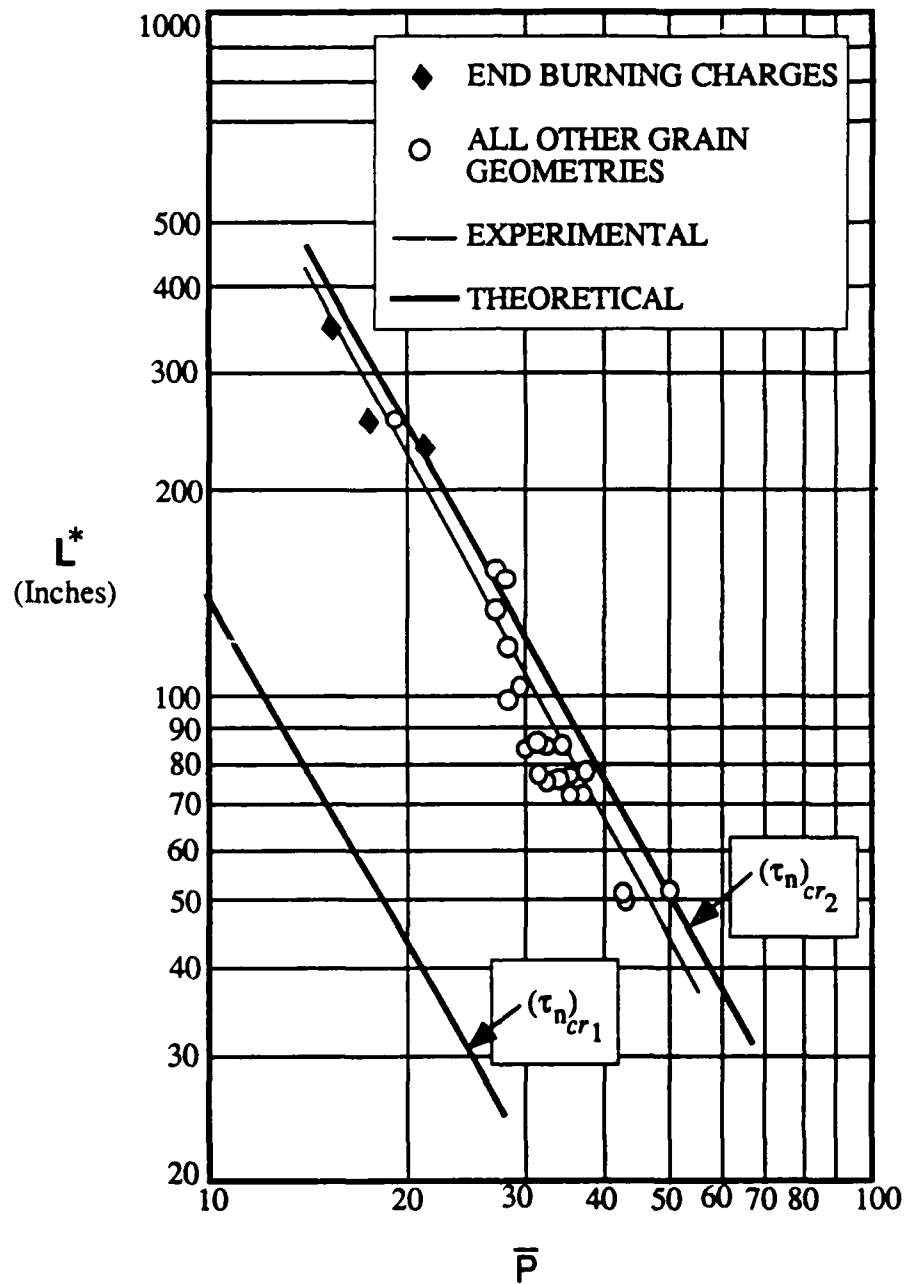
Fig. 7.8 Experimentally determined stability limit for JPL propellant 534 at 80 F.

(7.30) that both n and the response function are pressure-independent (a sufficient, but not necessary condition for $\ln L_2^*$ vs $\ln \bar{p}$ to be a straight line). Whatever the behavior of $\Re(\Omega)$ and $\bar{r}(\bar{p})$, $L_0^*(\bar{r})^2$ for a given propellant is determined by the value of

$$\frac{1}{\Omega_0}\sqrt{R_0^2 - 1}$$

corresponding to point(s) on the $R\cos \omega\tau = 1$ curve in Fig. 7.7 (pressure-dependent if $\Re(\Omega)$ is pressure-dependent).

The frequency corresponding to the stability limit is given by the definition of Ω, so

$$\omega_0 = \frac{(\bar{r})^2}{\kappa}\Omega_0 \tag{7.31}$$

which means ω_0 is proportional to $(\bar{r})^2$ if the response function $\Re(\Omega)$ is pressure independent, and ω_0 is then proportional to $\bar{p}^{-2\bar{n}}$ if n is also pressure independent (assumptions implicit in interpretations of experimental results in many reports). For the sake of perspective, it should be noted that the response function is rarely found to be completely independent of pressure, so the dependence of both L_0^* and ω_0 on pressure or burning rate is manifested not only through the $(\bar{r})^2$ factor in Eq. (7.28) and (7.31), but also through the dependence implicit in the factors involving R_0 and Ω_0.

To understand how this pressure dependence of the response function affects the stability limit through effect on R_0 and Ω_0, consider the R vs $\omega\tau$ curves in Fig. 7.7. These curves are based on QSHOD theory, with each curve corresponding to a different value of n. Assuming that n decreases as $\bar{P}$ increases (typical of many propellants at low pressure), R_0 and Ω_0 correspond to the intersection points on the $R\cos \omega\tau = 1$ curve. In this example, as pressure is increased, n decreases, R_0 decreases, and Ω_0 increases. The factor

$$\frac{1}{\Omega_0}\sqrt{R_0^2 - 1}$$

in Eq.(7.28) thus decreases with increasing pressure and burning rate, while the factor Ω_0 increases in Eq. (7.31). This situation corresponds to a response function such that the stability limit is on the upper branch of the R vs $\omega\tau$ curves (to the right of the maximum in the $\omega\tau$ vs Ω curve in Fig. 7.5). For a propellant with high magnitudes of the response function, the stability limit will occur on the lower branch of the R vs $\omega\tau$ response curve, and the effect on R_0 and Ω_0 of n decreasing with increasing pressure is different. In this case R_0 and Ω_0 both increase as pressure (and r) increase. These effects of pressure dependence of R_0 and Ω_0 have not been evaluated in past interpretations of experimental results. The strategy of examination here, based on expected effect of pressure dependence of n, is only an illustration of the nature of the problem. A real propellant may have a more complicated or different dependence of the problem. A real

propellant may have a more complicated or different dependence of response function on pressure than the QSHOD model used here. In any case, various dependence of $\Re(\Omega)$ should be reassessed and conclusions adjusted according to the outcome.

Behavior in the Oscillatory Domain

The foregoing discussion concerned relations among variables along the stability limit. However, stability limits are inferred experimentally from tests that oscillate, usually meaning that test conditions correspond to the unstable domain. Thus it seems reasonable to exploit the theory to forecast trends of oscillatory behavior and see how well these trends agree with experimental results. Assuming plausible values of A' and κ, and assuming temporarily a fixed value of $\bar{p}$ (and hence $\bar{r}$), the propellant will have a definite response function and L* can hence be related to Ω by Eq. (7.27). A different L* vs Ω will pertain for each $\bar{p}$, due to dependence of $\bar{r}$ on $\bar{p}$. Thus there is a family of L* vs Ω curves with $\bar{p}$ as a parameter. If the response function is pressure dependent, each L* vs curve should reflect that by using the appropriate value of $\Re \sin \omega \tau$ in Eq. (7.27). Using the response function curves in Fig. 7.7, the L* vs Ω curves are shown in Fig. 7.9. The appropriate values of p were assigned to curves in Fig. 7.7 by using the graphs of r vs p and n vs p in Fig. 7.10, which pertain to a specific propellant discussed in the next section. Thus the L* vs Ω curves reflect the pressure dependence arising from both $\bar{r}$ and the response function in Eq. (7.27) using a QSHOD model for the pressure dependence of $\Re(\Omega)$.

(FIGURE IN PREPARATION)

Fig. 7.9 Curves of L* and α vs Ω based on Fig. 7.7 and Eq. (7.27) and (7.32). The values of r and n were chosen for each p using Fig. 7.10.
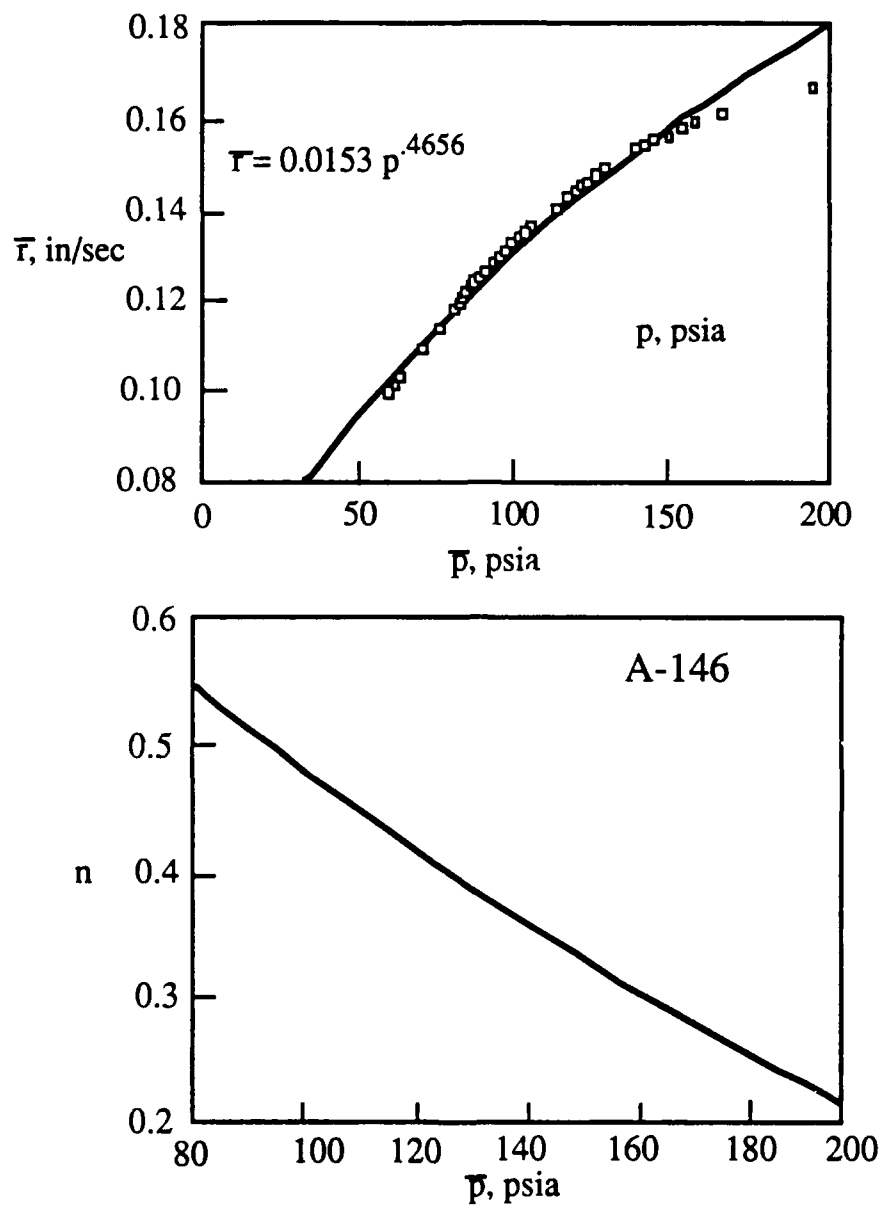
$$\bar{r} = 0.0153 \ p^{.4656}$$

Fig. 7.10 Burning rate and pressure exponent vs pressure for A-146 propellant (data from Ref. 7.10).

Also shown in Fig. 7.9 is the dependence of α on Ω for the above example, using Eq. (7.24) and (7.25) to get an expression for α vs Ω

$$\alpha = \frac{R\cos\omega\tau - 1}{A'L^*} = \frac{(\bar{r})^2}{\kappa}\left(\frac{R\cos\omega\tau - 1}{R\sin\omega\tau}\right)\Omega = \frac{(\bar{r})^2}{\kappa}\left(\frac{R^r - 1}{R^i}\right)\Omega \qquad (7.32)$$

The frequency is given for each pressure by

$$\omega = \frac{(\bar{r})^2}{\kappa}\Omega \qquad (7.33)$$

While Eq. (7.27), (7.32), and (7.33) permit one to calculate L^*, α, and ω vs Ω to illustrate trends as in Fig. 7.9, the range of trends plausible in the context of response function theory has not been fully explored. Fig. 7.11, for example, illustrates an unusual dependence of L^* on Ω that can arise within the context of QSHOD theory in which oscillatory solutions can occur for three different values of Ω at the same value of L^* (see Ref. 7.9). Unfortunately, there is very little direct information on response functions at the frequencies and pressures typical of L^* instability, so that discussion has been limited to plausible trends with approximate theories, and qualitative questions such as the dependence or independence of Ω on pressure. Even that question has not been resolved in the literature, although it could easily have been done if the measured data were accurate enough and the test conditions were consistent with the assumptions leading to Eq. (7.24) and (7.25) (questions that have not been carefully considered). Thus, if $\Re(\Omega)$ is pressure independent, a graph of $A'(\bar{r})L^*/\kappa$ vs Ω should be independent of p (see Eq. (7.27)). Such a graph is shown in Fig. 7.12 for test data for A-146 propellant (Ref. 7.10). This graph shows a well defined trend of $L_0^*(\bar{r})^2$ vs Ω, with moderate scatter of data that can be seen to include some systematic dependence on pressure. This "pressure spread" is in a direction indicative of high values of $R\sin\omega\tau/\Omega$ for a given Ω at higher pressure. Within the context of the QSHOD model, R decreases with increasing pressure due to a falling value of n (Fig. 7.11), while $\sin\omega\tau$ vs Ω in that model is independent of pressure. Thus the "pressure spread" in the data scatter in Fig. 7.12 is not explained by the pressure dependence encompassed in the QSHOD model, and remains unexplained. As we will see, a careful scrutiny of the L^* burner experimental data generally leaves a lot of unanswered questions, "blame" for which cannot presently be assigned unambiguously to either inadequacy of the response function model or inadequacy of the oscillator equations (Eq. (7.24 and 7.25). A further look at this issue is made in the following by using L^* burner data to calculate combustion response, and by comparing the results with QSPD theory.
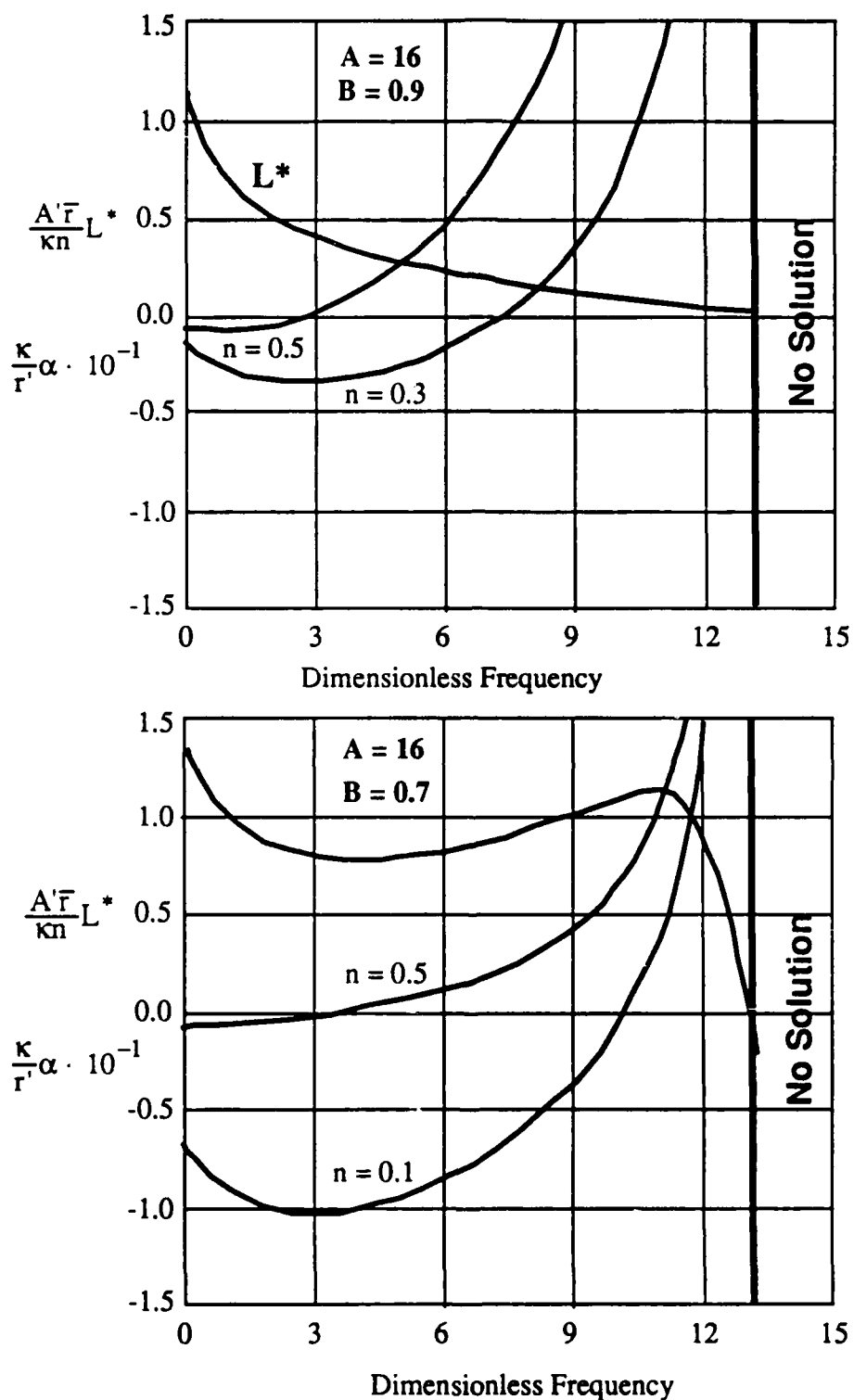
Fig. 7.11 Unconventional dependence of L* on Ω predicted by QSHOD theory for combinations of high values of the model parameters A and n with low values of B.
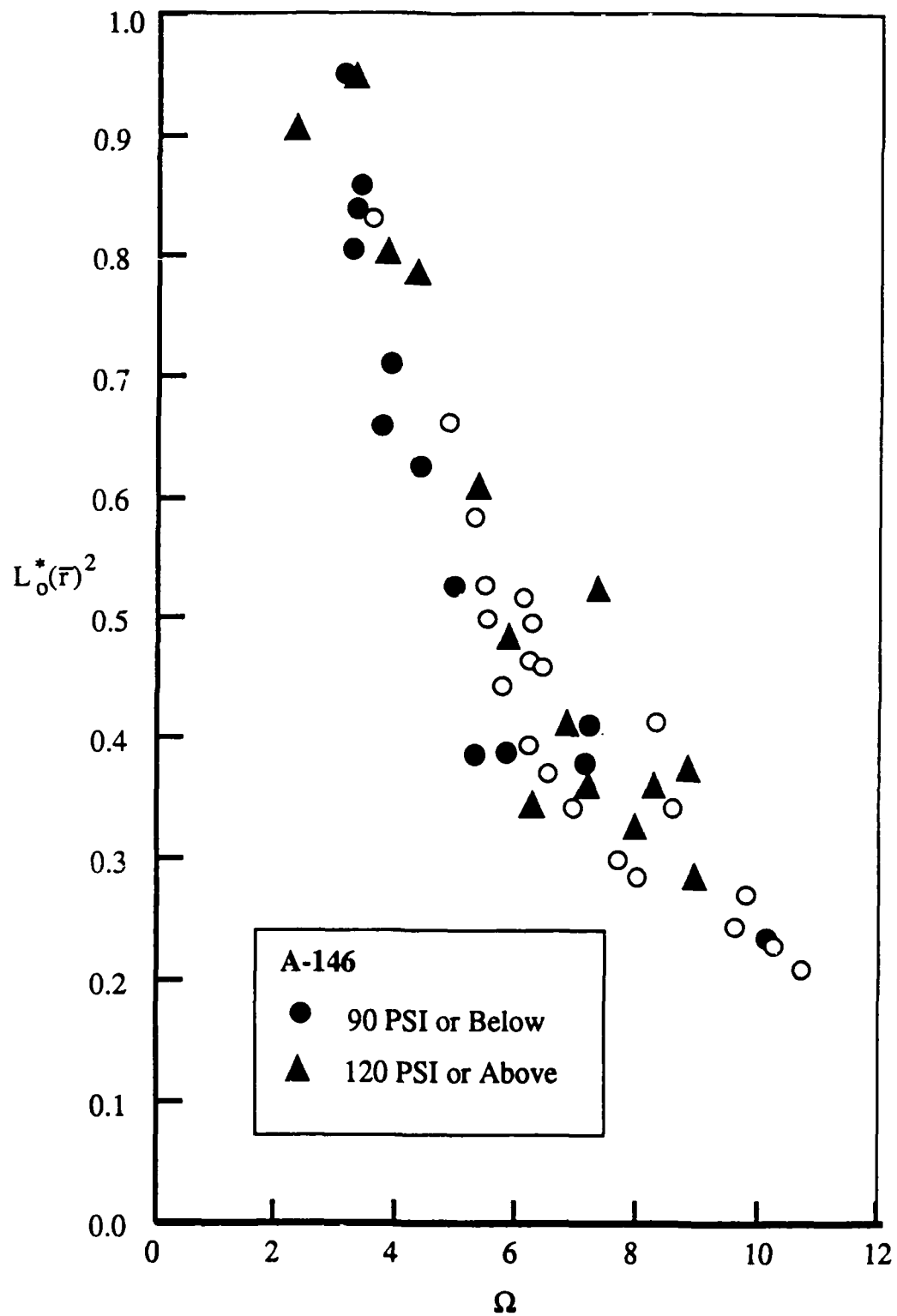
Fig. 7.12 Correlation of $L_0^*(\bar{r})^2$ vs Ω for A-146 Propellant

Calculation of Combustion Response

The oscillator equations (7.24 and 7.25) can be solved for R and $\omega\tau$ in terms of experimental variables, and R and $\omega\tau$ can then be calculated for tests in which growing oscillations permit determination of ω and α. Thus

$$\omega\tau = \tan^{-1}\left[\frac{A'\omega L^*}{1 + A'\alpha L^*}\right] \tag{7.34}$$

$$R = \frac{A'\omega L^*}{\sin\left\{\tan^{-1}\left[\dfrac{A'\omega L^*}{1 + A'\alpha L^*}\right]\right\}} \tag{7.35}$$

The above equations have been used by a few investigators to calculate from L* tests (Ref. 5, 10-15). The range of Ω over which the tests gave measurable κ is rather limited, so there has been no effort to fully evaluate the method, and some doubts have been raised about results. Such doubts generally question the adequacy of the response function model, rather than the adequacy of the experimental determination of R and $\omega\tau$ (Ref. 12-15). We have indicated earlier (e.g., 7.7) the trend in response $\Re(\Omega)$ as indicated by the QSHOD model. In Fig. 7.13 the actual data from tests on a specific propellant are shown, and permit a comparison of measured results with theory. The results are shown as R vs Ω and $\omega\tau$ vs Ω (corresponding to Fig. 7.5) and as R vs $\omega\tau$ (corresponding to Fig. 7.7).

Referring to Fig. 7.13a, QSHOD theory predicts that $\omega\tau$ vs Ω is a unique function independent of pressure (and independent of α to the extent that linear theory pertains). The results in Fig. 13 obviously do not conform to a simple $\omega\tau$ vs Ω curve. They show a trend to higher Ω for higher pressure tests, which helps in interpretation because it suggests that the results correspond to the region of positive slope of the $\omega\tau$ vs Ω function in Fig. 7.5. This inference can be drawn from the QSHOD models, as illustrated by the R vs $\omega\tau$ curves in Fig. 7.14, for an example where the curves cross the stability line on the lower branches of the R vs $\omega\tau$ curves (in contrast to Fig. 7.7). This is analogous to being on the positive $d(\omega\tau)/d\Omega$ part of an $\omega\tau$ vs Ω curve like that in Fig. 7.5. The test data fall in an area designated by the dotted envelope in Fig. 7.14, with the points along a given R vs $\omega\tau$ curve corresponding to all the QSHOD prediction of all data at that value of n (and, hence, p). The curves crossing the area at higher $\omega\tau$ (and higher Ω in this example) are the curves with lower n, and hence higher pressure (for A146 propellant, as per Fig 7.10). Examination of Fig. 7.7 will show that the opposite trend of Ω with pressure results when the R vs curves cross the stability line in the upper branches (corresponding to the negative $d(\omega\tau)/d\Omega$ regions in Fig. 7.5).

If we accept the QSHOD-based reasoning that the trend to higher Ω at higher pressure means that the experimental results correspond to the positive slope part of the $\omega\tau$ vs Ω function, then we can return to Fig. 7.13a, and note another
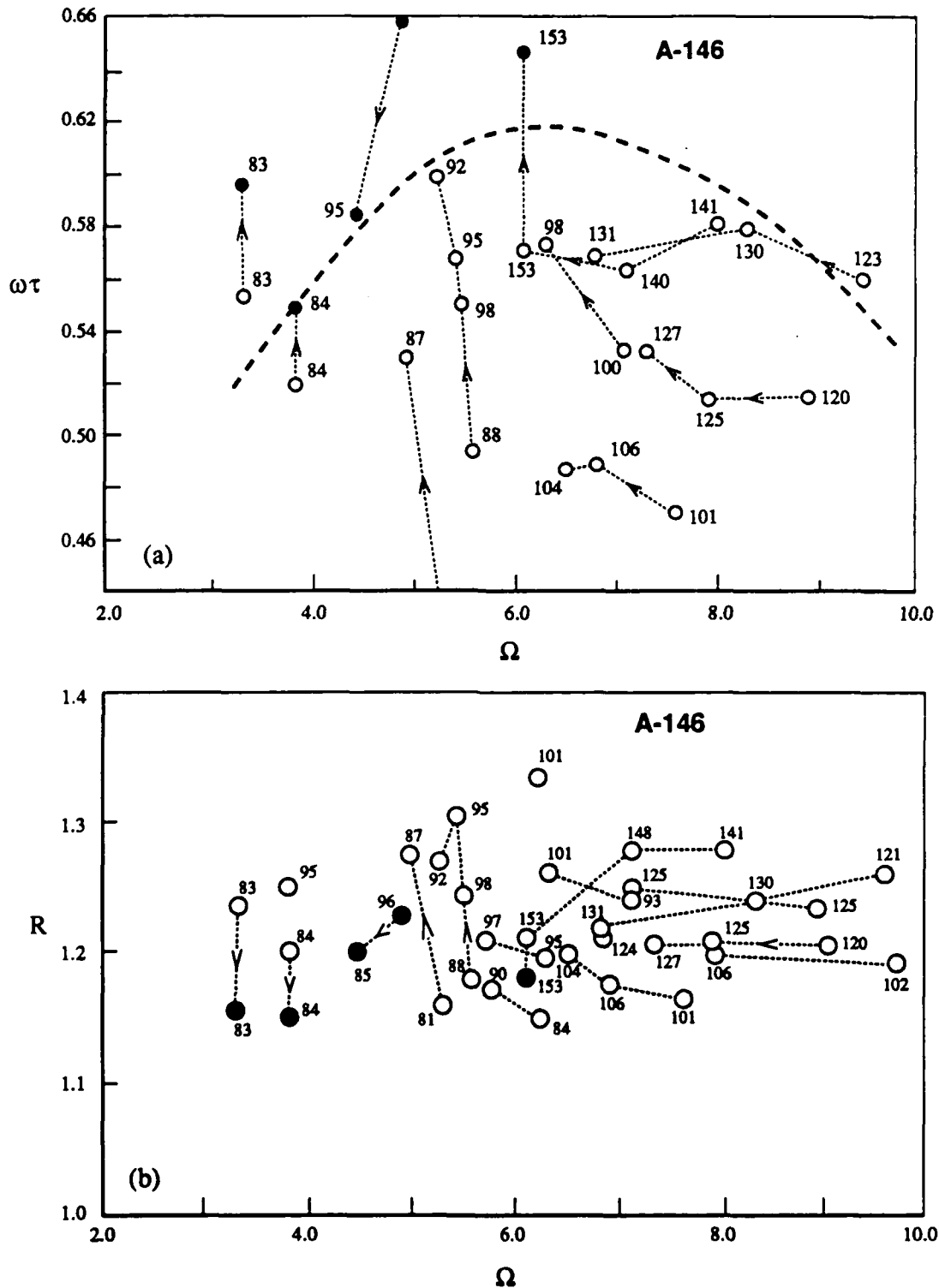
Fig. 7.13 Response function data for A-146 propellant based on Eq. (7.34) and (7.35) and data in Ref. 7.10. Solid symbols correspond to tests with negative α. The broken line in part a is an estimate of the stability limit based on the trend of the α data in Ref. 7.10. The broken line in part c is the stability limit defined by $R \cos \omega \tau = 1$. The dotted lines connect data points in sequential burns in single tests (arrows indicate time sequence).

Fig. 7.13   Response function data for A-146 propellant based on Eq. (7.34) and (7.35) and data in Ref. 7.10. Solid symbols correspond to tests with negative α. The broken line in part a is an estimate of the stability limit based on the trend of the α data in Ref. 7.10. The broken line in part c is the stability limit defined by $R \cos \omega \tau = 1$. The dotted lines connect data points in sequential burns in single tests (arrows indicate time sequence).
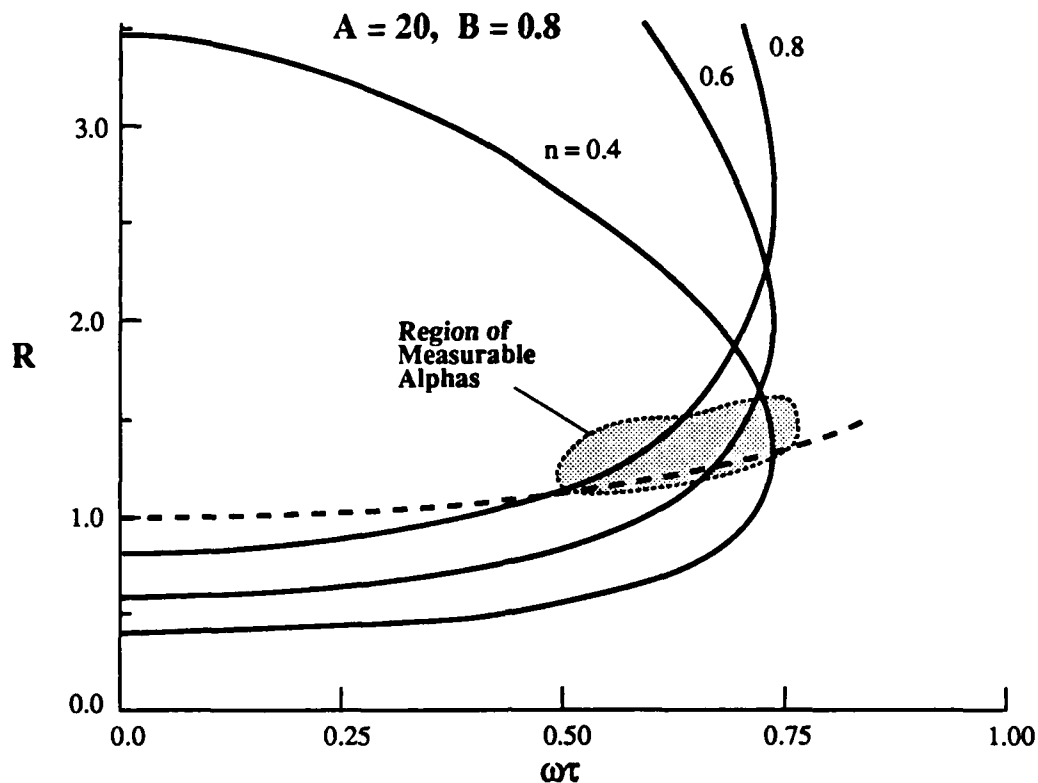
Fig.7.14 Response function map for stability limit on the lower branch of the R vs curves (QSHOD theory) with A=20 and B=0.8. The dotted envelope indicates the domain of tests with measurable positive α.

systematic trend in the data, that definitely is not forecast by the QSHOD theory. The data points connected by dotted lines represent points obtained from single tests that gave multiple burns as in Fig. 2b. These sequences occur at nearly constant p, increasing L*, and usually decreasing α and Ω consistent with points along a constant n QSHOD curve in Fig. 7.14. However, the points clearly differ systematically from the single α vs Ω curve required by theory, with the high α points tending to be at lower ωτ and higher Ω. An examination of the original data in Ref. 10 suggested that a reasonable ωτ vs Ω curve could be estimated for the stability limit, and such a curve is shown in Fig. 7.13. The divergence of the high α data from this curve may reflect nonlinear behavior, or may reflect systematic error in measurement or failure of assumptions in the model A more careful study is needed.

Referring to the R vs ωτ data in Fig. 7.13b, the trend of high pressure data to higher is shown here too, and is consistent with the location of the crossings of the constant pressure curves across the predicted region of test data in Fig. 7.14. However, the trend in multiple-burn sequences clearly do not conform to QSHOD

theory, which calls for decreasing R and $\omega\tau$ during such sequences. One might argue that the data corresponds to a pressure-dependent family of R vs $\omega\tau$ curves (Fig. 7.15) with the curves at lower pressure having higher R, consistent with the conditions in Fig. 7.14, biased by the systematic dependence on α in the multiple burn sequences. Looking at Fig, 7.13c, it is even more difficult to see argument with QSHOD theory, presumably because of both non-systematic error in determination of both R and $\omega\tau$, and the systematic dependence on time in a multiple burn sequence on both R and $\omega\tau$.

In summary, the "A-146 data"show that rough trends in data are consistent with theory,but that quantitative argument is not approached. The experimental method has not been fully evaluated and the assumptions in the model leading to Eq. (7.34) and Eq. (7.35) have not been evaluated A major effect on R and $\omega\tau$ that appears to be related to α prevents correlation of results with QSHOD theory; such an effect could be a nonlinear effect, but it seems premature to propose whether linearization in the oscillation model or the QSHOD model (or both) is responsible for failure to correlate the large α data. More careful testing to establish stability limit data might yield results consistent with the QSHOD model. Various papers that have identified data trends that do not conform to the QSHOD model (e.g., Ref. 11-15) probably should be re-examined with more suspicion of Eq. (7.34) and (7.35) (at large κ), more suspicion of the accuracy of determining Ω, L^*, and α (especially α), and with an effort to test the linear theory with low α data (a more critical look at the old test data should be a good starting point).

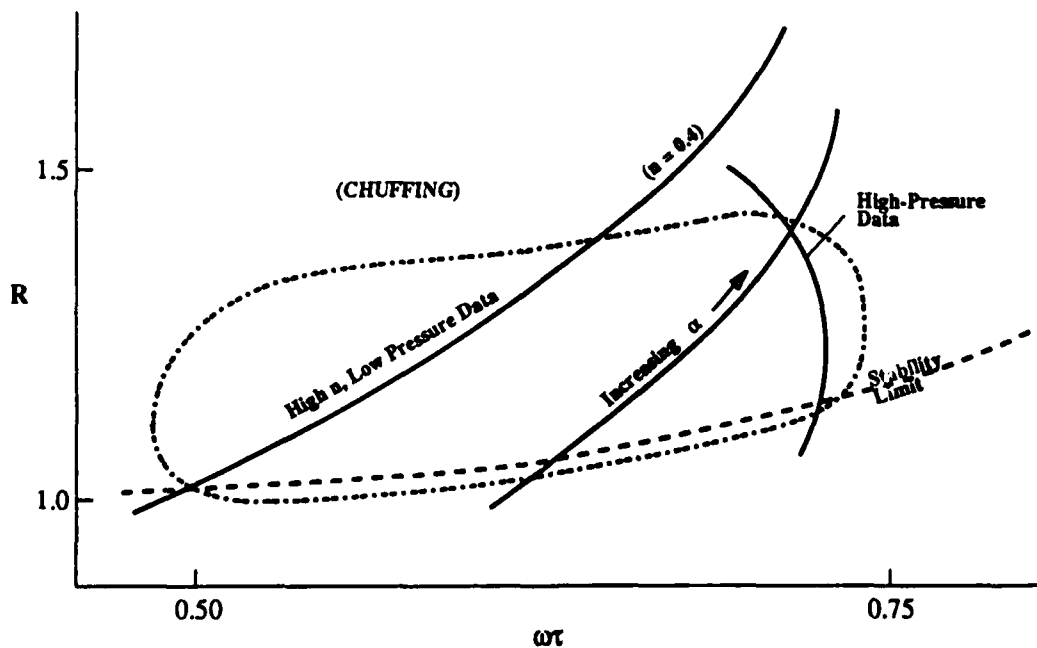

Fig.7.15 Sketch of R vs Ω showing the trends corresponding to the unstable domain in Fig. 7.14 and the data in Fig. 7.13b ·this figure is a sketch of the "data region" of Fig. 7.14: A and B have not been optimized to A-146 results).

7.4 ANOMALOUS BULK MODE OSCILLATIONS

Up to this point, this chapter has addressed primarily the concept of combustion response function driven oscillations, using linear models of both pressure-coupled combustion response and combustor oscillations. In addition, rather stringent limitations were imposed on distribution of combustion and on relative time constants in the system. In general, nature is more versatile than that, and it is appropriate to mention some realities that don't conform to the models Since state of knowledge is limited, these realities are mentioned primarily to help perspective in future research.

Spontaneous Combustion Oscillations

Some propellants will burn in an oscillatory way even in a nonoscillating environment (Ref. 4, 16-19). When such propellants are burned in a combustor, they produce pressure oscillations at the same frequency exhibited in a constant pressure chamber (Ref. 16). In an L* burner the system behavior with such a propellant corresponds to an oscillator (the combustor-flow system) responding to an independent forcing function (the combustion) at the frequency of the forcing function. The combustion response function is infinite at one frequency and zero elsewhere. While such behavior is uncommon (and usually unacceptable), it is related to a more common class of behavior that has been neglected and "mistreated". The oscillatory behavior reported in Ref. 16 was measured as oscillations in total luminosity of the burning area (constant pressure chamber), and the magnitude of the oscillations decreased as the burning area was increased; it was concluded that the oscillatory behavior was localized, and that contributions from different sites on a large surface were randomly phased so that there was no net oscillation in the total luminosity from large samples. However, this same propellant did drive burner oscillations at the propellant frequency, indicating that the sites on the surface were oscillating in phase. This means that the spontaneous oscillations are in some measure responsive to combustor oscillations (this was referred to in Ref. 18 as "phase coupling"), while retaining the characteristic frequency. The mechanism by which such phase coupling comes about has not been determined, but it is difficult to picture a mechanism that can shift phase without having some capacity to shift frequency as well. In other words, the combustion is responsive (probably to pressure oscillations), but only in a narrow frequency range, and probably in a very nonlinear way governed by phase correlation rules rather than by local response magnitude. A class of combustor instabilities referred to as "preferred frequency instability" (Ref.20) seems to be due to such combustion behavior. The extent of such behavior is presently unknown, but the trend of behavior of such a propellant in an L* burner would surely not conform with the description of L* instability discussed in this chapter.

Distributed Combustion

As noted earlier, the "short stay time" assumption in the combustor model poses the possibility that the combustion zone is not thin as assumed in the model. In the extreme case, combustion may not be complete at the nozzle entrance. The implications of this were considered in Ref. 21 and 22, but the difficulty of rigorous modeling has limited progress in understanding. Temperature oscillations (Ref. 23), luminosity oscillations (Ref. 4, 16, 18), and composition oscillations (Ref. 24) have been measured in L* burners, but no systematic results are available. It seems likely that distributed combustion effects would be important with nitrate ester propellants that are known to have extended combustion zones at low pressure, and with metalized propellants that give relatively slow burning metal droplets in the flow from the burning surface. While L* burner trends with such propellants have not been fully or systematically evaluated, they do show different trends than typical AP-HC binder propellants (Ref 114, 25). Some of these trends have probably been aggravated by tests that yielded data on oscillations (frequency) while the "mean" pressure was also changing (the absence of a reasonably steady time average pressure is indicative of poorly established burning (possibly due to incomplete combustion); consideration of oscillatory behavior during a poorly determined quasisteady state probably adds to the confusion of data without compensating revelations!

A further point is the assumption of short flushing time, mentioned in development of the model but not validated then. According to Eq.(7.25), the ratio of flushing time to period of oscillations is

$$\frac{\tau_{ch}}{T} = \frac{\tau_{ch}}{2\pi}\omega = \frac{R \sin \omega\tau}{2\pi} \qquad (7.36)$$

In L* instabilities, R is generally $1.0 < R < 1.3$. $\sin \omega\tau$ is necessarily less then 1.0, so the period of oscillation is always at least $2\pi/1.3$ times the flushing time . This result was used earlier to justify the isothermal assumption in Eq. (7.8). It also indicates that the residence time in the combustion chamber is less than

$$\tau_{ch} = 2\pi\frac{R \sin \omega\tau}{\omega} \qquad (7.37)$$

which is, for example, about 0.1 sec at 100 Hz. For AP composite propellants combustion is typically complete 1 mm from the burnings surface with an out flow velocity of 10 m/sec, corresponding to a combustion time of 10^{-3} sec. Some other propellants have longer combustion times, violating the thin combustion zone assumption.

Large Amplitude Behavior

Oscillations in L* burners usually reach peak-to-peak amplitudes that are 20-40% relative to mean pressure, and growth α's are usually determined from oscillations so severe as to cause quenching of burning (Fig. 7.2b). The number of cycles is often so small that conformance to exponential growth cannot be assessed. Frequency of oscillation is often changing (perhaps due to changing L*, perhaps due to changing amplitude during the growth of oscillation. As with the "α-dependent" trend of results with A-146 propellant discussed before, these effects appear to be related to nonlinear effects which may limit the use of the small perturbation model to correlation of stability limit data.

7.5 SUMMARY

The stability of combustion in bulk modes was chosen as an introduction to the stability concept because both the fluid dynamic behavior and the combustion-flow coupling are relatively simple. As a result, one would expect the instability behavior to be easily describable, and the analysis to be *relatively* tractable. In general, those expectations were met. Unfortunately, the state of the experimental data in the literature are in considerable disarray, due to lack of any agreement as to what should be measured and what correlation of variables would be most useful. The elementary theory is helpful in developing understanding of combustor stability, and in showing how the response function concept is used to represent the dynamic interaction of the combustion process and the combustor flow dynamics. A particular set of test data was chosen from the literature to illustrate how experimental data trend can be compared with prediction of elementary theory. The comparison proved to be a good means to discuss the predictions of the theory, but brought out some data trends that have not been noted previously, that suggest nonlinear or other effects not encompassed in the elementary theory. This outcome illustrates that the theory is still incomplete and the experiments not yet fully understood. In later chapters the same lesson will emerge repeatedly, but it is disconcerting that it emerges even in the context of the simplest form of solid propellant combustion instability.

NOMENCLATURE

A Parameter in the QSHOD response function model (see Chap. 6)

A' Parameter determined by propellant thermochemistry (see Eq.(7.6))

A Throat area of the nozzle

B Parameter in the QSHOD response function model (see Chap. 6)

C Proportionality factor in the steady state burning rate law (see Eq.(7.4))

C' Proportionality constant in L* stability limit equation (7.3)

C Nozzle discharge coefficient (see Eq. preceding Eq. (7.9))

f frequency, Hz, $\omega/2\pi$

L* V/A_t

M Amplitude of the oscillation in mass burning rate at the time t when the pressure amplitude is P.

m mass of gas per second

m_a mass accumulation rate

m_b mass burning rate

m_d mass discharge rate

$\hat{m}$ $\hat{m} = m - \bar{m}$ (instantaneous value, small perturbation)

n pressure exponent in the propellant burning rate "law" (see Eq. (7.5))

P amplitude of pressure oscillation

P_o amplitude at a chosen time, t = 0

p pressure

$\bar{p}$ time average pressure (e.g., over a cycle of oscillation)

$\hat{p}$ $p - \bar{p}$ (instantaneous value, small perturbation)

R   Magnitude of the combustion response function, M/P (assumed to be independent of amplitude)

R   Gas constant (R = $p\mu/T\rho$)

$\mathfrak{R}$ complex response function (see Fig. 7.4, Eq. (7.18) - (7.22))

$\mathfrak{R}^r$ Real part of $\mathfrak{R}$, $\mathfrak{R}^r$ = R cos $\omega\tau$

$\mathfrak{R}^i$ Imaginary part of $\mathfrak{R}$, $\mathfrak{R}^i$ = i R sin $\omega\tau$

$\bar{r}$ regression rate of the burning surface (mean value)

T   Temperature

t   time

V   Volume of the gas filled portion of the combustor

α Exponential growth rate constant for oscillations (Eq. (7.1), (7.2))

γ Ratio of specific heats of reaction product gas mixture

θ Phase lead of combustion oscillations relative to pressure oscillations, θ = $\omega\tau$

κ Thermal diffusivity of the propellant

μ Molecular weight of reaction product gas mixture

ρ Density of reaction product gas (also ρ_g)

ρ_s Density of the solid propellant

τ Time lead of combustion oscillation relative to pressure, τ = θ/ω

τ_{ch} Flushing time of the combustor, Eq. (7.10), (7.9)

τ_{tw} Relaxation time of the thermal wave in the solid phase portion of the combustion zone, τ_{tw} = $\kappa/(\bar{r})^2$

Ω Frequency of oscillations, nondimensional Ω = $\kappa\omega/(\bar{r})^2$

ω Frequency of oscillation, in radians/sec

$\bar{f}$ Overbar designates time-averaged value over one cycle.

$\hat{f}$ Caret mark designates small perturbation about mean value.

REFERENCES

7.1   Sehgal, R., and Strand, L. D., "A Theory of low-Frequency Combustion Instability in Solid Rocket Motors, "AIAA J 2,4 (1964), pp.696-702.

7.2   Strand, L. D, "Summary of a Study of Low Pressure Combustion of Solid Propellants, " JPL Technical Report 32-1242, April 1968

7.3   Kumar, R. N., "Some Experimental Results on the L-Star Instability of Metalized Composite Propellants, "AIAA Preprint 75-22, (January 1975).

7.4   Price, E. W., Rice, D. W., and Crump, J. E., "Low Frequency Combustion Instability in Solid Rocket Motors, "Naval Ordnance Test Station (China Lake, CA) NOTS TP 3524, July 1964.

7.5   Schoyer, H. F. R., "Results of Experimental Investigations of the L* Phenomenon, " JSR 17, 3 (May 1980), pp. 200-207.

7.6   Helmy, A. M., and Ramohalli, K. N. R., "Coated Oxidizer for Combustion Stabiity in Solid-Propellant rockets" AIAA Preprint 85-1111 (July 1985).

7.7   Price, E. W., "Exprerimental Observations of Combustion Instability," in Fundamentals of Solid Propellant Combustion, AIAA Progress Series Vol. 90, 1984, pp. 742-754.

7.8   Culick, F.E.C., "A Review of Calculations for Unsteady Burning of a Solid Propellant, " AIAA J 6, 12 (December 1968), pp. 2241-2255.

7.9   Dailey, B. J., "Analysis of L* and α Curves Generated by the Dennison and Baum Response Function," Report on Special Problems Course AE 8500, Georgia Institute of Technology, September 1985.

7.10 Beckstead, M.W., et al., "Combustion of Solid Propellants and low Frequency Combustion Instability," Naval Weapons Center,TP 4478, China Lake, CA, April 1968.

7.11   Beckstead, M.W., and Price, E.W., "Nonacoustic Combustor Instability," AIAA J 5, 11 (November 1967), pp. 1989-1996.

7.12   Beckstead, M.W., and Culick, F.E.C., "A Comparison of Analysis and Experiment for Solid Propellant Combustion Instability, "AIAA J 9, 1 (January 1971), pp. 147-154.

7.13   Boggs, T.L., and Beckstead, M.W., "Failure of Existing Theories to Correlate Experimental Nonacoustic Combustion Instability Data, "AIAA J 8, 4 (April 1970) pp. 621-631.

7.14   Schoyer, H.F.R, "Experimental Investigation into the L* Instability of Double Base Rocket Propellants, "Propellants and Explosives 3 (1978) pp. 88-96.

7.15   Beckstead, M.W. "Low Frequency Instability: A Comparison of Theory and Experiment, Combustion and Flame 12, 1 (October 1968) pp. 417-426.

7.16   Svetlichnyi, B., Margolis, A.D., and Pokhil, P.F., (reference being sought).

7.17   Margolis, Margolin, Levichek, *et al* ((reference being sought).

7.18   Price, E.W. "Review of the Combustion Instability Characteristics of Solid Propellants," in Advances In Tactical Rocket Propulsion, AGARD Conferencse Proceedings No. 1, Part 2, Chapter 5, Technivision Services, Maidenhead England, August 1968, pp. 141-194.

7.19   Inami, Y.H., and Shanfield, H., "Nonacoustic Combustion Pulsations of Ammonium Perchlorate Containing Aluminum,"AIAA J 2, 7 (July 1964). pp. 1314-1318.

7.20   Eisel, J. E., Horton, M. D., Price, E. W., and Rice, D. W. "Preferred Frequency Oscillatory Combustion of Solid Propellants "AIAA J 2, 7 (July 1964) pp. 1319-1323.

7.21   Tien, J.S., Sirignano, W.A., and Summerfield, M., "Theory of L-Star Combustion Instability with Tempeature Oscillations, "AIAA J 8, 1 (January 1970) pp. 120-126.

7.22   Schoyer, H.F.R., "Incomplete Combustion: A Possible Cause of Combustion Instability,"AIAA J 21, 8 (August 1983) pp. 1119-1126.

7.23   Schoyer, H.F.R. and de Bent, R.T.M.,"Experimental Verification of Temperature Fluctuations During Combustion Instability, "AIAA J 24, 2 (February 1986) pp. 340-341.

7.24   Eisel, J.R., Ryan, N. W., and Baer, A. D., "Combustion of NH C10 - Polyurethane Propellants: Pressure, Temperature and Gas-Phase Composition Oscillations," AIAA J 10, 12 (December 1972) pp. 1655-1661.

7.25   Kubota, N., and Kimira, J., "Oscillatory Burning of High Pressure Exponent Double-Base Propellants," AIAA J 15, 1 (January 1977) pp. 126-127.

EIGHT

COMBUSTOR STABILITY ANALYSIS

False facts are highly injurious to the progress of science, for they often endure long; but false views, if supported by some evidence, do little harm, for every one takes delight proving their falseness.

Charles Darwin, 1880

In spite of the considerable effort which has been made since 1960 in attempts to elucidate the phenomena of combustion instability, it is evident that many gaps exist in our base understanding of the phenomena.

G.F.P. Trubridge, 1969

8.1 INTRODUCTION

This chapter is devoted to a detailed description of the solution of the first-order oscillatory rocket flow field problem posed in Chapter 5. Emphasis is on analytical solutions in three spatial dimensions. This is the problem that forms the backbone of the current combustion instability theory and its implementation in computational form. The presentation is intended to aid the reader to the greatest extent possible in using the large body of literature on the subject. Special analyses introducing additional approximations (such as the assumption of one-dimensional flow) or additional physical effects left out of the standard analysis (such as effects of viscosity) will be examined for the purpose of highlighting some of the controversial issues in the accepted version of the theory. The handling of boundary conditions at burning surfaces by the admittance (or response function) method introduced in Chapter 4 and elaborated in Chapter 6 will receive special attention.

Virtually all accepted combustion stability assessment models are based on linearization of the conservation equations describing the time-dependent flow field and boundary conditions as described in Chapter 5. Although this approach limits the range of validity of the resulting algorithms, it has the valuable feature of providing considerable physical insight into the interactions between a multitude of variables and physical processes. Such insight cannot be gained, however, without close study of the resulting equations. One goal of this chapter is to take a searching look at the results in order to determine their shortcomings as they are applied in the rocket industry. There remain many unanswered questions pertaining to the validity and applicability of the theory in many cases of interest. In a few cases, it appears to be an adequate representation of the system behavior.

Plan for Chapter 8

The road map for this chapter is as follows. A brief historical summary is first undertaken to set the stage for the description of the analytical models. This supplements the more general historical material of Chapter 1; it emphasizes the origins of the theoretical treatment of combustion instability. The mathematical formulation of the rocket flow field developed in Chapter 5 is then used as the basis for a stability assessment model. This is done first in the simplest form possible with pressure-coupled combustion response as the principal source of driving energy. The thin combustion zone approximation will be exploited to the full extent. Classical methods of solution of the governing equations are reviewed, and the energy method is introduced as an especially useful approach. With the basic solution as a guide, the additional energy loss and gain mechanisms needed to analyze a complete rocket motor system are determined. Account is taken of distributed energy losses and gains such as those related to the two-phase flow of particulate material in the combustion gases. Effects of nozzle losses and viscous dissipation of acoustic energy at inert surfaces are added to the analysis. Wherever possible, analytical solutions are described; where the situation does not allow such simplifications, the required numerical approaches are identified.

The classical theory of combustion stability is based principally on a study of irrotational, compressible waves closely related to the acoustic waves described in Chapter 5. We will find it necessary to extend our view of the oscillatory rocket problem to include other types of oscillatory phenomena that may interact with the acoustic waves. It will be necessary to account for both thermal and vortical (rotational) oscillatory effects if a complete mathematical description is to be constructed. An introduction to these extensions will be presented after the classical theory has been carefully reviewed.

Finally, attention will be directed to several controversial issues related to incorporation of more realistic representations of the burning surface and both the mean and oscillatory gas flow. The concepts of *velocity coupling* and *flow turning* will be given special attention.

Chapter 9 provides further discussion of the results and details the implementation of computational stability algorithms. The resulting model will be applied there to typical motor situations, and its limitations will be demonstrated by comparison to actual experimental data. Areas requiring further research are identified. Discussion of velocity coupling and related phenomena are continued in Chapter 10 where the emphasis is on their nonlinear features.

Origins of Combustion Instability Theory

A short historical summary describing the origins of combustion instability theory provides a useful introduction to the chapter. The path to the theory in its present form has been a tortuous one. Early analyses were *ad hoc* attempts to deal

with specific experimental observations and did not constitute complete system models. An analysis by Grad [1949] was perhaps the first attempt to produce a comprehensive theory in this country; it had been preceded by others, notably in Britain, that are classified and not widely known here. Grad's paper is perhaps the first to associate acoustic waves with the observed pressure fluctuations in mathematical form. The work of Crocco and Cheng [1956] in liquid rocket instability was followed by a series of detailed analyses by McClure, Cantrell, Bird, and Hart [1965; 1960; 1962] that form the underpinnings of the general theory for solid rockets. These analyses were the first to treat all of the main features needed for a detailed physical understanding of the phenomenon in system form. Special cases such as the L* instability effect and others described earlier in the book form a parallel set of analyses that will not be treated in this chapter. Culick [1966; 1967; 1968; 1969; 1970; 1972; 1973; 1975; 1983] contributed numerous corrections and improvements and is thus considered by most members of the solid rocket community to be the author of the accepted theory. His work emphasized the need for careful application of mathematical expansion procedures. He developed both one-dimensional and three-dimensional versions of the basic theory and introduced a rational method for including the effects of particle damping. He also spearheaded the analysis of nonlinear effects to be discussed in Chapter 10. His work on velocity coupling and other flow related effects still represent the best that has been accomplished in the important area of combustion/flow interactions.

Accompanying the thread of valid theory we are tracing in this book, are a multitude of misconceptions that have arisen in attempts to address the rich variety of side issues and special cases. Unfortunately, many erroneous concepts are still in widespread use. This is one of the reasons combustion instability has appeared to the practical motor designer to be virtually unusable in ordinary design procedures. Instability problems are thus rarely anticipated. One must apparently know some "black art" in order to deal with problems after they show up in motor testing or after a system has already been deployed. Thus, as in earlier times, those working to correct or prevent instabilities are known as "magicians" as discussed in Chapter 1. Hopefully the material presented in this chapter and in Chapters 9 and 10 will help to dispel this misconception. Once one achieves an understanding of the nature of the assumptions being used and gains a clear view of what the various parts of the analysis are intended to accomplish, then their application in the development and design process esis fairly straightforward. Chapter 9 will emphasize the practical implementation of the theory developed here.

From the viewpoint of a typical manager in a solid propellant rocket company, instability theory is often deemed to be of limited value because it does not allow the determination of the *severity* or amplitude of the predicted oscillation. To many, the description of the problem in terms of growth rate of acoustic modes, seems to be exercise in futility. This is a built-in limitation of the first-order linearized theory; it allows only an assessment of the *stability* of the system, that is, the *tendency* for a particular mode of oscillation to grow or decay. Nevertheless, such knowledge is of great value if it is understood and applied correctly.

In fact, as will be demonstrated in Chapter 10, there is a direct relationship between the predicted rate of growth and the eventual limit or peak amplitude reached in finite-amplitude oscillatory behavior. So, even in its linearized form, the combustion instability theory provides useful design guidance if it is applied with understanding.

8.2 THE LINEAR GROWTH RATE

The object of all linearized motor stability analyses is the estimation of a set of numbers that contains all the available information. Each potential mode of oscillation is characterized at a given point in motor burn by its linear growth rate often represented by the symbol α. Before describing the methods used to calculate this important parameter, it is necessary to briefly discuss the philosophy of the calculation and to describe what it can and cannot tell us about the time-dependent operation of a rocket motor.

The basic assumption used to make the complex time-dependent flow problem tractable is that the departure from steady operation is very small. Earlier, this idea led us to expand the governing equations in terms of the amplitude of the gas oscillations, ϵ. This parameter is conveniently interpreted as the percentage oscillatory deviation of the pressure from its mean value. As long as we are only interested in very small values of this parameter (say in the range 10^{-4} to 10^{-3}) then the first-order set of equations should yield an adequate description of the situation. However, as will become evident in the mathematics of the analysis, this approach severely limits the information available in the solution. Only the system behavior near its *stability boundary* can be determined. Because of the linear nature of the formulation, the result of the calculation for a given mode of gas oscillation is an exponential growth indicating the tendency of that mode to grow or decay. This numerical result is a function of the geometry (and hence, the burn time), gas properties, and especially the sensitivity of the combustion process to the pressure fluctuations in the burning zone.

The analysis, in effect, fits an exponential curve to the time-average of each mode of oscillation. That is, the average amplitude of a certain mode n at a *given instant* will be found vary exponentially with time;

$$\left\langle p_n^{(1)} \right\rangle \equiv \frac{1}{\tau} \int_{t_o}^{t_o+\tau} p_n^{(1)} \, dt \approx e^{\alpha t} . \tag{8.1}$$

This is not an accurate representation of the actual manner in which the amplitude would change over a finite time in an actual system; it cannot deal with situations in which the system oscillations grow to a limit amplitude. It provides only an approximation to the rate of change at a given instant of time, the growth rate. A positive value of α indicates an oscillation with a tendency to grow (instability); a negative value implies stability. As applied in practice, the stability calculations yield numerical values for a for each assumed mode of oscillation at whatever times during motor operation are of interest. If α is large for a given mode, one often concludes that the system is more likely to oscillate in that mode. Interpre-

tation of the anticipated severity of instability from these numerical values is apparently an art, and no two investigators are likely to arrive at exactly the same conclusions in a given situation [Beckstead, 1971]. Further pursuit of this important practical point will be undertaken in discussions of the application of the theory in Chapter 9. Further insight will come as we turn to questions of finite-amplitude, nonlinear aspects of combustion instability in Chapter 10.

8.3 THE FIRST-ORDER STABILITY PROBLEM

A key element of the basic combustion stability model is a perturbed wave equation describing the influence of the flow environment on wave growth in the rocket combustion chamber. A brief review of the equations and boundary conditions from which this wave equation springs is in order before we proceed. The fundamental assumption to be made is that the amplitude of the pressure fluctuations is small (compared to the mean pressure). Thus it follows, as we have seen in Chapter 6, that the amplitude of the corresponding velocity oscillations is also small (compared to the speed of sound). This is the basis of a perturbation expansion scheme, which allows us to collect terms into groups with the same order of magnitude. The symbol ε will be used to represent the wave amplitude as before. A second perturbation parameter, the magnitude of the Mach number of the mean flow, M_b, yields the flexibility needed to incorporate driving and damping effects related to the chamber gas flow and, hence, the combustion processes that produce that flow. Table 6.1 is a map of the analytical procedure. In this chapter, we focus on the classical linear problem in which terms of first order in the wave amplitude and mean flow Mach number are retained. The need to treat the limit process in a careful and consistent manner was clarified in the work of Culick [1972]. Several previous instability theories were shown to be erroneous because of inconsistency in retention of terms in the equations. It is obviously incorrect to carry one or two terms of a given order while others of equal importance are ignored.

Following the expansion procedure described in Chapter 5, we first determine the linearized governing equations. For the moment we ignore viscous effects and the influence of the two-phase flow of particulate matter formed in the combustion process. Once the basic solution has been found, these and other effects can be incorporated by simple superposition owing to the linear nature of the formulation. Also, we will capitalize on the reversibility of the flow field in the absence of viscosity and other dissipative effects. The energy equation is thus satisfied automatically and in dimensionless form we find (see analyses leading to equations 5.96, 97) the governing equations

$$\frac{\partial p^{(1)}}{\partial t} + \gamma \nabla \cdot u^{(1)} = - M_b U \cdot \nabla p^{(1)} \tag{8.2}$$

$$\frac{\partial u^{(1)}}{\partial t} + \frac{\nabla p^{(1)}}{\gamma} = - M_b \left[u^{(1)} \cdot \nabla U + U \cdot \nabla u^{(1)} \right] + F^{(1)}, \tag{8.3}$$

where density has been replaced by pressure in the continuity equation by use of the isentropic relationship. $F^{(1)}$ is a body-force term we will use later to represent interaction with particulates in the mean flow. To emphasize that the oscillations described by the resulting equations are acoustical in nature, we follow the system of notation introduced in Chapter 5 by putting

$$p^{(1)} = p', \quad u^{(1)} = u', \tag{8.4}$$

where the prime will always indicate acoustic (irrotational) compressible gas motions throughout this text. This distinguishes the motion being analyzed from other types of oscillatory behavior that might be present. We will consider these later with special attention to the effects of vorticity transport and viscosity.

In Chapter 5 we solved the equations of motion for the special case of a closed chamber (no superimposed mean flow , $M_b = 0$). This led to the classical acoustic solutions. We are now interested in the interactions of such waves with the combustion gas flow. If we assume that it is sufficient to determine the system behavior at the stability boundary, that is for vanishingly small amplitudes of oscillation, then equations 8.2-3 will suffice for our current needs. We can proceed in much the same fashion followed in the acoustic wave examples of Chapter 5. That is, we expect the time-dependent gas motion to be a modified acoustic wave. As demonstrated in the simple acoustics case, there is much benefit in using either the pressure perturbation or the perturbation velocity potential as the main variable. This avoids the extra complexity of a vector wave equation that would result if velocity is used directly as the principal variable. We will adopt the customary choice of pressure as the variable. Thus we must combine equations 8.2 and 8.3 in such a way that the velocity vector is eliminated. This is accomplished by subtracting the divergence of the momentum equation (8.3) from the time-derivative of the continuity equation (8.2). The result is the perturbed wave equation

$$\frac{\partial^2 p'}{\partial t^2} - \nabla^2 p' = M_b \left[\gamma \nabla \cdot (u' \cdot \nabla U + U \cdot \nabla u') - U \cdot \nabla \frac{\partial p'}{\partial t} \right] - \gamma \nabla \cdot F^{(1)}, \tag{8.5}$$

where terms proportional to the mean flow Mach number have been collected on the right hand side of the equation. This suggests that a second perturbation be used with M_b as the perturbation parameter. This works because M_b is quite small in all practical cases, usually smaller than 10^{-2}. Since the left side is the acoustic wave equation, then equation 8.5 indicates that the problem can be treated as an acoustic wave motion that is slightly perturbed by the effects of the mean flow. Notice that $F^{(1)}$ is generated by particle drag in the mean flow and is properly grouped with the other $O(M_b)$ terms on the right side of 8.5.

It is also justified (on the basis of experimental evidence) to assume that the pressure fluctuations exhibit exponential time dependence since harmonic oscillations should dominate the unperturbed motion. Therefore,

$$p' = \eta(r) e^{i K t}, \tag{8.6}$$

where η is the mode shape (the spatial distribution of the pressure perturbation) and K is the perturbed frequency

$$K = k_i + O(M_b) = k_i + M_b(\omega_i - i\alpha_i) + O(M_b^2) \qquad (8.7)$$

The imaginary part, α_i, is the exponential growth rate of the wave and k_i is the unperturbed frequency of oscillation. ω_j is the effect of flow and combustion on the mode frequency. We have written K as an expansion in the mean flow Mach number, since we anticipate that modifications to the acoustic solution are of this order. The main objective of the linear combustion instability analysis is to estimate the value of α using acoustic mode frequencies to approximate ω. Since the velocity perturbation is of the acoustic variety, then it is related directly to the pressure; its time dependence must be the same. The body force is assumed to depend on the gas motion, so both u' and $F^{(1)}$ depend on time in the same way as p'. Thus

$$u' = q(r)e^{iKt} \qquad (8.8)$$

and

$$F^{(1)} = M_b f(r)e^{iKt}, \qquad (8.9)$$

where q and f are complex functions of the spatial coordinates to take account of phase shifts relative to the pressure field. Inserting 8.7 into the wave equation and cancelling the common exponential term yields the non-homogeneous Helmholtz equation

$$\nabla^2\eta + K^2\eta = M_b[iKU\cdot\nabla\eta - \gamma\nabla\cdot(q\cdot\nabla U + U\cdot\nabla q) + \gamma\nabla\cdot f], \qquad (8.10)$$

where the right-hand side is strongly influenced by the mean flow field.

Before further progress can be made we must investigate the boundary conditions that must be satisfied. That is, a complete boundary value problem must be defined to take account of the system geometry and the influence of the boundary effects such as combustion.

Perturbed Boundary Conditions

We assume that equation 8.10 governs the time-dependent gas motion in a control volume bounded by a control surface consisting of several types of boundaries. For instance, part of the boundary might consist of hard, inert walls such as those considered in the simple acoustic solutions of Chapter 5. Other types of boundaries at sites of propellant combustion where the mean flow originates are of obvious importance. Chapter 4 included an introduction to a simple means for accounting for the sensitivity of the combustion process to the presence of superimposed gas oscillations. Much more attention to the physical and chemical nature of this type of boundary is needed, but we will accept it for the present without further discussion. The boundary conditions on p' defined at the chamber surfaces can be determined by combining the definition for the propellant admittance or response function with the momentum balance. The latter is first written in the form of a condition on the component of the pressure gradient

normal to the wall. Defining **n** to be an outward pointing unit vector everywhere normal to the surface of the control volume as illustrated in Figure 8.1, and using 8.3 we write (after inserting 8.6, 8, and 9)

$$\mathbf{n} \cdot \nabla \eta = -\mathbf{n} \cdot \gamma [i K \mathbf{q} + M_b (\mathbf{q} \cdot \nabla \mathbf{U} + \mathbf{U} \cdot \nabla \mathbf{q} - \mathbf{f})] \qquad (8.11)$$

The value of this function must be specified at the various types of bounding control volume surfaces. This can be accomplished by using the admittance boundary condition. On inert surfaces this is just the hard-wall condition we used in Chapter 5 (see equation 5.110 and 5.112). On propellant surfaces it is assumed that there is a burning rate perturbation proportional to the local acoustic pressure defined as

$$\mathbf{n} \cdot \mathbf{u'} = -M_b \frac{1}{\gamma} A_b p' \qquad (8.12)$$

or, after factoring out the common exponential time dependence,

$$\mathbf{n} \cdot \mathbf{q} = -M_b \frac{1}{\gamma} A_b \eta \qquad (8.13)$$

A_b is the acoustic admittance in the form used by Culick [1966]. Other notations are sometimes used, and it is common practice to use the response function instead of the admittance. We will return to the subject of nomenclature after the basic solutions are in hand. Notice the great simplification that results if the admittance is taken to be a *property of the propellant*. That is, if it is not a function of position, wave amplitude, or wave geometry, then A_b is a simple ratio of the normal velocity amplitude at the burning surface to the local pressure amplitude. The admittance is taken to be only weakly dependent on boundary temperature, shear stresses, and other localized environmental variables. It is, however, strongly dependent on the frequency of the imposed pressure disturbance. On inert surfaces the normal component of velocity must vanish; we cannot restrict

Outward pointing unit vector **n**
is everywhere perpendicular to
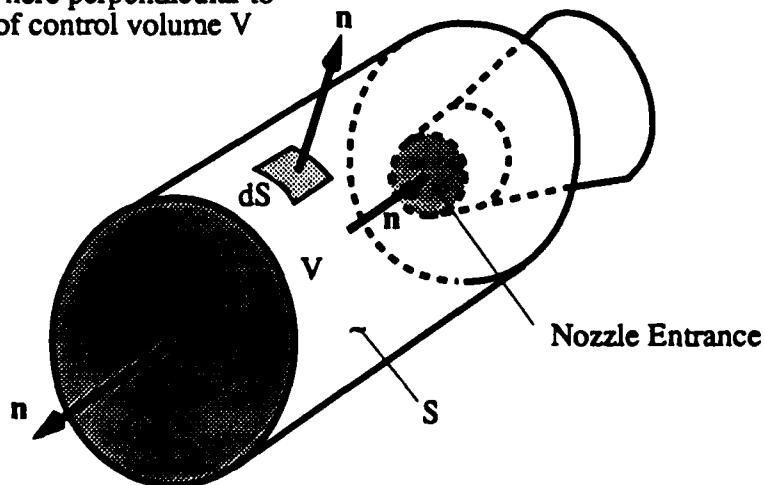surfaces of control volume V

Nozzle Entrance

Fig. 8.1 Control Volume and Control Surfaces

the parallel component of the fluctuating velocity without further discussion. One can treat the nozzle entrance region, an arbitrarily placed surface separating the compressible part of the nozzle flow from the chamber, by means of an nozzle admittance function A_n (to be discussed in detail later in the chapter). Thus, we put

$$\mathbf{n} \cdot \mathbf{q} = M_b \frac{1}{\gamma} A \eta = M_b \begin{cases} -\frac{1}{\gamma} A_b \eta & \text{on burning propellant surfaces} \\ 0 & \text{at inert surfaces} \\ \frac{M_e}{M_b} \frac{1}{\gamma} A_n \eta & \text{at the nozzle entrance surface} \end{cases} \qquad (8.14)$$

Combining 8.13 and 8.11, we find the boundary condition on the normal component of the pressure gradient at corresponding surfaces to be

$$\mathbf{n} \cdot \nabla \eta = M_b \{ iK A\eta - \gamma \mathbf{n} \cdot [(\mathbf{q} \cdot \nabla U + U \cdot \nabla \mathbf{q}) - \mathbf{f}] \} \qquad (8.15)$$

The combination of equations 8.10 and 8.15 constitutes a well-posed boundary value problem for the time-dependent gas motions in the chamber. Since the problem is a linear one, standard analytical methods can be used in determining its solution. We will demonstrate two methods each of which has certain advantages. These are chosen for their practicality and extendibility rather than for their mathematical elegance.

Solving for the Growth Rate

Several practical matters have not yet received attention. A few of these can be addressed easily at this point in the analysis. Others are quite difficult to handle, and not all have been properly implemented in instability prediction algorithms. For example, the scaling parameters used to define the dimensionless variables and the mean flow velocity vector and other parameters in the nonhomogeneous terms have been treated as though they do not vary with time. However, they are obviously not constant; in fact they may, in some instances, change quite rapidly with time. The chamber size and shape are altered as the burning surface regresses. The mean flow velocity and other gas properties can vary significantly during the motor run as the stagnation pressure changes. It is not clear that we have accounted for all of the inherent time-dependence in the problem. We will deal with this particular question in heuristic fashion by noting that although all of these quantities do vary in time they do so relatively slowly from the standpoint of the time scale we have adopted for the problem. That is, there may be many hundreds of cycles of oscillation during the time needed, say, for the axial flow velocity to change by a percent or two. Thus on the time scale of the waves (as conveniently measured by the period of oscillation, $\tau = 2\pi/\omega$) the variations in the chamber size, mean flow and thermodynamic parameters can be taken to be negligible. We often assume the scaling functions change slowly with

time and to the approximation of the problem as we have set it up these changes have negligible effect on the outcome of the calculation. These questions can be treated more formally using the methods of singular perturbation theory, two-time variable theory, or the method-of-averaging [Bogoliubov, 1961; Cole, 1968; Jeffrey, 1982 ; Krylov, 1957; Whitham, 1974]. This class of solution will be discussed at a more appropriate point in the presentation.

Other questions are not as easily swept under the rug. For instance, it is not at all certain that viscous effects do not play some essential role in the oscillatory behavior. We have already seen in Chapter 5 that rotationality of the flow field, that is the vorticity produced in the generation of gases at the burning surface, has a major influence on the velocity profiles and pressure distributions. Also, it is not obvious that the acoustic admittance properly accounts for the effects of wave orientation relative to the burning surface. The admittance boundary condition apparently only directly pertains to the *normal part* of the velocity fluctuations. Questions such as these have been addressed in development of the classical instability theory in an *ad hoc* manner usually by incorporation of corrections applied to the final growth rate expressions. Wave orientation questions have led to introduction of "velocity coupling", "flow turning", "admittance corrections" and so on. These items will be discussed separately and in depth in a separate section after we have deduced the basic instability results. As stated several times already, a most useful feature of the linearized theory is that corrective features can be introduced in most cases simply by adding them to the basic results.

Standard techniques have been developed for dealing with boundary value problems of the type characterized by nonhomogeneous linear differential equations with nonhomogeneous Neumann boundary conditions. The most direct and elegant approach is to apply the theory of Green's functions, which was designed to handle this class of problems. Since this approach is thoroughly discussed in elementary texts [Stakgold, 1979; Wylie, 1975] we will not describe it here. Culick applied this method formally in his seminal paper [Culick, 1966]. We will follow his notation fairly closely, since it is used in the formulation on which the standard stability assessment tools are based. Any variations in notation have been introduced only to clarify the approach. The material as originally published makes difficult reading for the typical rocket engineer.

There are in fact several ways to achieve the desired results without formal application of elegant mathematical techniques. Let us initially follow a physically motivated approach that uses many of the ideas that form the basis for the Green's function method, but without addressing its more abstract features. The method we will use is a standard approach applied in elementary vibration problems involving systems with distributed mass. The basic idea is that any oscillation of the system can be described as a linear superposition of a set of modes each of which satisfies the unperturbed problem. Thus for the present problem, the solution will be represented as a sum of acoustic modes. Each of these modes must have a relative amplitude chosen in such a way that their sum satisfies the boundary value problem we have formulated. In order that we can

arrive at some useful end result, it is first necessary that we highlight a few mathematical features of the acoustic solutions.

Since the unperturbed problem is linear, more complex solutions can be formed by superimposing simple solutions of the type we worked with in Chapter 6. Thus, we propose that the solution for our linear perturbed problem be written as

$$\eta = \sum_{i=1}^{\infty} A_i \eta_i ,$$ (8.16)

where i stands for the set of integers that describe a particular mode. If theproblem is three-dimensional, then each i represents a set of three mode integers as we defined them in Chapter 5.

Since the coefficients are not known *a priori*, we must construct some means to find them for the conditions of the problem. In fact, we will not need to determine them explicitly since the main goal is to determine the growth rate for each mode. That is, we are mainly interested in the imaginary parts of the complex eigenvalues, K, of the problem. Equation 8.16 is readily seen to be the equivalent of a Fourier series representation of the solution, and familiar ideas aassociated with such series are of great utility in our pursuit of the eigenvalues.

A most useful tool is the concept of orthogonality of the normal modes of the problem. This is the familiar Sturm-Liouville theorem reviewed at the end of Chapter 6, which states that the solutions of a linear boundary value problem form an orthogonal system of functions. Certain integrals over the problem domain have useful properties, and our approach will deliberately attempt to invoke them.

The problem we wish to solve can be expressed in the form of a nonhomogeneous Helmholtz equation and a corresponding nonhomogeneous boundary condition:

$$\begin{cases} \nabla^2 \eta + K^2 \eta = M_b g & (8.17) \\ \mathbf{n} \cdot \nabla \eta = - M_b h , & (8.18) \end{cases}$$

where

$$\begin{cases} g \equiv iK \, \mathbf{U} \cdot \nabla \eta - \gamma \nabla \cdot (\mathbf{q} \cdot \nabla \mathbf{U} + \mathbf{U} \cdot \nabla \, \mathbf{q}) + \gamma \nabla \cdot \mathbf{f} & (8.19) \\ h \equiv iK \, A \eta + \gamma \mathbf{n} \cdot [(\mathbf{q} \cdot \nabla \mathbf{U} + \mathbf{U} \cdot \nabla \, \mathbf{q}) - \mathbf{f}] . & (8.20) \end{cases}$$

Compare this to the unperturbed problem studied in Chapter 6:

$$\begin{cases} \nabla^2 \eta_i + k_i^2 \eta_i = 0 & (8.21) \\ \mathbf{n} \cdot \nabla \eta_i = 0 . & (8.22) \end{cases}$$

The experimental fact that the oscillations observed in rockets often have nearly the acoustic frequencies and mode shapes of the chamber is seen to be mathematically

expressed in equations 8.17 and 8.18. The departure from the acoustic equations (8.21 and 8.22) is very small since M_b is usually quite a small number. What we are interested in is the behavior of the system when it is oscillating near one of the resonant acoustic frequencies. Let us investigate a particular mode, say $i = j$. Then the pressure amplitude function can be written, following equation 8.16, as

$$\eta = \eta_j + \sum_{\substack{i=1 \\ i \neq j}}^{\infty} A_i \eta_i = \eta_j + O(M_b), \qquad (8.23)$$

and to satisfy 8.17, the correction to the acoustic solution j represented by the summation over the remaining acoustic modes must be of the order of the mean flow Mach number.

The simplest route to the growth rate is carry out these three steps:

(1) Multiply equation 8.17 by η_j
(2) Subtract equation 8.21 (with $i = j$) multiplied by η
(3) Integrate the result over the chamber volume

This leads to the expression

$$\int_V \left[\eta_j \nabla^2 \eta - \eta \nabla^2 \eta_j \right] dV + \left(K^2 - k_j^2 \right) \int_V \eta \eta_j dV = M_b \int_V g \eta_j dV. \qquad (8.24)$$

Notice that the process of volume integration enables us to use the orthogonality of the modes to isolate the term containing K (and with it the growth rate). However, we must first tackle the complicated-looking first term. This is accomplished by application of one of the basic forms of Green's integral theorem, which states that for any two scalar functions u and v with continuous second partial derivatives,

$$\int_V \left[u \nabla^2 v - v \nabla^2 u \right] dV = \int_S \mathbf{n} \cdot [u \nabla v - v \nabla u] dS. \qquad (8.25)$$

Thus, using the boundary conditions as expressed in 8.18 and 8.22, we find

$$\left(K^2 - k_j^2 \right) \int_V \eta \eta_j dV = M_b \int_V g \eta_j dV + M_b \int_S h \eta_j dS. \qquad (8.26)$$

Using the square of equation 8.7,

$$K^2 = k_j^2 + 2 k_j M_b \left(\omega_j - i \alpha_j \right) + O(M_b^2), \qquad (8.27)$$

one can solve for the growth rate and the frequency perturbation caused by the interaction of the waves with the mean flow and combustion. Remembering that

$$\int_V \eta_i \eta_j dV = \begin{cases} E_j^2 & i = j \\ 0 & i \neq j, \end{cases} \qquad (8.28)$$

the required stability information can be found from

$$
\left\{
\begin{aligned}
\omega_j &= \frac{1}{2k_j E_j^2} \Re\left[\int_V g\,\eta_j\,dV + \int_S h\,\eta_j\,dS\right] \\
\alpha_j &= -\frac{1}{2k_j E_j^2} \Im\left[\int_V g\,\eta_j\,dV + \int_S h\,\eta_j\,dS\right]
\end{aligned}
\right.
\tag{8.29}
$$

The growth rate and the accompanying frequency correction are found by taking the real and imaginary parts of the two integral terms as indicated. The frequency correction is too small to be of practical consequence. Expanding the expression for the growth rate yields

$$
\alpha = -\frac{1}{2k_j E_j^2} \Im
\begin{bmatrix}
\int_V [iK\,\mathbf{U}\cdot\nabla\eta - \gamma\nabla\cdot\mathbf{C} + \gamma\nabla\cdot\mathbf{f}]\,\eta_j\,dV + \\
+ \int_S [iK\,A\eta + \gamma\mathbf{n}\cdot\mathbf{C}]\,\eta_j\,dS
\end{bmatrix}
\tag{8.30}
$$

where $\mathbf{C}$ represents the convective acceleration terms

$$
\mathbf{C} = \mathbf{q}\cdot\nabla\mathbf{U} + \mathbf{U}\cdot\nabla\mathbf{q}
\tag{8.31}
$$

As we have noted before, this is an important part of the interaction between the waves and the mean gas flow. It must be handled with care. First, let us write it in a form that emphasizes that the mean flow is rotational as we discovered in Chapter 6 for a tubular propellant configuration. Thus, using equation 6.72,

$$
\mathbf{C} = \nabla(\mathbf{U}\cdot\mathbf{q}) - \mathbf{q}\times\nabla\times\mathbf{U} - \mathbf{U}\times\nabla\times\mathbf{q} = \nabla(\mathbf{U}\cdot\mathbf{q}) - \mathbf{q}\times\boldsymbol{\Omega}
\tag{8.32}
$$

where $\boldsymbol{\Omega}$ is the mean flow vorticity vector. Please note that the acoustic flow we are using to represent the oscillations is irrotational; no analogous unsteady vorticity term is carried. This is an important point we will return to shortly. Notice that the body force term appears only in the volume integral since it vanishes on all chamber surfaces by definition.

Equation 8.30 is the central result of all of combustion instability theory. There is little disagreement with the general result, but its interpretation and subsequent evaluation has been the subject of considerable controversy. To forge it into a useful tool, we must work algebraically with the integral terms. Equation 8.30 in its present form tells us only that growth depends on surface and volume effects yet to be evaluated. We must also attempt to uncover all of the physical content in order that we are guided to correct application of the results in assessment of system stability.

The most important feature of the result can be seen without any further algebra. Note that if there is no gas flow through the system ($M_b = 0$) then the

growth rate is zero. This emphasizes the central role played by the gas flow. It is obviously dangerous to neglect any feature of the chamber flow field in assessing the growth rate. Ironically, it is just such neglect, resulting from oversimplification of the fluid dynamics of the problem, that has led to much of controversy just mentioned.

It is now necessary to examine equation 8.30 more closely in order to both simplify it algebraically and to extract its physical essence. Let's tackle the most difficult part first. This is the volume integral containing the convective acceleration,

$$\int_V \eta_j \nabla \cdot \mathbf{C} dV = \int_V \eta_j \nabla \cdot (\nabla(\mathbf{U} \cdot \mathbf{q}) - \mathbf{q} \times \Omega) \, dV \qquad (8.33)$$

Using the vector identity

$$\nabla \cdot (u\mathbf{V}) = u\nabla \cdot \mathbf{V} + \mathbf{V} \cdot \nabla u \qquad (8.34)$$

and Gauss' theorem

$$\int_V \nabla \cdot \mathbf{V} dV = \int_S \mathbf{n} \cdot \mathbf{V} dS \qquad (8.35)$$

we can write

$$\int_V \eta_j \nabla \cdot \mathbf{C} dV = \int_V [\nabla \cdot (\mathbf{C}\eta_j) - \mathbf{C} \cdot \nabla \eta_j] dV$$

$$= \int_S \mathbf{n} \cdot (\mathbf{C}\eta_j) dS - \int_V \mathbf{C} \cdot \nabla \eta_j dV \qquad (8.36)$$

Notice that the surface integral produced in this transformation exactly cancels the one already appearing in equation 8.30. Thus,

$$\alpha = -\frac{1}{2k_j E_j^2} \Im \left[\begin{array}{l} \int_V [iK \mathbf{U} \cdot \nabla \eta + \gamma \mathbf{C} \cdot \nabla \eta_j + \gamma \nabla \cdot \mathbf{f}] \eta_j dV + \\ + \int_S iK \, A \, \eta \, \eta_j \, dS \end{array} \right] \qquad (8.37)$$

Now concentrate on the remaining part of the convective term. It is useful to note that in evaluating **C**, we can replace terms with η and **q** with the unperturbed acoustic wave (mode j) results, since to do otherwise would violate our original assumption that only terms to first order in M_b will be retained. Thus, using the unperturbed form of the momentum equation (6.105),

$$\mathbf{q} = -\frac{i}{\gamma k_j} \nabla \eta \qquad (8.38)$$

and the convective volume integral becomes

$$\int_V C \cdot \nabla \eta_j dV = -\frac{i}{\gamma k_j}\int_V [\nabla(U \cdot \nabla \eta_j) - \nabla \eta_j \times \Omega] \cdot \nabla \eta_j dV \quad (8.39)$$

Now, the second term is zero, since the cross product of U with $\nabla \eta_j$ is perpendicular to $\nabla \eta_j$; the dot product is zero. That is

$$(\nabla \eta_j \times \Omega) \cdot \nabla \eta_j \equiv 0$$

Therefore, the growth rate expression becomes

$$\alpha = -\frac{1}{2E_j^2}\left[\begin{array}{c} \int_V \left[\eta_j U \cdot \nabla \eta - \frac{1}{k_j^2}\nabla(U \cdot \nabla \eta_j) \cdot \nabla \eta_j \right] dV \\ + \int_V \frac{\gamma}{k_j}\eta_j \nabla \cdot f^{(i)} dV + \int_S A^{(r)}\eta_j^2 dS \end{array} \right] \quad (8.40)$$

where the supersripts (r) and (i) refers to the real and imaginary parts respectively.

This can be further simplified by dint of several lines of vector algebra. First recall Green's theorem in the form

$$\int_V (\nabla v \cdot \nabla u + v\nabla^2 u)dV = \int_S n \cdot (v\nabla u)dS \quad (8.41)$$

This is actually an intermediate form used in the derivation of the more general result described in equation 8.25. Applying this to the second volume integral term (what remains of the convective acceleration), we find

$$\frac{1}{k_j^2}\int_V \nabla(U \cdot \nabla \eta_j) \cdot \nabla \eta_j dV = \frac{1}{k_j^2}\int_S (U \cdot \nabla \eta_j)n \cdot \nabla \eta_j dS$$
$$- \frac{1}{k_j^2}\int_V [U \cdot \nabla \eta_j]\nabla^2 \eta_j dV \quad (8.42)$$

where ($U \cdot \nabla \eta_j$) represents the scalar (v) and η_j is the scalar (u) in Green's function as expressed in 8.41. The surface integral vanishes because

$$n \cdot \nabla \eta_j = 0 \quad (8.43)$$

on all the surfaces. This is a statement that the normal part of the fluctuating velocity vector is zero at the bounding surfaces to within the order of the mean flow Mach number. Remembering the unperturbed wave equation (8.21), it is

useful to replace the term involving the Laplacian with

$$\nabla^2 \eta_j = -k_j^2 \eta_j \tag{8.44}$$

Therefore

$$\frac{1}{k_j^2} \int_V \nabla(U \cdot \nabla \eta_j) \cdot \nabla \eta_j \, dV = \int_V [U \cdot \nabla \, \eta_j] \eta_j \, dV \tag{8.45}$$

which is identical to the first volume integral term in 8.40. Each of the terms can be converted into surface integrals by again using the vector identity from 8.34. We find

$$\int_V [U \cdot \nabla \, \eta_j] \eta_j \, dV = \int_V \left[U \cdot \nabla \, \frac{\eta_j^2}{2} \right] dV = \int_V \left[\nabla \cdot \left(U \frac{\eta_j^2}{2} \right) - \frac{\eta_j^2}{2} \nabla \cdot U \right] dV \tag{8.46}$$

The last term is zero because the mean flow is divergence-free (incompressible). The remaining volume integral can be converted to a surface integral by means of Gauss' theorem. Finally, the growth rate expression reduces to its classical form

$$\alpha = -\frac{1}{2E_j^2} \left[\int_S n \cdot U \eta_j^2 \, dS + \int_S A^{(r)} \eta_j^2 \, dS + \int_V \frac{\gamma}{k_j} \eta_j \nabla \cdot f^{(i)} dV \right] \tag{8.47}$$

The same result will be found in a much simpler way by using energy methods in the next section. The reason for tackling the wave equation directly as we have just done is that it highlights all of the approximations being made. This is not as clear-cut in the energy approach. We gain this advantage at the expense of some fairly difficult vector calculus.

Let us review the features of the growth rate formula that we have constructed. The second term is the well-known pressure-coupled driving contribution. The surface integral has been broken into two parts; one over the burning surface showing the effect of combustion on the growth, and one over the nozzle entrance representing the damping due to convection of wave energy out of the system through the nozzle. The remaining surface integral shows that the mean flow interacts with the pressure fluctuations at the surfaces in such a way that work is done on the system. This is a positive contribution to growth at the burning surfaces, since n · U is negative at that point; it represents a net loss of energy at the nozzle entrance. The remaining term will be used to represent damping due to forces produced by interaction of the waves with particulates suspended in the gas flow. All of the physical interpretations are easier to deduce in energy form as we will see in the next section.

Notice that the final result does not include a term indicating any influence from the rotational mean flow although we went to great lengths to retain a realistic mean flow model. This was first discovered by Culick [1966]. It seems to indicate that rotational flow effects are of little importance in combustion instability since the effects of mean flow vorticity do not show up in the growth rate formula. This has led to the widely held conclusion that rotational effects in the fluctuating part of the flow are also of no importance. We have already seen in Chapter 5 that this is a dangerous point of view. It has led to much confusion and to many incorrect stability assessments. This and other corrections to the simple formula must be deduced. Also, additional mechanisms affecting the system stability must be described mathematically in a form compatible with 8.30. Much of the remainder of this chapter will be devoted to this important part of the job. Before starting, it is useful to introduce an alternate point of view that will aid us in our physical interpretation of the growth rate stability computations.

8.4 APPLICATION OF ENERGY BALANCE METHODS

In discussing the coupling of waves to combustion in Chapter 6 it was established that the flow of energy could be interpreted as pdV work done on the the waves in the combustion zone. This suggests that the system consisting of the chamber gases and the reactive boundary zones can be described from the thermodynamic point of view with an energy balance analysis. Although, as we shall see, this leads to the same expression for the growth rate already deduced directly from the vector mechanics of the problem, it also deepens our understanding of the interplay between the driving and damping mechanisms involved. More importantly, it establishes a powerful tool for the investigation of nonlinear aspects of combustion instability. We will need these if we are to understand finite-amplitude behavior and self-limiting as they are observed in actual oscillatory motor operation.

Energy budget analyses have been used in acoustics problems since the time of Kirchhoff [1877] who first derived an energy balance equation analogous to its much used thermodynamic counterpart. The energy method was in fact the basis of much of the early work on combustion instability [McClure, et al, 1960, 1965]. Some of these results were later questioned on the basis of the unjustifiable retention of certain terms in the expansion process [Culick, 1972]. As pointed out throughout our exploitation of the asymptotic expansion method, it is essential that terms be carried or rejected in a given level of analysis in a completely consistent way. To do otherwise is to risk incorrect conclusions as to the relative importance of various physical effects. It renders physical interpretations useless in some instances.

An important advantage of the energy balance method is that it allows us to work with quantities that are scalars rather than vectors as employed in section 8.3. This simplifies the algebra to a great extent. Nevertheless, it should not be thought that this makes it less important to pay close attention to the details.

Careless application of the energy method has led to incorrect results in many past analyses. Thus, as in the last section, we will carefully outline the detailed procedure. This may seem to be a pedantic exercise to some, but there are many examples of incomplete (or incorrect) arguments in the literature. These can lead to important errors especially if they are used as the basis for *extensions* to the theory. An important goal of the energy approach to be presented here is that it lays the foundation for a tool that can be used to extend combustion instability theory. This is especially important in the study of nonlinear effects. In the case of finite-amplitude oscillations, use of the vector methods becomes extremely complicated unless one resorts to purely numerical procedures. The additional difficulties associated with the latter approach have been described in detail earlier. Again, analytical methods are of great importance in setting the stage for the complete CFD solutions of the future. For now, a carefully designed energy balance tool will be of great utility in verifying and interpreting our linear results.

Conversion of the Equations to Mechanical Energy Form

The beginning is the same as that for the perturbed wave equation approach. The continuity and momentum balances as written in equations 8.2 and 8.3 are the starting point. The first step is to change the momentum equation to energy form by multiplying through by the velocity. This is physically based on the idea that the rate of energy change (per unit volume) in the gas is the force times the velocity. Since the momentum equation represents the force balance acting in the volume of gas, then multiplication by the oscillatory velocity yields the rate of change of kinetic energy per unit volume. To this we add terms representing the rate of change of potential energy. These are obviously related to the pressure fluctuations, and are found by multiplying the continuity equation by the pressure (divided by γ^2). Thus, we find

$$\frac{\partial}{\partial t}\left[\frac{p'^2}{2\gamma^2} + \frac{u'\cdot u'}{2}\right] = -\frac{1}{\gamma}\nabla\cdot(p'u') - M_b\left[U\cdot\nabla\left(\frac{p'^2}{2\gamma^2}\right) + u'\cdot C - \frac{u'\cdot F}{M_b}\right] \quad (8.48)$$

The prime notation for the fluctuating quantities emphasizes that the acoustic approximation is to be used. We follow Kirchhoff in identifying the combination of terms on the left as the *acoustic energy density* of the oscillatory field:

$$e' \equiv \frac{p'^2}{2\gamma^2} + \frac{u'\cdot u'}{2} \quad (8.49)$$

Of central concern is the rate at which the total oscillatory energy changes in response to driving by the combustion process and to various loss and gain mechanisms within the chamber volume and at its surfaces. Actually what we are most interested in is the time-averaged rate of change, since this determines whether or not the wave amplitude is growing or decaying at a given time.

Guided by this idea, we integrate the energy density over the volume to compute the total oscillatory energy contained in the chamber and then take the time average. The time-averaged acoustic energy in the system in a particular mode at a given instant is

$$E' = \int_V \langle e' \rangle dV \tag{8.50}$$

Triangular brackets denote the time average defined by

$$\langle f \rangle \equiv \frac{1}{\tau} \int_{t_o}^{t_o + \tau} f \, dt \tag{8.51}$$

where for harmonic oscillations, τ is the period. Thus our analysis is based on the energy balance

$$\frac{\partial E'}{\partial t} = \int_V \left\langle -\frac{1}{\gamma} \nabla \cdot (p' u') - M_b \left[U \cdot \nabla \left(\frac{p'^2}{2\gamma^2} \right) + u' \cdot C - \frac{u' \cdot F}{M_b} \right] \right\rangle dV \tag{8.52}$$

Before attempting to use this result, it is very important to set up the proper protocol for evaluating the various combinations of mean and oscillatory velocity, and oscillatory pressure. This is an important step that is often not explained properly in the literature. Notice that there are several quadratic combinations of fluctuating quantities. If we treat these carelessly we might conclude that their time-averages are zero. For instance, consider the combination p'^2 that appears in the energy density. Assume p' represents a harmonic oscillation of the form

$$p' = \eta e^{iKt}$$

The complex form is used to take advantage of the simplifications in accounting for phase angles and so on. It is necessary to treat the square of p' with care. It is quite easy to make a serious error here, one that has invalidated many analyses in the past. The situation arises whenever products with sinusoidal time dependence appear in the evaluations. This occurs both in the application of energy methods where we are dealing with quadratic combinations of the acoustic variables and in nonlinear problems (see equation sets 5.77-5.80) and (5.81-5.84) developed earlier for use in nonlinear analyses). It is tempting to write

$$p'^2 = \eta^2 e^{i2Kt} = \eta^2[\cos(2Kt) + i\sin(2Kt)] \tag{8.53}$$

which would lead to erroneous results. Notice that the time average is zero. The term in equation 8.49 involving the velocity would behave in a similar way, and we would reach the conclusion that the time-averaged acoustic energy in the waves is zero, clearly an incorrect interpretation. To get the correct result, it is first necessary to express the components in real notation. After the multiplication is done, one may revert to complex form if desired. For compatibility with the vector stability analysis, we assume that the oscillations are harmonic such that the complex wave number is

$$K = k - iM_b \alpha \tag{8.54}$$

where k may contain a frequency correction of the order of the mean Mach number as in equation 8.7. Then, using the same notation as before, the pressure and velocity may be written as

$$p' = \eta e^{iKt} = \eta e^{M_b \alpha t} e^{ikt} \tag{8.55}$$

$$u' = \frac{\nabla \eta}{\gamma k} e^{M_b \alpha t} (- i e^{ikt}) \tag{8.56}$$

Before these can be used in products with other harmonically oscillating quantities, we must convert to real form. this is accomplished by taking the real part. Thus, pressure and velocity are given by

$$p' = \eta e^{M_b \alpha t} \cos kt \tag{8.57}$$

$$u' = \frac{\nabla \eta}{\gamma k} e^{M_b \alpha t} (\sin kt) \tag{8.58}$$

and we can use these forms safely in quadratic combinations. The usual convention is to measure the phase of any quantity with respect to the pressure fluctuations. Thus we see as before that the velocity is out of phase by $\pi/2$ radians with the pressure. For situations in which we don't know the phase relationship of a quantity relative to the pressure, we need a slightly different approach. For example, we are carrying a term F representing an as yet unevaluated force such as that produced in the gas by solid particles. For this we write, as before

$$F = M_b f e^{iKt} = M_b e^{M_b \alpha t} [f^{(r)} + i f^{(i)}] e^{ikt} \tag{8.59}$$

where f is a complex function that will be fleshed out later. The real part is

$$F = e^{M_b \alpha t} [f^{(r)} \cos kt - f^{(i)} \sin kt] \tag{8.60}$$

and both real and imaginary parts of f must be retained to allow the phase angle to be unconstrained.

Notice that we are carefully retaining terms of the order of the mean flow Mach number in the perturbed wave number. This is done for compatibility with the remainder of the equation since we are attempting to deduce the effect of terms of this order on the system energy. All quantities must be carried to this order of accuracy in order that we do not lose important contributions.

One additional idea provides useful guidance. Observe that if we take the time-average too literally, the entire left side of the equation vanishes along with the growth rate a that we wish to estimate. Let us introduce the ideas of the two-variable expansion method, which is closely related to the "method of averaging" familiar to workers in nonlinear mechanics [Kevorkian, 1966; Cole, 1968; Krylov and Bogoliubov, 1947]. It should be clear that we are dealing with more than one time scale in tracking growth and decay of acoustic waves in a rocket chamber. There is a "fast" time variable represented by the rapid oscillations at the acoustic mode frequency; there is also a slow scale representing the slow evolution of the

system energy or slow changes in chamber size and mean properties. The latter are clearly related to the relatively slow motion of the gas in the chamber. Thus, we formally introduce slow and fast variables by defining

$$\begin{cases} \hat{t} = \dfrac{\bar{a}}{L}t^* = t = \text{ Fast Time Variable} & (8.61) \\[2ex] \tilde{t} = M_b t = \dfrac{v_b}{L}t^* = \text{ Slow Time Variable .} & (8.62) \end{cases}$$

We will not need the full machinery accompanying this approach until we tackle some nonlinear problems, but the definitions can be used to advantage even in the simple situation we are now evaluating. When we need to integrate with respect to time we put

$$\frac{d}{dt} = \frac{d\hat{t}}{dt}\frac{\partial}{\partial\hat{t}} + \frac{d\tilde{t}}{dt}\frac{\partial}{\partial\tilde{t}} = \frac{\partial}{\partial t} + M_b\frac{\partial}{\partial\tilde{t}} \ . \tag{8.63}$$

Let us illustrate the technique by carrying out the operations indicated on the left of equation 8.48. Inserting the (real) pressure and velocity expressions as written earlier, we find

$$\left(\frac{\partial}{\partial t} + M_b\frac{\partial}{\partial\tilde{t}}\right)\left\{\frac{e^{2\alpha\tilde{t}}}{2\gamma^2}\int_V \left(\eta^2\cos^2 kt + \nabla\eta \cdot \nabla\eta\sin^2 kt\right)dV\right\} =$$

$$= \left(\frac{\partial}{\partial t} + M_b\frac{\partial}{\partial\tilde{t}}\right)\frac{e^{2\alpha\tilde{t}}}{2\gamma^2}\int_V \eta^2 dV \ . \tag{8.64}$$

Since we are working with the time average, the derivative with respect to the fast time variable is zero. For the left side this is true even without taking the time average, because the two terms combine to give a result independent of the fast variable. However, notice that the exponential term involving the growth rate naturally involves the slow variable. This validates are definition for the slow variable, since α clearly describes the relatively leisurely evolution of the global system amplitude. Thus we find for the left side

$$M_b\frac{E_i^2}{\gamma^2}e^{2\alpha\tilde{t}}\alpha, \tag{8.65}$$

where the mode normalization constant again appears naturally. If we can evaluate the terms remaining on the right of equation 8.52 then we can easily solve for the growth rate. We have now established all of the ideas needed to do this. Unfortunately, although we are working with a scalar equation, it is still necessary to evaluate some vector functions. Notice this was already necessary in simplifying the volume integral of the gradient terms in equation 8.64 by application of Green's Theorem. Thus we will need to use some of the same vector identities required in the previous section.

Determining the System Growth Rate

The energy balance can now be written out as

$$M_b \frac{E_i^2}{\gamma^2} e^{2\alpha \tilde{\tau}} \alpha =$$

$$= \int_V \left\langle -\frac{1}{\gamma} \nabla \cdot (p'u') - M_b \left[U \cdot \nabla \left(\frac{p'^2}{2\gamma^2} \right) + u' \cdot \nabla(U \cdot u') - \frac{u' \cdot F}{M_b} \right] \right\rangle dV \tag{8.66}$$

and we must evaluate the four integrals on the right-hand side. The first integral immediately transforms to a surface integral by means of Gauss' theorem. If we assume that the normal velocity fluctuation is governed by the local pressure as before, then we can write

$$n \cdot u' = M_b \frac{1}{\gamma} A^{(r)} p' \tag{8.67}$$

where A is the general admittance function as defined in equation 8.14. Although we assume A is zero on surfaces other than the burning propellant and nozzle entrance, it may not be. Any real surface is reactive to some extent. This effect is neglected in most rocket analyses. A noteworthy exception is the case of a liquid motor chamber containing a perforated lining installed for the purpose of suppressing acoustic oscillations. Such liners are designed so that the perforations form tiny Helmholtz resonators that absorb acoustic energy. For now, we will retain the interpretations introduced earlier. The second integral is handled much as it was in the last section. Use the vector identity of equation 8.34 to write

$$U \cdot \nabla \left(\frac{p'^2}{2\gamma^2} \right) = \nabla \cdot U \frac{p'^2}{2\gamma^2} - \frac{p'^2}{2\gamma^2} \nabla \cdot U \tag{8.68}$$

and after using the incompressiblity of the mean flow to put the second term to zero, we can convert the first term to a surface integral by use of Gauss' theorem. The result is

$$-M_b \int_S n \cdot U \left\langle \frac{p'^2}{2\gamma^2} \right\rangle dS = -e^{2\alpha \tilde{\tau}} \frac{M_b}{2\gamma^2} \int_S n \cdot U \frac{\eta^2}{2} dS \tag{8.69}$$

The third term requires a little more work. Again use identity 8.34 and notice that retention of the surface term involving the normal velocity fluctuation would introduce an effect of second order in M_b. This is inconsistent with the order of terms retained. Thus

$$-M_b \int_V \langle u' \cdot \nabla(U \cdot u') \rangle dV = M_b \int_V \langle (U \cdot u') \nabla \cdot u' \rangle dV + O\left(M_b^2\right) \tag{8.70}$$

Inserting the approximations for $\mathbf{u}'$,

$$-M_b\int_V \langle \mathbf{u}' \cdot \nabla(\mathbf{U} \cdot \mathbf{u}')\rangle dV = e^{2\alpha\tilde{\tau}}\frac{M_b}{k^2\gamma^2}\int_V \langle ((\mathbf{U} \cdot \nabla\eta)\nabla \cdot \nabla\eta \rangle dV$$

$$= e^{2\alpha\tilde{\tau}}\frac{M_b}{k^2\gamma^2}\int_V \langle (\mathbf{U} \cdot \nabla\eta)\nabla^2\eta \rangle dV \qquad (8.71)$$

The Laplacian term can be removed by use of the Helmholtz equation

$$\nabla^2\eta = -k^2\eta \qquad (8.72)$$

Keep in mind that we are approximating the effects on the right hand side to first order in M_b. Thus, again assuming an incompressible mean flow we find

$$-M_b\int_V \langle \mathbf{u}' \cdot \nabla(\mathbf{U} \cdot \mathbf{u}')\rangle dV = -e^{2\alpha\tilde{\tau}}\frac{M_b}{2\gamma^2}\int_S \mathbf{n} \cdot \mathbf{U}\frac{\eta^2}{2}dS \qquad (8.73)$$

which is identical to the second integral involving the mean flow as given in 8.69.

To evaluate the term involving $\mathbf{F}$ we write

$$M_b\int_V \left\langle \mathbf{u}' \cdot \frac{\mathbf{F}}{M_b}\right\rangle dV = M_b\int_V \langle \mathbf{u}' \cdot \mathbf{f}e^{iKt}\rangle dV, \qquad (8.74)$$

and taking the time average,

$$M_b\int_V \left\langle \mathbf{u}' \cdot \frac{\mathbf{F}}{M_b}\right\rangle dV = -e^{2\alpha\tilde{\tau}}\frac{M_b}{2\gamma k}\int_V \nabla\eta \cdot \mathbf{f}^{(i)}dV. \qquad (8.75)$$

Applying identity 8.34 yet again,

$$M_b\int_V \left\langle \mathbf{u}' \cdot \frac{\mathbf{F}}{M_b}\right\rangle dV = -e^{2\alpha\tilde{\tau}}\frac{M_b}{2\gamma k}\left\{\int_S \mathbf{n} \cdot \mathbf{f}^{(i)}\eta dS - \int_V \eta\nabla \cdot \mathbf{f}^{(i)}dV\right\}, \qquad (8.76)$$

and the surface term vanishes because the normal component of $\mathbf{f}$ is zero at the surface. Remember that by definition, $\mathbf{F}$ arises from volume interactions within the gas flow.

Finally, we can assemble the various pieces, divide through by the common terms, and solve for the growth rate:

$$\alpha = -\frac{1}{2E_j^2}\left[\int_S \mathbf{n} \cdot \mathbf{U}\,\eta_j^2\,dS + \int_S A^{(r)}\eta_j^2\,dS + \int_V \frac{\gamma}{k_j}\eta_j\nabla \cdot \mathbf{f}^{(i)}dV\right], \qquad (8.77)$$

which is identical with the previous analysis as given in equation 8.47.

8.5 INTERPRETATION OF GROWTH RATE FORMULA

Before developing the growth rate equation further, it is necessary to examine the basic result we have derived from the standpoint of its physical content. The validity of the entire analysis depends on correct interpretation and application of growth rate formula. It makes little sense to embellish the analysis with a multitude of additional loss and gain corrections unless the basic result is understood in depth. We will find it necessary to question certain boundary conditions that have not appeared as a result of our use of acoustic waves to represent the oscillatory flow field. This leads to a major modification of the growth rate formula. However, we pause here to assess what we have found to this point. The plateau we have reached corresponds to the classical combustion instability treatment, the one that is used as the basis for all stability prediction methodology employed in the rocket industry.

Physical meaning is readily attached to the three major growth rate contributions identified in equation 8.77 (or 8.47). The earlier discussion in Chapter 6 based on simple thermodynamics is helpful in this regard. The mechanical energy associated with the gas oscillations is modified by work done at the chamber boundaries or within the control volume. This is a simple application of the first law of thermodynamics. The third term represents the work done in moving solid particles (say aluminum oxide smoke) formed in the combustion process. This is mainly a loss effect; we will deal with it computationally in Chapter 9.

The first of the three stability integral terms, the one involving the mean flow of combustion gases from the burning surface, is perhaps the most difficult to understand. In fact, the early investigators did not include this term; many analyses assumed that only energy flux from the oscillatory combustion process (as represented by the second term incorporating the acoustic admittance) affects the wave growth. Careless application of simple analyses such as the one described in section 6.2 has led to considerable confusion. It is not that the simple approach is wrong; in fact, the results are in agreement with the more complete analyses we have just carried out. The intuitively obvious contributions such as driving by the pressure-sensitive propellant burning rate come quite easily. Others, such as the first term in 8.77 do not follow as readily from simple arguments; they can only be found by careful application of a correct (and complete analysis) of the combined mean and oscillatory flow field.

Notice the great similarity between the first and second integral terms. As we have already decided, the second term describes work done by combustion at the boundaries. By analogy, the first term represents the convective transport of wave energy into the chamber by the mean flow. Both terms contribute to the energy balance at the burning surface, and are of comparable magnitude. This is the result of the manner in which the problem as been scaled. For instance, we were led to include the mean flow Mach number as factor in our definition of the response function (see equation 8.14) simply because all of the perturbing effects

on the right side of the wave equation are proportional to M_b. Whether waves grow or decay depends on the sign of the *net* effect. Wave energy changes depend on the relative size of the real part of the admittance and the gas injection velocity. The contribution of the mean flow at the surface is always a gain; the flow is into the chamber, and the magnitude of $-\mathbf{n} \cdot \mathbf{U}$ is positive, thus providing a positive contribution to the growth rate. It is important to understand the signs on various terms. Some investigators have chosen to define the unit normal **n** to be positive in the direction inward into the chamber. This makes the growth rate formula look a little neater, but it has been the experience of the authors that it leads to confusion. The typical user of the results is an engineer trained in the traditional way with a minimum of thermodynamics and fluid mechanics and the associated vector mathematics. The unit normal vector **n** used in standard courses and text books is almost invariably defined to be positive outward from the control volume. We have adhered to this convention so that there can never be ambiguity in signs. Pointing **n** inward is a convenience in the present situation, but there are many others in which the opposite is true. Thus, the best approach is to use a consistent definition throughout. This may seem to be a trivial matter to experienced analysts, but to a newcomer, anything that can be done to ease the burden of special interpretations is worthwhile.

The situation is similar at other boundaries. At the nozzle entrance, the first term always contributes an energy loss because the flow is out of the system ($-\mathbf{n} \cdot \mathbf{U}$ is negative).

Reexamination of the Boundary Conditions at the Burning Surface

Of major importance is a careful assessment of the boundary conditions that were imposed in evaluating the integral expressions in the two growth rate derivations. We closely follow Culick's interpretations in this regard [Culick, 1972; Culick, 1966a; Culick, 1966b]. He found by comparing the standard three-dimensional form (as written in Equation 8.77) to the analogous one-dimensional growth rate formula that there are terms appearing in the final one-dimensional formula (Culick 1973) that do not correspond to any of the terms in the three-dimensional form. His position on this finding is best expressed in his own words (Culick 1972): "The essential point is that the one-dimensional formulation implicitly accounts for viscous processes occurring in the flow adjacent to the lateral boundaries. If those terms correctly representing boundary layer effects can be identified in the one-dimensional analysis, then they may be incorporated in certain results of the three-dimensional analysis." Notice that the problem identified is one in which the wave motions are *parallel* to the chamber boundary (as they must be in the one-dimensional case). Culick indicated that ". . . the classical three-dimensional formulation does not reduce to the one-dimensional results, and. . . it is not possible, within the strict three-dimensional analysis, to handle coupling at the boundary when the main wave motions are parallel to the boundary. Both of these difficulties are removed by patching the three-dimen-

sional analysis." The latter is a statement of the origin of the "flow-turning" correction. What was done in implementing this correction was to simply add terms from the one-dimensional calculations that did not appear in the three-dimensional analysis.

The heart of the matter is that certain important features of real fluid behavior have not been addressed explicitly in the analysis leading to the growth rate. Nothing is wrong if the waves impinge normally on the surface. The difficulty lies in accounting for the behavior of the waves near the burning surface when gas motion is parallel to it. It is quite likely that the one-dimensional model gives useful guidance in this regard. By its very nature, it requires that the momentum changes implied by the geometry are addressed. The waves are obviously parallel to the duct, but in representing the driving effects due to mean flow and combustion, the momentum fluctuations invoked are normal to the axis. So, why aren't similar effects introduced in a natural way into the three-dimensional analysis. The reason is that to do so requires that we solve the analog to the mean flow analysis discussed in Chapter 5. In that analysis, we found that in attempting to satisfy a realistic boundary condition, *we were forced to account for the generation and transport of vorticity at the chamber boundaries*. Clearly, the key to the matter is to incorporate physically realistic boundary conditions into the three-dimensional, time-dependent flow. This requires that we discuss items that have received scant attention in the classical stability literature.

The very essence of the problem is that we must find a way for parallel wave motions to satisfy the no-slip condition at all solid boundaries, especially the one on the burning propellant surface. That is, we must find a way to correct for the fact that the gas oscillations cannot be purely acoustical if they are parallel to the burning surface. We must account for the generation and propagation of *time-dependent vorticity*. We will do this by showing that it is necessary to account for an entirely different type of wave. The acoustic waves are irrotational. We must allow for rotational waves. These are sometimes referred to as *shear waves*. They appear in many guises. One is in the form of vortex shedding formed when there are steep gradients in the mean flow profiles such as in flow over bluff protrusions into the flow channel.

Of more interest in the present situation are shear waves generated at the burning surface itself. Previous investigators have neglected this problem by application of standard acoustic boundary layer results (for instance, see the discussion by Williams [1985]). These are certainly appropriate at inert chamber boundaries. We will find that the presence of the strong blowing at the burning surface renders the boundary layer approach totally inadequate. The convection of vorticity by the mean flow, rather than diffusion as in the boundary layer situation, makes a dramatic difference in the way it affects the oscillating flow field throughout the chamber.

There are many reasons to believe that the use of the one-dimensional analysis to provide these corrections is not likely to lead to reliable results in all cases. Thus we devote the remainder of this chapter to the important question of

satisfying physically realistic boundary conditions. We will review recent experimental data that give considerable guidance. Unfortunately, we will find it necessary to carry out additional computations that are of complexity comparable to those already undertaken. Fortunately, the results are in the form of linear corrections to the stability analysis; they are readily incorporated into the standard results. This process has not yet taken place in the stability assessment tools used by the rocket industry. Hopefully the modifications can be accomplished in the near future. As we will demonstrate, they lead to a major improvement in the agreement of the analysis to experimental reality. They remove the need to use one-dimensional approximations to what are inherently three-dimensional physical effects. They also lead to a rational way to account for velocity coupling. They provide a bridge to the subject of turbulent effects accompanying pressure oscillations. Clearly, an important step in understanding the role of *turbulence* in combustion instability is to gain a thorough understanding of the *laminar* effects the precede the appearance of turbulence.

8.6 ROTATIONAL FLOW EFFECTS : VISCOSITY AND VORTICITY

Let us now carefully construct a realistic model for the interaction of acoustic waves with a burning propellant surface. Emphasis will be on the proper handling of waves with parallel incidence to the burning surface. Although the necessary theory will be developed in a general form that correctly dovetails with all of that presented earlier, we will make detailed evaluations for a simple chamber geometry that we have used consistently to introduce basic ideas. It has frequently been useful to carry out details for the case of a tubular internal burning propellant charge. This closely approximates the motor geometries used in the majority of solid rockets. It allows us to use analytical solutions to the greatest extent possible and provides an improved view of the underlying physics of the problem.

Characteristics of the Mean Flow

A brief review of the mean flow field will lead us in the right direction. As we have seen throughout the analysis, the steady flow plays an important role in the support of the superimposed acoustic oscillations. The gas flow enters the chamber in a direction perpendicular to the burning surface. This implies that the steady part of the flow is rotational; vorticity is introduced at the surface and is carried through the chamber by the mean gas motion. Viscous effects (the no-slip condition) account for the normal influx at the surface, but there is no boundary layer because vorticity is rapidly convected away from the surface. Viscous shear stresses are small and can be neglected in mathematical representations of the flow field. Typical mean flow velocity vectors found by such an inviscid, rotational model are illustrated in Figure 8.2(a). Cold flow studies

Chamber Centerline

*Porous Surface
(or Burning
Propellant)*

(a) Steady Flow Velocity Vectors at Three Stations in Laminar Zone

Chamber Centerline

*Acoustic
Boundary Layer*

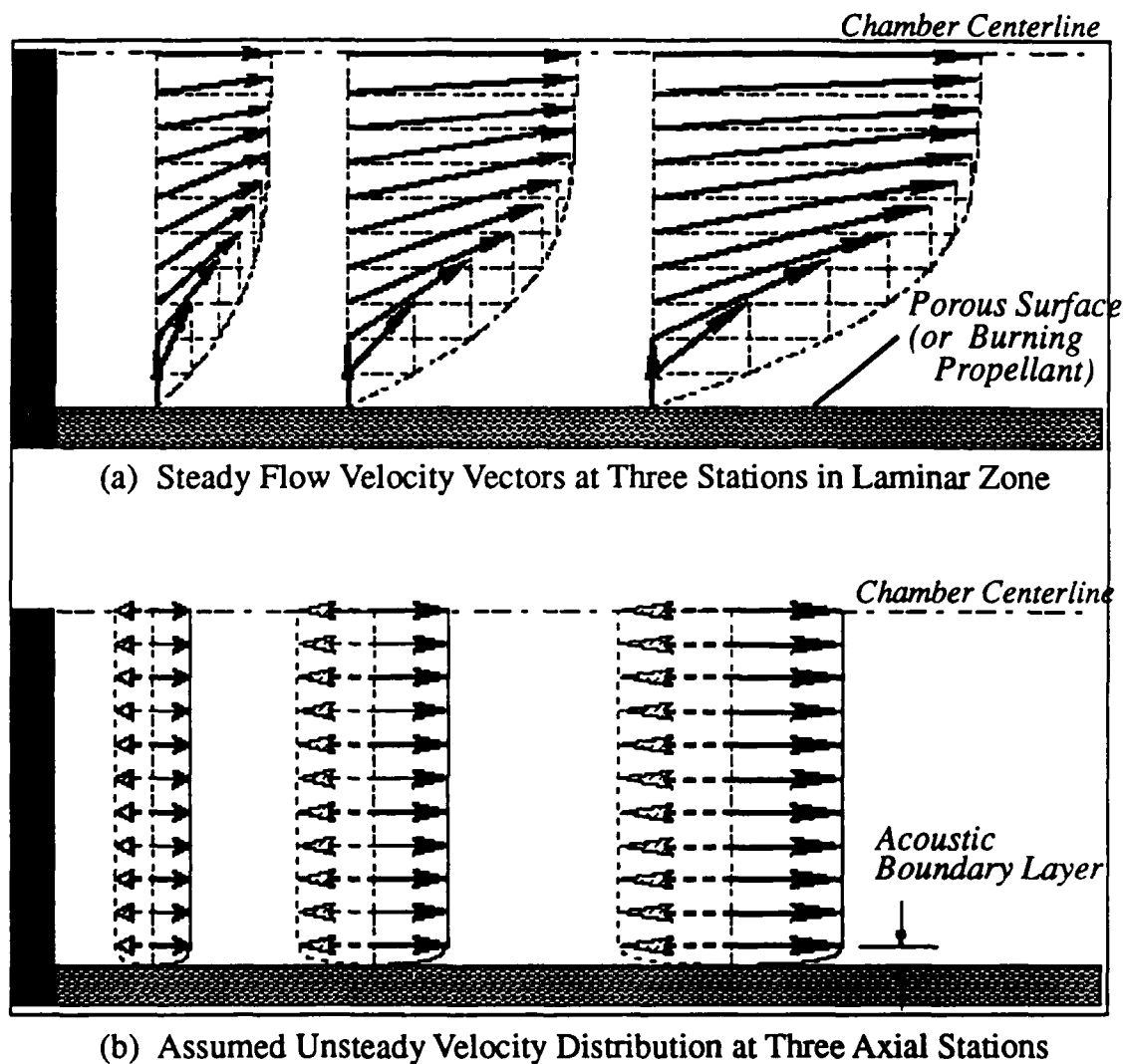(b) Assumed Unsteady Velocity Distribution at Three Axial Stations

Fig. 8.2 Mean Flow (a) and Assumed Unsteady Velocity Profiles (b)

[Dunlap, 1974] have verified this picture in detail and closely agree with analytical models for the mean flow in a tubular motor [Culick, 1962]. An important finding is that the nature of the velocity distribution changes dramatically as the axial distance from the head-end approaches a critical value in long chambers. The presence of turbulent gas motions is clearly indicated. The laminar flow region in the forward end of the chamber will be the focus of attention here. Clearly, a thorough understanding of the laminar behavior must preface serious consideration of turbulent interactions.

The classical model for pressure oscillations superimposed on this mean flow does not take account of several potentially important factors. Most analyses utilize standard acoustic assumptions; an important one is that the fluctuations represent an inviscid process and that the oscillating field is irrotational. If time-dependent rotational flow is addressed, it is most often assumed to exist only in "thin acoustic boundary layers" near the surfaces. Figure 8.2(b) shows the type

of motion usually envisioned; the velocity phase angle relative to pressure is assumed constant across the radius. The boundary effects are often neglected entirely, and one finds many references in combustion instability literature to the "cross-flow" velocity near the surface implying that it can be determined from the simple one-dimensional irrotational acoustic picture of the flow as illustrated. This does not take account of either the actual velocity distribution near the surface or the phase of the velocity fluctuations relative to the pressure wave system. More importantly, from the combustion stability viewpoint, it does not account for modification by boundary effects of the radial time-dependent gas velocity at the burning surface; detailed knowledge of the radial velocity component and its dependence on geometrical and physical parameters is required in stability assessments.

Pressure fluctuations affect the local burning rate with the result that there is a fluctuating flow velocity normal to the surface. This is the pressure coupling theappeared as the principal source of acoustic energy in our stability equation (8.47). The processes by which the normal fluctuations transfer energy into the assumed *parallel* acoustic field are not clearly portrayed in the linearized acoustic instability theory. The flow turning idea introduced earlier is intended to accouunt for this, but it is based on an extension of the one-dimensional analysis. The accompanying physical descriptions of such processes invariably suggest the presence of vorticity transport and viscous forces, but details do not appear in the analyses. In fact, they cannot appear because it is necessary to have a two-dimensional flow in order to invoke even the simplest viscous process. Shear flows are two-dimensional. Accepted models cannot directly incorporate viscous effects, since the flow-turning models consist of an *ad hoc* extension of one-dimensional analyses into multidimensional form. Again, this is a signal that more information concerning the gas motion near the burning surface is needed.

Other interactions with the burning surface include the controversial notion of velocity coupling. This form of coupling cannot be correctly modeled without taking into account the velocity amplitude and phase distributions in the vicinity of the burning zone. Nevertheless, existing velocity coupling models ignore such effects. The simple acoustic model (Figure 1) is usually assumed, with the "cross-flow" affecting the time-dependent combustion taken to be the one-dimensional acoustic velocity far from the surface.

Furthermore, effects of particle damping depend crucially on a correct model of the momentum transfer between the particle and gas phase velocities. It is obvious that accurate knowledge of the time-dependent flow field dynamics is essential in a correct estimation of the damping. It would have been premature to evaluate the particle interaction force F that appeared in our earlier growth rate calculation on the basis of simple acoustic velocity fields. More information on the actual gas motions is needed. This is one of several elements in the standard stability evaluation method that is in great need of revamping.

Information from Cold Flow Experiments and CFD Simulations

Recent cold-flow experiments [Brown, *et al*, 1986] have dramatically demonstrated that the simplified thinking described in the introductory material cannot represent a correct portrayal of the flow field under the conditions described. The experiments were executed as part of a study of velocity coupling. The apparatus consists of a porous tube with mean gas flow (nitrogen) entering normally through the surface and exiting through a choked nozzle; axial acoustic waves are excited by a rotating valve at the nozzle end. Of central interest here are the hot wire measurements of axial acoustic velocity distributions. Figures 8.3 and 8.4 show data points from six separate tests carried out under identical thermodynamic and geometrical conditions. The data in figure 8.3 were taken at the first axial mode resonance (84 Hz). Data are normalized to the center-line reference velocity. The heavy dashed line superimposed on the plots show the expected (acoustic) velocity distribution. Figure 8.4 is the corresponding phase angle distribution relative to the pressure fluctuations. Measurements were taken by traversing a two-axis hot-wire probe radially at a location several inches from the closed end of the chamber.
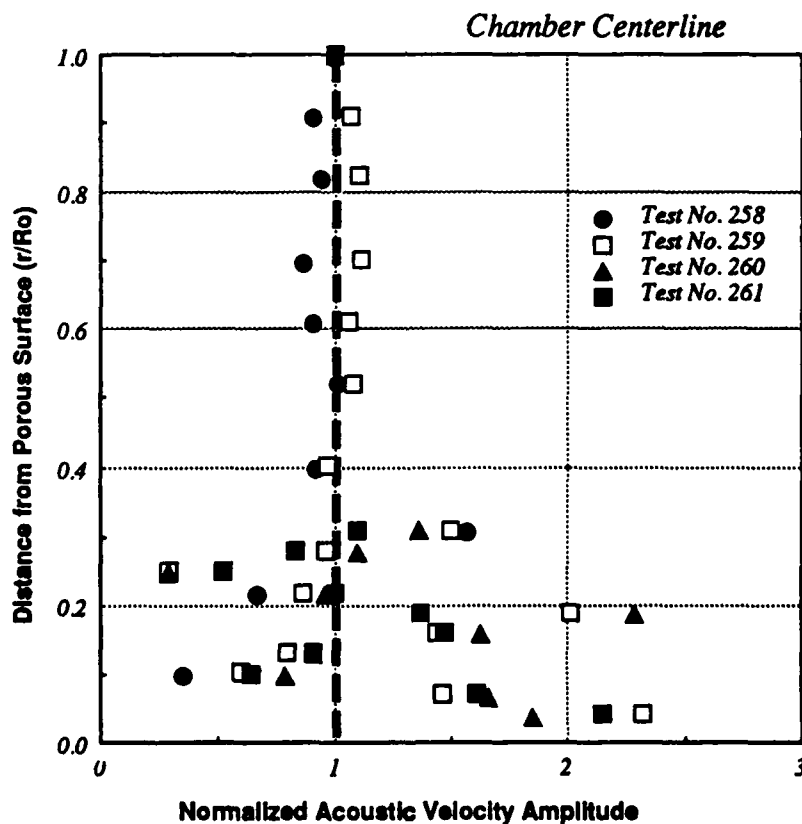

Fig. 8.3 Measured Fluctuating Velocity Distribution at 84 Hz [Brown, 1986]
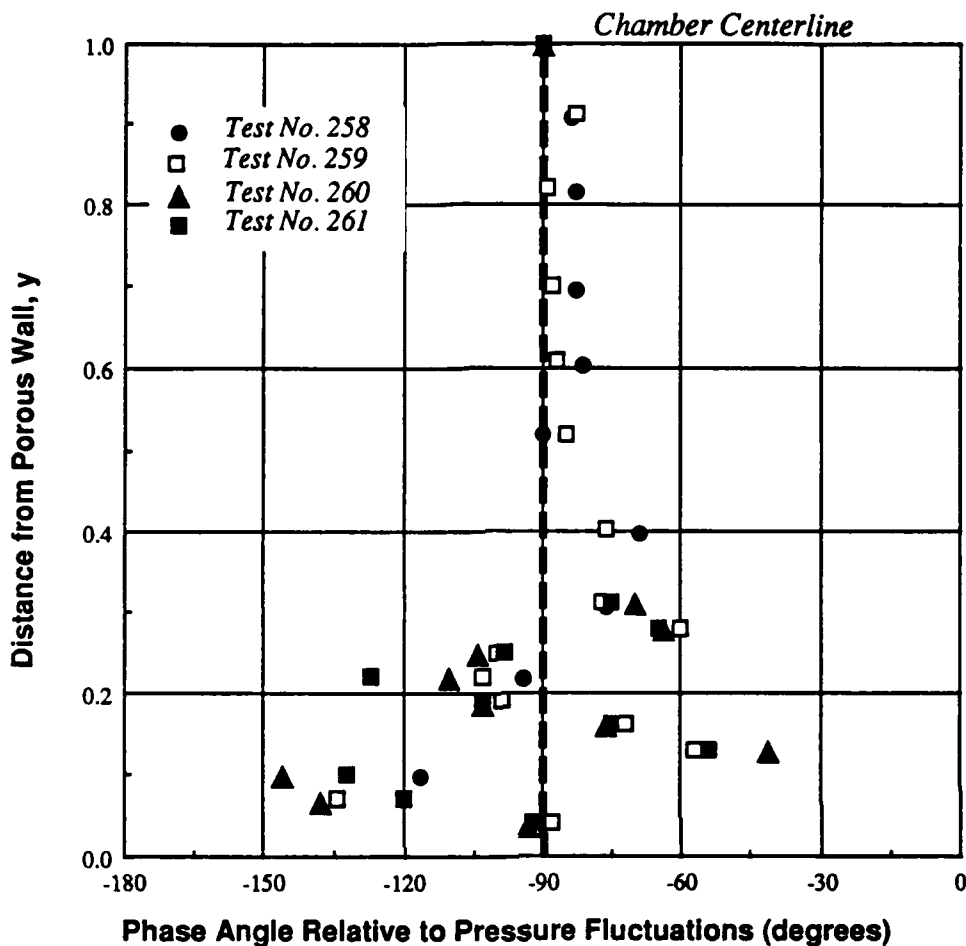
Chamber Centerline

Fig. 8.4 Measured Fluctuating Velocity Phase Angle at 84 Hz [Brown, 1986]

The time-dependent velocity and phase distributions are completely different than those expected on the basis of linearized acoustic theory. There appears to be *strong radial dependence* of both the wave amplitude and phase with largest deviations from the acoustic plane wave near the porous wall. Deviations apparently decrease as the chamber axis is approached. The expected plane wave behavior is limited (for the conditions of the test) to a small volume near the axis of the chamber. In the absence of a correlating theory, the plots suggest that there are large random errors in the measurements. However, at any given radial position there seems to be reasonably good reproducibility suggesting that an organized behavior is responsible for the deviations.

Brown [1986] has suggested that these dramatic departures from classical ideas are the result of time-dependent rotational flow effects. His interpretation of the data is based on an analogy with the mean flow. Since there is strong blowing, it is plausible that oscillatory viscous stresses are negligible and that time-dependent vorticity is generated at the boundaries and is transported by

mean flow convection. The normal mean influx boundary condition, which applies to both the steady and unsteady gas motions, leads to the generation of vorticity that affects the entire field since it is generated at the surface and is convected with the mean flow. The fluctuating velocity normal to the surface must "turn" so that it merges smoothly with the axial acoustic motions in the volume of the chamber. Since the fluctuating component must satisfy a no-slip boundary condition (the oscillating mass flux must enter the chamber at 90° to the surface), then an oscillatory component of vorticity must also be generated.

Brown's hypothesis is that the surface-generated vorticity accounts for the marked influence on the wave structure observed experimentally. An important question to be resolved is the role played by shearing stresses generated within the chamber volume by viscous effects in the propagation of the rotational flow oscillations. Since the mean flow field solution does not exhibit a direct dependence on viscosity, it is plausible that viscous forces do not, as Brown suggests, affect the fluctuating flow field directly. However, the observed gas motions are reminiscent of the vorticity wave effects predicted in analyses by Flandro [1974a, 1974b]in which an axial velocity overshoot is generated near the burning surface and decays radially due directly to viscous drag. Applicability of these earlier theories is one of the questions to be investigated in what follows.

Two groups have recently used computationl fluid dynamics (CFD) simulations of a rocket chamber to investigate effects of realistic fluid mechanics on the interactions between the mean flow and the fluctuating field. The paper by Vuillot and Avalon of ONERA [1988] shows computed time-dependent velocity profiles quite reminiscent of that shown in figure 8.4. As they point out, the results agree with Flandro's approximate solution, but exhibit an axial dependence that does not show up in the simplified analysis. Axial dependence is an important feature that ties in closely with the ideas of velocity coupling as we will see in the following analysis. The CFD work by Baum and Levine [86, 87, 88, 89] indicate similar effects and emphasize the importance of viscous stresses and vorticity transport on the development of acoustic waves near a propellant surface.

Incorporation of Effects of Viscosity and Vorticity Transport

The analysis has three main goals: (1) to determine the role (if any) played viscosity in determining the time-dependent flow field in the vicinity of a burning propellant surface and throughout the chamber, (2) to ascertain the basic dependence of rotational flow effects on chamber geometry and the physical characteristics of the gas flow, and (3) to establish the proper direction for further evaluation of the effects of the time-dependent shear effects on motor stability assessment procedures. The cold flow data offer a unique opportunity to validate the theoretical results directly and to expose any weaknesses therein. Two analytical approaches are described. In the first, and simplest one, viscous forces are ignored completely. In the second, viscous forces are retained along

with the associated mathematical complications. A numerical approach is required in evaluating the results. However, a full computational (CFD) attack is not used in order that emphasis can be focused on physical interpretation of the results. The finite-difference, Navier-Stokes solver approach has been used recently in work by Vuillot and Avalon [1988] and by Baum and Levine [1988, 1989]. However, a simpler model, more easily incorporated into existing combustion stability assessment tools, is badly needed now; this need strongly motivates the approach described.

The notation and normalization conventions follow those introduced in Chapter 5. It will now be necessary to retain terms that were neglected in the developments of the first part of this chapter. We must now find a way to accout for the rotational effects that are thrown out when the acoustic wave assumption is used. Assuming a compressible, Newtonian, ideal gas, the system is governed by the continuity, momentum, energy and state equations (see discussions in Chapter 5 leading to equation 5.73-5.76)

$$\frac{\partial \rho}{\partial t} + \nabla \cdot \rho u = 0 \tag{8.78}$$

$$\rho \left[\frac{\partial u}{\partial t} + \nabla \frac{u \cdot u}{2} - u \times \nabla \times u \right] = -\nabla P + \delta^2 \left[\frac{4}{3} \nabla (\nabla \cdot u) - \nabla \times \nabla \times u \right] \tag{8.79}$$

$$\rho \left[\frac{\partial T}{\partial t} + u \cdot \nabla T \right] = (\gamma - 1) \left[\frac{\partial P}{\partial t} + u \cdot \nabla P \right] + F \cdot u + \frac{\delta^2}{P_r} \nabla^2 T \tag{8.80}$$

$$P = \rho T , \tag{8.81}$$

where $\delta^2 = v_0 / a_0 R_0$ is the inverse of the reference Reynolds number based on the cylinder radius and speed of sound. P_r is the Prandtl number. Other assumptions that have been made in writing the energy equation are: 1) no radiative heat transfer, 2) no internal heat generation, 3) constant specific heats, thermal conductivity, and viscosity, and 4) no mechanical dissipation within the fluid. The latter assumption implies that terms of order of the square of the wave amplitude and smaller are to be neglected.

Since oscillations of small amplitude about the mean gas flow are to be considered, it is appropriate to employ perturbation expansions of the form

$$\begin{cases} P = 1 + p^{(1)} + \cdots \\ \rho = 1 + \rho^{(1)} + \cdots \\ T = 1 + T^{(1)} + \cdots \\ u = M_b U + u^{(1)} + \cdots , \end{cases} \tag{8.82}$$

where superscript (1) is used to identify time-dependent fluctuating quantities of first-order based on the amplitude of the acoustic pressure field,

$$\varepsilon \equiv \left| p^{(1)} \right| . \tag{8.83}$$

These expansions are inserted into 8.78-8.81 and terms are collected according to the ordering implied by the limiting process

$$\underset{\varepsilon,\, M_b \to 0}{\text{Lim}} \left(\frac{\varepsilon}{M_b}\right) \to 0 \tag{8.84}$$

The behavior of the resulting zeroth-order terms governs the mean flow and the terms of first-order in the wave amplitude ε represent the superimposed gas oscillations.

Steady Flow

Several features of the assumed mean flow require review. If axial variations in propellant burning rate (or gas injection speed through analogous porous walls) are ignored, the solution for the steady velocity field is found to be (see analyses in section 5.3)

$$U = U_r e_r + U_z e_z = - \frac{\sin\left(\frac{\pi r^2}{2}\right)}{r} e_r + \pi z \cos\left(\frac{\pi r^2}{2}\right) e_z. \tag{8.85}$$

Figure 8.2(a) shows this solution at several axial stations. The flow is rotational because the no-slip boundary condition has been accommodated. The solution was based on the inviscid form of the equations ($\delta = 0$) but retaining rotational flow effects [Culick, 1966]. Although the results exhibit good agreement with experiments, it is useful to analytically validate the approach by demonstrating that the mean viscous shear stresses have negligible effect. The axial shear force (per unit volume) is given by

$$F_z = M_b \delta^2 \left[\frac{1}{r}\frac{\partial}{\partial r}\left(r\frac{\partial}{\partial r}U_z\right) + \frac{\partial^2 U_z}{\partial z^2}\right] = \tag{8.86}$$

$$= - M_b \delta^2 \pi^2 z \left[\pi r^2 \cos\left(\frac{\pi r^2}{2}\right) + 2\sin\left(\frac{\pi r^2}{2}\right)\right].$$

Figure 8.5 is a plot of the distribution of this force showing that maximum axial shear is applied at a point about 20% of the radius from the boundary; as one might expect, it is zero at the centerline ($y = (1 - r) = 1$). The magnitude is very small, since it is proportional to the product of the injection Mach number and the acoustic Reynolds number. These are both very small quantities. Typical values are in the ranges

$$\begin{cases} 1 \cdot 10^{-4} < M_b < 1 \cdot 10^{-3} \\ 1 \cdot 10^{-7} < \delta^2 < 1 \cdot 10^{-6} \end{cases} \tag{8.87}$$

and it is seen that this yields forces in the axial momentum balance that are very much smaller than those corresponding to pressure and inertial terms. In the case of the mean flow, the vorticity produced because of normal injection is rapidly convected to fill the entire chamber; the shearing stresses and associated viscous forces are everywhere negligible compared to inertial and pressure forces.
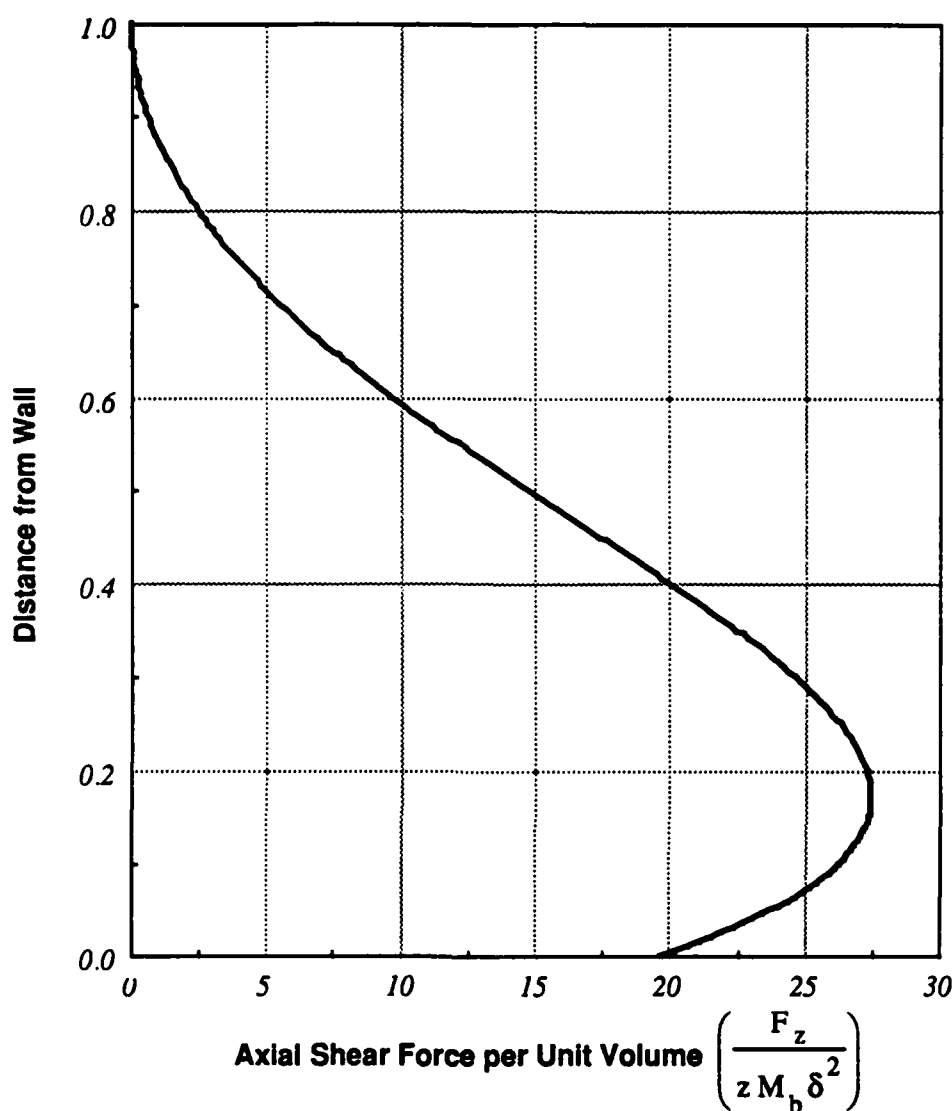
Fig. 8.5 Mean Axial Shear Force Distribution (evaluated at z = 1, distance of one chamber radius downstream from chamber head-end)

To summarize, a simple, inviscid, rotational mean flow model accurately represents the steady gas motion in a tubular rocket grain or porous tube. As Brown suggests, it is therefore plausible that the time-dependent flow could behave in analogous fashion. That is, it appears that viscous effects might also be negligible in the unsteady flow. Classical acoustic boundary layers are then only generated at inert surfaces. The strong blowing spreads the vorticity generated at active surfaces into the chamber volume by a convective rather than a diffusive transport mechanism. The peculiar behavior exhibited in the experimental data could then be the result of time-dependent vorticity transport. These possibilities must be carefully assessed along with their implications in terms of combustion instability modeling.

Time-Dependent Calculations

The unsteady motion is governed, to first-order in wave amplitude, by the set

$$\frac{\partial \rho^{(1)}}{\partial t} + \nabla \cdot \mathbf{u}^{(1)} = - M_b \nabla \cdot \rho^{(1)} \mathbf{U} \tag{8.88}$$

$$\frac{\partial \mathbf{u}^{(1)}}{\partial t} = - M_b \left(\nabla \mathbf{u}^{(1)} \cdot \mathbf{U} - \mathbf{u}^{(1)} \times \nabla \times \mathbf{U} - \mathbf{U} \times \nabla \times \mathbf{u}^{(1)} \right) - \frac{\nabla p^{(1)}}{\gamma} +$$

$$+ \delta^2 \left[\tfrac{4}{3} \nabla (\nabla \cdot \mathbf{u}^{(1)}) - \nabla \times \nabla \times \mathbf{u}^{(1)} \right] \tag{8.89}$$

$$\frac{\partial T^{(1)}}{\partial t} + M_b \mathbf{U} \cdot \nabla T^{(1)} = \frac{(\gamma - 1)}{\gamma} \left[\frac{\partial p^{(1)}}{\partial t} + M_b \mathbf{U} \cdot \nabla p^{(1)} \right] + \frac{\delta^2}{P_r} \nabla^2 T^{(1)} \tag{8.90}$$

$$p^{(1)} = \rho^{(1)} + T^{(1)} \tag{8.91}$$

In most combustion stability calculations, the viscous terms are dropped on the basis of analogies with the mean flow behavior as described in the last subsection. This leads to a perturbed acoustic wave equation (equation 8.5). Solution of this equation (retaining of terms of the order of the steady flow Mach number, M_b) leads to the standard model for combustion stability assessment (equation 8.47). Boundary conditions are written in the form of an admittance (or response function) at the burning surface that relates the oscillatory burning rate to local pressure fluctuations. The assumption of acoustic motion implies that the gas motion is irrotational or *lamellar*. The energy equation collapses to a statement that the flow is isentropic.

These assumptions eliminate two additional wave-like components that will be shown to have significant impact on the representation of the composite unsteady flow. These are: 1) vorticity or shear waves due to the rotationality of the unsteady flow and 2) thermal wave effects resulting from effects of viscous diffusion on the unsteady temperature distribution. The latter are partially addressed in the usual modeling of the admittance boundary condition; the thermal wave in the solid propellant is matched to an approximation of the temperature fluctuations accompanying the acoustic waves in the burning zone. The temperature is the main variable determining the instantaneous burning rate. One usually neglects the gas phase effects (the "quasi-steady" assumption) related to thermal wave propagation in the boundary zone. In order to understand the unexpected features discovered in the cold flow simulation, it is necessary to reexamine such assumptions. To emphasize that there are three distinct types of wave behavior, it is useful to break the equations into three sets, each describing one of the components. This is done by *splitting* the velocity, pressure, and temperature such that

$$\mathbf{u}^{(1)} = \mathbf{u}' + \tilde{\mathbf{u}}$$

$$p^{(1)} = p' + \tilde{p} \tag{8.92}$$

$$T^{(1)} = T' + \tilde{T}$$

where primes refer to the lamellar (acoustic, irrotational) part and tilde indicates the solenoidal (incompressible, rotational) part. Thus, the unsteady gas motion is governed by the two independent sets:

Acoustic

$$\begin{cases} \dfrac{\partial p'}{\partial t} + \gamma \nabla \cdot u' = -M_b \nabla \cdot p'U & (8.93) \\[2mm] \dfrac{\partial u'}{\partial t} + \dfrac{\nabla p'}{\gamma} = -M_b(\nabla u' \cdot U - u' \times \nabla \times U) + \delta^2 \dfrac{4}{3}\nabla(\nabla \cdot u^{(1)}) & (8.94) \end{cases}$$

Vortical

$$\begin{cases} \nabla \cdot \tilde{u} = 0 & (8.95) \\[2mm] \dfrac{\partial \tilde{u}}{\partial t} + \dfrac{\nabla \tilde{p}}{\gamma} = -M_b(\nabla \tilde{u} \cdot U - \tilde{u} \times \nabla \times U - U \times \nabla \times \tilde{u}) - & \\[2mm] \qquad\qquad - \delta^2 [\nabla \times \nabla \times \tilde{u}] & (8.96) \\[2mm] \dfrac{\partial \tilde{T}}{\partial t} + M_b U \cdot \nabla \tilde{T} = \dfrac{(\gamma - 1)}{\gamma}\left[\dfrac{\partial \tilde{p}}{\partial t} + M_b U \cdot \nabla \tilde{p}\right]\dfrac{\delta^2}{P_r}\nabla^2 \tilde{T} & (8.97) \end{cases}$$

The irrotational viscous term on the right of the acoustic momentum equation represents the effects of normal strains that are negligible for small-amplitude oscillations; the shearing strains of most potential importance appear in the solenoidal equations emphazing the effects of vorticity generation and transport. Note that the part of the energy equation corresponding to the acoustic field collapses to the isentropic relationship and has already been used to eliminate the density in equations 8.93 and 8.94 as we did earlier. Thus, the acoustical formulation is based on the assumption that the pressure fluctuations behave isentropically.

Departures from isentropicity are to be represented by the vortical equations. Note that a vortical pressure, sometimes called the "pseudosound" is included in the vortical set. This is often assumed to be zero; in fact it is negligible in the present situation as verified by CFD solutions of the problem. The pressure field is very nearly acoustic. If this is so, then the energy equation 8.97 is independent of 8.95 and 8.96 and it governs what is often called entropy waves. We will refer to these simply as thermal waves.

Boundary conditions are the usual ones including a symmetry condition at the chamber axis and the no-slip condition at all bounding surfaces including transpiring walls such as a burning propellant or porous sidewall. After solutions for all three parts of the unsteady problem have been found, they must be super-imposed in such a way that the boundary conditions are correctly satisfied. For example, it is necessary that $u^{(1)}$ go to zero at the wall. The acoustic and vortical components must either each be zero or be equal in magnitude and opposite in sign at solid surfaces. Since, in the case of parallel acoustic waves, u' is not zero at the boundary, then it must be balanced by a nonzero value of $\tilde{u}$.

Acoustic Solutions

This part of the problem was thoroughly discussed in Chapter 5. The focus of attention for the moment will be the unperturbed solution of the wave equation that results from combination of equations 8.93 and 8.94. The perturbations of the order of the mean Mach number play a central role in the combustion instability problem since growth of wave amplitude is controlled by terms of this and higher orders, and their effects in the composite problem will be discussed in detail later.

For the moment, let us assume that the irrotational part of the flow is represented by the axial plane standing wave system

$$p' = \Re\left[e^{i\omega t}\cos kz \right] = \cos \omega t \cos kz \tag{8.98}$$

$$u'_z = - \Re\left[i e^{i\omega t}\sin kz \right] = \sin \omega t \sin kz \tag{8.99}$$

in which the acoustic velocity lags the pressure by a 90° phase angle.
ω is the dimensionless frequency

$$\omega \equiv \frac{\omega_o R_o}{a_o} \tag{8.100}$$

and k is the corresponding axial wavenumber ($k = \omega$).

When the $O(M_b)$ terms are accounted for (as we did in sections 8.3 and 8.4), one finds that the magnitude of the acoustic disturbance either grows exponentially or decays depending on the admittance characteristics of the injection boundary, nozzle boundary representation, and other loss or gain effects such as particle damping. For the axial wave system, any radial gas motions must be of the order of M_b or smaller.

Inviscid Vortical Solutions

The effects of vorticity will now be addressed in a direct manner by solving for the rotational wave effects. Since the vortical oscillations are in effect driven by the acoustical motions, then it is appropriate to assume that

$$\mathbb{U} \approx f(r,z) e^{i\omega t}\sin kz \tag{8.101}$$

This insures that the composite solutions will combine with the acoustic velocity to satisfy the no-slip boundary condition, and will be used in all forms of the vortical motion to be derived.

We will find that 8.96 represents another type of wave equation describing waves of vorticity. Unlike the acoustic wave equation, it describes a "broadband" oscillator that respond to the superimposed acoustic fluctuations. That is, it does not exhibit specific frequency eigenvalues. It does however respond to the acoustic signal more strongly in a certain frequency range. This range tends

to be on the low side of the acoustic scale.

Let us first test Brown's hypothesis by assuming at the outset that viscous forces are not important because of the strong convective effect at the solid boundaries of the chamber. The axial component of the vortical momentum equation (z-component of 8.96) can be written as

$$\frac{\partial \tilde{u}_z}{\partial t} = - M_b \left[\frac{\partial}{\partial z} (U_z \tilde{u}_z) - \Omega \tilde{u}_r - U_r \zeta \right] - \delta^2 \frac{1}{r} \frac{\partial}{\partial r} (r\zeta) \quad (8.102)$$

where the mean and oscillatory vorticity are, respectively

$$\Omega = |\nabla \times U| = \left(\frac{\partial U_r}{\partial z} - \frac{\partial U_z}{\partial r} \right) = - \pi^2 r z \sin\left(\frac{\pi r^2}{2} \right), \quad (8.103)$$

$$\zeta = |\nabla \times \tilde{u}| = \left(\frac{\partial \tilde{u}_r}{\partial z} - \frac{\partial \tilde{u}_z}{\partial r} \right). \quad (8.104)$$

The radial velocity component is of the order of the mean flow Mach number (this is justified by the admittance boundary condition, which sets the magnitude of the radial oscillations), thus terms involving the radial vortical velocity component are negligible. The terms involving the axial rate of change are of the order of M_b. Subject to later verification, it is assumed that terms involving gradients in the radial direction are not negligible. Thus to first-order the axial vortical disturbance is governed by

$$\frac{\partial \tilde{u}_z}{\partial t} + M_b U_r \frac{\partial \tilde{u}_z}{\partial r} = 0 \quad (8.105)$$

assuming that viscous effects are negligible. This will be recognized as a simple wave equation with the radial mean flow velocity in the role of the (variable) speed of propagation of the wave. A solution is easily found that, when combined with the acoustic part, correctly satisfies the no-slip boundary condition. This result is

$$\tilde{u}_z = - \sin\left[\omega t + \left(\frac{\omega}{\pi M_b} \right) \ln \tan\left(\frac{\pi r^2}{4} \right) \right] \sin kz \quad (8.106)$$

and the composite velocity solution to zeroth order in M_b is

$$u^{(1)} = \left\{ \sin \omega t - \sin\left[\omega t + \left(\frac{\omega}{\pi M_b} \right) \ln \tan\left(\frac{\pi r^2}{4} \right) \right] \right\} \sin kz\, e_z + O(M_b) \quad (8.107)$$

Notice that since the equation of motion is of first-order in its radial dependence, then only one spatial boundary condition can be satisfied. Since the entire problem is dominated by the blowing wall no-slip condition, this is the one that we are forced to address. This leaves the behavior at the chamber axis uncontrolled. Attempting to satisfy the symmetry condition at the axis leads to a trivial solution, so the one shown is the only possibility. The composite solution clearly

satisfies the no slip condition. Figure 8.6 is a plot of the radial variation of the composite wave amplitude. The vortical solution represents a traveling shear wave generated at the surface and propagating radially due to mean flow convection. *This is precisely the time-dependent analog of the mean flow solution.* The spatial wavelength of the motion decreases radially and approaches zero at the axis (because the propagation speed is proportional to the radial mean flow, U_r, which goes to zero at the axis). The amplitude varies periodically, but its maximum value is independent of radial position. The vortical effect causes a periodic overshoot of the axial velocity with a maximum value of twice the acoustic wave amplitude.

Figure 8.7 shows this solution with the 84 Hz cold flow data superimposed. Parameters used in the evaluation correspond to those used in the cold flow testing. The agreement between the simple solution and the data in the vicinity of the boundary is remarkably good, but the agreement degrades rapidly as the
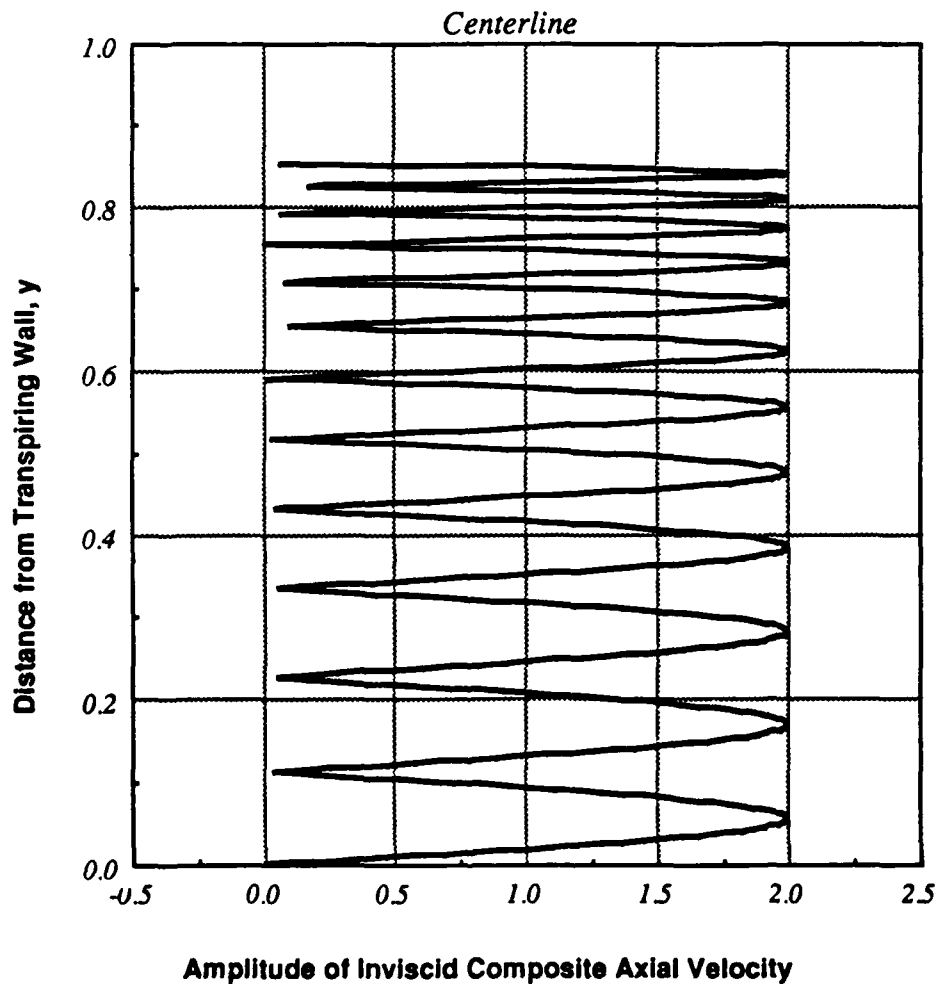
Fig. 8.6 Plot of Inviscid Composite Axial Velocity Distribution

chamber centerline (y = 1) is approached. For emphasis, note that the theoretical result correlates favorably with the measured data for perhaps the first quarter of the distance from the porous surface. The presence of oscillatory spatial behavior exhibited in the experimental data becomes quite apparent with the superposed shear wave plot as a guide to the eye. However, the data show a rapid decay in overshoot amplitude as the axis is approached. Near the surface, the maximum overshoot in the data is typically about twice the centerline amplitude, as the theory predicts.

To achieve an acceptable solution, it is necessary that the source of the radial decay of the shear wave be identified. The decay is not the result of the radial mean velocity U_r decreasing to zero at the chamber axis. It is apparent that the analogy with the mean flow is not complete, and viscous effects must be included in the solution. The physical reasons for this are apparent. The unsteady flow causes a gas particle emerging from the transpiring surface to change direction (relative to its mean flow streamline) repeatedly as it moves into the
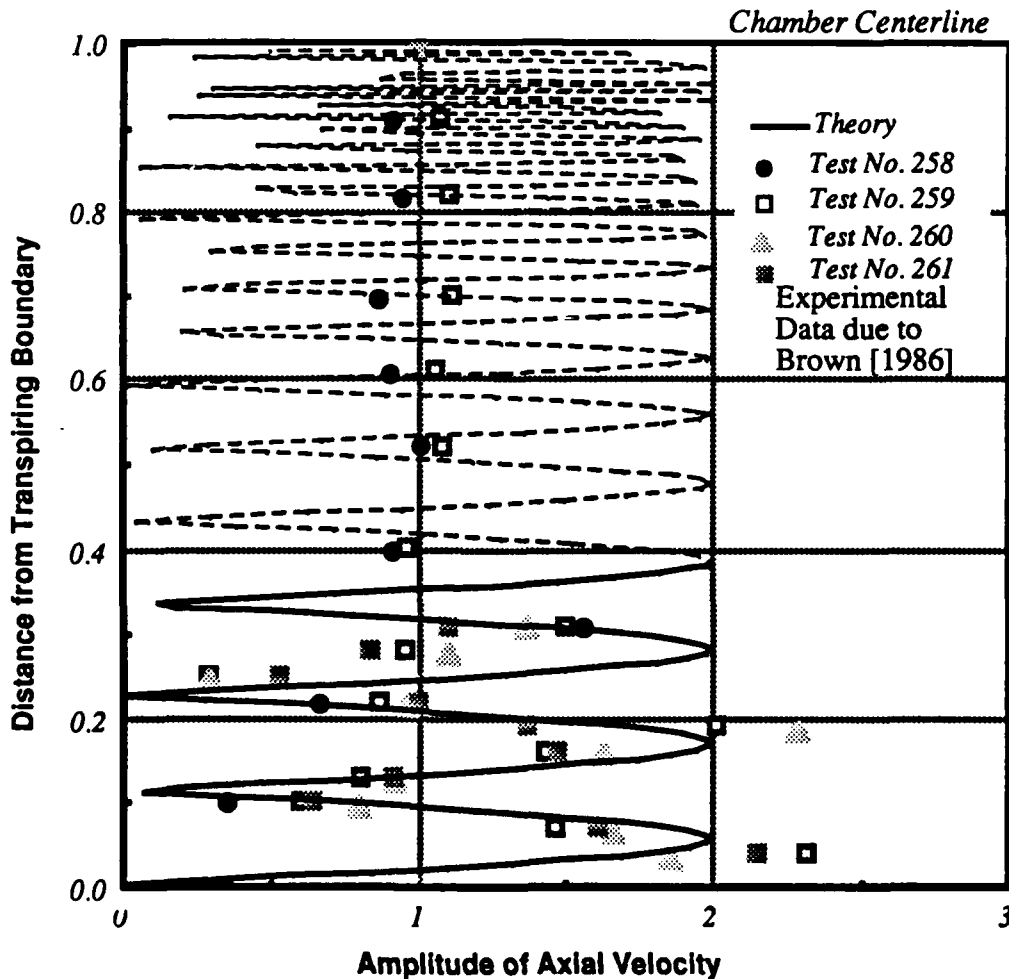

Fig. 8.7 Comparison of Inviscid Composite Axial Velocity to Cold Flow Data

chamber with the mean flow. Near the surface, the radial velocity is large and the associated shear is small; viscous forces may be negligible as Figure 8.7 indicates they are for the cold-flow tests. However, as the particle moves closer to the axis, the number of reversals per unit radial distance traveled becomes much larger and the shear stresses may become important and viscous decay of the oscillations dominates the behavior. The shear stress is proportional to the rate at which the velocity changes in the radial direction,

$$\tau \sim \frac{\partial u_z}{\partial r} \approx \frac{\Delta u_z}{\Delta r} \tag{8.108}$$

The acoustic velocity amplitude divided by distance traveled by the particle in one fourth the acoustic period provides a reasonable estimate for the velocity gradient. Near the wall

$$\tau \sim \frac{2\omega}{\pi M_b} \tag{8.109}$$

and the ratio of the dimensionless frequency to the mean flow Mach number appears naturally. Not unexpectedly this is the same combination of parameters that controls the inviscid solution. Thus, for high frequency or small injection Mach number, the shearing stress may not be negligible near the surface, and becomes even larger as the centerline is approached. Therefore for the conditions in the cold-flow tests and in most rockets, viscous forces must be included in the formulation. Also notice that this result verifies that the radial derivative term (second term) in equation 8.108 is properly retained as assumed even though it is multiplied by the mean flow Mach number.

To summarize, an inviscid, rotational correction to the plane acoustic wave representing the unsteady generation of vorticity at the injection boundary allows satisfaction of the no-slip boundary condition but does not properly represent the flow in the interior of the chamber. The theory agrees with the experimental data only in the vicinity of the injection surface. *We must therefore conclude that Brown's hypothesis does not apply either in the porous tube experiment or in the majority of rocket motor situations.* It is necessary to include effects of viscous drag if solutions are to be found that match all physical constraints on the system. Therefore we must, unfortunately, give up the simplicity of the inviscid approach when dealing with the time-dependent flow in a rocket motor.

Vortical Solutions with Viscous Corrections

Again focus on the leading terms in the expressions for axial velocity fluctuations. The viscous terms must be retained because the radial gradient of the axial velocity is large for small mean flow Mach numbers and for the frequency ranges of interest. Therefore, the axial vortical velocity is governed to zeroth order in the mean flow Mach number by

$$\frac{\partial \tilde{u}_z}{\partial t} + M_b U_r \frac{\partial \tilde{u}_z}{\partial r} = \delta^2 \frac{\partial^2 \tilde{u}_z}{\partial r^2} + O(M_b) \tag{8.110}$$

The order of the differential equation is raised by retention of the viscous terms and it is now possible to satisfy an additional boundary condition. In particular, one can satisfy both the symmetry condition at the chamber centerline and the no-slip condition. Several terms multiplied by are not shown in this approximate formulation. These control the dependence of the solution on axial position, z. We will pay close attention to these additional terms later. To include them we must deal with another spatial dimension; a much more complex strategy will be needed to find the solutions. For now we will concentrate on the behavior at a fixed axial location and ignore the small terms that are explicitly dependent on z.

It is useful (but not necessary) to employ the methods of singular perturbation theory by introduction of a stretched radial coordinate, η. Put

$$\eta \equiv \frac{M_b}{\delta^2} y = \frac{M_b}{\delta^2} (1 - r).$$
(8.111)

This in effect properly scales the radial variations so that they are compatible with axial variations in the parameters. Rewriting equation (8.110) in terms of the new radial coordinate yields

$$\frac{\partial^2 \tilde{u}_z}{\partial \eta^2} + U_r \frac{\partial \tilde{u}_z}{\partial \eta} - \lambda^2 \frac{\partial \tilde{u}_z}{\partial t} = 0,$$
(8.112)

where

$$\lambda \equiv \frac{\delta}{M_b},$$
(8.113)

is an important scaling parameter, which is of the order o unity in most rocket motors and in the cold flow experiments. Unfortunately, although 8.112 is linear, the coefficients are variable; U_r is a complicated function r (see equation (8.85)). The problem is apparently not solvable in closed form unless the radial mean flow velocity function is modified. If frequency is sufficiently high and/or the blowing Mach number is low, a simple solution can be derived as shown by Flandro [1974a, 1974b, 1983]. Please note that we are not talking of an "acoustic boundary layer" in this problem. The vortical effects are expected to penetrate deeply into the chamber volume.

Approximate Viscous Solution

Since closed-form solutions are of great value in paving the way to more complete ones, let us review the approximate solution. The approximation to be used amounts to the assumption that variation in the radial mean flow velocity occurs slowly compared to the radial rate of decay of $\tilde{u}_z$. The result is valid in a region sufficiently close to the transpiring boundary. In this region, $U_r \sim -1$, and equation (8.112) is easily solved. One finds

$$\tilde{u}_z = e^{i\omega t} e^{-\xi \eta} \sin (kz)$$
(8.114)

where ξ is the solution of the complex quadratic equation

$$\xi^2 + \xi - i\left(\omega \lambda^2\right) = 0 \qquad (8.115)$$

The real and imaginary parts of ξ for a physically acceptable solution are

$$\begin{cases} \xi^{(r)} = \dfrac{1}{2}\left(\dfrac{\omega \lambda^2}{\xi^{(r)}} - 1\right) \\[2mm] \xi^{(i)} = \sqrt{\dfrac{1}{8}\left[-1 + \sqrt{1 + (4\omega \lambda^2)}\right]} \end{cases} \qquad (8.116)$$

The real part controls the rate of viscous damping and the imaginary part determines the phase shift and propagation speed of the shear wave as can be seen when the real part of the composite solution is written out:

$$\mathbf{u}^{(1)} = \left\{ \sin(\omega t) - e^{-\left(\xi^{(r)}\frac{M_b}{\delta^2}\right)y} \sin\left[(\omega t) - \left(\xi^{(i)}\frac{M_b}{\delta^2}\right)y\right]\right\} \sin(kz)\,\mathbf{e}_z \qquad (8.117)$$

Notice that two Reynolds numbers control the behavior of the system. These are described in Table 1 together with their physical interpretations.

Table 1. Dimensionless Groups in Viscous Time-Dependent Flow

| Group	Definition	Physical Interpretation	Typical Values
$\dfrac{M_b}{\delta^2} = R_{ei}$	$\dfrac{v_b R_o}{v_o}$	Injection Reynolds number. Ratio of mean flow inertial force to viscous force	$2 \cdot 10^3$ to $7 \cdot 10^4$
$\dfrac{\omega}{\delta^2} = R_{ea}$	$\dfrac{\omega_o R_o^2}{v_o} = \dfrac{2\pi f R_o^2}{v_o}$	Acoustic Reynolds number. Ratio of acoustic wave inertial force to viscous force	$1 \cdot 10^5$ to $2 \cdot 10^7$
$\omega\lambda^2 = \dfrac{R_{ea}}{R_{ei}^2}$	$\dfrac{\omega_o v_o}{v_b^2}$	Ratio of Acoustic Reynolds number to square of injection Reynolds number	$1 \cdot 10^{-3}$ to $1 \cdot 10^{-1}$
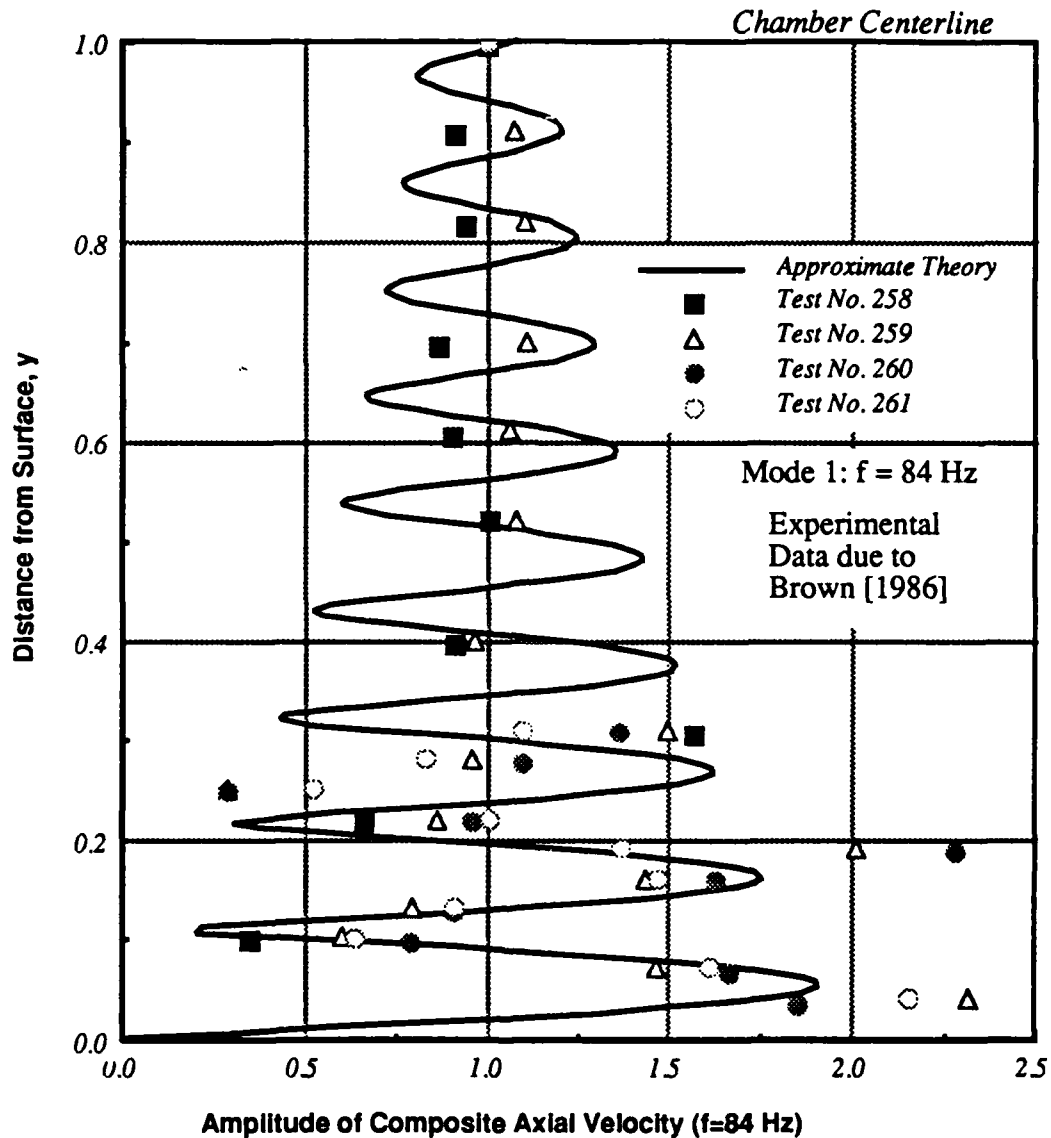
Fig. 8.8 Comparison of Approximate Viscous Solution to Cold Flow Data

It happens that the limit to the range of validity of the approximate solution falls between the two cold-flow experimental frequencies. Figures 8.8 and 8.9 compare the measured axial velocity amplitude to the theory for both the first chamber mode (f = 84 Hz) and the second mode (f = 168 Hz). Again, the agreement is acceptable only near the wall. Because of the relatively low frequency, the exponential decay (assuming U_r = constant = -1) does not reduce the amplitude rapidly enough to satisfy the centerline boundary condition. The agreement with the data is significantly better, however, than it was in the inviscid calculations. The poor agreement in the inner half of the tube is clearly the result of ignoring the dependence of U_r on the radius; it goes to zero at the axis. For the second mode, the approximate solution works fairly well. Thus the approximate
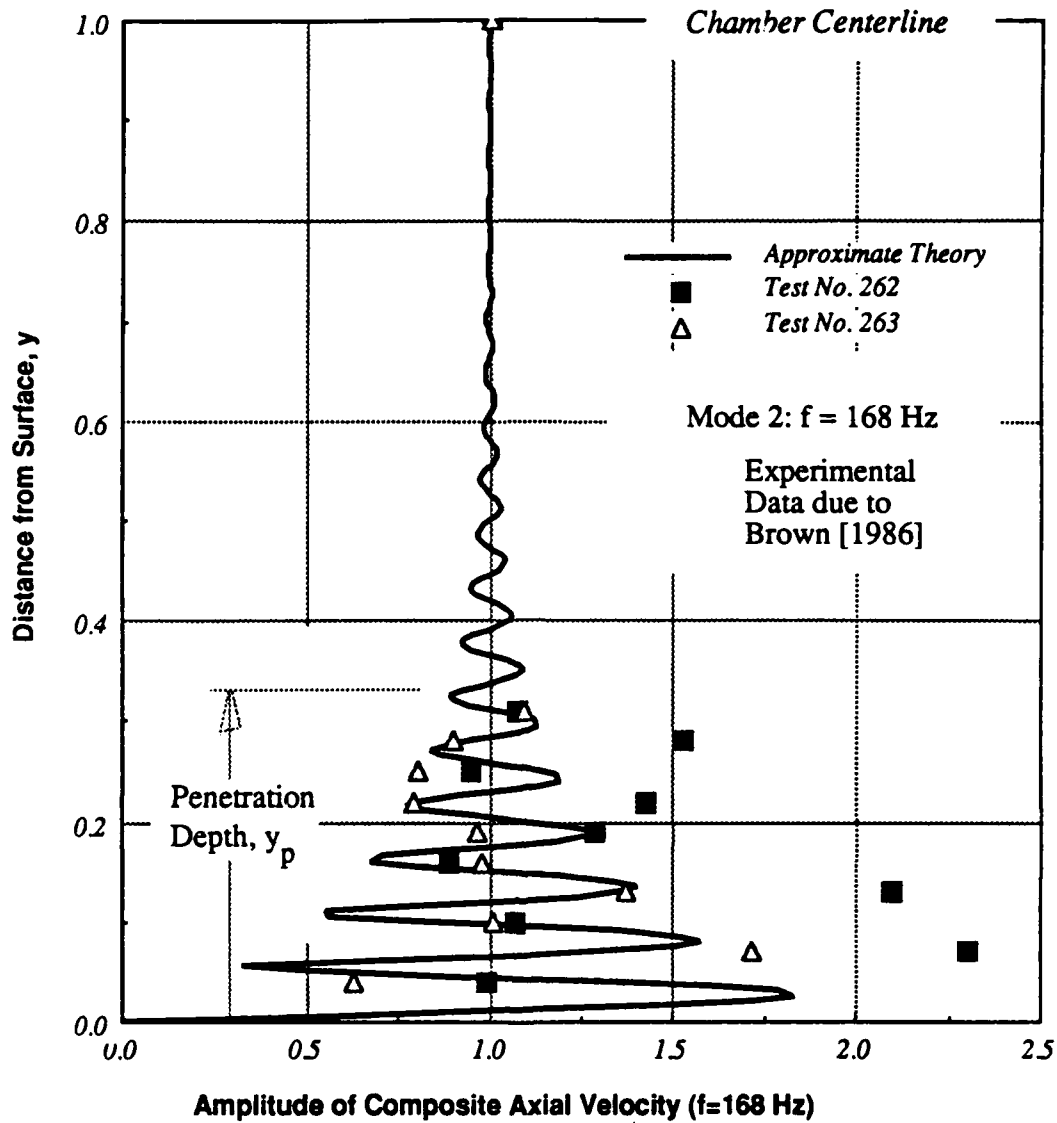
Fig. 8.9 Comparison of Approximate Viscous Solution to Cold Flow Data

theory is usable in problems in which the *penetration depth* of the decaying shear wave is less than, say, half the chamber radius. Otherwise, it is necessary to solve the complete problem as described by equation (8.102). This we will do shortly. Before so doing, it is useful to determine the range of conditions for which the closed-form model applies.

The penetration depth is defined by determining the radial position at which the shear wave amplitude decays to less than, say, 1% of the acoustic amplitude. This depth, measured from the burning surface, is

$$y_p \cong - \frac{\delta^2 Ln\,(0.02)}{2\,M_b\,\xi^{(r)}} \qquad (8.118)$$

Figure 8.10 is a plot of constant values of y_p on a Reynolds number map. The vertical axis corresponds to acoustic Reynolds number, Re_a; the horizontal axis corresponds to the injection Reynolds number, Re_i. Since the approximate theory is not appropriate if the penetration depth is too large, points to the right of the solid curve (corresponding to $y_p = 0.5$) are not well represented by the approximate solution. Points corresponding to the two cold-flow data sets, a typical tactical rocket, and to a large SRM booster are shown on the plot. For the rockets, lowest-order longitudinal modes are assumed. The approximate theory is not sufficiently accurate for either the first-mode cold-flow simulation or the
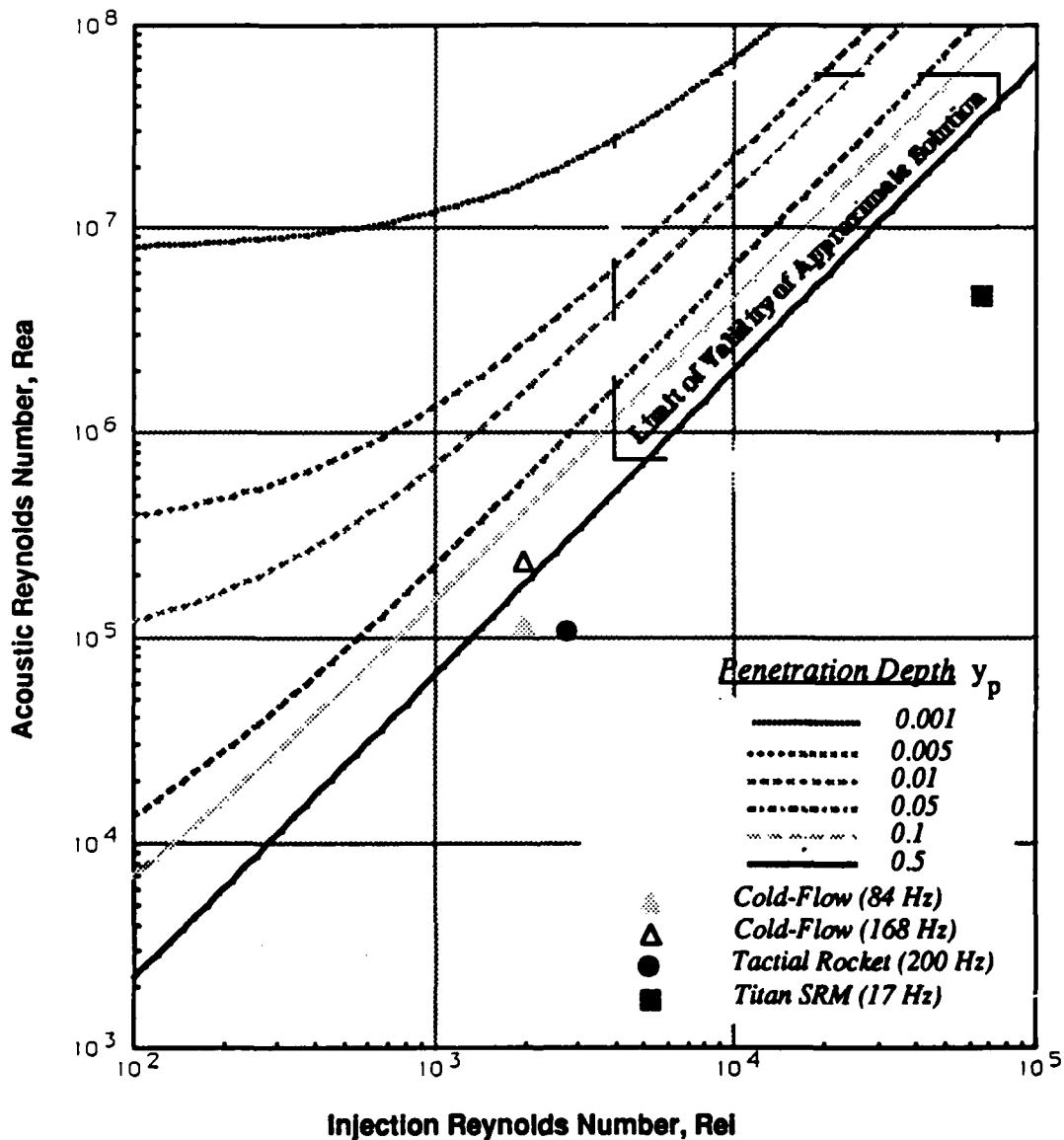

Fig. 8.10 Lines of Constant Penetration Depth on Acoustic Reynolds Number vs Injection Reynolds Number Map

rockets shown. A large volume of the chamber is subjected to the shear wave effects for these configurations. For higher axial modes or for high-frequency tangential oscillations, the approximate theory is adequate in most cases.

To summarize the approximate calculations, it will be noted that in acuality, a large range of actual rocket motor combustion oscillations are covered by the theory. Only when the frequency is relatively low, as it is in the lowest order axial modes, does the need for a more complete solution appear. It is very interesting to note that in most cases of axial mode oscillations, the shear waves penetrate deeply into the core of the flow field unlike the simple acoustic boundary layer effects that have been previously assumed to account for vortical effects. This observation brings into question many of the standard analyses used to model combustion instability. For example, it is clear that the radial variations in velocity amplitude and phase will greatly affect results such as the particle damping calculations that assume a much simpler velocity profile. Perhaps the failure of classical instability theory in a large number of axial mode instability situations can be partially attributed to complications of this sort.

Detailed Solution for the Axial Viscous Motion

In order to determine the vortical solution with a realistic mean flow profile, we must resort to numerical solutions. This might appear quite simple at the outset. For example, one might expect that a simple numerical integration starting at the sidewall with initia. conditions from the approximate solution is a viable approach. However, *the differential equations are numerically stiff*, and this approach fails. It is necessary to integrate backward, starting from the centerline with values satisfying the symmetry condition. A differential correction or "shooting" approach then allows adjustment of the starting conditions to satisfy the conditions at the transpiring boundary. Although this may seem a complicated approach, it far less so than dependence on full finite-difference integration of the Navier-Stokes equations. The algorithm is simple and can be readily appended to any standard instability programs. The axial effects are readily accounted for.

Figures 8.11 and 8.12 show the amplitude and phase distributions for the numerical solution. Data from the 84 Hz cold-flow simulation are superimposed. All boundary conditions are now satisfied. The approach to zero at r=0 of the radial mean velocity, U_r, drives the vortical disturbance to zero at the axis as required. Agreement with the data is remarkably good. There is apparently some experimental error, since it is difficult to precisely locate the hotwire probe in the small (4" diameter) tube, especially for points very close to the boundary of the porous tube. Four data points, two from Test 259 and one each from Tests 260 and 261 lie beyond the upper theoretical velocity overshoot limit of 2. The reasons for this discrepancy have not been determined. Nevertheless, the data follow the theoretical trends quite closely. This is especially surprising for the phase angle data, since it is difficult to measure these accurately.

Normalized Acoustic Velocity Amplitude

Fig. 11 Com,   ˙˙on of Numerical Results to Experimental Data
Axial Velocity Magnitude vs y (First Mode, f = 84 Hz)
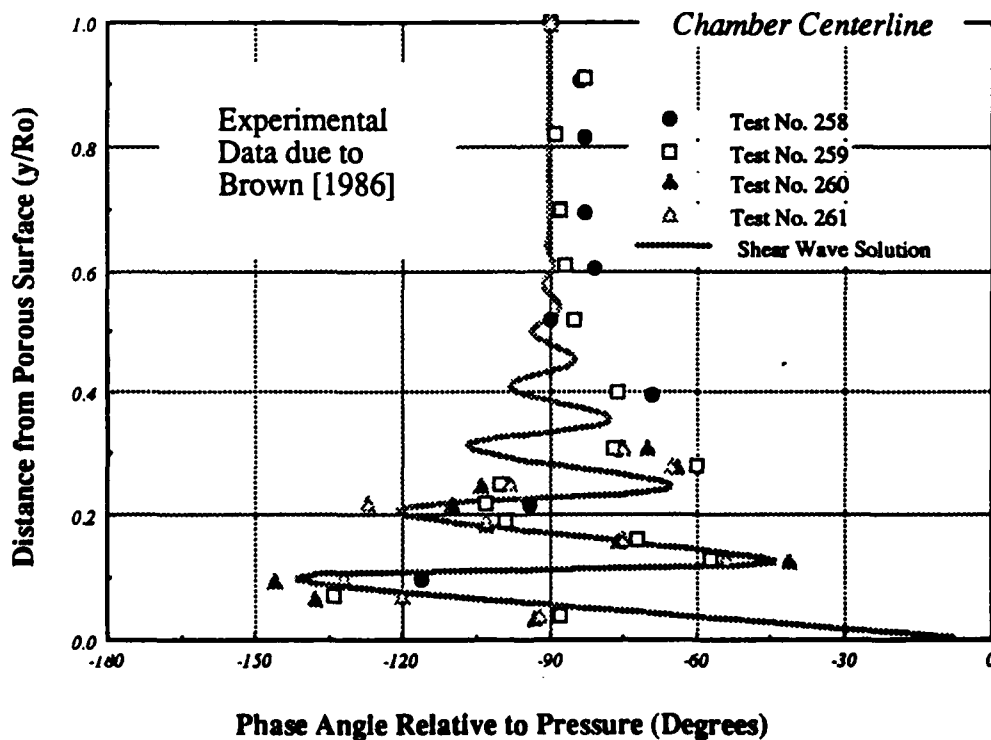

Phase Angle Relative to Pressure (Degrees)
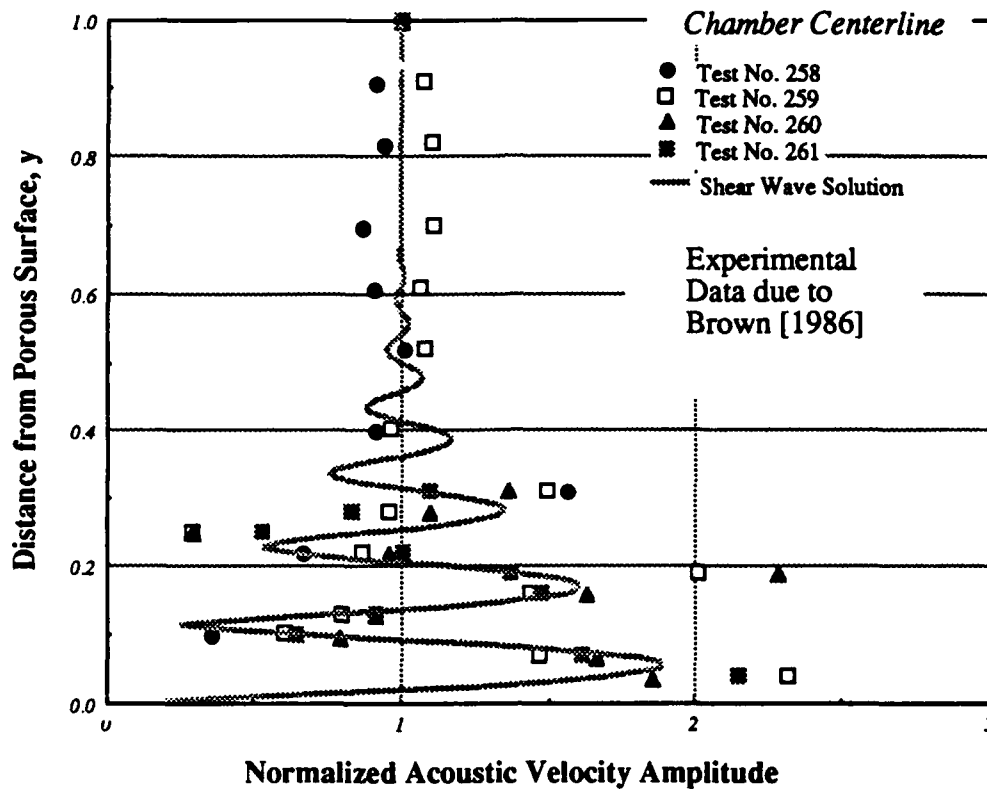
Fig. 12 Comparison of Numerical Results to Experimental Data
Axial Velocity Phase Angle vs y (First Mode, f = 84 Hz)

8.7 SUMMARY

The theoretical basis for current combustion instability models was reviewed in detail using two distinctly different analytical approaches. The result is a simple formula for the linear system growth rate. Three basic elements determine the tendency of the wave amplitude to grow or decay. The first is a convective transport of acoustic energy from the burning surface (a gain) into the nozzle (a loss). The second is the classical pressure coupled response of the combustion to the incident wave. This produces either a gain or a loss contribution depending on the sign of the admittance function describing the sensitivity of the combustion processes to pressure fluctuations. The third effect carried through the analysis in symbolic form is the influence of drag of solid particles moving through the flow. The details of this loss effect are presented in Chapter 9.

Since the problem is linear, the growth rate formula can be enhanced by simply adding other gain and loss effects. This cannot be done carelessly, because the validity of the system predictions are only as good as the weakest element of the analysis. A list of enhancements including particle losses, losses at inert surfaces, nozzle damping, effects of losses in the boundary materials and propellant, and heat transfer is discussed in detail in Chapter 9.

In assessing the boundary conditions used in performing the basic stability analysis, we discovered that certain constraints on the oscillatory flow were not accommodated. In particular, it is necessary to account for the vorticity generated near the propellant surface as a result of the no-slip contraint on the axial acoustic velocity component. These show that vorticity transport markedly affects the time-dependent velocity distributions in wave systems in rocket motor flows. The motion consists of perturbations to the assumed axial acoustic plane waves caused by traveling shear waves formed at the surface and convected away from it with the mean flow. Shear waves are generated because the flow must enter the chamber radially; vorticity is thereby introduced. This is the direct analog of the corresponding rotational mean flow effects.

The existence of the disturbance does not require the presence of viscous forces in the volume of the chamber (other than those implied in the normal injection process). However, the viscous shear forces induced in the time-dependent case are of the order of inertial forces and cannot be neglected in mathematical modeling. They act to damp the shear waves as they propagate toward the axis. Additional effective damping results from the interaction with the radial mean flow. The result is a set of rapid radial fluctuations in the amplitude and phase of the time-dependent flow; the expected plane wave motion is confined to a small volume near the chamber axis.

The penetration depth of the perturbations depends on two Reynolds numbers, one related to the injection speed of the gases, the other to the acoustic particle velocity or frequency. For longitudinal modes of oscillation, these effects dominate the gas motions. For high frequency waves, such as tangential

mode oscillations, the region of vortical activity is thin compared to the chamber dimensions; at sufficiently high frequency the penetration depth is within the burning zone. In this case, effects of the velocity fluctuations can influence the time-dependent combustion as in classical velocity coupling. This behavior corresponds to studies by Tien [1972] and Flandro [1982].

Near the injection surfaces or burning propellant, the velocity magnitude overshoots that of an acoustic plane wave by a factor approaching two. There are also significant phase distortions. The phase angle near the surface is closer to a 0° lag than the 90° assumed in previous theories based on a purely acoustic representation of the oscillation flow. This has profound effects on the particle damping and other effects that depend on the velocity distribution and its phase relative to the pressure waves.

For low-order axial modes and injection speeds typical of rocket combustion, the shear waves fill the chamber. The concept of velocity coupling As it applies to lower frequency oscillations, especially for axial modes, is greatly affected because existing theory assumes an oscillating velocity profile quite different than the one observed in the experiments and demonstrated in the theory presented here.

Much work remains to be accomplished in determining the impact of rotational flow effects on growth and decay of combustion oscillations in rockets. It is expected that inclusion of these effects will significantly improve both physical understanding and predictive capability in combustion instability problems.

REFERENCES

Anderson, J. D. (1982). Modern Compressible Flow. New York, McGraw-Hill Book Company.

Andreev, N. N. (1955). "Concerning Certain Second-Order Quantitites in Acoustics." Soviet Physics-Acoustics. 1(2):

Avalon, G., J. Pascal and F. Cauty. (1987). Experimental Investigation of a Type of Solid Propellant Velocity Coupling.

Awad, E. (1983). Nonlinear Acoustic Instabilities in Combustion Chambers.

Baum, J. D. and J. N. Levine. (1986). "Numerical Study of Flow Turning Phenomenon", AIAA Paper 86-533, AIAA Aerospace Sciences Meeting, Jan. 1986.

Baum, J. D. and J. N. Levine. (1987a). Acoustic-Mean Flow Interactions.

Baum, J. D. and J. N. Levine. (1987b). "Acoustic Energy Exchange Through Flow Turning", AIAA Paper 87-217, AIAA Aerospace Sciences Meeting, Jan 1987.

Beckstead, M. W. and F. E. C. Culick. (1971). "A Comparison of Analysis and Experiment for Solid Propellant Combustion Instability." AIAA J. 9: 147-154.

Beddini, R. A. (1986). "Injection-Induced Flows in Porous-Walled Ducts." AIAA J. 24(12): 1766-1773.

Bell, W. A., B. R. Daniel and B. T. Zinn. (1973). "Experimental and Theoretical Determination of the Admittances of a Family of Nozzles Subjected to Axial Instabilities." J. Sound and Vibration. 30: 179-190.

Betchov, R. (1958). "Nonlinear Oscillations in a Column of Gas." Physics of Fluids. 1(No. 3): 205-212.

Bird, J. T., F. T. McClure and R. W. Hart. (1963). Acoustic Instability in the Transverse Modes of Solid Propellant Rockets.

Blokhintsev, D. I. (1956). Acoustics of a Nonhomogeneous Moving Medium.

Bogoliubov, N. N. and Y. A. Mitropolsky. (1961). Asymptotic Methods in the Theory of Non-linear Oscillations. Hindustani Publishing Co.

Brigham, E. O. (1974). The Fast Fourier Transform. Englewood Cliffs, NJ, Prentice-Hall.

Brown, R. S., A. M. Blackner, P. G. Willoughby and R. Dunlap. (1986). Coupling between Velocity Oscillations and Solid Propellant Combustion. AIAA 24th Aerospace Sciences Meeting. **Paper 86-0531:**

Brown, R. S. and R. J. Muzzy. (1970). "Linear and Nonlinear Pressure Coupled Combustion Instability of Solid Propellants." AIAA J. 8(8): 1492-1500.

Brownlee, W. G. (1964). "Nonlinear Axial Combustion Instability in Solid Propellant Motors." AIAA J. 2(2): 275-284.

Brownlee, W. G. and G. H. Kimball. (1966). "Shock Propagation in Solid-Propellant Rocket Combustors." AIAA J. 4(6): 1132-1134.

Brownlee, W. G. and F. E. Marble. (1960). An Experimental Investigation of Unstable Combustion in Solid Propellant Rocket Motors. ARS Progress in Astronautics and Rocketry: Solid Propellant Rocket Research.

Butcher, A. G. and M. W. Beckstead. (1979). A Comparison of Predicted and Measured Acoustic Stability Using SSP. 16th JANNAF Combustion Meeting. III: 475-504.

Cantrell, R. H. and R. W. Hart. (1964). "Interaction between Sound and Flow in Acoustic Cavities: Mass, Momentum, and Energy Considerations." J. Acoustical Society of America. 36: 697-706.

Chester, W. (1964). "Resonant Oscillations in Closed Tubes, J. Fluid Mechanics." J. Fluid Mechanics. 18: 44.

Chu, B. T. and S. J. Ying. (1963). "Thermally Driven Nonlinear Oscillations in a Pipe with Traveling Shock Waves, Physics of Fluids." Physics of Fluids. 6, No. 7(November): 1625-1637.

Cole, J. D. (1968). Perturbation Methods in Applied Mechanics. Waltham, Massachusetts, Blaisdell Publishing Company.

Crocco, L. and S. I. Cheng. (1956). Theory of Combustion Instability in Liquid-Propellant Rockets. AGARDograph No. 8. London, Butterworths Scientific Publications.

Culick, F. E. C. (1970). "Stability of Longitudinal Oscillations with Pressure and Velocity Coupling in a Solid Propellant Rocket." 2(2):

Culick, F. E. C. (1971). "Nonlinear Growth and Limiting Amplitude of Acoustic Waves in Combustion Chambers." 3(1): 1-16.

Culick, F. E. C. (1972). Interactions Between the Flow Field, Combustion and Wave Motions in Rocket Motors.

Culick, F. E. C. (1973). "The Stability of One-Dimensional Motions in a Rocket Motor." 7: 165-175.

Culick, F. E. C. (1975a). Nonlinear Behavior of Acoustic Waves in Combustion Chambers.

Culick, F. E. C. (1975b). "Stability of Three-Dimensional Motions in a Combustion Chamber." 10: 109-124.

Culick, F. E. C. (1976). "Nonlinear Behavior of Acoustic Waves in Combustion Chambers." Astronautica Acta. 3(9): 715-756.

Culick, F. E. C. (1966a). "Acoustic Oscillations in Solid Propellant Rocket Chambers." Astronautica Acta. 12(2): 113-126.

Culick, F. E. C. (1966b). "Rotational Axisymmetric Mean Flow and Damping of Acoustic Waves in a Solid Propellant Rocket." AIAA J. 4(8): 1462-1463.

Culick, F. E. C. (1967). "Calculation of the Admittance Function for a Burning Surface." Astronautica Acta. 13(3): 221-238.

Culick, F. E. C. (1968). "A Review of Calculations for Unsteady Burning of a Solid Propellant." AIAA Journal. 6: 2241-2255.

Culick, F. E. C. (1973). "The Stability of One-Dimensional Motions in a Rocket Motor." 7: 165-175.

Culick, F. E. C. (1983). An Introduction to Velocity Coupling in Solid Propellant Rockets.

Culick, F. E. C. and K. Magiawala. (1977). Measurements of Energy Losses Associated with Interactions between Acoustic Waves and a Steady Flow Field.

Culick, F. E. C. and K. Magiawala. (1979). "Excitation of Acoustic Modes in a Chamber by Vortex Shedding." 64(No. 3):

Culick, F. E. C. and E. H. Perry. (1969). "T-Burner Data and Combustion Instability in Solid Propellant Rockets." AIAA J. 7: 1204-1205.

Culick, F. E. C., E. W. Price and e. al. (1969). T-Burner Manual.

Curle, N. (1955). "The Influence of Solid Boundaries upon Aerodynamic Sound." Proc. Royal Society, Series A. **231**:

Currie, I. G. (1974). Fundamental Mechanics of Fluids. New York, McGraw-Hill Book Comapny.

Denison, M. R. and E. Baum. (1961). "A Simplified Model of Unstable Burning in Solid Rocket Propellants." ARS J. 3(6): 1112-1121.

Dickinson, L. A. (1962). "Command Initiation of Finite Wave Axial Combustion Instability in Solid Propellant Rocket Motors." ARS J. 32: 643-644.

Drazin, P. G. and W. H. Reid. (1981). Hydrodynamic Stability. Cambridge, Cambridge University Press.

Dudley, D. P. and R. D. Waugh. (1976). Standardized Stability Prediction Method for Solid Rocket Motors.

Dunlap, R. and e. al. (1974). "Flowfield in the Combustion Chamber of a Solid Propellant Rocket Motor." AIAA J. 12(10):

Dunlap, R., G. A. Flandro, R. A. Beddini, R. S. Brown and H. McDonald. (1987). Internal Flow Field Study.

Flandro, G. A. (1982a). "Energy Balance Analysis of Nonlinear Combustion Instability." J. Propulsion and Power. 1(3): 210.

Flandro, G. A. (1982b). Nonlinear Time-Dependent Combustion of a Solid Rocket Propellant.

Flandro, G. A. (1986). "Vortex Driving Mechanisms in Oscillatory Rocket Flows." J. Propulsion and Power. 2(3): 206-214.

Flandro, G. A. (1967). Rotating Flows in Acoustically Unstable Rocket Motors.

Flandro, G. A. (1969). Acoustic Combustion Instability in Flight Application Solid Propellant Rocket Motors (Final Report).

Flandro, G. A. (1973). The Influence of Mean Flow on Rocket Motor Combustion Instability.

Flandro, G. A. (1974). "Solid Propellant Acoustic Admittance Corrections." J. Sound and Vibration. 36(No. 3):

Flandro, G. A. (1979). Influence of Vortex Shedding on Acoustic Instability in Solid Propellent Motors.

Flandro, G. A. (1980). Stability Prediction for Solid Propellant Rocket Motors with High-Speed Mean Flow.

Flandro, G. A. and H. R. Jacobs. (1975). Vortex Generated Sound in Cavities. Aeroacoustics: Jet and Combustion Noise, Progress in Astronautics and Aeronautics. MIT Press.

Flandro, G. A. (1982), "Nonlinear Time-Dependent Combustion of a Solid Rocket Propellant", 19th JANNAF Combustion Meeting, Greenbelt, MD.

Folkman, S. (1980). Investigation of Pressure Oscillations in the Space Shuttle SRM QM-3 Test.

Fox, R. W. and A. T. McDonald. (1985). Introduction to Fluid Mechanics. New York, John Wiley & Sons.

Friedly, J. C. and E. E. Peterson. (1966). "Influence of Combustion Parameters on Instability in Solid Propellant Motors: Part I - Development of Model and Linear Analysis." AIAA J. 4(9): 1605-1610.

Grad, H. (1949). Comm. Pure Appl. Math. 2(79):

Hansen, A. C., F. M. Prater and G. A. Flandro. (1971). Generation of Acoustic Waves in a Cavity by Injection of a Turbulent Jet (Also Masters thesis by A. C. Hansen).

Hart, R. W., J. F. Bird, R. H. Cantrell and F. T. McClure. (1964). "Nonlinear Effects in Instability of Solid Propellant Rocket Motors." AIAA J. 2: 1270-1273.

Hart, W. R. and F. T. McClure. (1959). "Combustion Instability: Acoustic Interaction with a Burning Propellant Surface." J. Chem. Phys. 30(9): 1501-1514.

Hersh, A. S. and B. Walker. (1983). Experimental Investigation of Rocket Motor Flow Turning Losses.

Hersh, A. S. and B. Walker. (1984). Experimental Investigation of Rocket Motor Flow Turning Losses.

Horton, M. D., R. L. Coates, M. Krashin and M. W. Beckstead. (1972). Velocity Coupling Analysis.

Ingard, K. U. (1959). "Influence of Fluid Motion Past a Plane Boundary on Sound Reflection, Absorption and Transmission." J. Acoustical Society of America. **31**: 1035-1036.

Jeffrey, A. and T. Kawahara. (1982a). Asymptotic Methods in Nonlinear Wave Theory. Boston, Pitman Advanced Publishing Program.

Jeffrey, A. and T. Kawahara. (1982b). Asymptotic Methods in Nonlinear Wave Theory. Boston, Pitman Advanced Publishing Program.

Karamacheti, K. (1969). Some Features of an Edge-Tone Flow Field.

Keller, J. B. (1955). "Reflection and Transmission of Sound by a Moving Medium." J. Acoustical Society of America. **27**(6): 1044-1047.

Kinsler, L. E., A. R. Frey, A. B. Coppens and J. V. Sanders. (1982). Fundamentals of Acoustics. New York, John Wiley & Sons.

Kirchhoff, G. (1877). Vorlesungen uber Mathematiche Physik: Mechanik. Leipzig, Teubner.

Koopman, G. H. (1967). "The Vortex Wakes of Vibrating Cylinders at Low Reynolds Numbers." J. Fluid Mechanics. **28**:

Krylov, N. M. and N. N. Bogoliubov. (1957). Introduction to Nonlinear Mechanics. Princeton, Princeton University Press.

Kurosaka, M. (1977). "Cumulative Nonlinear Distortion of an Acoustic Wave Propagating Through Non-Uniform Flow." J. Fluid Mechanics: 83. **83**(part 4): 751-773.

Kurosaka, M. (1982). Ranque-Hilsch Effect Revisited: Temperature Separation Traced to Orderly Spinning Waves or 'Vortex Whistle'.

Lengele, G. (1975). "A Model Describing the Velocity Response of Composite Propellants." AIAA J. **13**: 315-322.

Levine, J. N. and J. D. Baum. (1983). "A Numerical Study of Nonlinear Instability Phenomena in Solid Propellant Rocket Motors." AIAA J. **21**: 557-564.

Levine, J. N., J. D. Baum and R. L. Lovine. (1983). "Pulsing of Solid Propellant Rocket Motors: A Numerical and Experimental Study." J. Spacecraft and Rockets. 20(March-April): 150-157.

Levine, J. N., J. D. Baum and R. L. Lovine. (1984). "Pulse Triggered Instability in Solid Propellant Rocket Motors." AIAA J. 22: 1413-1419.

Levine, J. N. and F. E. C. Culick. (1974). Nonlinear Analysis of Solid Rocket Combustion Instability.

Liepmann, H. W. and A. Roshko. (1957). Elements of Gasdynamics. Galcit Aeronautical Series. John Wiley & Sons, Inc.

Lighthill, M. J. (1952). "On Sound Generated Aerodynamically." Proc. Royal Society, Series A. 231:

Lin, C. C. (1967). The Theory of Hydrodynamic Stability. Cambridge, Cambridge University Press.

Lovine, R. L. and R. C. Waugh. (1976). Standardized Stability Prediction Method for Solid Rocket Motors.

Markham, J. J. (1952). "Second-Order Acoustic Fields: Energy Relations." Physical Review. 86: 712.

Maslen, S. H. and F. K. Moore. (1956). "On Strong Transverse Waves Without Shocks in a Circular Cylinder." J. Aeronautical Sci. 23: 583-593.

Mathes, H. B. (1980a). Assessment of Chamber Pressure Oscillations in the Shuttle Solid Rocket Booster Motor.

Mathes, H. B. (1980b). A New Assessment of Chamber Pressure Oscillations in the Shuttle SRB.

Mathes, H. B. (1983). Analysis of Acoustic Chamber Pressure Oscillations in Shuttle High-Performance SRB's.

Mathes, H. B. (1979). Assessment of Chamber Pressure Oscillations in the Shuttle SRB.

Mathes, H. B. and C. J. Bicker. (1976). Combustion Stability Predictions for Space Shuttle Solid Propellant Rocket Motors.

Mathes, H. B. and C. J. Bicker. (1985). Analysis of Longitudinal Chamber Pressure Oscillations in Shuttle SRB's During Flight. JANNAF Combustion Meeting.

Mathes, H. B. and C. J. Bicker. (1985). Analysis of Longitudinal Chamber Pressure Oscillations in Shuttle SRB's During Flight.

McClure, F. T., J. F. Bird and R. W. Hart. (1962). "Erosive Mechanisms for Nonlinear Instability in the Axial Mode of Solid Propellant Rocket Motors." ARS J. 3(3): 374-378.

McClure, F. T. and H. R. W. (1965). Theory of Acoustic Instability in Solid-Propellant Rocket Combustion.

McClure, F. T., H. R. W. and B. J. F. (1960). Solid Propellant Rocket Motors as Acoustic Oscillators. Solid Propellant Rocket Research. New York, Academic Press.

Michalke, A. (1965). "On Spatially Growing Disturbances in an Inviscid Shear Layer." J. Fluid Mechanics. 23:

Miles, J. W. (1957). "On the Reflection of Sound at an Interface of Relative Motion." J. Acoustical Society of America. 29: 226-228.

Mitchell, C. E., Crocco, L. and W. A. Sirignano. (1969). "Nonlinear Longitudinal Instability in Rocket Motors with Concentrated Combustion." (?): 35-63.

Morfey, C. L. (1967). Energy-Balance Equations in Acoustics. Unstable Combustion of Advanced Solid Propellants.

Morse, P. M. and K. U. Ingard. (1968). Theoretical Acoustics. New York, McGraw-Hill Book Company.

Myers, M. K. (1980). "On the Acoustic Boundary Condition in the Presence of Flow." J. Sound and Vibration. 71(3): 429-434.

Nayfeh, A. H. (1973). Perturbation Methods. New York, John Wiley & Sons.

Nayfeh, A. H., J. E. Kaiser and B. S. Shaker. (1974). "Effect of Mean Velocity Profile Shapes on Sound Transmission through Rectangular Ducts." J. Sound and Vibration. 34(3): 413-423.

Nayfeh, A. H., J. E. Kaiser and D. P. Telionis. (1975). "Acoustics of Aircraft Engine-Duct Systems." AIAA J. 13: 130-154.

Nussbaumer, H. J. (1982). Fast Fourier Transforms and Convolution Algorithms. New York, Springer-Verlag.

Pierce, A. (1981). Acoustics. New York, McGraw-Hill Book Company.

Press, W. H., B. P. Flannery, S. A. Teukolsky and W. T. Vetterling. (1986). Numerical Recipes: The Art of Scientific Computing. Cambridge, Cambridge University Press.

Price, E. W. (1979). "Velocity Coupling in Oscillatory Combustion of Solid Propellants." AIAA J. **17**: 799-800.

Price, E. W. (1977). Combustion Instability in Solid Rocket Motors.

Price, E. W. (1979). "Velocity Coupling in Oscillatory Combustion of Solid Propellants." **17**: 799-800.

Price, E. W. and J. W. Sofferis. (1958). "Combustion Instability in Solid Propellant Rocket Motors." **28**(No. 3): 190-192.

Ribner, H. S. (1957). "Reflection, Transmission and Amplification of Sound by a Moving Medium." J. Acoustical Society of America. **29**: 435-441.

Riemann, B. (1953). On Propagation of Plane Air Waves of Finite Amplitude. The Collected Works of Bernhard Riemann. New York, Dover.

Rockwell, D. (1982). Oscillations of Impinging Shear Layers. AIAA Aerospace Sciences Meeting.

Rosenhead, L. (1963). Laminar Boundary Layers. Oxford, The Clarendon Press.

Sankar, L. N. and Y. Tassa. (1982). "A Strongly Implicity Procedure for Steady Three-Dimensional Flows." AIAA J. **20**(5):

Schlichting, H. (1979). Boundary-Layer Theory. McGraw-Hill Series in Mechanical Engineering. New York, McGraw-Hill Book Company.

Shackelford, B. W., H. B. Mathes and R. H. Sforzini. (1985). Space Shuttle Solid Rocket Motor Ballistic Response to Motor Case Material Change.

Shapiro, A. H. (1953). The Dynamics and Thermodynamics of Compressible Fluid Flows. New York, Ronald Press.

Sigman, R. K. (1985). "Boundary Condition for Rocket Motor Stability." AIAA J. 23(7): 1079-1085.

Sigman, R. K. and B. T. Zinn. (1983). "A Finite Element Approach for Predicting Nozzle Admittances." J. Sound and Vibration. 88(1): 117-131.

Sirignano, W. A. and L. Crocco. (1964). "A Shock Wave Model of Unstable Rocket Combustors." AIAA J. 2(July): 1285-1296.

Sotter, J. G. and G. A. Flandro. (1968). "Unstable Combustion in Rockets." Scientific American. 12(12):

Stakgold, I. (1979). Green's Function and Boundary Value Problems. New York, John Wiley & Sons.

Stewartson, K. (1964). The Theory of Laminar Boundary Layers in Compressible Fluids. Oxford, The Clarendon Press.

Sutton, G. P. (1986). Rocket Propulsion Elements. New York, John Wiley & Sons.

Swithenbank, J. and G. Sotter. (1964). "Vortex Generation in Solid Propellant Rockets." AIAA J. 2(7): 1297-1302.

Temkin, S. (1967). Nonlinear Gas Oscillations in a Resonant Tube..

Tien, J. S. (1972). "Oscillatory Burning of Solid Propellants Including Gas Phase Time Lag." 5:

Tsui, C. and G. A. Flandro. (1977). "Self-Induced Sound Generation by Flow Over Perforated Duct Liners." J. Sound and Vibrations. 50(3):

Van Dyke, M. (1964). Perturbation Methods in Fluid Mechanics. Applied Mathematics and Mechanics. New York and London, Academic Press.

Van Dyke, M. (1975). "Computer Extension of Perturbation Series in Fluid Mechanics." SIAM J. Appl. Mech. 28: 720-734.

Van Moorhem, W. K. (1982). "Flow Turning in Solid Propellant Rocket Combustion Stability Analyses." AIAA J. 20(10): 1420-1425.

Van Moorhem, W. K. (1980). An Investigation of the Origin of the Flow Turning Effect in Combustion Instability.

Van Wylen, G. J. and R. E. Sonntag. (1978). Fundamentals of Classical Thermodynamics. New York, John Wylie & Sons.

Vogt, G. (1982). Flow Generated Noise in a Simulated Rocket.

Vuillot, F. and P. Kuentzmann. (1986). "Flow Turning and Admittance Correction: An Experimental Comparison." J. Propulsion. 2(4): 345-353.

Vuillot, F. and G. Avalon. (1988). "Acoustic-Mean Flow Interaction in Solid Rocket Motors Using Navier-Stokes Equations" AIAA Joint Propulsion Conference, 1988.

Whitham, G. B. (1974). Linear and Nonlinear Waves. New York, John Wiley & Sons.

Williams, F. A. (1985). Combustion Theory. Menlo Park, CA, The Benjamin/ Cummings Publishing Co., Inc.

Wolfram, S. (1988). Mathematica. A System for Doing Mathematics by Computer. Redwood City, CA, Addison-Wesley Publishing Co.

Wylie, C. R. (1975). Advanced Engineering Mathematics. New York, McGraw-Hill Book Company.

Yang, J. Y. S. (1970). Unsteady Pressure Response of a Burning Solid Propellant Surface.

Yang, J. Y. S. and G. A. Flandro. (1971). "Acoustic Wave Amplification in Solid Rockets by Discrete Mass Injection." AIAA J. :

NINE

COMBUSTOR STABILITY COMPUTATION

In spite of the considerable effort which has been made since 1960 in attempts to elucidate the phenomena of combustion instability, it is evident .. that many gaps exist in our base understanding of the phenomena.

G.F.P. Trubridge, 1969

9.1 INTRODUCTION

The multitude of separate analyses and analytical tools we have collected in previous chapters must now be assembled into a usable stability assessment package. What is needed is a systems analysis tool that can be easily applied to realistic rocket motor geometries by analysts working in industrial settings. It must incorporate the best possible set of representations for all gain and loss mechanisms. As brought out in our detailed study of some of these mechanisms, the level of reliability varies greatly among the various contributing parts. Some areas simply have not been correctly treated. One difficulty that is impossible to avoid is that each element in a collection of separate analyses of varying complexity cannot be expected to be of uniform quality. Since it is a system analysis that we need, then the final analytical tool may be only as good as its weakest component. It is therefore no surprise, that stability prediction methodology only appears to work in some of the cases to which has been applied. This has led to a general distrust of stability assessment programs, and motor developers often carry out stability calculations only if they are required to do so contractually.

In what follows, we will review the state of development of the standard stability approach, its history, and recent improvements and additions. Great care will be taken to identify the weak links in the method and its implementation. An important task will be to review several important additional gain and loss terms that have not already been accounted for. Suggestion are also made for improvements in each program element. Finally, we will review the track record of the standardized stability prediction method in application to actual motor systems over the past twenty-three years.

9.2 ORIGINS OF THE STANDARD STABILITY APPROACH

A brief historical summary of the origins of the standard stability prediction methodology provides a useful framework for this chapter. Later sections describe the various loss and gain mechanisms that must be added to the basic linear stability analysis described in Chapter 8 to bring it to the status of a system analysis tool. The way in which understanding of these mechanisms has evolved will aid us in assembling the parts needed for more reliable stability prediction programs than the ones now used by the rocket industry.

Before 1969, each propulsion company dealt with combustion instability in an *ad hoc* manner; there was little, or no, inclination to develop a system analysis approach. This changed when the serious Minuteman Stage 3 combustion instability problem arose. The progress in analysis, coupled with apparent success of the T-burner method for determining the response characteristics of the propellant convinced concerned government agencies and the major motor contractors that a standardized stability prediction scheme was both feasible and desirable. It was expected to promote more efficient communication between the several universities, government laboratories, and rocket manufacturers.

The goals of the Standardized Stability Prediction Program sponsored by the Air Force Rocket Propulsion Laboratory were to develop computational procedures and digital computer programs for

- Standardized analysis of motor combustion instability

- Parametric studies of motor port and grain geometries for stability

- Reduction of experimental combustor data

It was intended that the procedures developed in the program would become the industry-wide standard for stability calculations. This has in effect come to pass, although most companies have made modifications in the program to fit their special needs. Several revisions to the program have been made since it was first released; the most recent appearing in 1987. These have not brought major changes to the approach, but were aimed at general sprucing up of the various algorithms.

SSPP Program Capabilities

The SSSP consists actually of two main program modules:

- Axial Mode (one-dimensional)

- Multi-dimensional

The first module is based on Culick's one-dimensional stability model [Cu-

lick, 1973]. It is intended for use in situations likely to be dominated by longitudinal acoustic oscillations with no important gas motion in the transverse direction. The acoustic modes and corresponding frequencies are determined analytically by means of simple trigonometric or hyperbolic functions.

The second module represents a more general computational tool intended for port geometries that can support more complex modes of oscillation. The NASTRAN finite element program is employed for calculating mode shapes and frequencies for two classes of motor geometry. Both axisymmetric (with port area variations in the axial direction allowed, but limited to a constant cyclic symmetry number) and more general grain shapes (constant planar cross section along the longitudinal axis) are accommodated.

Each program incorporates several stability elements that represent the various gain and loss mechanism. The effects included are:

1. Pressure Coupling - This is based on the analysis presented in Chapter 8. The Flandro admittance correction [Flandro,1974a; 1974b] (a simplified version of the vortical effects described in 8.5) can be selected in addition to or in place of the Flow Turning Loss (which it is intended to replace). Values for the propellant admittance function must be supplied as input.

2. Velocity Coupling - The classical form of velocity coupling is accommodated. It attempts to account for effective erosive velocity at each station along the propellant surface and includes a model of the threshold effect.

3. Particulate Damping - The Tempkin-Dobbins [1966] analysis is used to account for the drag loss due to particles in the gas. Particle sizes are distributed in bimodal log-normal form. Each component of the distribution has a specified standard deviation and mean diameter.

4. Flow Turning Loss - This is the correction introduced by Culick [1972] to account for failure to incorporate realistic boundary conditions in the multidimensional analysis. This is done by extension of results from the one-dimensional analysis.

5. Nozzle Damping - Since there was controversy at the time of program inception as to the proper manner for representing the nozzle, the program requires the user to specify the nozzle admittance function. In the intervening years, most users have found that use of the simple short-nozzle theory is a reliable approach [Crocco and Cheng, 1956; Buffam, 1967; Crocco and Sirignano, 1967].

6. Wall Losses - Viscous damping and thermal losses at inert boundaries are calculated using a simple acoustic boundary layer model.

7. Distributed Combustion - Since metal additives continue to burn as they move away from the propellant and into the chamber, there is an associated potential driving (or damping). This calculation requires volumetric combustion rate to be specified by the user.

8. Mode Coupling - This correction, based on Culick's early nonlinear one-dimensional analysis [Culick, 1971], may be selected in the longitudinal mode module.

9. High Flow Mach Number Corrections - An attempt was made to incorporated corrections for high-speed flow effects. This element was not fully developed, and to the knowledge of the authors, was never utilized in practice.

Each of the factors on which the Standard Stability Prediction Program is based will be subjected to careful scrutiny in this chapter. We will attempt to update the background analyses whenever possible or appropriate. The intent is to clarify the underlying assumptions, limitations, and numerical implementation of each gain and loss contribution. Areas requiring renewed attention are identified, and suggestions are made for detailed improvements at several points. Actually, as the discussion unflolds, it will be apparent that only a fraction of the theoretical work that has been accomplished over several decades is implemented in the program. This a result of the dominating influence of a few individuals who have strongly affected the field of study.

The reader must be careful to properly interpret the remarks and suggestions made in following sections. All of these are intended to be strictly constructive. The SSPP was designed at a time when many of the basic parts of the stability analysis were still under development. It remains to this time as the only available method for motor stability assessment. It has been updated several times; the last one just a year before this was written. Nevertheless, much improvement is possible. Hopefully what is presented here will represent a contribution to future development of a much needed engineering tool.

NONLINEAR COMBUSTION INSTABILITY

Nonlinearity in waves manifests itself in a variety of ways, and in the case of waves governed by hyperbolic equations, the most striking is the evolution of discontinuous solutions from arbitrarily well behaved initial data.

A. Jeffrey and T. Kawahara 1982

All real processes are nonlinear; however, they are only "slightly nonlinear." If this were not true, then it is doubtful that the human intellect, and the scientific disciplines that are its most important offspring, would ever have evolved.

Anon., 1973

10.1 INTRODUCTION

Whenever we do not succeed in our prediction or explanation of some oscillatory phenomenon in solid rocket motors, it is traditional to explain our failure as being due to the "nonlinearity of the problem." This is a phrase that, loosly translated, means "we haven't the faintest idea of what happened." However, in many cases, the situation is truly governed by physical effects that are not well-represented by a linear analysis of the type we have relied upon throughout the earlier parts of this book. If a truly practical approach to combustion instability is to evolve, it is necessary that tools for dealing with nonlinear behavior be developed. This development must be supported at many levels. The usual tendency is to attack just one feature or to use just one approach. Success will come only if *all the tools available* are put to use in an organized and mutually supporting manner. These tools consist of

- Experimental procedures using cold flow simulation

- Experiments using laboratory-scale burners or motors

- Experiments in full-scall hot motor firings

- Computational Experiments employing CFD techniques

- Analyses that extend successful parts of the linear theory into
  the nonlinear range

Organization of Chapter 10

This chapter devoted to the very important topics of nonlinear behavior of time-dependent rocket motor flow, the analysis of such behavior, and the experimental procedures for studying it. As has been continuously emphasized in previous chapters dealing with the analysis of the combustion instability problem, whenever finite amplitude oscillations are present there is a high liklihood that one or more of the attributes of nonlinear behavior will appear.

The experimental basis for nonlinear behavior is extensive. In fact, the first experimental observations of combustion instability resulted from nonlinear effects such as the frequently observed mean pressure shift that sometimes leads to explosive failure of the motor. The experimental literature contains references to a plethora of nonlinear effects, some rather subtle in nature, others more dramatic such as the mean pressure excursion just described. It will become apparent that the most important threat to system performance attributable to combustion instability comes about as the result of nonlinear behavior. Thus it is of great importance to develop appropriate means for the analytical modeling of these effects. Without such tools, evaluation of experimental data and formulation of corrective strategies becomes a nearly impossible task. Much remains to be accomplished in this regard, especially in the nonlinear modeling of the combustion zone itself.

A vital problem in combustion instability modeling is the prediction of the limit amplitude expected in a given combustor. That is, information regarding the *severity of oscillatory behavior* nearly always missing. Motor development program managers often express great frustration because of the lack of information from instability models regarding the *level* of the oscillatory pressure amplitude. It is necessary to understand that linear models are simply not capable of producing this information. They yield only an indication of the *probability* that oscillatory behavior will or will not occur. However, there is a relationship that we will identify between the linear growth rate and the maximum oscillation amplitude (often referred to as the limit amplitude), but linear theory does not yield direct information on this important aspect of system behavior. In the past, there have been cases where concern over a particular mode showing a high predicted growth rate has led to such a concentration of attention and resources on its elimination that another with much smaller predicted growth is neglected and yet rises to disastrous amplitude when motor testing commences.

Only by extending combustion instability modeling into the nonlinear regime can estimates of limit amplitude be accomplished. The present status of this class of modeling is carefully assessed and is found to be in need of much attention. The potential role of computational tools based on CFD techniques is discussed. Handling of instrumentation and interpreting data in experimental study of nonlinear instability also requires special attention. Again, much remains to be accomplished even though the basic problem involved was the first of the combustion instability effects to be observed and is by far the most damaging to motor

operation when it occurs in the field.

10.1 CLASSIFICATION OF NONLINEAR BEHAVIOR

Before attempting to introduce the modeling of nonlinear oscillatory flows , it is beneficial to briefly review the types of behavior that have been identified in several decades of experimentation. Much can be learned by classifying these observations. This information is invaluable in formulating the appropriate analytical or computational attack on the problem. For the benefit of readers not familiar with the jargon of nonlinear combustion instability. Words such as "triggering", "limit-cycles", and "D.C. shift" will occur frequently in the discussion.

Table 1 is a summary of characteristics often associated with nonlinear combustion instability. It seldom happens that more than one or two of the attributes are present simultaneously. There are situations in which certain combinations of attributes always appear together. Such occurrences give valuable guidance in the search for understanding of underlying physical origins.

TABLE 10.1

ATTRIBUTES OF NONLINEAR COMBUSTION INSTABILITY

1. Finite Amplitude Pressure Oscillations

2. Multiple Harmonic Components in Wave Spectrum

3. Appearance of Traveling Steep Fronted Pressure Waves

4. Limit Cycle Behavior at a Well-Defined Limiting Amplitude

5. Triggering - Oscillations Started by Pulsing of Otherwise Stable System

6. Modification of Mean Burning Rate with Resultant DC Shift in Chamber Pressure

7. Unexpected Torques or Sideforces

8. Secondary Flows Such as Axial Vortices or Cellular Recirculation Patterns

9. Velocity Coupled Propellant Response to Acoustic Fluctuations

10. Transition to Turbulent Motions in Combustion Zone
Before proceeding it is necessary to understand the way in which the word

"instability" is to be interpreted in the following discussions. *Instability* pertains to the mathematical description of a system whose amplitude grows without limit. As indicated in Chapter 8, a stability analysis seeks to determine, usually on the basis of a simple linearized model, whether or not the system is stable to an infinitesimal disturbance. That is, whether or not the amplitude of a very small departure from a rest state of the system will grow or decay. Such an analysis cannot answer questions related to finite amplitude motions except in very special situations. The word "instability" is used here in the broad sense that it describes the presence of oscillatory behavior whether or not the associated wave motions are in the process of growing, decaying, or have reached a finite limit cycle.

As already discussed, the time-dependent gas motions in a rocket system are inherently nonlinear. Thus a finite disturbance is quite likely to provoke a nonlinear response of one of the types described in Table 10.1. The principal goal of nonlinear combustion stability analysis is to provide some predictive capability in this regard.

The literature is replete with examples of unexpected nonlinear behavior. Each of these has required some special *ad hoc* treatment in motor development programs. This is a costly and time-consuming approach that does not take advantage of the considerable experimental and analytical data base. It also does not take account of the close interrelationships between a number of the nonlinear attributes. An important goal of this chapter is to make this literature as accessible as possible to the reader.

Only some of the nonlinear attributes listed in Table 10.1 may be simultaneously present in an oscillating combustion chamber. For example, a situation often observed is that of an apparently linear acoustic disturbance growing to finite amplitude and then reaching a stable limit cycle without any evidence of harmonics or transition to steep wave fronts. Another common example is the appearance of steep fronted waves with a rich supply of harmonics in its spectrum without an associated D.C. shift in the mean pressure. On the other hand, the D. C. Shift phenomenon is sometimes observed in situations where no steep wave front is discernible in the data (although the waves have a relatively large amplitude). To be useful, any theoretical models must be capable of treating any of these cases as well as the more common one in which steep wavefronts, rich harmonic content, and the D. C. shift appear together with a finite limit cycle.

Before attempting any computations, it is necessary that we discuss each of the nonlinear attributes shown in Table 10.1 in more detail. We must establish what situations give rise to each of the effects, and must attempt to give a preliminary assessment of the relationship to basic motor design parameters. It is obviously necessary to gain some familiarity with the nonlinear features so that they can be properly recognized in experimentation. Since there is such a rich set of interrelated phenomena to be covered, it is essential to acquire this initial familiarity so that the roots of each type of behavior and its relationships to other types of nonlinear behavior can be recognized in the analysis.

Finite Amplitude Pressure Oscillations

Let us first be a little more precise about what we mean by "finite amplitude" oscillations. It is especially important to understand the implications in terms of use of acoustic modes of the motor chamber as a means for describing the gas motions. The simplest definition for "finite amplitude" is that the pressure waves are *measurable*. That is that the gas oscillations can be detected by instruments with typical resolving capability. This is not a very precise definition, and it implies that nonlinear behavior is automatically present if the waves can be resolved by instrumentation such as pressure gages located at the chamber peripheries or by strain gages attached to the outer surface of the pressure vessel. Nevertheless, often true that if oscillations can detected by the usual types of instrumention then the system is exhibiting some form of nonlinear oscillatory behavior.

A situation that is often encountered is one in which detectable oscillations are present with an amplitude that reaches a maximum that may vary slowly (compared to the period of the fluctuations). This is what we will call "limit cycle" behavior (to be defined and discussed in more detail shortly). The attainment of a limit cycle is a clear indication of nonlinear behavior. Careful study of the material in Chapter 8 will suggest that a linear system (or at least a linear model of the type of system we are interested in) cannot operate in a limit cycle. Even if the limit cycle amplitude is very small compared to the chamber mean pressure (recall that this is defined to be the ratio of the instantaneous wave amplitude to the mean chamber pressure), it is necessary to classify the system as exhibiting nonlinear oscillations. The reasons for this will become evident as we analyze the problem. We will see that nonlinear features must be present in the system to give rise to limit cycle behavior.

The system described in the last paragraph may sometimes exhibit a monomodal pressure distribution. That is, it may be possible to describe the oscillatory pressure field using just one of the acoustic modes as a model. The frequency of the oscillation and the mode shape of the wave may appear to match a particular acoustic mode nearly exactly. Nevertheless, as we will show, if a limit amplitude is present, then the system must be described as *nonlinear*.

It is often possible to observe transient waves of relatively small amplitude that appear to be growing exponentially as required for a linear system. It is the usual assumption that these are adequately described by the linear analysis, making it possible to determine system features such as propellant admittance or response function from the data. This must be done with some care, because, as we shall see, the apparent exponential growth rate can be significantly affected by nonlinear influences if the wave amplitude is sufficiently large. It is thus quite difficult to measure attributes of the linear system in test devices that behave in a nonlinear fashion. Precise measurement of the linear admittance or response function can only be attained if data is taken quite close to the stability boundary, that is for very small (and difficult to measure) amplitudes. This fact explains at

least part of the well-known discrepancies between experimental response function measurements taken in different equipment by different investigators as discussed in earlier chapters. It also helps to explain the data scatter found in the results from a single type of device carefully operated by a single investigator.

In this brief discussion we have encountered one of the several practical difficulties of nonlinear oscillatory motor behavior. That is, if the oscillations are large enough to be measured, then we must be prepared to address nonlinear aspects of the physics of the system. This is not to say that linear analysis is of no use. What we wish to emphasize is that *one must carefully treat predictions based on linear theory and be especially careful in applying the ideas of linear theory to data from unstable motor systems*. We will continually return to this theme as we attempt to construct a usable nonlinear model for rocket motor pressure fluctuations.

Multiple Harmonic Components in Wave Spectrum

A feature of nonlinear motor behavior is often that the spectrum contains many harmonic components. It is often possible to associate each of these harmonics with an acoustic mode of the chamber. However, as emphasized in the last subsection, there are commonly occurring situations in which a single mode attains a finite amplitude limit cycle without the presence of other acoustic components. Thus, multiple harmonics are not a necessary condition for nonlinear behavior, although there are many practical situations in which many acoustic components must be present to describe the gas motions. The shock-like waves in unstable tactical rockets involving predominantly longitudinal oscillations are a case in point. This situation is described in more detail in the next paragraphs.

Much of the existing theory of nonlinear instability [Culick, 1971, 1975a, 1976; Levine and Culick, 1974; Levine and Baum, 1983], is based on the idea of energy exchange between the several acoustic modes used in describing the system mathematically as we have done in previous chapters (see the discussions at the end of section 5.6). Several of the nonlinear attributes can be ascribed to migration of energy between modes, usually from the low-order (low frequency) to the higher-order (high frequency) modes. This concept is closely related to the steepening of the wave system into a shocklike pattern to be discussed in the next subsection. However, the mathematical process used does not always account for nonisentropic losses that accompany steep wave fronts. A practical scheme for correcting the results for these important losses will be introduced at an appropriate point in the analyses to follow.

Traveling Shock Waves

It is often assumed that nonlinear behavior is characterized by the presence of steep fronted waves. Indeed, such waves are clearly nonlinear according to the definitions we are utilizing. However, as described in the previous subsection,

there have been many cases exhibiting a self-limited wave with nearly sinusoidal acoustic wave characteristics. Thus steepening of the wavefront (implying the presence of acoustic harmonic components) is not a requirement for nonlinear behavior.

There are, on the other hand, many important practical situations in which the system is dominated by shock-like, steep-fronted waves. This situation appears frequently in motor designs susceptible to *longitudinal* acoustic oscillations. We will identify the characteristics of such systems as we proceed. It appears that transverse wave motion are not susceptible to steepening effects (see the excellent description of nonlinear transverse waves by Maslen and Moore [1956]). Thus one often observes nearly sinusoidal oscillations in motors dominated by transverse instabilities.

Since longitudinal oscillations often exhibit a steep-fronted waveform, the gas motions are often assumed to be quite different from those we have used to represent the system in earlier chapters. There have been many studies of finite amplitude waves in ducts and combustors based on treatment of the wave structure from the standpoint of traveling shock waves. The classical works by Chester [1964] and others have emphasized this point of view. However, it turns out that to adopt this approach in the rocket motor stability problem is not as productive as *extending* the linear analyses that we have already constructed.

There have been several models of nonlinear motor behavior based on shock waves [Sirignano and Crocco, 1965; Mitchell, Crocco, and Sirignano, 1969], but these have not been widely accepted for use in practical motor analysis. There are obviously many benefits in employing a model which extends the accepted linear point of view. It is this approach that we will follow in the remainder of the chapter. Thus, we will not consider the shock wave instability theories in any detail although they represent a very interesting and elegant approach to the problem.

What we will try to accomplish in the remainder of this subsection is to show that the acoustic perturbation analysis (with vortical corrections) contains in it what is needed to describe finite-amplitude, steep-fronted waves. This is a subject that has been somewhat controversial in the past, so, as usual, we will insert a fair amount of mathematical detail to clarify the situation. For instance, it will be demonstrated that a *traveling* shock wave structure can be synthesized from *standing* acoustic modes of the chamber. Thus we can use a set of small-amplitude standing waves to describe a finite-amplitude traveling wave. This only works if we can find a way to correct for energy losses due to the nonisentropic nature of this form of wave motion.

Limit Cycle Behavior

The approach to a peak amplitude or limit cycle is a feature frequently associated with nonlinear motor oscillations. As we will demonstrate in this chapter, in order for the system to attain a composite wave amplitude that changes only

slowly on the time scale of the period of the oscillations, there must be nonlinear elements in the system energy gain/loss balance. Such a behavior will be described as a *limit cycle* in accordance with the terminology of the theory of nonlinear oscillations (see the excellent texts on this subject [Minorski, 1962; Krylov and Bogoliubov, 1957; Stoker, 1950; Bogoliubov and Mitropolsky, 1961; Jordan and Smith, 1977]). This does not mean that observations taken in a a motor firing at a time when the amplitude is changing rapidly are not nonlinear. In fact will will shortly describe a situatio₁ ⁻ ich the system amplitude may be changing nearly exponentially as predicted b₋ near theory, but is still dominated by nonlinear influences.

As we have frequently pointed out, prediction of limit cycle amplitudes should be one of the main goals of rocket instability analysis. It is this information that is of most interest to the motor designer and especially the end-user. One of the defects of the linear theory is that it only provides an estimate of the tendency for the wave system to increase in amplitude. It is valid only at the stability boundary where the amplitudes are exceedingly small. What is needed is the capability to predict what the time-history of the actual wave amplitude will be over many cycles of oscillation. Typically, it will change slowly on the time scale of the oscillations because it is governed by the motor chamber geometry, size, and thermodynamic parameters that also change slowly. We will attempt to show that by carrying out the analysis at a given point in time assuming all of these parameters are fixed, one can arrive at a useful estimate of the instantaneous system limit amplitude. Carrying this procedure out at other burn times then allows us to construct a time-history of the development of any of several possible composite modes of oscillation. This is a capability yet to be fully achieved, but should be a goal for the combustion stability community.

One of the earliest attempts to devise a nonlinear theory for solid rocket motor combustion instability was that based on mode coupling effects by Culick [1971]. In this theory, it is assumed that the main nonlinear influence stems from the fact that the acoustic components of the composite wave structure are not independent of one another. This is closely tied to the concept of wave steepening, a classical demonstation of nonlinear acoustics in which an initially sinusoidal wave of finite amplitude steepens into a shock wave. The final wave can be decomposed (as we will soon demonstrate) into a set of superposed standing acoustic components. Thus, the steepening process can be described as a migration of the energy initially contained in the fundamental sinusoidal wave into a large number of harmonics.

Wave steepening in longitudinal oscillatory flows is governed by the same physics that leads to the breaking of a surface wave on a liquid or the steepening of the wavefront in a shock tube. The passage of the wavefront increases the local temperature of the gas particles, and thus the speed of sound behind the wavefront is raised causing the following particles to "catch up". The result is a tendency for the wave to attain a steep-fronted shocklike structure. Modeling of these effects as a function of time is one of the aims of nonlinear analysis. In fact, it is often

assumed that the steepening effect is the main process involved in nonlinear behavior. This represents a cascading of the initial energy distribution in the system into a new configuration with the energy flow usually (but not always) in the direction of the higher modes of oscillation. This process is described as "mode coupling" and is the origin of steep wave fronts in a rocket motor. Thus, if nonlinear loss mechanisms are too weak to rapidly dissipate the energy flux from the lower to the higher harmonics, then the acoustic wave tends to steepen into a shock wave.

It is often the case that both energy required to excite a particular acoustic mode and the dissipation inherent in that mode increase as the wave number increases. This is clearly depicted in our earlier discussions of the acoustic modes. One measure of the energy associated with a particular mode is the normalization function E_i^2 as it was derived in Chapter 8. Evaluation of this function for a given wave geometry shows that the energy inherent in a given mode increases with the mode index. That is, higher-order modes require more energy to reach a given amplitude. This explains the lowest order modes are almost always the ones to be driven to large amplitude in practice.

It is clear from the discussion of stability characteristics of the acoustic modes of a particular system in Chapter 8 that the lower order modes are always easier to excite for the reasons just cited. That is, for a given amplitude it requires less energy to amplify the wave and the relative effect of dissipative mechanisms is generally smaller. This explains why the lower order modes are the ones inevitably observed experimentally and why very high frequency motions are normally not of great importance. They are simply too difficult to excite unless some very unusual high frequency external sc rce of energy is attached to the system.

In many practical problems, only the fundamental mode (or one of the other lower order modes) can be strongly excited because the others are strongly damped. It is possible in this situation that large limiting amplitudes are reached while the waveform remains sinusoidal. In this situation mode coupling may *not* play a role in the nonlinear system behavior.

There are many other situations in which several modes are involved in a nonlinear instability with each component reaching a limit amplitude in the nonlinear range. It is quite often the case that the *relative amplitudes* of the component acoustic waves do not change as the system amplitude evolves with time. Figure 10.1 shows such a wave. Notice that over many cycles of oscillation there is no discernible change in the shape of the waveform. This shape will be shown to be the result of the relative phases and amplitudes of the acoustic components. In this situation there is negligible transfer of energy between modes; if this was not so, then the mode shape would change noticeably with time. Mode coupling requires that the wave *shape* change continuously with time.

The point of introducing two situations frequently encountered in practice in which no mode coupling is present is that in such cases the analysis of the system behavior is greatly simplified. Since it is our object to clarify the subject of

nonlinear motor behavior to the greatest possible degree, we will carefuly assess this special situation. In so doing, the various elements of the motor system that contribute to the limit amplitude, triggering behavior, and DC shift characteristics will be brought into focus. While mode coupling may well be a dominant mechanism in some situations, treating it as the central theme of nonlinear instability tends to complicate the analysis and makes it more difficult to identify the most important system features. Again, our objective is to enhance physical understanding of the behavior and the relationship of the analytical findings to the motor design process. Everything covered in this chapter is presented with this as the guiding principle.

The Triggering Phenomenon

Another important feature associated with the nonlinear characteristics of a system is its ability to be forced into oscillation. This is an important feature from the operational standpoint because motors that exhibit stable operation under normal circumstances (that is, the system is linearly stable) can oscillate violently if they are pulsed beyond a certain threshold wave amplitude. The pulse that triggers this particularly nasty form of instability can be caused by passage of pieces of propellant or insulator through the nozzle. This momentary reduction in throat area tends to initiate a fairly steep (one rich in harmonic content) reflected wave back into the combustion chamber. If the amplitude of this pulse is sufficiently high, the system can sustain the oscillation under certain circumstances. A similar situation involves motors that exhibits a limit cycle oscillation with an acceptably small amplitude that is driven into oscillatory behavior at a much more destructive amplitude by a pulse.

Since natural triggering can occur in unexpected ways in the field, a method of testing has been evolved in which test motors are deliberately pulsed one or more times during burn to determine their susceptibility to triggered oscillations. It is obviously a matter of practical necessity to illuminate the geometrical, chemical, and thermodynamic features of the motor system that contribute to this suceptibility.

We will demonstrate that triggering is a natural consequence of the nonlinear sensitivity of the energy gain/loss balance to the wave amplitude. One of the goals of the analysis to be undertaken will be to identify motor parameters and relationships between parameters that affect the triggering response.

10.2 CONNECTION BETWEEN LINEAR AN NONLINEAR BEHAVIOR

An important task is to identify those combinations of geometry, propellant variables, and other system parameters that give rise to the various nonlinear attributes. It cannot be overemphasized that this is the major goal of all of the analytical efforts. Only in some cases has success been achieved. The design implications of nonlinear combustion stability modeling are fairly obvious. A

major goal, yet to be achieved, is the capability to estimate the limit amplitude or the triggering amplitude of a given system. However, progress in this direction is finite, and the present state of development is carefully assessed. It is believed by some investigators that this goal can be best achieved by means of computational fluid dynamics algorithms. The current state of progress in this regard is compared to the purely analytical models that have been developed. Clearly, both points of view must be utilized in a mutually supportive manner. As has been demonstrated so often in other fields, use of a strictly numerical strategy often does not take advantage of the sharply honed insight resulting from a more approximate analytical method. Again, for the most rapid progress toward the goal of a predictive nonlinear instability capability, both methods must be used in a synergistic fashion. The goal is to produce analytical results that can be used to interpret data. In many practical situations, elaborate numerical calculations are simply not justified since the required input information is not available[2].

It is natural to think of nonlinear instability as separate and distinct from linear combustion instability considerations. However, the nonlinear characteristics of the system are strongly dependent on the linear characteristics. Nonlinear modeling cannot be successful without a complete and reliable linear model. Thus continuing efforts to improve the linear analyses are justified in support of nonlinear modeling.

It will be shown that there is a direct relationship between the linear analyses of Chapter 8 and the nonlinear models to be discussed here. From this it will be demonstrated that a system with a large linear growth rate as predicted by the linearized instability calculation can indeed be expected to exhibit a larger finite limit cycle amplitude than one with a relatively small linear growth rate. This expectation has been used as an "article of faith" in the interpretation of the linear results for many years. Thus it will be possible to rationalize this often used criterion for deciding whether a particular instability prediction justifies serious corrective actions.

Conceptual Model of Nonlinear Behavior

Before addressing the very complex set of conservation equations describing the nonlinear fluid dynamics of a solid propellant combustion chamber, it is beneficial to introduce a simple conceptual model as an aid to understanding the physical processes that must be confronted. This enables one to focus on the key elements of the problem without the burden of tracking the simultaneous interactions of many variables such as pressure, temperature, density, and the three velocity components. Not to mention the important shear wave corrections described in Chapter 8.

A simple chamber geometry such as that shown in Figure 10.2 is useful. It consists of a tubular propellant grain with combustion on the internal surface only. Suppose that this chamber initially supports an acoustic oscillation in only the fundamental longitudinal mode. The origin of this wave motion is not of

concern at this point. It could have arisen from random fluctuations such as turbulence if the system is linearly unstable at the mode frequency. It could also have been initiated by a controlled pressure pulse at the chamber boundary or within the burner cavity. Whether or not nonlinear behavior will follow depends upon a myriad of system parameters and geometrical features. If the system damping is light, or if the system is linearly unstable (positive linear growth rate a), then certain nonlinear affects will appear if the wave persists for a sufficiently long time.

Wave Steepening - An Example of Modal Superposition

It is useful to demonstrate the utility of the superposition concept by applying it to a situation that will be of direct use in our analytical treatment of nonlinear combustion instability. It is well-known that one can superpose two traveling-waves to produce a standing-wave solution. In elementary treatment of the wave equation this is the way the standing-wave concept is often introduced. For instance in the simple one-dimensional wave equation we treated earlier (see equation 5.113) it is readily shown by direct substitution that the most elementary solutions are of the form

$$p^{(1)} = f(z-t) + g(z+t), \qquad (10.1)$$

where $f(z-t)$ and $g(z+t)$ are two independent arbitrary functions of the special combinations of the spatial variable z and the time t, $(z-t)$ and $(z+t)$. This is d'Alembert's famous solution to the wave equation and the special variables define the two families of *characteristic* curves describing the motion in the z-t plane. Figure 10.3 shows characteristics for a waveform advancing in the +z direction. Each of the characteristic lines has a slope equal to the reciprocal of the speed of sound (in the present case this is unity since we are working in a dimensionless system with the speed of sound as the characteristic speed). These lines are intimately related to the Mach lines familiar to the reader who has studied gasdynamics. The waves we are discussing are "weak" in that their amplitudes must be regarded as very small. Otherwise the linearized equations would break down. Notice that in use of the linearized equations to describe the waves in the gas flow we are specifically ignoring nonlinear effects. All parts of the wave in the figure propagate at the same speed. This is a comforting feature of linear waves that we will soon be required to give up.

The form of the general solution given in 10.1 applies for any function of the characteristic variables. The two solutions

$$p_1 = \tfrac{1}{2}\cos k(z+t) \quad \text{and} \quad p_2 = \tfrac{1}{2}\cos k(z-t) \qquad (10.2)$$

fit this specification. These represent two harmonic traveling-waves of equal amplitude propagating in opposite directions. If we combine the linear solutions, we find as a composite solution

$$p^{(1)} = p_1 + p_2 = \tfrac{1}{2}[\cos k(z+t) + \cos k(z-t)]. \qquad (10.3)$$

The result can be manipulated by means of standard trigonometric identities to yield

$$p^{(1)} = \cos kz \cos kt, \qquad (10.4)$$

which is just the solution we found earlier that satisfies the rigid-wall boundary conditions. The combination is a *standing-wave*. That is, the two propagating waves interfere with each other in such a way that node points appear at points that can be interpreted as chamber boundaries. This is a very special situation; the resulting wave is fixed. It has no traveling-wave crest of the type that characterizes the fundamental solutions in 10.1.
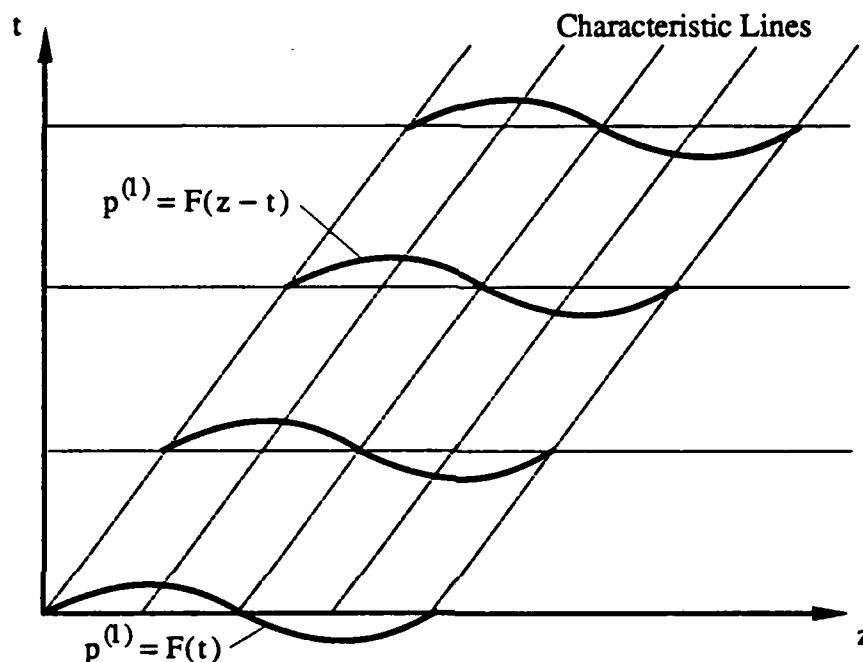

Fig. 10.3 Propagation of a Weak Wave in the z-t Plane
(Rightward Propagating Wave Illustrated)

It is not as well known that combinations of *standing-waves* can be used to represent a *traveling-waveform*. Let us first describe situations in which this could be important. As a simple case consider a finite-amplitude standing-wave in a closed tube. We could arrange that the wave have an initially sinusoidal waveform, and it could thus be be considered, at least for an instant, as a finite-amplitude acoustic wave. However, this configuration is not stable. To make it stable the amplitude would have to be infinitesimal and there could be no dissipative or heat-transfer effects present. The fact that finite-amplitude is specified implies that some of the effects of nonlinearity must come into play. This situation is analogous to one that was first studied by Riemann for the case of a propagating wave [Riemann, 1953]. He found that finite sinusoidal waves tend to steepen into shockwaves.

A simple explanation for this distortion or steepening is that as the wavefront traverses the gas it heats it and increases the local speed of sound in parts of the wave where pressure increased above the ambient and decreases the speed of propagation where it is below the undisturbed pressure. Thus, gas elements

behind the wave front have a higher propagation speed. That is, their characteristic lines have different slopes. This is illustrated in Figure 10.4, which shows the evolution of an initially sinusoidal traveling-wave. At a special time and location (depends on the initial amplitude and shape of the disturbance), the characteristic lines cross. At this point we say the wave has steepened into a *shock wave*. Although the figure implies that the process of steepening continues beyond this point, resulting in a *breaking* wave as shown in the upper part of the drawing, such behavior is not possible in gas dynamics. Something like this does occur in the analogous free-surface waves; breaking ocean waves are familiar to all surfers.
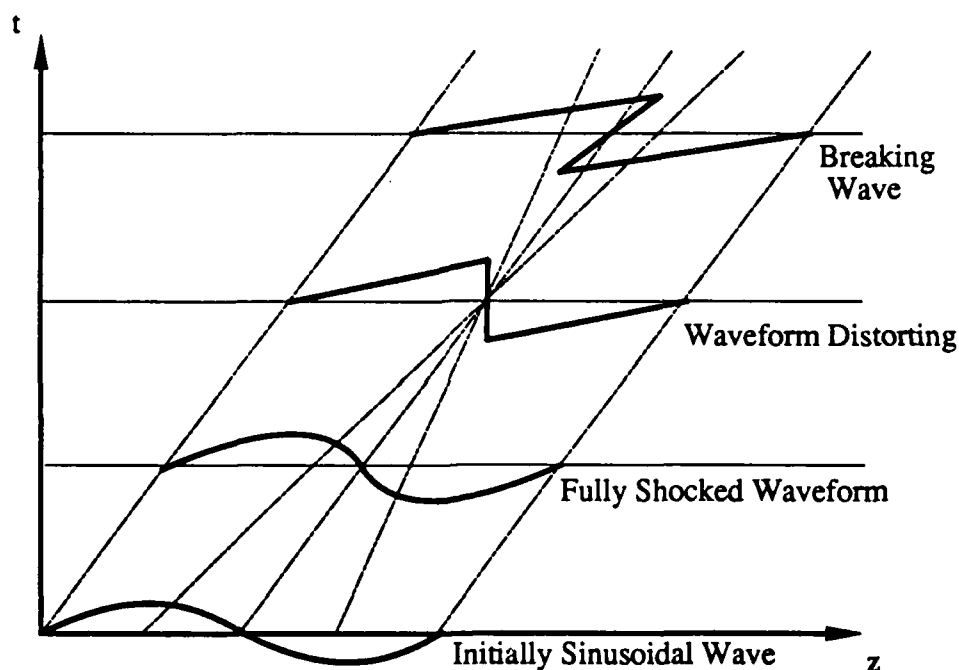

Fig. 10.4 Steepening Effect in Finite Amplitude Wave

In the present case of a standing-wave, the same distorting elements are present and the initially sinusoidal shape cannot remain unchanged. It may not be clear at first glance exactly what this distortion will eventually lead to, but the trends are easy to determine. Consider an initial finite-amplitude waveform with a shape identical to the first acoustic mode as shown in Figure 10.5. The upper plot is the pressure distribution; the lower plot shows the acoustic particle velocity. At the instant shown all of the gas is moving to the right (away from the high-pressure area and towards the low-pressure zone, as one would expect). Remember that the speed of sound in an ideal gas is proportional to the temperature. That is

$$\bar{a} = \sqrt{\gamma\, R\bar{T}_o} = \sqrt{\gamma\, R\bar{T}(1 + \varepsilon T^{(1)} + \dots)} ,$$ (10.5)

The propagation speed must be higher at the left (high-pressure side) than at the right (low-pressure side) because the temperature variations in the gas are in phase with the pressure. The gas particles tend to "bunch up" on one side. That is, our initially sinusoidal wave is *steepening*. If this motion is extrapolated it will be seen that we have the beginnings of a shock front moving to the right. If the pressure distribution had started 180 degrees out of phase from that shown, that is, with the high-pressure at the right end, a shock moving to the left would have been initiated. A little reflection will suggest that what must ultimately result is a shock front bouncing back and forth between the endwalls of the tube. Such gas motions have been frequently observed in axial-mode combustion instability [Brownlee, 1964; Brownlee and Kimball, 1966; Dickinson, 1962; Sirignano and Crocco, 1964; Temkin, 1967].
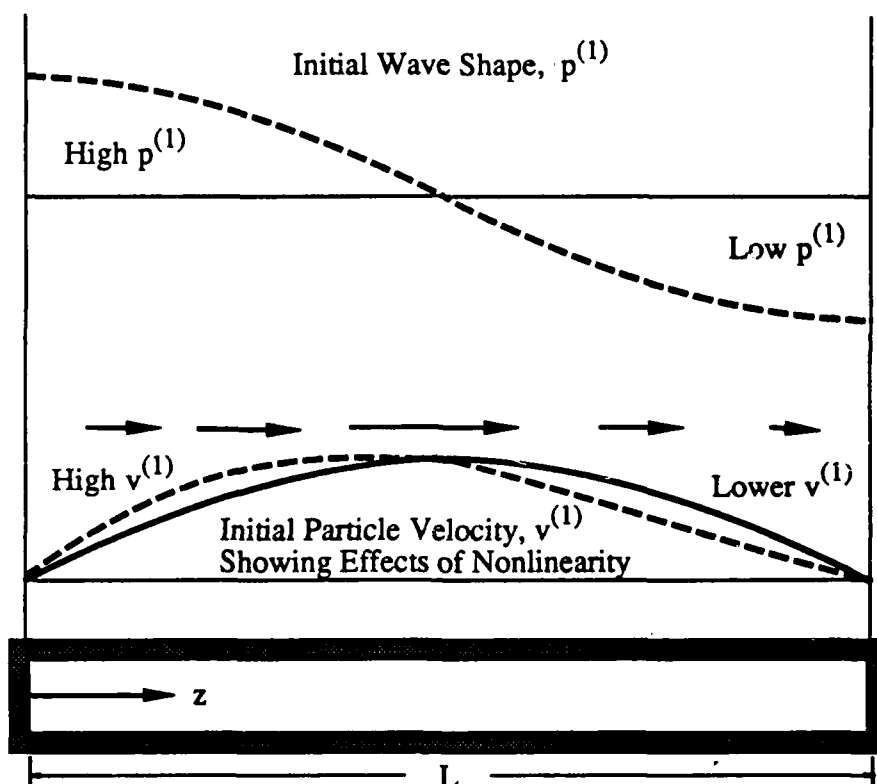

Fig. 10.5 Development of a Traveling Wave in a Closed Tube

Remember that acoustic waves representing the appropriate solutions to the boundary-value problem are *standing-waves*. The relationship, if any, to this *traveling* steep-fronted wave may not be immediately clear. We will now demonstate that a superposition of standing acoustic modes can represent a traveling steepfronted wave. This is useful information, because it bridges the gap between linearized models of combustion instability and the nonlinear behavior that is so often of concern in practice. This bridge will be used to advantage in this chapter.

It greatly simplifies the incorporation of linearized stability theory into the context of nonlinear instability and clarifies the physical meaning of a variety of system energy loss and gain mechanisms.

Linear waves can be added together in any way we like as long as they are individually solutions of the appropriate differential equations and boundary conditions. Assuming a one-dimensional system, we can superpose (dimensionless) pressure and corresponding velocity components to represent more complex situations. Thus, one can write

$$p^{(1)} = \sum_{n=1}^{N} A_n \cos(k_n z) \cos(k_n t - \phi_n) \qquad (10.6)$$

$$u^{(1)} = \frac{1}{\gamma} \sum_{n=1}^{N} A_n \sin(k_n z) \sin(k_n t - \phi_n) \, k \,, \qquad (10.7)$$

where the coefficients A_n at this point are completely arbitrary and N can represent any number of modes. ϕ_n is the relative phase angle and k_n is the wave number or dimensionless frequency. Now redefine ε slightly so that it represents the *composite* amplitude of the set of modal components. Solutions for the A_n can be found in many ways. One way is to allow steep wavefronts in the formulation and to solve for the resulting wave system [Betchov, 1958; Chester, 1964; Chu and Ying, 1963; Sirignano and Crocco, 1964]. Analyses like this are quite complicated, and it would be inappropriate to introduce them at this point. For now, we will take an easier tack. We can assume a wave shape and use Fourier analysis to find the coefficients. The results match those found directly from the nonlinear governing equations using the method of characteristics or similar approaches. Our solution is valid only for small-amplitude waves because it is to be composed of solutions of the equations derived on the basis of the small-amplitude limit.

Assume that some experimental data exhibits a pressure waveform of the shape shown in Figure 10.6. By *waveform* we mean the repeating shape of the disturbance as it appears in a time-domain plot. Now apply the simplest form of the Euler-Fourier formulas for any function f(t),
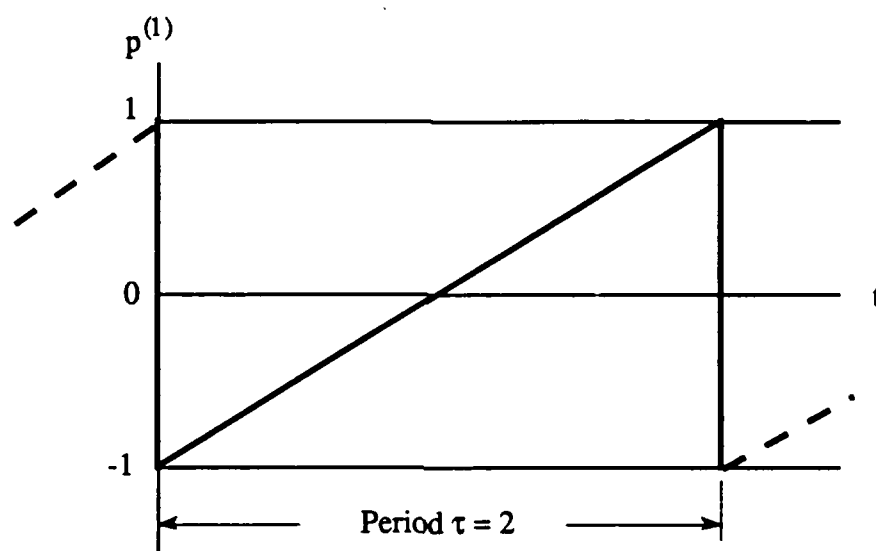
$$f(t) = \frac{a_o}{2} + \sum_{n=1}^{\infty} a_n \cos\left(\frac{n\pi t}{\tau/2}\right) + b_n \sin\left(\frac{n\pi t}{\tau/2}\right), \qquad (10.8)$$

where

$$a_n = \frac{2}{\tau} \int_0^\tau f(t) \cos\left(\frac{n\pi t}{\tau/2}\right) dt \qquad \text{and} \qquad b_n = \frac{2}{\tau} \int_0^\tau f(t) \sin\left(\frac{n\pi t}{\tau/2}\right) dt$$

to the waveform shown in the figure. The expression for the assumed sawtooth waveform is

$$p^{(1)} = f(t) = (t - 1) \qquad 0 < t < \tau \qquad (10.9)$$

Fig. 10.6 Assumed "Sawtooth" Waveform at z = 0

Assuming that the wave has the same frequency as the fundamental axial acoustic mode, the period of oscillation is

$$\tau = \text{Period} = \frac{2\pi}{k_1} = 2 \tag{10.10}$$

and we can evaluate the Euler coefficients by using 10.8. The results are

$$a_n = A_n \cos \phi_n = 0$$
$$b_n = A_n \sin \phi_n = -\frac{2}{n\pi} \tag{10.11}$$

Therefore

$$A_n = -\frac{2}{n\pi}, \quad \phi_n = \frac{\pi}{2} \qquad n = 1, 2, 3 \ldots \tag{10.12}$$

Since all the phase angles are 90o, the final solution can be written in the simple form

$$\left\{
\begin{aligned}
p^{(1)} &= -\sum_{n=1}^{N} \frac{2}{n\pi} \cos(n\pi z) \sin(n\pi t) && (10.13) \\
u^{(1)} &= \frac{1}{\gamma} \sum_{n=1}^{N} \frac{2}{n\pi} \sin(n\pi z) \cos(n\pi t) \, \mathbf{k} && (10.14)
\end{aligned}
\right.$$

Figure 10.7 shows the predicted *spectrum* for the waveform. This is compared to a spectrum as it would be determined using a wave analyzer or spectral analysis computer program. The sharp spikes in the theoretical spectrum would appear as shown in actual experimental data; because of the manner in which theinformation is handled using "fast-fourier transform" or FFT algorithms [Brigham, 1974]. Agreement improves as more terms are retained.
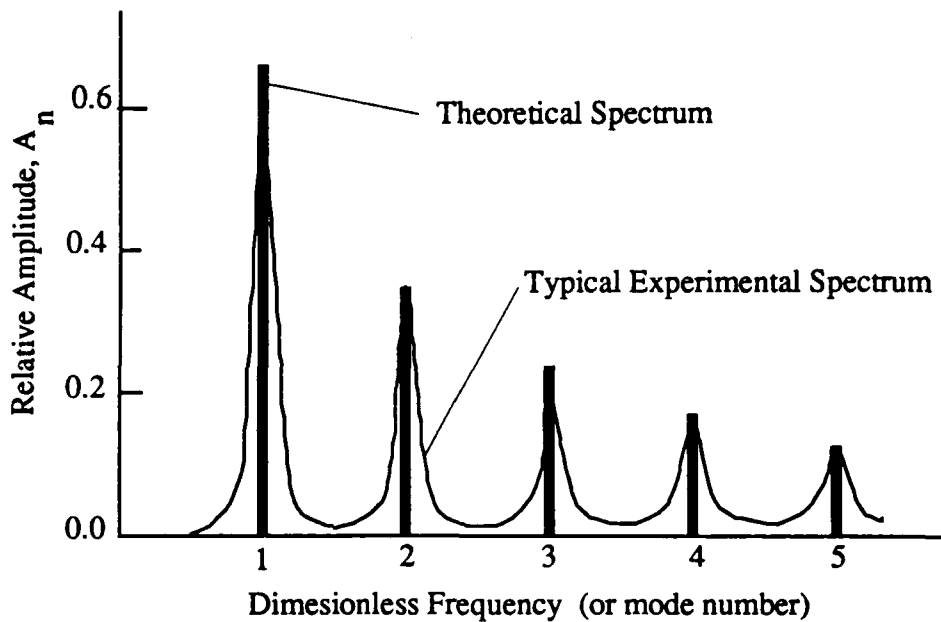
Fig. 10.7 Spectrum of "Sawtooth" Traveling Wave in a Closed Chamber

To demonstrate that we have, in fact, represented a traveling steep-fronted shock wave, Figure 10.8 shows the composite waveform plotted vs. position at several times during one wave cycle. The number of terms used in evaluation of the series (equation 6.165) was $N = 30$. The to-and-fro motion of the wave front at the frequency of the fundamental acoustic mode is apparent. Notice the characteristic phase shift as the pressure front reflects from the right-hand boundary and begins its travel down the channel to the left. The Gibbs overshoot near the front (always associated with Fourier series representations) is also evident. The thickness of the wavefront decreases as more terms are included in the series.

The superposition of acoustic modes to represent a traveling steep-fronted waveis a useful device for accessing key nonlinear features of combustion instability because it connects nonlinear behavior to the linear theory in the simplest way possible. The linear problem is the arena in which a vast majority of the work has been accomplished, and in which the most complete physical understanding is available. In the nonlinear arena are to be encountered the most important practical problems still requiring attention.

In the example of mode superposition just explored we did not attempt to expose the physical processes by which the steepening into a sharp wave front occurs. Steepening involves some nonlinear processes in which coupling between the acoustic modes must be involved. There may be a flow of energy from the lower to higher modes. In the real problem, some energy is lost in this process and ends up eventually in the form molecular motion or heat. All of this behavior is dictated by the second law of thermodynamics, and we will need to account for a variety of loss and gain mechanisms in addition to this one. This will be a necessary step if we are to be able to make useful predictions of the tendency for wave amplitudes to grow in a rocket experiencing unstable combustion.
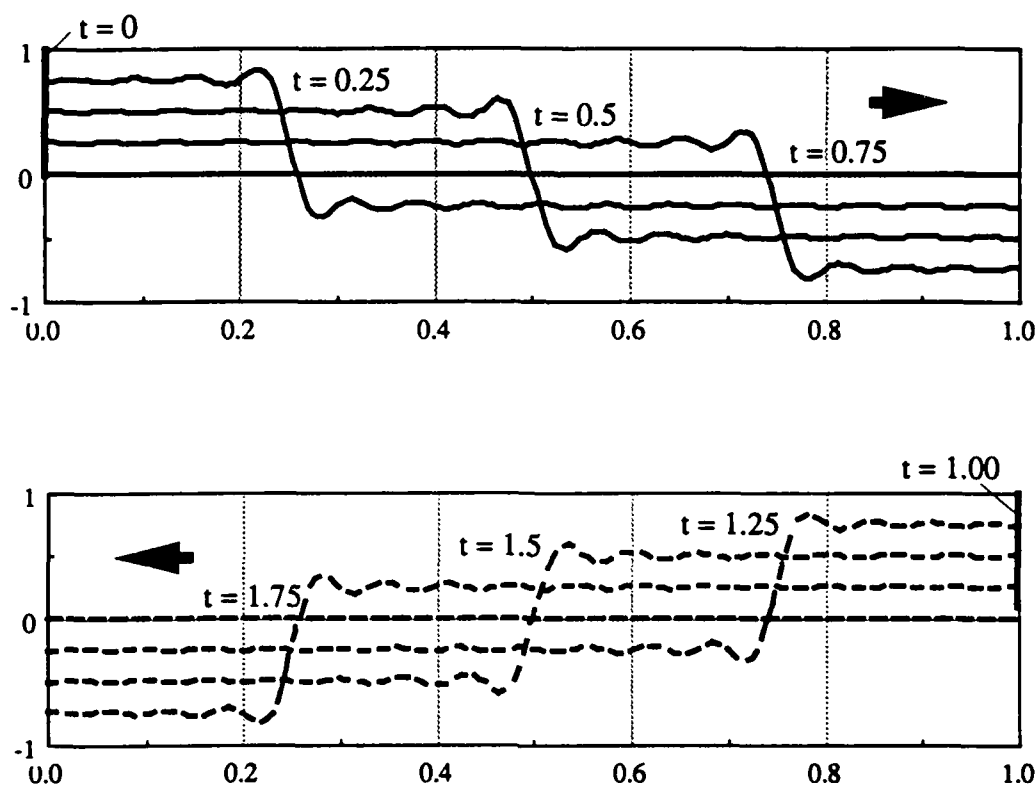
Fig. 10.8 Motion of a Traveling Steep-Fronted Wave in a Closed Chamber

An additional observation is necessary at this point. The reader will see that the subject of wave steepening was approached using a one-dimensional model. One must inquire as to the effects of the three-dimensionality of the problem. What influence will viscous stresses in the gases, especially at the chamber walls, have on the evolution of the wave? Also, one must ask if steepening effects are to be expected in transverse modes. Is a standing tangential mode, say the (0, 1, 0) mode we studied earlier, subject to steepening effects? Some answers to these questions were found many years ago [Maslen and Moore ,1956]. Their perturbation analysis of tangential modes in a combustor led to the conclusion that transverse modes do not steepen into shocklike structures. However, flow visualization studies of liquid rockets experiencing severe tangential mode instability were highly suggestive that steep wave fronts were present [Sotter and Flandro, 1968]. Sotter described them as "traveling detonation waves", but whether this definition really fits the physical situation has never been established. These are points that we will explore in more detail later in the chapter after we have assembled a few more necessary tools.